A stress analysis method for fatigue life prediction of welded structures

by

Rakesh Kumar Goyal

A Thesis
presented to the University of Waterloo
in fulfillment of the
thesis requirement for the degree of
Doctor of Philosophy
in
Mechanical Engineering

Waterloo, Ontario, Canada, 2015

AUTHOR'S DECLARATION

I hereby declare that I am the sole author of this thesis. This is a true copy of the thesis, including any required final revisions, as accepted by my examiners.

I understand that my thesis may be made electronically available to the public.

Abstract

In the case of structural weldments, the procedure for estimating fatigue life requires information concerning geometry of the object, loads and material. Detailed knowledge of stress fields in the critical regions of weldments is used to determine the fatigue life. The main theme of the research discussed in this thesis is to provide details of the methodology which has been developed to determine peak stress and associated non-linear through thickness stress distribution at the critical weld toe location by using only the geometry dependent stress concentration factors along with appropriate unique reference stress calculated in an efficient manner e.g. without modeling geometrical weld toe details. The peak stress at the weld toe can be subsequently used for estimating the fatigue crack initiation life. The non-linear through thickness stress distribution and the weight function method can be used for the determination of stress intensity factors and for the analysis of subsequent fatigue crack growth.

Accurate peak stress estimation requires 3D fine mesh finite element (FE) models, accounting for the micro-geometrical features, such as the weld toe angle and weld toe radius. Such models are computationally expensive and therefore impractical. On the other hand, stresses at sharp weld corners obtained from 3D coarse FE meshes are inaccurate and cannot be used directly for fatigue life estimations. A robust, sufficiently accurate, efficient and practical approach is proposed for fatigue life estimation of welded structures based on 3D coarse mesh FE models.

Another objective is to establish a methodology which is capable of accounting for the actual variability of stress concentration factors at welds, welding defects such as misalignment and incomplete penetration resulting from manufacturing processes. The proposed approach is capable of accounting for the effects from use of different material and effect of residual stresses from welding process. Residual stress information is obtained from a welding process simulation model, which has been validated against measured residual stress data.

The proposed methodology has been validated using numerical and experimental data by analyzing different weldments of varying geometrical and load configurations.

Further, the applicability of the stress field obtained from the proposed methodology is demonstrated by using it in a forward looking “Total Fatigue Life” concept based only on the fracture mechanics approach.

Acknowledgements

I would like to express my sincere appreciation to my supervisor Professor Grzegorz Glinka for his guidance, strong technical support, and helpful discussions throughout the thesis work. I feel great sense of pride in being associated with him and this feeling will stay alive with me forever.

Also I would like to thank my guru and technical mentor Dr. El-Zein Mohamad for his encouragement and unconditional support. Thanks to him for showing me the way and providing the flexibility to walk along that path while still working. Thanks to my friends Dr. Eric Johnson, Dr. Kuen Tat Teh and Dr. Peter Huffman for their support with the fatigue testing and many technical discussions. My special thanks go to Dr. John Goldak for teaching me everything I know in the field of welding process simulation.

Besides my advisor, I would like to thank the rest of my thesis committee: Prof. Heikki Remes, Prof. Hamid Jahed, Prof. Hyock Ju Kwon and Prof. Scott Walbridge.

I would also like to thank Dr. Sergey Bogdanov, Dr. Semyon Mikheevskiy, Aditya Chattopadhyay, and James Wong for their friendship and support especially during my initial days at Waterloo.

Most of all I would like to thank my wife Nupur Goyal for her love, patience, and endless support without which this would not have been possible. Finally, I would like to express my profound gratitude to my Parents for their support and encouragement throughout my education and professional career.

Dedication

To my wife Nupur and my son Pulkit

Table of Contents

List of Figures

List of Tables

Nomenclature

2D	2-Dimensional
3D	3-Dimensional
a	Crack size
a_i	Initial crack size
a_f	Final crack size
b	Fatigue strength exponent
c	Fatigue ductility exponent
2c	Crack length on the surface
a/c	Crack aspect ratio
C, p, m, γ	Material constants in the Fracture Mechanics equations
$\bar{d}$	Distance away from the weld toe
E	Young's modulus
2e/t	Misalignment to thickness ratio in the cruciform joint
ESED	Equivalent strain energy density
F	External force
FEA	Finite Element Analysis
FAT	Fatigue design class
G	Strain energy release rate
GMAW	Gas Metal Arc Welding
I	Moment of Inertia
K	Stress intensity factor
K_A	Stress intensity factor at the deepest point A of semi-elliptical crack

K_B	Stress intensity factor at the surface point B of semi-elliptical crack
$K_{t,}$ $K_{t,n}$	Stress concentration factor
K'	Cyclic strength coefficient
K_{th}	Threshold stress intensity factor
$K_{t,hs}^{m}$	Membrane hot spot stress concentration factor
$K_{t,hs}^{b}$	Bending hot spot stress concentration factor
K_f , K_w	Fatigue notch factor
K_{max}	Maximum stress intensity factor
K_{min}	Minimum stress intensity factor
K_{sa}	Multi-linear structural stress concentration factor
L,l	Length, width
h, h_p	Fillet weld leg size of the base and attachment plate respectively
m	Slope of S-N curve
$m_A(x,a)$	Weight function at the deepest point A of semi-elliptical crack
$m_B(x,a)$	Weight function at the surface point B of semi-elliptical crack
M, M_b, M_c	Bending moment
N	Number of cycles
n'	Cyclic strain hardening exponent
N_f	Total fatigue life
N_i	Fatigue crack initiation life
N_p	Fatigue crack propagation life
P, P_t, P_b	Applied load
P_s	Probability of survival

R	Stress ratio (ratio of minimum stress to maximum stress)
σ_{RS}, RS	Residual stress
S, σ	Stress
S-N	Stress-life curves
SIF	Stress intensity factor
SWT	Smith-Watson-Topper fatigue damage parameter
t, t_p	Thickness of the base and attachment plate respectively
TIG	Tungsten Inert Gas (Arc Welding)
x, y	Through-thickness distance from the weld toe
x_{NA}	Represents the X-coordinate of the neutral axis
y_{NA}	Represents the Y-coordinate of the neutral axis
Y	Geometry factor
ε	Strain
ε_f'	Fatigue ductility coefficient
ε_{max}^a	Elastic plastic strain at weld toe
$\varepsilon - N$	Strain-life curves
ν	Poisson's ratio
σ_b	Bending stress
σ_{ENS}	Effective notch stress (using 1mm notch radius)
σ_f'	Fatigue strength coefficient
σ_{hs}	Hot spot stress
σ_{hs}^m	Hot spot membrane stress
σ_{hs}^b	Hot spot bending stress

σ_m	Membrane stress
σ_{max}^a	Actual max stress at the weld toe
σ_n	Nominal stress
σ_{nl}	Non-linear stress at weld toe
σ_{nom}	Nominal stress in the base plate
σ_{peak}	Peak stress or max elastic notch stress
σ_r	Residual stress
σ_{sH}	Hot spot structural stress by Haibach
σ_{uts}	Ultimate tensile strength
σ_{weld}	Weld stress
$\sigma(y)$	Stress distribution along Y-axis
$\sigma(y_i)$	Nodal stress value at distance y_i from weld toe
$\sigma_{xx}(y)$	Normal stress (XX component) distribution along Y-axis
$\sigma_{yy}(x)$	Normal stress (YY component) distribution along X-axis
σ_{ys}	Monotonic yield strength
ρ, r	Actual notch radius
ρ_f	Fictitious notch radius
ρ^*	Microstructural support length of the material
θ	Weld toe angle
$\tau_{xy}, \tau_{yz}, \tau_{zx}$	Shear stress components
δ_{el}	Finite element size
ΔK	Stress intensity factor range
Δy_i	Distance between two adjacent nodes of FE model

$\Delta\varepsilon^{a}$	Actual elastic plastic strain range
$\Delta\epsilon_{k}$	Elasto-plastic strain range
$\Delta\sigma_{\mathrm{hs}}$	Hot spot stress range
$\Delta\sigma_{\mathrm{k}}$	Notch stress range (welded joint)
$\Delta\sigma_{\mathrm{n}}$	Nominal stress range
$\Delta\sigma_{\mathrm{peak}}$	Peak stress or max elastic notch stress range
$\Delta\sigma_{\mathrm{per}}$	Permissible stress range
$\Delta\sigma_{\mathrm{s}}$	Structural stress range (parent material)
$\Delta\sigma^{\mathrm{a}}$	Actual stress range

Chapter 1 Introduction and Research Objectives

1.1 Background and challenges in the fatigue design of welded joints

Welding is one of the most extensively used joining processes to build structural components, equipment, machines, bridges and cranes. Most of the structural components in the automobile, rail-road, aerospace, shipbuilding, agriculture and construction industries are designed for a specified fatigue life. In welded structures, the most obvious location of fatigue failure is either at the toe or root of the weld. It is very important to design welded structures in a way so that there is no premature fatigue failure of weld joints along with the universal requirement that design should be economical. *Accurate fatigue life estimation of welded joints, at early design stage, is the key* to achieve these contradictory requirements.

Current industry practices emphasize the increased use of virtual product design, verification, and validation methods, such as the use of finite element analysis techniques. This helps to reduce the dependence on expensive and time consuming prototype building and testing along with the added advantage of accelerated insertion of products in the design cycle. This further helps to reduce the overall product development time, enabling faster launch of products in the market. However, when it comes to the virtual design, analysis and fatigue life estimation of welded structures, it offers many *challenges* to the design and verification engineers due to the level of complexities involved as discussed in the next few paragraphs.

Practically, it is difficult to have 100% discontinuity free welds even in the case of most mechanized and robotic welds. Therefore, most of the welding codes allow for certain levels of discontinuities e.g. porosity, misalignment, convexity, concavity, undercut etc. If the size of these discontinuities exceeds the permissible tolerance range, as specified in the welding standards, these discontinuities are considered as weld quality defects requiring either repair or scrap of the welded component. These discontinuities can result in high stress concentration, decreasing the fatigue life of a welded joint in service.

Further, the weld micro geometrical features such as the weld toe radius and angle can create very high levels of stress concentration, affecting the fatigue life of welded

structures significantly. None of the welding codes (e.g. AWS D14.3) provide permissible tolerance range for these weld micro geometrical features, probably because of the following reasons a) Effect of these micro geometrical features on the fatigue life is so high that they have to be accounted for during the design b) Sufficient statistical data is not available in the literature as it is expensive and time consuming to measure these features for production weldments c) Depending on the welding process and technique, there is high variability in these parameters. Most of the welding codes require that stress concentration created by these weld micro geometrical features must be accounted for during the design process. Although due to the small size and complex nature of these features, detailed and large size fine mesh FEA models are needed to capture the stress concentration effect.

The welding process itself adds more complexities such as the altered chemical composition, microstructure and hence physical and mechanical material properties of the weld joint. Further, the complex thermal cycles from welding heat input can lead to distortion and a residual stress state in and around the welded joint, detrimental to fatigue life of the weld joint.

All of these *challenges* sufficiently explain the point that fatigue life estimation of the welded structures is a complex task. The objective of the research work presented in this thesis is to help address these *challenges.*

Fatigue is a process which causes irreversible damage or failure of a component subjected to repeated loading. Fatigue life comprises of the crack initiation life and the subsequent long-crack propagation life up to the final fracture. The crack may be a semi-elliptical surface crack, about 0.5mm in depth and 2mm in length. Fatigue process originates at the stress concentration points, such as at the weld toe in case of welded structures. Both the fatigue crack initiation and propagation stages are controlled by the magnitude and the distribution of stresses in the potential crack plane. A concise yet highly informative flow chart (Figure 1-1) has been given by the SAE committee and is reproduced here, describing the information path for stress and fatigue analysis. The essential inputs required for any fatigue life analysis are the geometry, load history and

material properties. Stress-strain analysis needs to be performed to obtain appropriate stress or strain information as required by the method used for fatigue analysis.

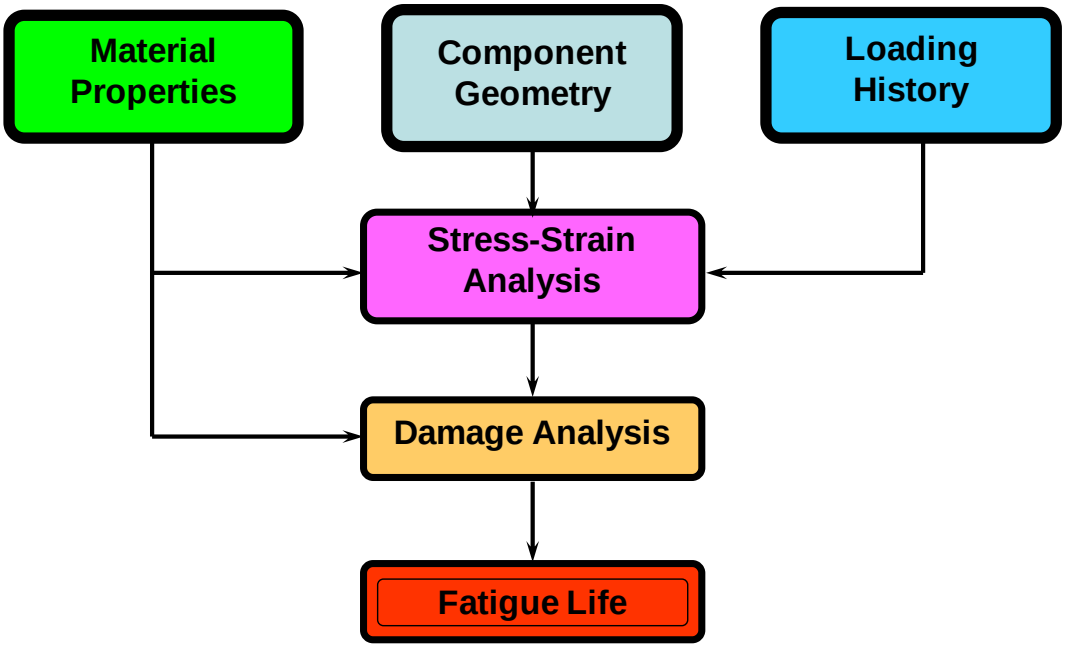

Figure 1-1: Stress and fatigue analysis flow chart [1]

In this work, the local strain life approach and the fracture mechanics approach have been utilized. The strain life approach and the fracture mechanics approach helps to determine the fatigue crack initiation life and the fatigue crack propagation life respectively. As shown in Figure 1-1, stress-strain analysis is the first important step towards fatigue life estimation. Accurate estimation of the fatigue life requires information about the appropriate stress-strain data. Local peak stress at the weld toe (or root), σ_{peak} is the main stress parameter which affects the fatigue life of a weldment at the critical location. For conducting the strain-life fatigue analysis (ε - N method) the magnitude of peak stress or peak stress history is required. For conducting crack propagation analysis using the fracture mechanics approach, non-linear through thickness stress distribution at the critical section is required. This non-linear through thickness stress distribution and the weight function method can be used for the determination of stress intensity factors and for the analysis of subsequent fatigue crack growth. Therefore, determination of the stress concentration and stress distribution at the critical locations in the welded structure plays an important role for the fatigue analysis.

It is known that stress concentration factors for the weld geometry are highly dependent on the micro geometrical features such as the weld toe radius and angle but also sensitive to the modes of loading. Depending on the welding techniques (manual versus robotic), process capabilities and the skill level of welding operators, shape and size of these weld micro geometrical features and hence the stress concentration factors could vary significantly, which could significantly impact the fatigue life. So it is critical to account for this variability of the stress concentration factors while determining the appropriate stress-strain information required for the fatigue life estimation.

1.2 Research objectives

The purpose of the methodology proposed in this thesis is to utilize an approach that would require the stress concentration factors independent of the load configuration and appropriate reference stresses to be used. The only parameters needed for the estimation of peak stress and the stress distribution induced by any combination of loads are only the geometrically unique stress concentration factors and the appropriate reference or nominal stresses.

The fatigue life prediction of complex welded structures, based on the stress analysis carried out with the Finite Element Analysis (FEA) methods, can be executed in many different ways with varying degrees of time consumption and accuracy. A large size FE model will increase both the time for the model preparation and the computational time. The large and complex FEA models may include the analysis of several critical locations and complex boundary conditions. The complex FE meshes on the other hand require substantial computing resources. The time required to solve such problems may make the fatigue evaluation and optimization process prohibitive. The ideal way to obtain detailed stress field information for welded structures , as required for fatigue life estimation, is to use 3D fine mesh finite element analysis models which have the capability to capture micro-geometrical features i.e. weld toe radius and angle. It however requires significant amount of time and efforts to model and solve 3D fine mesh FE model of even a simple weld joint e.g. double fillet T-joint. Doing such a detailed FE analysis is almost impractical for large size real welded structures such as the boom of an excavator arm. If a 3D coarse mesh model with larger size finite elements is used instead of a fine mesh

model, stresses at the sharp weld corner become inaccurate due to the singularity and hence cannot be directly used for fatigue life estimation. Advanced FEA modeling tools are able to automatically generate 3D coarse mesh FEA models in very short time. However because of the above described limitation with 3D coarse mesh FE models, benefits from the use of these advanced modeling tools cannot be realized to the full extent.

As a part of this research, a methodology has been developed to determine the peak stress σ_{peak} and the associated non-linear through thickness stress distribution $\sigma(y)$ at the critical weld toe location (Figure 1-2) by using only the geometry dependent stress concentration factors along with the appropriate unique reference stress quantities calculated in an efficient manner e.g. without modeling micro geometrical weld toe details. One of the main objectives of the research in this thesis is to develop new procedures to extract the stress data from simplified finite element models of the complex welded structures and to use the data for fatigue life predictions. It is believed that the method proposed in this thesis will help to make the design period shorter and to decrease the project cost, while the accuracy of the stress analysis could remain same as that one obtained from the complex 3D finite element models.

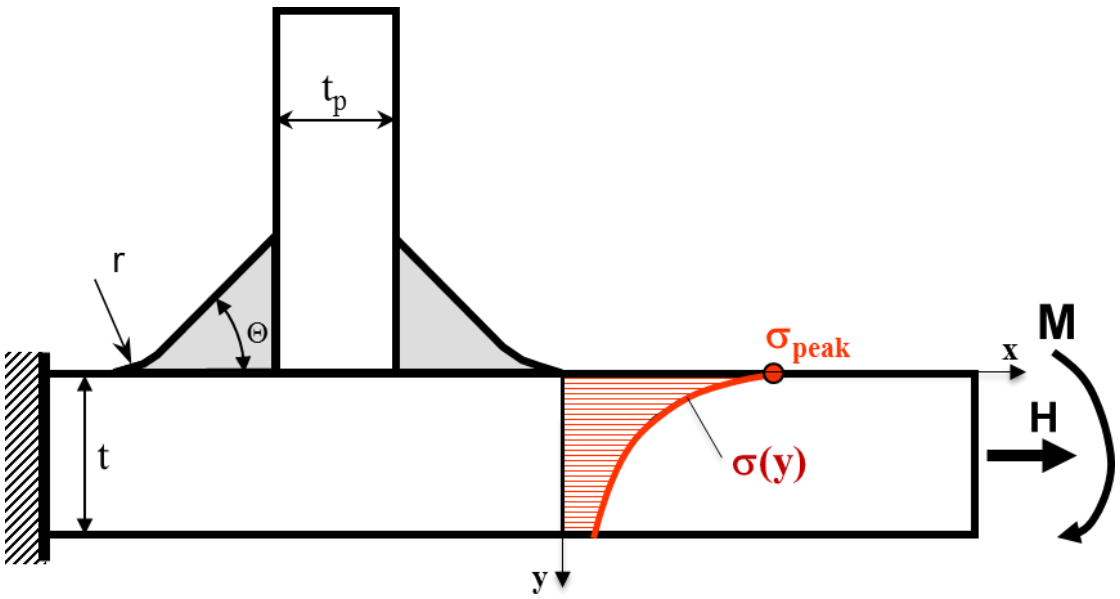

Figure 1-2: Peak stress and through thickness stress distribution at the critical weld toe location in a double fillet T-joint subjected to axial and bending loads

Further, residual stresses generated due to the complex thermal cycles from the welding process are generally of tensile nature near the weld toe region and needs to be accounted for along with the structural stresses in an appropriate manner during the fatigue life estimation. In this work, residual stresses from the welding process have been estimated using advanced process simulation package and the same have been accounted for the fatigue life estimation in an appropriate manner.

The present research proposes a new methodology which helps to determine the appropriate stress field as necessary for fatigue life estimation from the simplified FEA models of the large size welded structures and also provides the ability to account for the variability effects from the manufacturing process (stress concentration, residual stress, and defects like joint misalignment and incomplete penetration) to allow more robust fatigue life estimations.

Many different approaches for the fatigue life analysis are currently available. The nominal stress method was the most common method in the past until more confidence was developed in the other fatigue life analysis methods. The structural stress method and the notch stress methods have also gained acceptance due to their reasonably good life prediction capabilities. However these methods have limitations to account for many factors such as the effect of actual micro geometrical features of the weld joint, effect of actual residual stress and the effect of change in material type (e.g. these methods do not differentiate between the fatigue life estimation for mild steel versus advanced high strength structural steel). Also these methods use stress analysis procedures requiring special meshing rules which make them highly difficult to apply for the real large size welded structures. The proposed methodology for the fatigue life estimation of welded structures is more robust and efficient than the currently available methods in many aspects. The proposed method enables to use analysis results from 3D coarse mesh FEA model which is efficient in terms of computational efforts. Further, it provides a scientific approach to account for many factors which are otherwise ignored or conservatively assumed. Overdesign can be avoided, weight and hence cost reduction can be achieved while designing safe weld joints by using the proposed method.

Objectives of the proposed methodology are summarized as follow:

- Provide an efficient method for modeling large size welded structures which considerably reduces the computational time associated with 3D fine mesh FEA models.
- Provide a method to utilize output results from 3D coarse mesh FEA models to determine the peak stress and the through thickness stress distribution around the weld toe.
- Provide a method accounting for the appropriate stress concentrations, which are unique to the geometry of weld joint and independent of the load along with appropriate reference stress quantities.
- Provide a method to account for the variability of stress concentration due to the manufacturing process or technique, by allowing the use of realistic values of weld micro geometrical features i.e. weld toe radius and angle.
- Provide a method to account for the welding defects such as incomplete penetration and/or misalignment.
- Provide a method to evaluate the effect of welding residual stresses on the fatigue life of welded structures.
- Provide a method with the ability to account for the effect of using different materials so that benefits from the use of high strength steel can be realized more effectively.

The proposed methodology in this thesis includes the following steps:

1. Conduct 3D finite element analysis using efficient coarse mesh model for the complete large size welded structure.

2. Determine the through thickness normal stress distribution in the critical cross section.

3. Determine the membrane and bending hot spot stresses using the proposed methodology by post-processing of the extracted coarse mesh FE stress output data.

4. Estimate the stress concentration factors using the best empirical formulae available, accounting for the weld micro geometrical parameters obtained from the statistical measured data of real welded structures.

5. Calculate the peak stress at the weld toe and the through thickness stress distribution at the critical plane.

6. Conduct welding process simulation to determine residual stress at the weld toe and the through thickness residual stress distribution profile based on the welding procedures and parameters used during the actual production of welded structures.

7. Conduct the fatigue life analysis for weld joints, both crack initiation and crack propagation, accounting for the effects of the welding residual stresses.

Listed below are some of the major contributions from this research:

1. The mid-thickness segment of any through thickness stress field shows the same stress distribution, regardless of the FE mesh resolution (fine or coarse).

2. The relationship between the bending moment obtained from the middle half thickness segment of the section and the actual total bending moment at the weld toe section has been developed.

3. A method to determine the peak stress and the through thickness stress distribution at the weld toe has been developed, based on the data obtained from 3D coarse mesh FE model, required for the strain life and the fracture mechanics methods respectively.

4. An evaluation of the residual stress in the welds using welding process simulation tool.

5. A method to account for the combined effect of welding residual stress along with structural stress on the fatigue life has been formulated and validated.

6. A “forward looking concept” of the total fatigue life is demonstrated, validating that it could be possible to estimate the total fatigue life using the fracture mechanics approach only. Applicability of the stress field data (obtained using proposed 3D coarse mesh methodology) for the total fatigue life concept is demonstrated as well.

1.3 Outline of the thesis

This thesis has been organized in the following manner. Chapter 1 provides an introduction to the need for accurate fatigue life prediction of welded joints, limitations with the current methods in brief, objectives of the proposed methodology along with its benefits. Chapter 2 presents a review of the literature pertinent to this research field and provides principles of both the fatigue analysis and the fracture mechanics. Chapter 3 explains the objectives of the proposed research in details and development of the methodology for fatigue life analysis of weldments. Chapter 4 presents the verification of the proposed methodology. Chapter 5 presents the experimental fatigue life test results, its comparison with the estimated fatigue life using numerical methods and details of the forward looking approach on 'total fatigue life' concept only based on the fracture mechanics.. Chapter 6 presents the future work for potential enhancements in the proposed methodology Finally, Chapter 7 outlines the summary and conclusions.

Chapter 2 Review of Fatigue Analysis Methods

2.1 Fatigue Life Analysis Methods

Welded structures are very common in the off-road vehicles like agriculture and construction machines. These machines are required to perform services in the field under fatigue loads and are designed to meet certain life goals. A major mode of failure for the structural weld joints in these machines is fatigue failure. Weld joints are generally the weakest link between joined members and the fatigue failures are initiated and propagated through the welds. In order for these machines to perform their function adequately without fatigue failures, it becomes important that designers have an accurate method for establishing fatigue life in general and more specifically for the weld joints. Considering the importance, criticality and complexity of the subject enormous amount of research efforts have been (and are being) carried out, resulting in extensive amount of literature on various fatigue life estimation methods. This chapter covers the details of existing methods for stress analysis and fatigue life assessment of welded structures and associated challenges.

Fricke [2] presented a review paper showing summary of various fatigue life prediction approaches developed up to 2002 for seam welds. Niemi [3] and Fricke [4] have presented detailed recommendations concerning stress determination for fatigue analysis of welded components, more recent developments are covered by Hobbacher and Radaj in reference [5,6]. The importance of this subject is obvious because of the fact that other than independent researchers, various organizations across the globe like IIW, ASME, and SAE etc. have been working through several joint research programs to establish standard guidelines for analyzing the welded joints and estimating service life of welded structures. Comprehensive design guide and subsequently many updates have been issued by the International Institute of Welding (IIW) on 'recommendations for the fatigue design of welded components and structures'. Different fatigue life estimation methods are usually distinguished by the parameter used for description of fatigue life. Fatigue life can be determined using various methods; accordingly the assessment criteria and level of stress-strain information required are different, as shown in Table 2-1 e.g. the nominal stress (S-N) method uses the nominal stress (σ_n) parameter, the local strain-life (ε-N)

method uses the peak stress (σ_{peak}) parameter and the fracture mechanics (da/dN-ΔK) method uses the actual through thickness stress distribution $\sigma(y)$ for fatigue life estimation (see Figure 2-3). Most of the proposed methods for fatigue life estimation can be broadly classified into three categories: The nominal stress method, the local strain life method and the fracture mechanics method. The hot spot stress method and the effective notch stress method were developed through modifications of the S-N method. Details for these two methods along with the three main methods have been covered in the next sections.

Table 2-1: Inputs required for the three main fatigue life estimation methods

Fatigue Life Method	Assessment	Information
The nominal stress method	S-N curve of weldment	Structural detail
The local strain life method	ε-N curve of material	Peak notch stress
The fracture mechanics method	Stress intensity factor at the crack tip	Through thickness stress distribution

2.2 The Nominal Stress Method

The nominal stress method is based on the global geometry and does not account for the local effects, neither at macro level (weld shape and size) nor at micro level (such as weld toe or root). Application of this approach requires fatigue S-N curves, which are generated through fatigue testing of either small specimens or near full scale structures. All macro geometrical factors such as the discontinuity effects induced by various attachments and all micro geometrical factors such as the local notch effects from the weld geometry are included in the fatigue strength obtained experimentally. In order to properly apply this method the nominal stress range $\Delta\sigma_n$ should be clearly defined and the structural discontinuity should be comparable with one of the classified details used in design rules for generating the fatigue S-N curves.

Wohler [7] performed many laboratory fatigue tests under repeated bending stresses during the period of 1850 and 1860. These experiments were concerned with the railway axle failures and are considered to be the first systematic investigations of the fatigue phenomenon. Using the stress amplitude versus life (S-N) diagrams, Wohler showed that the fatigue life decreased with the increase of the stress amplitude and that below certain

stress amplitude, the test specimens did not fail. Thus, Wohler introduced the concept of the S-N diagram and the fatigue limit. He pointed out that the amplitude of stress was more important in fatigue than the maximum stress. Goodman's [8] contribution included the development of a model accounting for the mean stress effect on fatigue of metals. In 1910, Basquin [9] proposed an empirical law to mathematically describe the fatigue S-N curves. He showed that in the finite life region the S-N curve could be represented as a linear log-log relationship. During the period of 1920s and 1930s, fatigue of materials had evolved as a major field of scientific research. Investigations in that period focused among others on fatigue damage accumulation models such as by Palmgren [10]. The linear damage-accumulation hypothesis was also proposed by Miner [11].

Step by step procedure for the fatigue life estimation using the S-N method is shown in Figure 2-1 and is also summarized below:

1. Analysis of external forces acting on the welded structure (Figure 2-1 a),
2. Analysis of internal loads in a chosen cross section of a component (Figure 2-1 b),
3. Selection of individual notched component in the structure (Figure 2-1,c)
4. Selection (from ready-made family of S-N curves) or construction of S-N curve adequate for given weldment (Figure 2-1,d,e),
5. Identification of the stress parameter used for the determination of the S-N curve (nominal/reference stress),
6. Determination of analogous stress parameter for the actual element in the structure, as described above,
7. Identification of appropriate stress history (Figure 2-1,f),
8. Extraction of stress cycles (rainflow counting) from the stress history (Figure 2-1,g),
9. Calculation of fatigue damage (Figure 2-1,h),
10. Fatigue damage summation (Miner- Palmgren hypothesis) (Figure 2-1,i),
11. Determination of fatigue life in terms of number of stress history repetitions, N_{blck}, (No. of blocks) or the number of cycles to failure, N (Figure 2-1,j).
12. The procedure has to be repeated several times if multiple stress concentrations or critical locations are found in a component or structure.

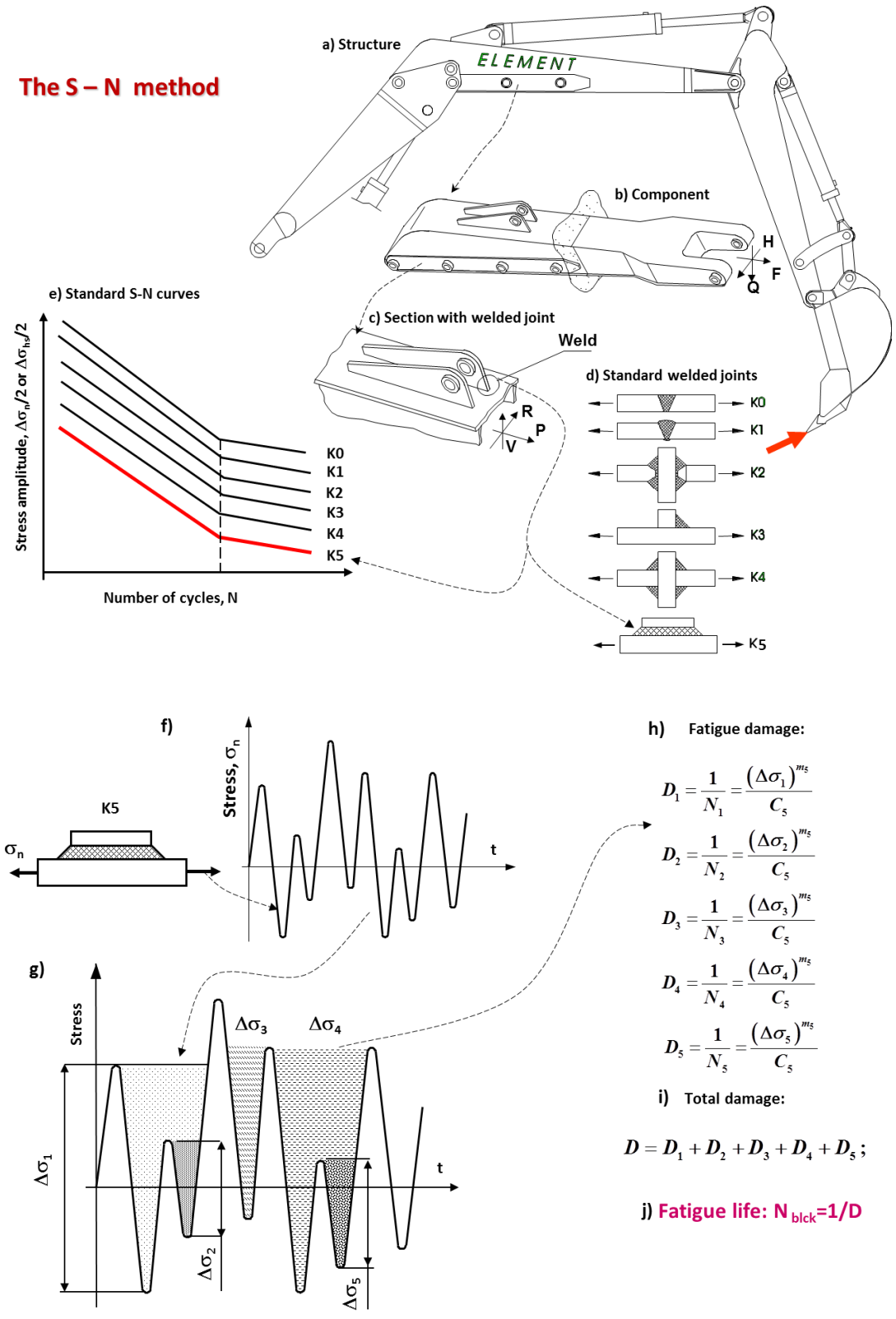

Figure 2-1: Steps in fatigue life prediction procedure based on the S-N approach [1]

Several standards and guidelines were developed based on the statistical evaluation of relevant fatigue tests performed in the 1970s. Around 30 years later, the International Institute of Welding [12] issued more comprehensive set of S-N curves along with catalogue of details for steel as well as aluminum alloys. The fatigue design categories of welded structural details are mentioned by FAT, fatigue design class, along with a specific number. The number following FAT designates the allowable nominal stress range $\Delta\sigma_n$ (in MPa) at N = $2x10^6$ cycles with the survival probability, P_s = 97.7%.

Even though this method appears to be easy for practical application but it has several limitations. Nominal stress is an average stress in a welded joint, so each type of unique structural detail needs special fatigue curve. The application of this concept not only requires defining and estimating the nominal stress value but also its permissible value with reference to a corresponding classified structural detail. The selection of an appropriate S-N curve for damage calculation can be very subjective, since the weld details have been classified not only based on the joint geometry, but also the dominant loading mode. Various factors which cause scatter in fatigue life data such as variations within the detail in dimensions, welding procedures etc. are not considered in this approach. So there may be a situation when this method is either not applicable, difficult to apply or may be very conservative resulting into unnecessary costlier designs.

This approach does not differentiate between crack initiation and propagation life as the calculated service life represents the final fracture. There is no formal guidance available for the designer or analyst on how to calculate the nominal stress using finite element analysis (FEA) as typically FEA estimates the notch stress. Sometimes the stress at a distance of 1 or 1.5 times wall thickness away from weld toe is assumed as nominal stress but that's rather subjective and is highly mesh dependent.

To include the effect of residual stresses, slopes in Wohler S–N curves were shifted down to a slope (m) of 2.7 from 3 based on the experimental studies. This effect has been evaluated and is limited for the stress ratio, R = $\sigma_{min}/\sigma_{max}$= 0.5 [5]. The use of this shifted curve does not help to account for the actual residual stress present in the specific weld structure being analyzed.

2.3 The Hot Spot Stress Method

The nominal stress concept is easier to use in the case of a simple weld joint but it is not practical to determine nominal stress and then select one of the design S-N curves for the analyzed complex welded joint. Moreover, by nature the fatigue process is a local phenomenon and cannot be fully described by nominal (global) stress. Another method called as hot spot stress method was developed, which accounts for macro geometric effects such as the shape and size of welds. Structural or hot spot or geometric stress, are all the synonyms referring basically to the same approach. The fatigue design philosophy for the welded components, based on the hot spot stress concept, was introduced first in the design guidelines for tubular joints in the offshore structures [13,14]. The size of the tubular components used in offshore industry made it difficult to determine the fatigue behavior and strength experimentally. With the introduction of the finite element method (FEM), the structural stress variant which was developed for the tubular connections in steel constructions (roofs, bridges, off-shore structures) gained importance and led to the hot spot structural stress concept as a codified procedure of fatigue assessment [15]. As per this approach, fatigue strength is mainly affected by the normal stresses perpendicular to the weld length, so accordingly the structural stress concept basically estimates the fatigue life under loading in this direction. The hot-spot stress concept is based on the stress values closer to the weld toe, which includes the stress concentration effect of the welded joint, but excludes the local notch effect of the weld (toe) itself. This stress is then used in combination with appropriate S-N curve, determined experimentally, representing the notch effect of the weld toe. The hot spot stress approach accounts for the dimensional variations within particular structural detail eliminating one of the major limitation with the nominal stress approach. This approach is really useful when nominal stress cannot be defined easily and structural discontinuity cannot be compared with any classified details in included design. However the variation in local geometry of the weld toe is still one of the main reasons for scatter in the fatigue test results. A major challenge in using this approach is to define and estimate the structural hot spot stress and then select the appropriate hot spot stress design S-N curve.

The conventional approach to estimate the structural hot-spot stress is the linear or quadratic extrapolation of strains measured at two or three reference points ahead of the

weld toe. As per the recommendations from International Institute of Welding (IIW), distances of the reference points from the weld toe of 0.4t/1.0t (Figure 2-2) or 0.4t/0.9t/1.4t are used as a common practice, where t is the plate thickness. An underlying assumption is that the local stress increase due to the notch at the weld toe disappears within 0.4t. At the plate edges, quadratic extrapolation over reference points at the fixed distances from the weld toe (4/8/12 mm) has been recommended as plate thickness is not considered a suitable parameter to define reference points at the plate edges.

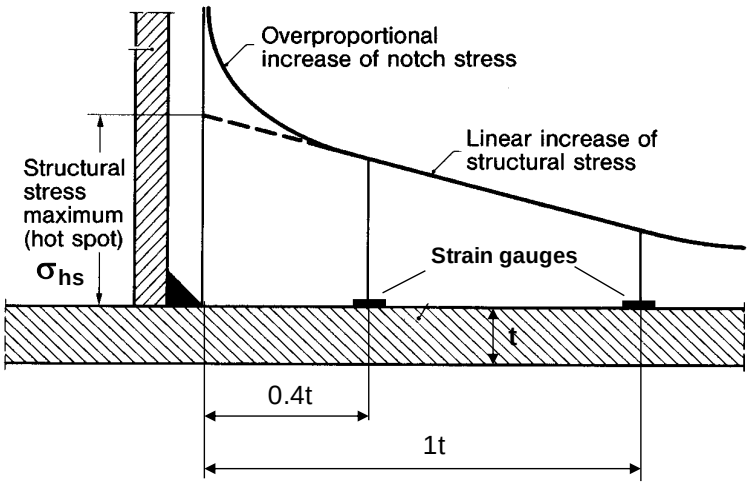

Figure 2-2: Experimental definition and determination of the hot spot stress

Due to the complex nature and large size of welded structures, it is needed to utilize FEA tools to determine the required stress-strain quantities for fatigue life analysis. In the commercial-vehicle sector the fatigue resistance, by contrast, is often verified experimentally. However, there is still a need for computer-aided methods, particularly when it is necessary to assess the fatigue lives for very short production runs or special design solutions. Moreover, even the development of series-production parts gives rise to a number of different design versions, and it is not possible to investigate the fatigue behavior of all of them experimentally. Therefore it is necessary to predict the fatigue lives using the accurate stress data. However the determination of stress data for the fatigue analyses requires solving complex boundary problems using the Finite Element method. The Finite Element Analysis (FEA) was developed in 1950's. Later it was applied to solving the stress analysis problems. By the early 70's, FEA was limited to expensive mainframe computers owned by the aeronautics, automotive, defense, and

nuclear industries. Since the rapid decline in the cost of computers and the phenomenal increase in the computing power, the FEA method has become a very popular and high precision daily engineering tool. The FE method helps designers to predict the stress and fatigue life of a component or structure by modeling the effects of cyclic loading on the behavior of material structures. Such an analysis can reveal the areas where the crack initiation and propagation is most likely to occur. Unfortunately the FE stress analysis results can be affected by the finite element meshing and the element properties. Some recommendations concerning the finite element modeling and evaluation of the hot spot stress are given by Huther [16] and Fricke [4]. These recommendations are based on the extensive round-robin stress analyses of various welded structures. Niemi and Tanskanen [17] as well as Fricke and Bogdan [18] have also developed some procedures for the hot spot stress evaluation.

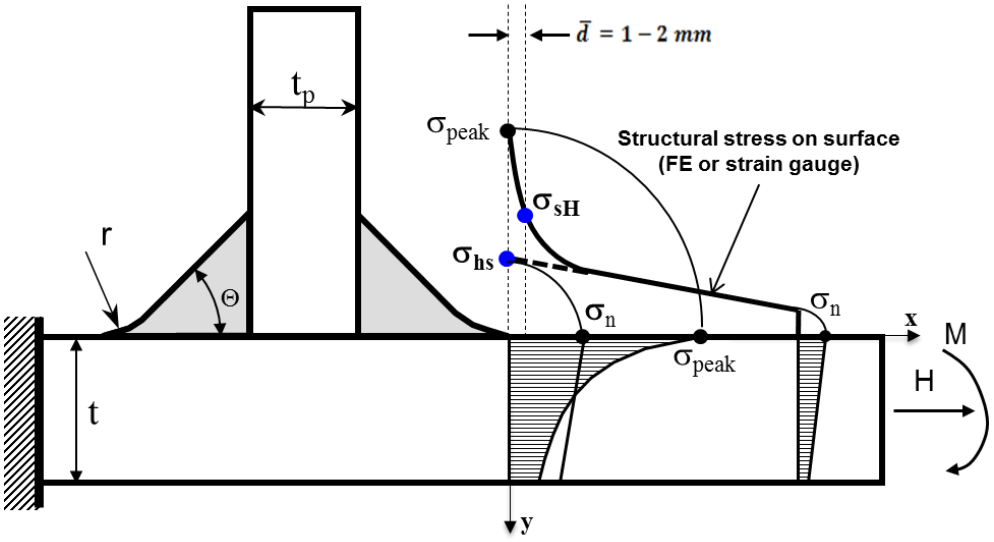

Figure 2-3: Haibach's procedure to calculate hot spot structural stress (σ_{sH}) based on strain at distance $\bar{d}$ from the weld toe and its comparison to the codified procedure of linear extrapolation (σ_{hs})

Several variations to this approach have been developed mainly focused on different methods to estimate the hot spot structural stress. Peterson, Manson and Haibach proposed a method to estimate the structural stress range $\Delta\sigma_{hs}$, by measuring the stress or strain at a certain distance away from the weld toe during 1960 [19]. Haibach proposed to obtain the hot spot structural stress (σ_{sH}) based on strain at distance $\bar{d}$ from the weld toe,

its comparison to hot spot structural stress (σ_{hs}) obtained using method of linear extrapolation is shown in Figure 2-3. Detailed case studies and recommendations for estimation of the hot spot stresses had been presented by Maddox [20,21] and Niemi [22]. These case studies showed that the results obtained from the stress analysis are strongly dependent on the finite element mesh and the element properties.

Modified structural stress approach was proposed by Dong [23,24] by building upon structural stress definition by Radaj [25] to evaluate the structural hot spot stress at the weld toe directly from the finite element results by using the principles of elementary structural mechanics. This method was demonstrated on several examples of 2D simple welded joints and is claimed to be a mesh-insensitive approach. However it has few limitations such as the joint misalignment is not taken into account in the structural stress. This means that the effect of misalignment has been included in the master S–N curve to the extent misalignment was present in the test specimens. This approach fails at in-plane notches such as the welded edge gussets, where plate thickness is no more a relevant parameter for defining the reference points needed for the stress estimation and does not have provision to account for the actual residual stress [26].

Xiao and Yamada [27] proposed unconventional structural stress concept which considers the structural stress estimated at 1mm depth below the weld toe (on the expected crack path) as the relevant fatigue parameter. Structural stress 1mm in depth takes the thickness or size effect directly into account, in contrast to the stress in a depth chosen in proportion to the thickness of the plate. Noh et al. [28] demonstrated that the fatigue lives determined in fatigue tests and plotted against the structural stress 1mm in depth below the weld toe result in a sufficiently narrow scatter band whose lower bound meets the design S–N curve JSSC-D in the Japanese design code, which corresponds to the curve FAT 100 in the IIW recommendations.

Poutiainen and Marquis [29] proposed another modified structural stress method based on the multi-linear stress distribution consideration through the plate thickness and the stress concentration factor K_{sa}. This method basically extends the structural stress method by modifying linear structural stress with the normal stress distribution in the weld throat plane σ_{weld} as shown by the stress distribution (A) in Figure 3-1. The proposed method

has not considered the stress distributions for partial or full-penetration welds. Another limitation, it does not consider the case when the welded attachment itself is loaded.

The main drawbacks of the hot spot stress method are, the limitation to surface crack failures (as only the surface stress is considered) and the uncertainty of extrapolation procedure. The designer should be very careful in designing the joint and making sure that the weld joint will not fail from the root or the internal defects as this method is not suitable for the weld root failures analysis. Although many recommendations have been made, the extrapolation procedures available to date still lack consistency for general applications. The results are often questionable due to the fact that these stresses can be strongly dependent on the mesh-size and the loading modes [17]. For gusset joints with hot spots at the edge, width plays major role rather than thickness on the geometric effect, as the stress distribution approaching the weld toe does not depend on thickness. In this type of hot spot, structural stress distribution due to the gusset geometry and the weld fillet are both non-linear and they occur in the same plane. Consequently, it is not easy to distinguish between the local effect of weld toe geometry and the effect of the structural discontinuity in such details. A special problem is related to structural distortions caused by the fabrication process such as axial and angular misalignments, are difficult to account for using this approach [30].

Welds of different types (butt or fillet) or with different geometries may have different fatigue strengths even though the structural stress is the same. This approach makes no distinction between the effects of membrane and the shell bending components on the crack propagation life. This approach does not provide enough clarity on how to account for the residual stress as present in structure being analyzed. Hot spot stress design S-N curves (expressed as fatigue class, FAT number), include the effect of high tensile residual stresses as present in tested samples, but any beneficial effect of lowering the residual stresses arising from stress relaxation procedures cannot be accounted for.

2.4 The Effective Notch Stress Method

This approach uses the linear elastic effective notch stress range $\Delta\sigma_{ENS}$ as an estimation parameter. Radaj [25] proposed that local stress can be evaluated directly without the need of stress concentration factor (SCF) or fatigue notch factor, based on Neuber's

micro-structural support hypothesis by suggesting an additional fictitious notch radius, ρ_f. He proposed to use $\rho_f = 1$mm for steel considering worst-case conditions (assuming a sharp notch exist at the weld toe) along with underline assumption of the plane strain condition at the notch and the von-mises strength criterion for the ductile material.

Fatigue effective notch stress (ENS) depends on the notch root radius, which is fictitiously enlarged

$$\rho_f = \rho + s\rho^* \quad (2.1)$$

Where ρ is the actual notch radius, ρ^* is the microstructural support length of the material, and s is a factor depending on the multiaxiality of the notch stress state and the applied strength hypothesis. A worst case fatigue analysis is based on $\rho = 0$ which results into $\rho_f = 1$mm for mild steels welds.

As per the ENS method, an irregular notch at the weld toe can be replaced by an effective one with a radius of 1mm. The fatigue assessment is then done by the use of a single universal Wohler S–N curve. The resistance Wohler S–N curves of FAT225 and FAT72 have been recommended for steel and aluminum respectively based on the large set of fatigue test experiments. As the notch stress accounts for the weld micro features, the conversion of K_t to K_f is implicitly included and no special procedure is required.

The elastic notch stress concept was originally restricted to the high-cycle fatigue range [31,32]. However later, notch stress concept was also extended for application in the medium-cycle and low-cycle fatigue range as per IIW recommendations. As originally proposed, uniform reference notch radius $\rho_f = 1$mm at sharp weld notches (sheet thickness t≥5mm) combined with the design S–N curve FAT 225 (steel weld joints) can result in non-conservative results in case of mild weld notches. IIW recommendations restricted the applicability of the S–N curve FAT 225 by prescribing a minimum fatigue notch factor, K_w=1.6, at the weld toe or root and by proving additionally that the parent material outside the weld notch provides a sufficient fatigue strength with respect to the structural stress at that location [15]. Considering low fatigue lives or high local stress levels, the design S–N curve FAT 225 must be limited by FAT 160 x K_w (with $K_w \geq 1.6$), Figure 2-4. The limitation is given by transformation of the curve FAT 160 relating to the

parent material in the local system. For this, the weld notch factor K_w of the weld under consideration has to be derived as the ratio of the maximum effective notch stress σ_{ENS} for $\rho_f = 1$ mm to the relevant hot spot structural stress σ_{hs} . The described procedure corresponds to performing two assessments independently and using the less conservative result: weld notch stress (according to $K_w \geq 1.6$) compared with the curve FAT 225 and relevant structural stress outside the weld notch compared with the curve FAT 160.

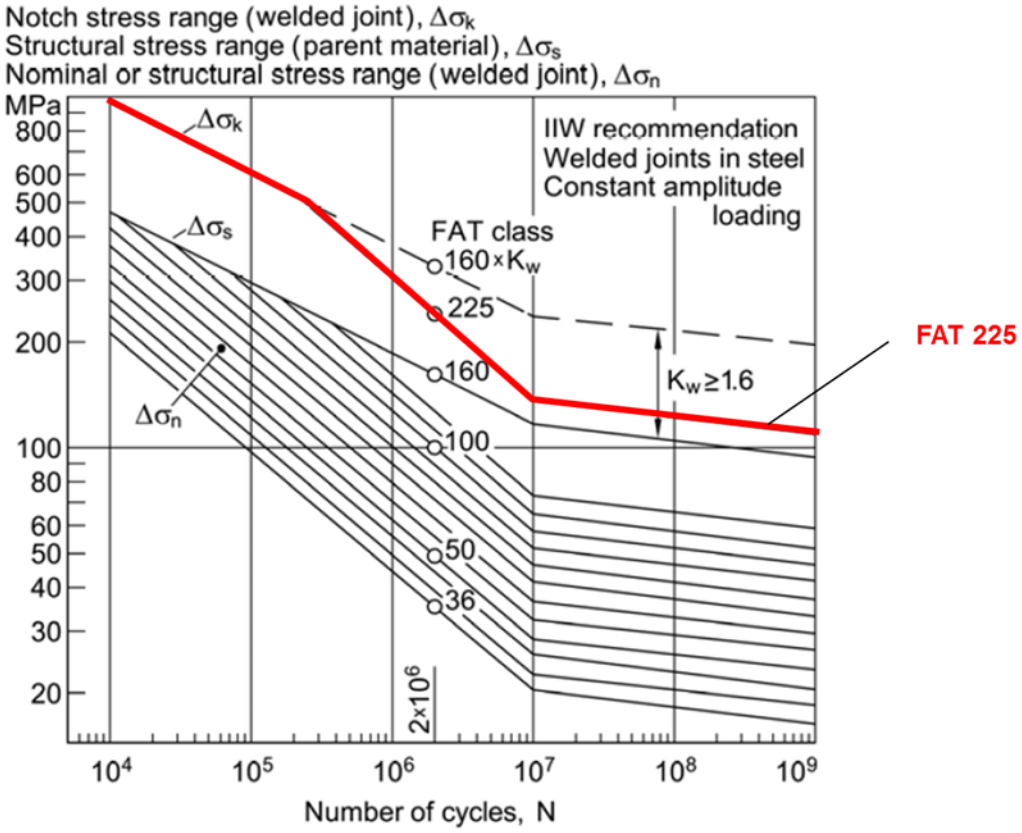

Figure 2-4: Limitation to the design S–N curve FAT 225 (relating to reference notch radius ρ_f =1mm by FAT 160 x K_w with weld notch factor $K_w \geq 1.6$; according to the IIW recommendations [15]

Benefits of the ENS approach lies in the fact that many of the variables which cannot be accounted for in other approaches can be considered here such as the weld quality specifically the weld profile (leg lengths), weld toe angle, shape and size of undercuts and the effects of multi-axial loading. In addition, this approach helps to optimize the geometry of fillet-welded joints with respect to the fatigue as the most geometrical influence factors can be taken into account. This approach has also been recommended

for weld root assessment. One of the major limitations with this approach is that estimation of effective notch stress requires large size fine mesh FE models, which are computationally very expensive [33] hence the approach is limited to 2D FE models. Other limitation is to account for the actual residual stress present in the weld joint.

2.5 The Local Strain Life Method

The local strain life method has the capability to account for the effects from macro as well as micro geometrical features. The notch or the local strain life approach uses elasto-plastic strain range $\Delta\epsilon_k$ as an estimation parameter. This method was initially developed for the non-welded components and was later extended to the weld joints as the weld toe usually has local plasticity. This concept is focused on crack initiation life whereas the nominal or the hot spot stress methods estimate the fatigue life to final fracture. The fatigue life expressed as numbers of load cycles comprises of the technical crack initiation life and the subsequent long-crack propagation life up to final fracture. The technical crack may be a surface crack, about 0.5 mm in depth and 2 mm in length. The technical crack initiation life comprises the microstructural crack initiation life and the short-crack propagation life up to the technical crack size. In the un-notched specimens, most of the total life may be consumed in microstructural crack initiation. In sharply notched specimens, on the other hand, the crack initiation life may be very short, but initiated cracks are arrested to some extent.

Langer [34] studied fatigue under variable amplitude loading and separated the fatigue life into the crack initiation and crack propagation phases and suggested a damage sum of 1.0 for both phases. He also wrote that the application of his hypothesis required determination of the fatigue curves analogous to the nominal stress-life curves. Neuber [35] investigated the notch effect on the monotonic and cyclic deformation of engineering materials. The idea that plastic strains were responsible for the fatigue damage was formulated by Coffin [36] and Manson [37]. Working independently on problems associated with fatigue, Coffin and Manson proposed an empirical relationship between the number of stress reversals to the fatigue failure and the plastic strain amplitude. This idea was promoted later by Topper [38] and Morrow [39] and, along with the development of Neuber's rule [40] and rainflow cycle counting method by Matsuishi and

Endo [41], form the basis for the current notch strain-life fatigue analysis. As an alternative to Neuber's rule, Glinka [42] proposed equivalent strain energy density (ESED) approach for estimating elasto-plastic stresses and strains (localized yielding) at the notches and cracks. For an elasto-plastic notch strain analysis, cyclic stress-strain curves are used which are determined from tests on small smooth specimens.

As per the strain life approach, the pseudo linear elastic stress range, $\Delta\sigma_{peak}$ along with the maximum stress value, $\sigma_{peak,max}$ at the weld toe is used for calculation of the actual stress, σ^{a}_{max} and the elastic-plastic strain, ε^{a}_{max} . Either the Neuber [40] or the ESED [43] rule can be used along with the Ramberg-Osgood material cyclic stress-strain curve to find these two unknowns. For the various notations in eqns. 2.1 to 2.11, refer Figure 2-5.

$$\frac{\left(\sigma_{\text{peak,max}}\right)^2}{\text{E}} = \sigma^{\text{a}}_{\text{max}}\varepsilon^{\text{a}}_{\text{max}} \quad - \text{The Neuber rule} \tag{2.2}$$

$$\varepsilon^{\text{a}}_{\text{max}} = \frac{\sigma^{\text{a}}_{\text{max}}}{\text{E}} + \left(\frac{\sigma^{\text{a}}_{\text{max}}}{\text{K}'}\right)^{\frac{1}{\text{n}'}}$$

$$- \text{The material Ramberg} - \text{Osgood stress strain curve} \tag{2.3}$$

The elasto-plastic strain range and the associated stress range are calculated in a similar manner with the difference that stress-strain curve is expanded by the factor of 2.

$$\frac{\left(\Delta\sigma_{\text{peak}}\right)^2}{\text{E}} = \Delta\sigma^{\text{a}}\Delta\varepsilon^{\text{a}} \quad - \text{The Neuber rule} \tag{2.4}$$

$$\Delta\varepsilon^{\text{a}} = \frac{\Delta\sigma^{\text{a}}}{\text{E}} + 2\left(\frac{\Delta\sigma^{\text{a}}}{2\text{K}'}\right)^{\frac{1}{\text{n}'}} \quad - \text{The expanded material stress strain curve} \tag{2.5}$$

The equivalent strain energy density (ESED) method provides more accurate calculation compared to the Neuber's rule especially when dealing with the geometries having high stress concentration factors where the Neuber's rule can overestimate these values.

$$\frac{\left(\sigma_{\text{peak,max}}\right)^2}{2\text{E}} = \frac{\left(\sigma^{\text{a}}_{\text{max}}\right)^2}{2\text{E}} + \frac{\sigma^{\text{a}}_{\text{max}}}{\text{n}' + 1}\left(\frac{\sigma^{\text{a}}_{\text{max}}}{\text{K}'}\right)^{\frac{1}{\text{n}'}} \quad - \text{The ESED rule} \tag{2.6}$$

$$\varepsilon^{\text{a}}_{\text{max}} = \frac{\sigma^{\text{a}}_{\text{max}}}{\text{E}} + \left(\frac{\sigma^{\text{a}}_{\text{max}}}{\text{K}'}\right)^{\frac{1}{\text{n}'}} - \text{Ramberg osgood material stress strain curve} \tag{2.7}$$

Similarly the elasto-plastic strain range and associated stress range are calculated with stress-strain curve expanded by the factor of 2.

$$\frac{\left(\Delta\sigma_{peak}\right)^2}{2E} = \frac{(\Delta\sigma^a)^2}{2E} + \frac{2.\Delta\sigma^a}{n' + 1}\left(\frac{\Delta\sigma^a}{2K'}\right)^{\frac{1}{n'}} \quad \text{The ESED rule} \tag{2.8}$$

$$\Delta\varepsilon^a = \frac{\Delta\sigma^a}{E} + 2\left(\frac{\Delta\sigma^a}{2K'}\right)^{\frac{1}{n'}} \quad -\text{The expanded material stress strain curve} \tag{2.9}$$

Next step is to calculate the number of cycles, Ni, needed to initiate the fatigue crack at the weld toe by using the Manson and Coffin [44] equation and stress parameters, σ_{max}^{a} and $\Delta\varepsilon^a$, actual maximum stress at the weld toe and the actual strain range respectively.

$$\frac{\Delta\varepsilon^a}{2} = \frac{\sigma_f'}{E}(2N_i)^b + \varepsilon_f'(2N_i)^c \tag{2.10}$$

The mean stress effect can be accounted for by incorporating the SWT [38] damage parameter along with the Manson-Coffin curve.

$$\sigma_{max}^{a}\frac{\Delta\varepsilon^a}{2} = \frac{(\sigma_f')^2}{E}(2N_i)^{2b} + \varepsilon_f'\sigma_f'(2N_i)^{b+c} \tag{2.11}$$

The strain life approach does not provide clarification on the crack size after subjecting the welded joint to N_i loading cycles. Literature suggests to use the initial crack size, a_i=0.5-0.8mm for a semi-elliptical crack for most of the engineering problems.

The procedure for predicting the fatigue crack initiation life is graphically shown in the Figure 2-5 and is summarized below:

1. Determine the external loads on the structure (Figure 2-5a).
2. Calculate the internal loads in the structure (Figure 2-5b).
3. Determine the critical points (Figure 2-5c) in the structure.
4. Calculate the peak stress at the critical points (Figure 2-5e).
5. Define the peak stress history (Figure 2-5f).
6. Determine the elasto-plastic stress-strain response at the critical points (Figure 2-5g).
7. Obtain the stress-strain hysteresis loops (Figure 2-5h).
8. Determine the fatigue damage and fatigue life (Figure 2-5i, j, k, l).

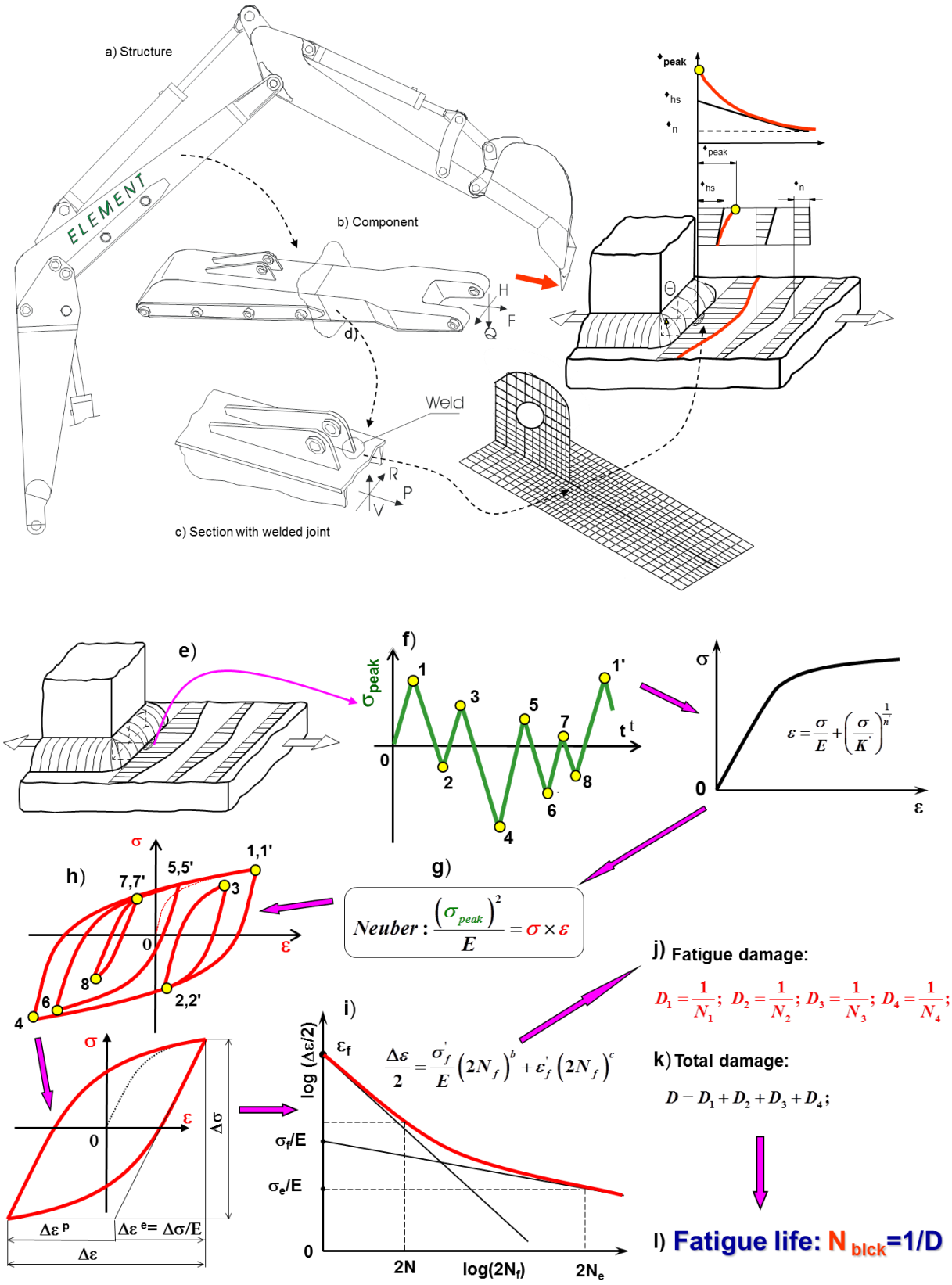

Figure 2-5: Steps in fatigue life prediction based on the strain-life approach [1]

2.5.1 Effect of residual stress on fatigue crack initiation life

The welding processes present a number of technical challenges to the designer, manufacturer, and end-user of the welded structures. The Gas Metal Arc Welding (GMAW) process is widely used especially for the joining of structural components in agricultural and construction industry. This process consists of heating, melting and solidification, of the parent metals and filler material in the localized fusion zone, by a transient heat source to form a joint between the parent metals. The heat source causes highly non-uniform temperature distributions across the joint and the parent metals. The complex thermal cycles from welding result in the formation of residual stresses in the joint region and distortion of the welded structure. Both the weld residual stress and the distortion can significantly impair the performance and reliability of the welded structures. For example, not including residual stress in the engineering stage could significantly reduce the fatigue life of a component, which is one of the dominant modes of failures of the welded structures. From the manufacturing perspective, meeting the design tolerance, quality issues and fixture design becomes a major issue, which is generally designed through heuristic methods and experimental trials.

In the current industrial practice, welding processes are developed largely based on the experiments incorporating an engineer's knowledge and experience of the previous similar designs. Simulation tools based on finite element (FE) method are very useful to predict welding distortions and residual stresses at the early stage of product design and welding process development. However, the complexity of welding processes and the complex geometry of real engineering components have made the prediction of welding distortions and residual stresses a very difficult task. Literature review of the various available welding process simulation models is covered in [45], a paper presented from this research work. A common drawback of many of these codes is that they do not have the capability to handle complex geometry from real structures and also they do not capture the micro structural transformations and their effects during welding.

Residual stresses in a component or structure are caused by incompatible internal permanent strains. They may be generated or modified at every stage of the component life. Welding is one of the most frequent causes of residual stresses and typically

produces large tensile stresses near welds whose maximum value is approximately equal to the yield strength of the base material.

The residual stress cannot be added linearly to the actual stress at the notch tip. However for the fatigue crack initiation analysis, the residual stress effect can be accounted for by adding it to the pseudo-elastic stress in the Neuber's formula (Figure 2-6).

$$\frac{(K_t S + \sigma_r)^2}{E} = \sigma_2 \epsilon_2 \tag{2.12}$$

Where: σ_r is the residual stress

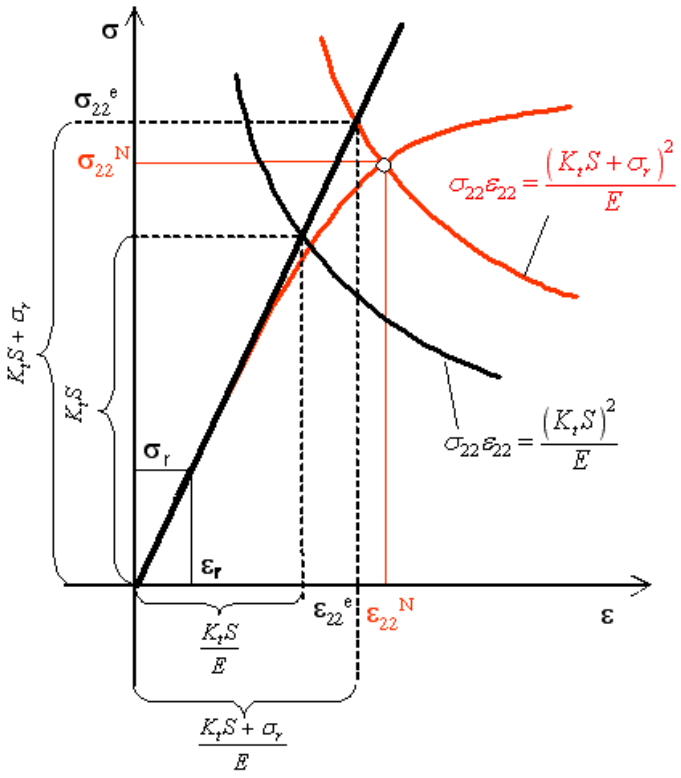

Figure 2-6: Neuber's rule in the presence of residual stresses

The effect of the residual stress on the first reversal is shown in Figure 2-6. The residual stress causes the increase of the stress and strain induced by the first reversal (the set-up cycle). Since the notch stress-strain response must lie on the stress-strain curve and Neuber's hyperbola, the intersection of these two curves provides the actual values for the stress and strain. It should be noted that this point will be used as an origin of the new coordinate system for calculating the stress and strain induced by the next reversal.

The effect of the tensile and compressive residual stress on the resultant notch tip stress-strain response induced by the same cyclic load is shown in Figure 2-7. If the direction of the residual stress and the first stress reversal induced by the applied load are different, the effect of residual stress is more visible than in cases where the residual stress and the applied stress are the same nature, i.e. both are tensile or compressive.

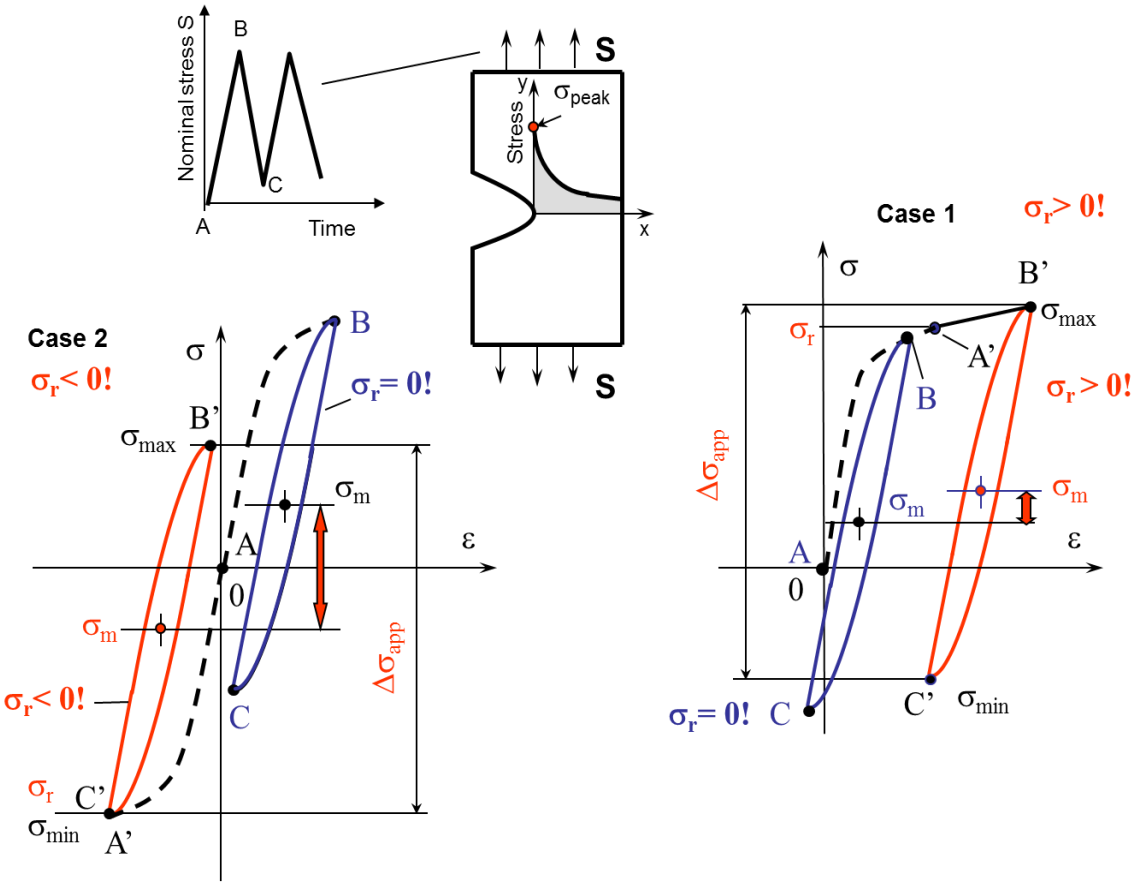

Figure 2-7: Residual stress effect on the stress-strain response at the notch tip, B'C'- stress cycle corrected for the residual stress effect, BC- stress cycle without residual stress effect (see the difference in the change of the mean stress)

2.6 The Fracture Mechanics Method

The Fracture Mechanics approach to the fatigue life prediction or the da/dN- ΔK method is a technique based on the analysis of fatigue crack propagation. The combination of the load/stress and the geometry is represented by the stress intensity factor (SIF), K, in the case of monotonic load. The range of the stress intensity factor, ΔK, is used in the case of

cyclic loading. The stress intensity factor range, ΔK, is the most important parameter governing the fatigue crack growth. Progress in the fracture mechanics came with the pioneering studies of Irwin [46]. He introduced the stress intensity factor, K, and pointed out its importance in determination of the static strength of cracked bodies. Irwin has stated that when the stress intensity factor, K, reaches a certain critical magnitude exceeding the "fracture toughness" of the material, instant fast fracture occurs. Paris showed that the fatigue crack growth rate, da/dN, could also be described by using the stress intensity factor range ΔK. The Paris equation [47] is used up to day, although it does not account for the mean stress effect on the fatigue crack propagation. In 1970's, Paris [48,49] demonstrated that a threshold stress intensity factor exists below which the fatigue cracks would not grow. Elber [50] demonstrated the importance of the crack tip closure on the fatigue crack growth. He developed a qualitative model showing that the fatigue crack growth was controlled by the effective stress intensity factor rather than by the applied stress intensity factor range. The crack closure model is commonly used in the current fatigue crack growth analysis. The history of the crack propagation approach for the fatigue assessment has been compiled by Paris in [51].

The fracture mechanics approach assumes an existing initial crack whereas the local strain life approach calculates the crack initiation life. So, it estimates the crack propagation life from an initial crack size to certain final size (critical crack size, which if exceeded will cause final brittle fracture). IIW recommended using initial crack size of a_i=0.15mm for a conservative fatigue life estimation. Later, some publications suggested a_f=0.5mm for the mechanical engineering applications, however there is no general accepted size as it would probably vary depending on the material, the loading conditions and the inspection capabilities. This approach also helps to determine the crack size and shape. Thus it is an important approach for setting expectations on the material toughness specifications, fabrication tolerances, quality assurance requirements, level of inspection and its frequency. Application of this approach has been successfully demonstrated through various case studies such as evaluating the effect of special geometrical influence factors on the fatigue life, e.g. the effects of a longitudinal attachment, the effects of misalignment for the load-carrying cruciform joints [52] and the effects of undercuts and the residual stresses at misaligned butt-joints [53].

In the case of welded structures with high stress concentrations (sharp fillets at the weld toe) the fatigue crack initiation portion of the fatigue life could be relatively small and could take relatively large number of cycles to propagate the crack before final fracture occurs. Depending on the geometry, load configuration or other factors, relative proportions of the crack initiation and propagation life could vary significantly. This emphasizes that there is need to estimate the crack propagation portion of the fatigue life accurately as well. The simplest fatigue crack growth relation is that one proposed by Paris [54].

$$\frac{da}{dN} = C(\Delta K)^m \tag{2.13}$$

To account for the effect of stress ratio, R during crack propagation, several expressions of the crack growth relation have been proposed e.g. by Walker [55] , Forman [56] and Kujawski [57].

Noroozi et al. [58,59] proposed the following relation to account for the effect of the mean stress or the stress ratio R:

$$\frac{da}{dN} = C\,[(K_{max})^p\,(\Delta K)^{1-p}]^\gamma \tag{2.14}$$

Where: C, p, m and γ are the material constants; K_{max} represents the maximum stress intensity factor and accordingly $\Delta K = K_{max} - K_{min}$ represents the stress intensity factor range. The fatigue crack propagation life N_p can then be calculated by analytical or numerical integration as below.

$$N_p = \int_{a_i}^{a_f} \frac{da}{C(\Delta K)^m} \quad \text{or} \quad N_p = \int_{a_i}^{a_f} \frac{da}{C\left(K_{max}^p \Delta K^{1-p}\right)^\gamma} \tag{2.15}$$

For the structural applications, most of the welded structures are complex in terms of the load and geometrical configurations, so it is not possible to find the stress intensity factors from the handbooks. To estimate the stress intensity factors for the cracks in complex weld joints, the weight function technique [60] has been recommended and the same has been utilized in this work.

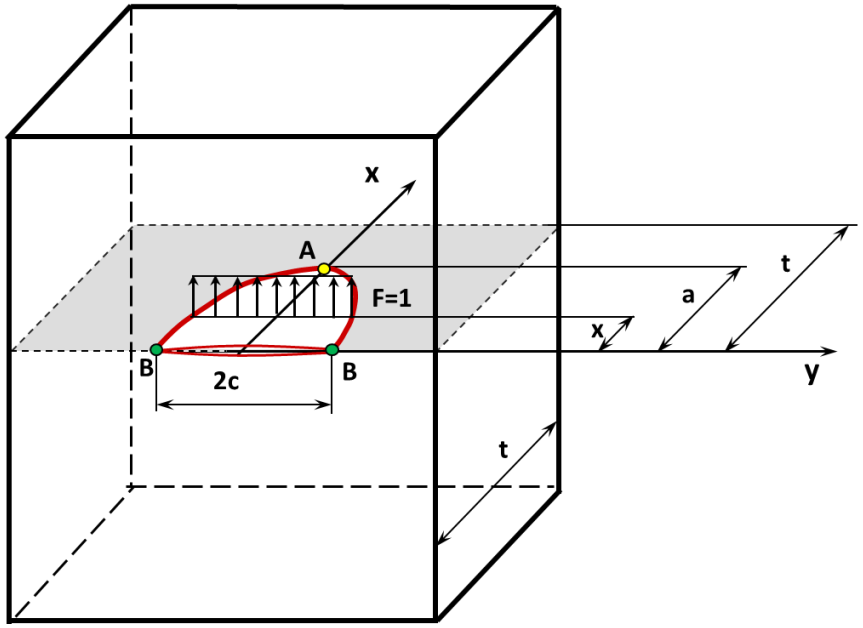

Figure 2-8: Weight function notation for a semi-elliptical crack in finite thickness plate

The weight functions (2.16) and (2.17) and the stress intensity factors for a semi-elliptical surface crack can be calculated at both points A (the deepest point in the crack) and point B (the surface tip point) as shown in Figure 2-8.

$$m_A(x,a) = \frac{2F}{\sqrt{2\pi(a-x)}}\left\{1 + M_{1A}\left(1-\frac{x}{a}\right)^{\frac{1}{2}} + M_{2A}\left(1-\frac{x}{a}\right) + M_{3A}\left(1-\frac{x}{a}\right)^{\frac{3}{2}}\right\} \quad (2.16)$$

$$m_B(x,a) = \frac{2F}{\sqrt{\pi x}}\left\{1 + M_{1B}\left(\frac{x}{a}\right)^{\frac{1}{2}} + M_{2B}\left(\frac{x}{a}\right)^{1} + M_{3B}\left(\frac{x}{a}\right)^{\frac{3}{2}}\right\} \quad (2.17)$$

Parameters M_{1A}, M_{2A}, M_{3A}, M_{1B}, M_{2B} and M_{3B} are given in the Appendix A.

Once the weight function is known, the stress intensity factor K can be calculated by integrating the product of the stress distribution $\sigma(x)$ in the prospective crack plane and the appropriate weight function $m(x,a)$, see Figure 2-9.

$$K_A = \int_0^a \sigma(x)\, m_A(x,a)\,dx \quad \text{at point A} \quad (2.18)$$

$$K_B = \int_0^a \sigma(x)\, m_B(x,a)\,dx \quad \text{at point B} \quad (2.19)$$

Thus, the calculation of the stress intensity factors by the weight function method requires the knowledge of the stress distribution, $\sigma(x)$, in the prospective crack plane in the un-cracked body (Figure 2-9). The biggest benefit in using the weight function technique lies in the fact that stress distribution, $\sigma(x)$, in the potential crack plane needs to be determined from one time analysis of the un-cracked FE model, which when combined with the weight functions helps to estimate the stress intensity factors for most of the weld joints, required for the fatigue crack growth analysis. This eliminates the need of modeling actual crack and time consuming and complex analysis necessary for the determination of SIFs.

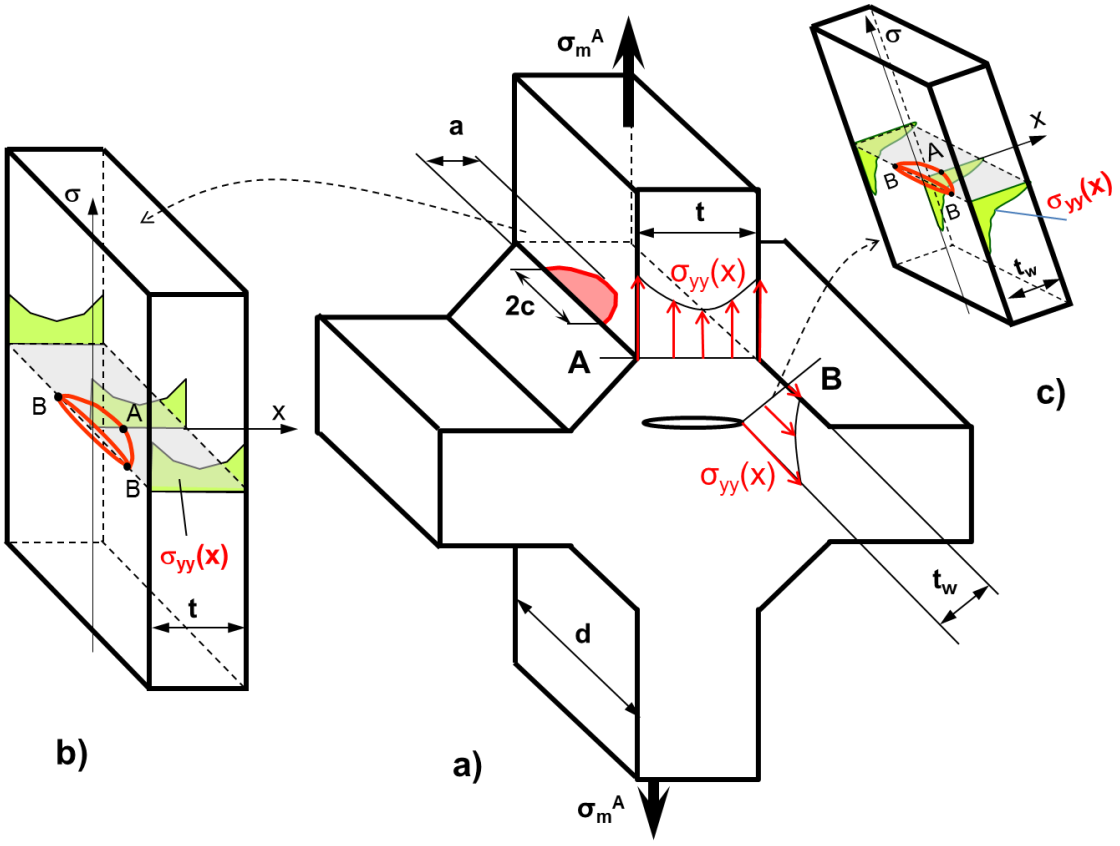

Figure 2-9: Critical locations in a cruciform weldment; a) general geometrical configurations of the joint, b) crack model for the failure from the toe (section A), c) crack model for the failure from the weld root (section B)

A cruciform joint is shown in the Figure 2-9 as an example. The through thickness stress distribution obtained from the un-cracked FE model is subsequently applied virtually to

the crack surfaces (Figure 2-9) and integrated together with the weight function. Finally the product of the stress distribution $\sigma(x)$ and the weight function $m(x,a)$ needs to be integrated over the entire crack surface area to estimate the stress intensity factors required for the crack growth analysis. The stress intensity factor calculations need be repeated after each crack increment induced by the subsequent load cycles so the stress intensity factor is calculated for the instantaneous (actual and varying) crack size and geometry. Such a method enables simultaneous simulation of both the crack growth and the crack shape evolution.

The procedure for predicting the fatigue crack propagation life is graphically shown in the Figure 2-10 and is summarized below:

1. Analysis of external loads on the structure and the component (Figure 2-10a),
2. Analysis of internal loads in a chosen cross section of the component (Figure 2-10b),
3. Selection of individual welded joints in the structure (Figure 2-10c),
4. Identification of appropriate nominal or reference stress history (Figure 2-10d),
5. Extraction of stress cycles (rainflow counting) or reversals from the stress history (Figure 2-10e),
6. Determination of the stress intensity factor (i.e. the factor Y) for postulated or existing crack, (Figure 2-10f):
    I. Indirect method:
        a) Analyze the un-cracked weldment and determine the stress field, $\sigma(x,y)$, in the prospective crack plane; normalize the calculated stress distribution with respect to the nominal or any other reference stress, i.e. $\sigma(x,y)/\sigma_n$,
        b) Choose appropriate weight function and calculate stress intensity factor
    II. Direct method:
        a) Determine the stress $\sigma(x,y)$ or displacement field $U(x,y)$near the crack, or the strain energy release rate (G),
        b) Calculate stress intensity factor using the same
7. Determination of crack increments for each stress cycle (Figure 2-10h),
8. Determination of the number of cycles, N, necessary to grow the crack from its initial size, a_i up to the final size, a_f.

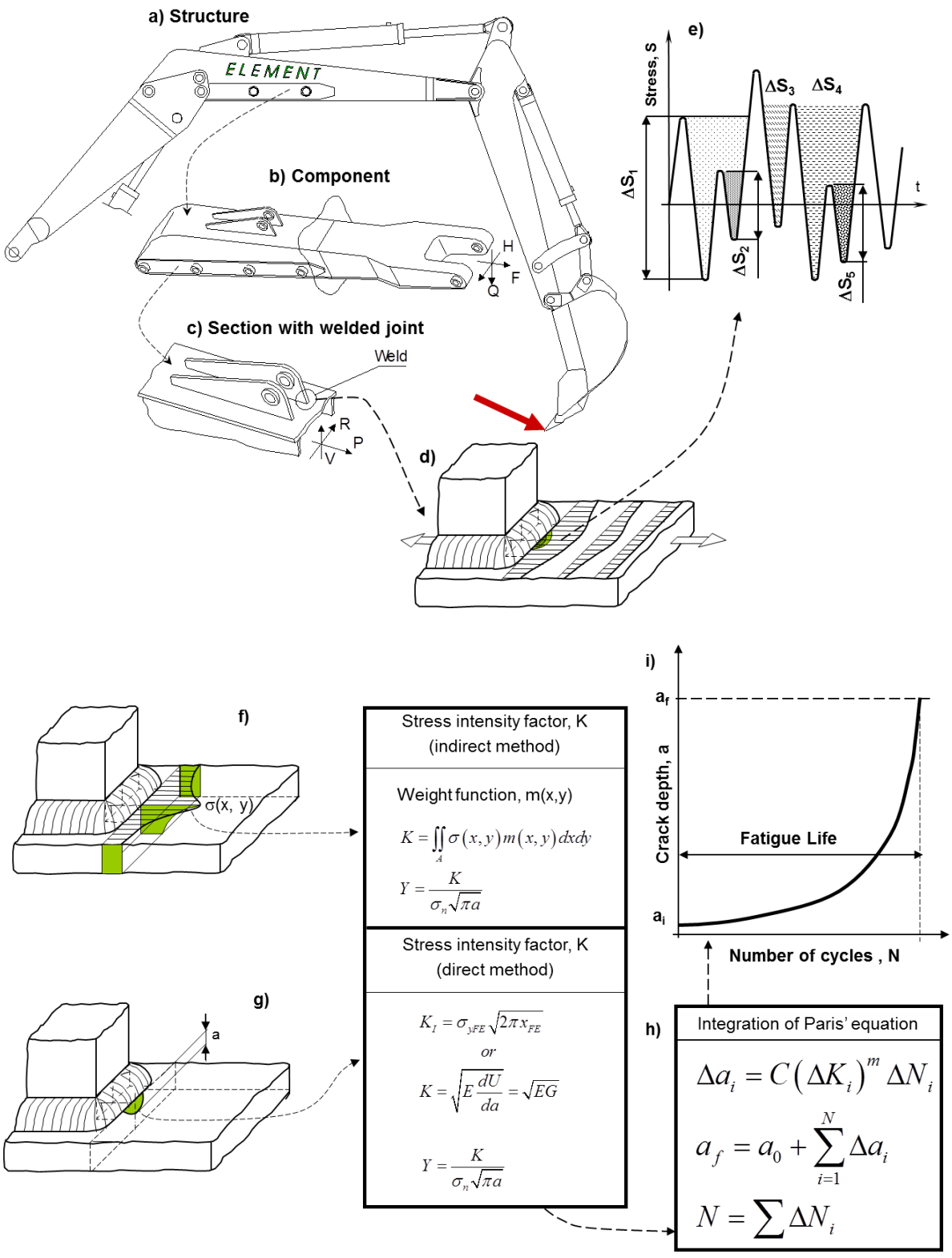

Figure 2-10: Steps in fatigue life prediction based on the da/dn-ΔK approach [1]

2.6.1 Effect of residual stress on fatigue crack propagation life

Machine and structural components may contain residual stresses. It has been found that the compressive residual stresses can be beneficial, while the tensile residual stresses can considerably reduce the fatigue life. For the fatigue crack propagation analysis, the effect of the residual stress is accounted for by considering its influence on the effective residual stress intensity factor resulting from the joint action of the load and the residual stress.

The effective stress intensity factor can be defined as:

$$\mathrm{K}^{\mathrm{eff}} = \mathrm{K}^{\mathrm{apl}} + \mathrm{K}^{\mathrm{res}} \tag{2.20}$$

Subsequently, the effective maximum and minimum stress intensity factors can be calculated as:

$$\mathrm{K}_{\mathrm{max}}^{\mathrm{eff}} = \mathrm{K}_{\mathrm{max}}^{\mathrm{apl}} + \mathrm{K}^{\mathrm{res}} \tag{2.21}$$

$$\mathrm{K}_{\mathrm{min}}^{\mathrm{eff}} = \mathrm{K}_{\mathrm{min}}^{\mathrm{apl}} + \mathrm{K}^{\mathrm{res}} \tag{2.22}$$

The equations above can be used to calculate the stress intensity factor range, $\Delta\mathrm{K}$, and the effective stress ratio, $\mathrm{R}^{\mathrm{eff}}$.

$$\Delta\mathrm{K} = \mathrm{K}_{\mathrm{max}}^{\mathrm{eff}} - \mathrm{K}_{\mathrm{min}}^{\mathrm{eff}} = \mathrm{K}_{\mathrm{max}}^{\mathrm{apl}} - \mathrm{K}_{\mathrm{min}}^{\mathrm{apl}} \tag{2.23}$$

$$\mathrm{R}^{\mathrm{eff}} = \frac{\mathrm{K}_{\mathrm{min}}^{\mathrm{eff}}}{\mathrm{K}_{\mathrm{max}}^{\mathrm{eff}}} = \frac{\mathrm{K}_{\mathrm{min}}^{\mathrm{apl}} + \mathrm{K}^{\mathrm{res}}}{\mathrm{K}_{\mathrm{max}}^{\mathrm{apl}} + \mathrm{K}^{\mathrm{res}}} \tag{2.24}$$

The simple superposition of the applied and residual stress intensity factors (eqns. 2.21 and 2.22) leads to the stress intensity factor range not affected by the presence of the residual stress. However, this is not entirely true because the effective stress intensity factor range does depend on the effective stress ratio, R^{eff}. The crack closure model is most often used to determine the effective stress intensity factor range, ΔK^{eff} . The simplest variation of the crack tip closure model is the empirical one proposed by Kurihara [61].

Kurihara [61] suggested the following expression to calculate the effective stress intensity factor range depending on the effective stress ratio, R^{eff}.

$$\Delta K^{eff} = U\Delta K = U\left(K_{max}^{apl} - K_{min}^{apl}\right) \quad (2.25)$$

Where:

$$\begin{cases} U = \dfrac{1}{1.5 - R^{eff}} & \text{for} -5 \leq R^{eff} \leq 0.5 \\ U = 1 & \text{for } R^{eff} > 0.5 \end{cases} \quad (2.26)$$

In effect both the stress ratio and the stress intensity factor range are influenced by the presence of residual stresses. Therefore, the effective stress intensity factor range ΔK^{eff} is subsequently entered into the Paris equation (eqn. 2.13) for the fatigue crack growth analysis.

The stress intensity factors, K_{max}^{eff} and K_{min}^{eff}, can be calculated with the help of appropriate weight function providing that the residual stress and the applied stress distributions in the prospective crack plane are known.

Total fatigue life can then be calculated as sum of the fatigue crack initiation life (eqn. 2.11) and the fatigue crack propagation life (eqn. 2.15).

2.7 Geometrical, load and material factors influencing fatigue life

Thickness of geometry (plate thickness) has significant effect on the fatigue life. Thickness correction factors have been recommended for nominal and hot spot structural stress approaches. Local concepts such as the local strain life method and the fracture mechanics method do not require any such correction as the effect of thickness is implicitly included.

Misalignment in axially loaded joints leads to an increase of stress in the welded joint due to the occurrence of secondary shell bending stresses. The resulting stress is calculated by stress analysis or by using the formulae for the stress magnification factor. It has been proved in the literature that misalignment is a very important factor in fatigue. Misalignment in weld joints could result into significant increase of stress levels e.g. 30% increase in butt joints and 45% increase in the cruciform joints as reported in [5]. Not only the misalignment can increase the level of stress, but it can also change the location of failure as demonstrated in Chapter 6.

Residual stress can play significant role on the fatigue life of welded joints as also mentioned in sections 2.5.1 and 2.6.1. In the nominal or structural stress approach residual stress effect is included by the fatigue resistance of the given FAT values, as FAT values are determined from representative welded samples already containing residual stresses. So the S-N curves are supposed to have built-in effect of residual stress. Local concepts require that the residual stress be determined and accounted for life estimation. Today, many techniques are available such as grinding, annealing, shot peening, TIG dressing, laser peening, ultrasonic peening etc. which help to change the residual stress state from tensile to compressive along with reducing the stress concentration factor at the weld toe. If any of these techniques are used, literature recommends using a bonus factor on the fatigue resistance values. IIW has recommended improvement factors for grinding, TIG dressing, hammer and needle peening. However these factors only provide a minimum value of the improvement effect. There are other challenges though e.g. the difficulty in estimation of the accurate residual stresses, as there are many parameters affecting the residual stresses such as the welding sequence, the process parameters and the welding fixture constraints. The prediction of residual stress needs to be improved in order to make fatigue assessments more accurate [5]. Once the residual stresses are known, an appropriate procedure needs to be applied in order to account their effect correctly for fatigue life assessment. Accurate estimation of residual stress, their possible relaxation in the process zone and method to account them plays an important role otherwise it can lead to considerable errors in predicted life [62].

Weld toe geometry such as the weld toe radius and angle, is responsible for the stress concentration at the weld toe and hence is an important factor towards estimation of the fatigue life. Important factors like inhomogeneous material, residual stresses, exact geometrical characteristics (weld toe radius, angle) are either not considered or assumed approximately as per available approaches [32]. Most of the weld fatigue life assessment methods rely either on S-N curves determined from experimental test (real weld toe geometry for joint under consideration can be different than experimental samples used for generating S-N curves) or use fictitious weld toe radius (1mm as per notch stress concept). Depending on the joint type and the manufacturing practices, there could be large variation in weld toe geometry, accounting for which is required to accurately

estimate the fatigue life of weld joints. Any change of micro weld features caused by life improvement methods such as grinding or peening etc. needs to be captured and accounted for accordingly.

High strength steels are characterized by a longer crack initiation period. The earliest numerical investigation on the local approach for welded joints was performed by Lawrence [63]. Residual stresses even play increased role in the case of high strength steels. Residual stresses which reach the yield limit substantially change the fatigue strength especially of higher-strength steels, increasing it in the case of compressive stresses and lowering it in the case of tensile stresses. Many of the fatigue life prediction methods do not consider the difference between mild steel and high strength steel from the fatigue life analysis prospective. The same FAT class is recommended for any type of steel. There are definitely some advantages in using higher strength steels over mild steel in terms of fatigue. Better design consideration e.g. locating the weld joint in the lower stress areas helps to retain some advantages of higher strength steels enhancing the fatigue life for the weld joints. Better methods to capture the benefits in fatigue life from the use of high strength steel are needed.

Chapter 3 The Proposed Methodology

3.1 Stress distribution in weld joints

Typical stress distributions in a weld joint are as shown in Figure 3-1. The stress distributions shown in this figure represent the following:

- Normal stress distribution in the weld throat plane (A),
- Through the thickness normal stress distribution in the weld toe plane (B),
- Through the thickness normal stress distribution away from the weld (C),
- Normal stress distribution along the surface of the plate (D),
- Shear stress distribution in the weld throat plane (E),
- Linearized normal stress distribution in the weld toe plane (F).

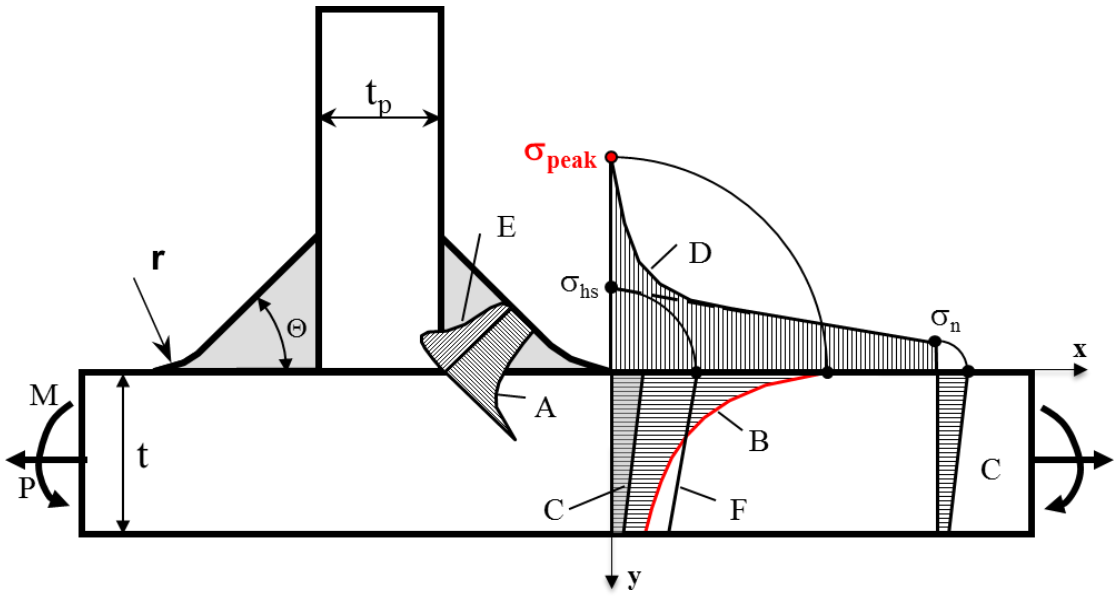

Figure 3-1: Various stress field distributions in a T-joint with transverse fillet welds

The stress distribution C is obtained from the axial load P and the bending moment M (Figure 3-1) by using the simple membrane and bending formulae such as eqns. (3.1) and (3.2).

$$\sigma_m = \frac{P}{t\,L} \tag{3.1}$$

Where: t – plate thickness, L-plate width, P- axial force.

$$\sigma_b = \frac{M\,c}{I} \qquad (3.2)$$

Where: M-bending moment, c-distance from the neutral axis, I-moment of inertia of the critical cross section

However a more realistic non-linear stress field in a complete welded structure is practically impossible to obtain using analytical analysis, therefore the finite element method is found to be more convenient. An additional challenge, to find out all the necessary details of the various stress fields as those shown in Figure 3-1, is that accurate geometrical and FE modeling techniques of welded structures are required.

The stress state at the weld toe is multi-axial in nature. But the plate surface is usually free of stresses, and therefore the stress state at the weld toe in general reduces to one non-zero shear and two in-plane normal stress components (Figure 3-2). Due to stress concentration at the weld toe the stress component σ_{xx} normal to the weld toe line is largest in magnitude and it is predominantly responsible for the fatigue damage accumulation in this region. Therefore for the fatigue analysis of welded joints, it is sufficient in practice to consider only the stress component σ_{xx} i.e. its magnitude and distribution across the plate thickness as shown in Figure 3-2.

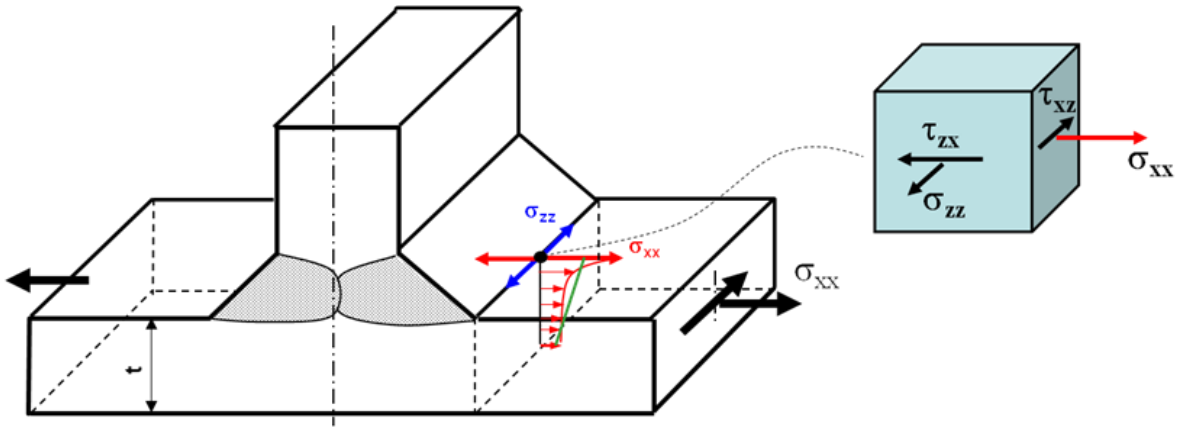

Figure 3-2: Multiaxial stress state at the weld toe

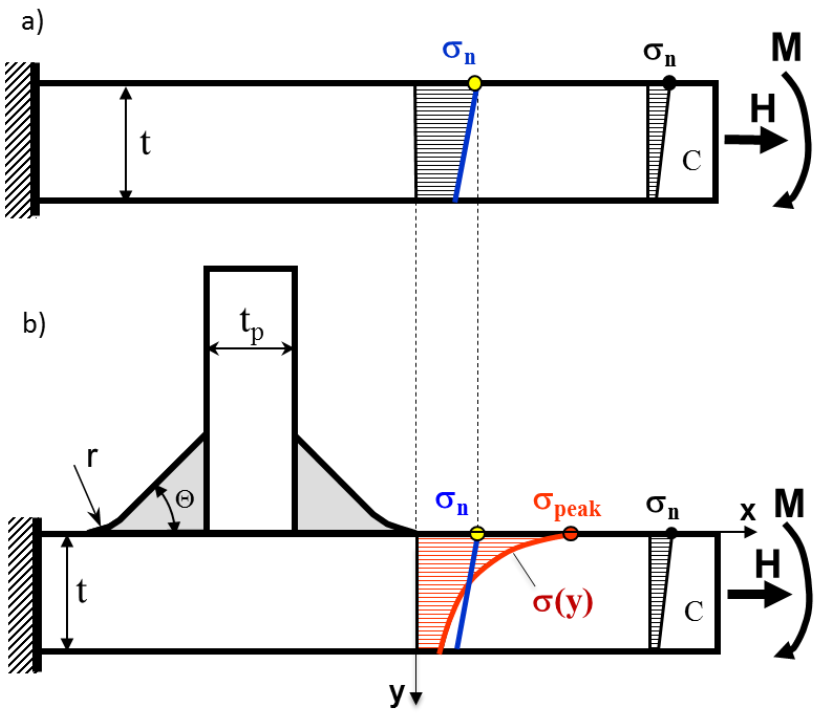

Figure 3-3: Various stress quantities in (a) plate and (b) weldment

The nominal stress, σ_n in a plate without any attachments or notches (Figure 3-3a) can be determined using simple tension and/or bending stress formula.

$$\sigma_n = \frac{H}{A} + \frac{M\,t}{2\,I} \tag{3.3}$$

After adding the attachment plate by welding (Figure 3-3b), it changes the stiffness in the weld region resulting in stress concentration at the weld toe and the non-linear through-thickness distribution, represented by eqns. 3.4 and 3.5 respectively.

$$\sigma_{peak} = \sigma_n\, K_{t,n} \tag{3.4}$$

$$\sigma(y) = \sigma_n\, f(y) \tag{3.5}$$

The peak stresses at the weld toe can be determined using stress concentration factors available in the literature and the appropriate reference stresses. These stress concentration factors are unique for the given geometry and the mode of loading. However, weldments are often subjected to multiple loading modes, and therefore it is not easy to define a unique nominal or reference stress. For this reason, the use of classical stress concentration factors is limited to the simple geometry and the load

configuration for which they were derived. The nominal membrane and bending stresses, actually nonexistent in the weld joint, are the same as in the un-welded plate. Nominal stress, σ_n in a weldment is nothing but the characteristic stress of statically equivalent linear stress distribution. Unfortunately, determination of the meaningful nominal stress in complex welded structures is difficult and often non-unique such as in the case of joint shown in Figure 3-4. Nominal stress, σ_n in such a case can be determined using eqn. 3.6, which shows that it is not unique and is dependent on L.

$$\sigma_n = \frac{\int_{-L/2}^{L/2}\int_{-t}^{0}\sigma\,(x,y)\,dxdy}{t\,L} = \frac{P}{t\,L} \tag{3.6}$$

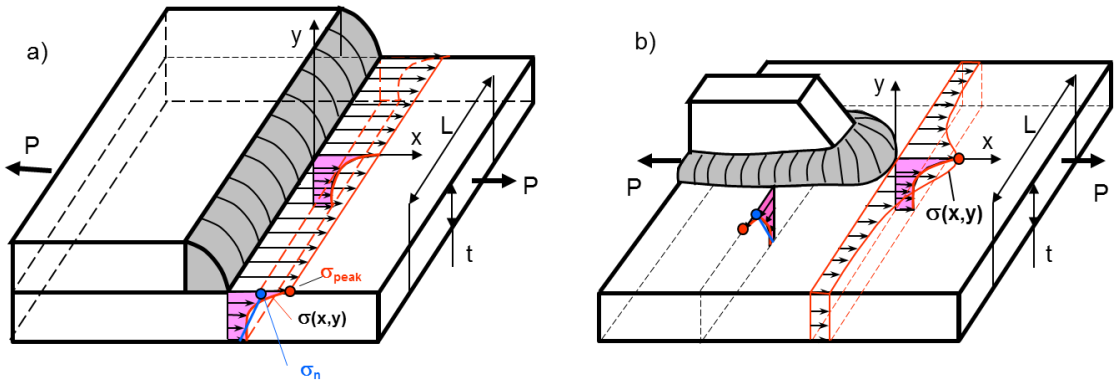

Figure 3-4: Limitation of the nominal stress method

Therefore the structural stress σ_{hs} often termed as the 'hot spot stress', is used in some cases, originally applied in the offshore structures industry. The hot spot stress has the advantage that it accounts for the effect of the global geometry of the structure and the existence of the weld, but it does not account for the micro geometrical effects such as the weld toe radius, r, and weld angle, θ. The through thickness stress distribution in the plate thickness at the weld toe section is usually non-linear and so, the stress parts can be separated, which are the membrane, the bending and the non-linear peak stress. Structural stress is defined as the sum of the membrane stress (σ^m) and the bending stress (σ^b), obtained by assuming linear statically equivalent stress distribution with the mid-plate-thickness as the neutral point, see Figure 3-5. The remaining stress is nonlinear due to the local notch effect [64].

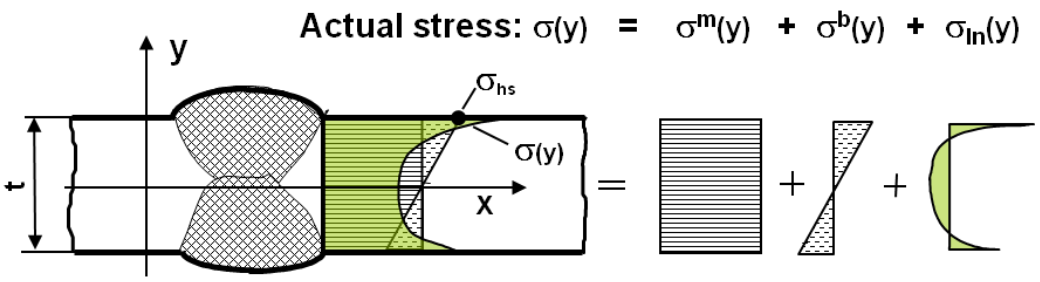

Figure 3-5: Decomposition of the stress field in the weld toe plate cross section

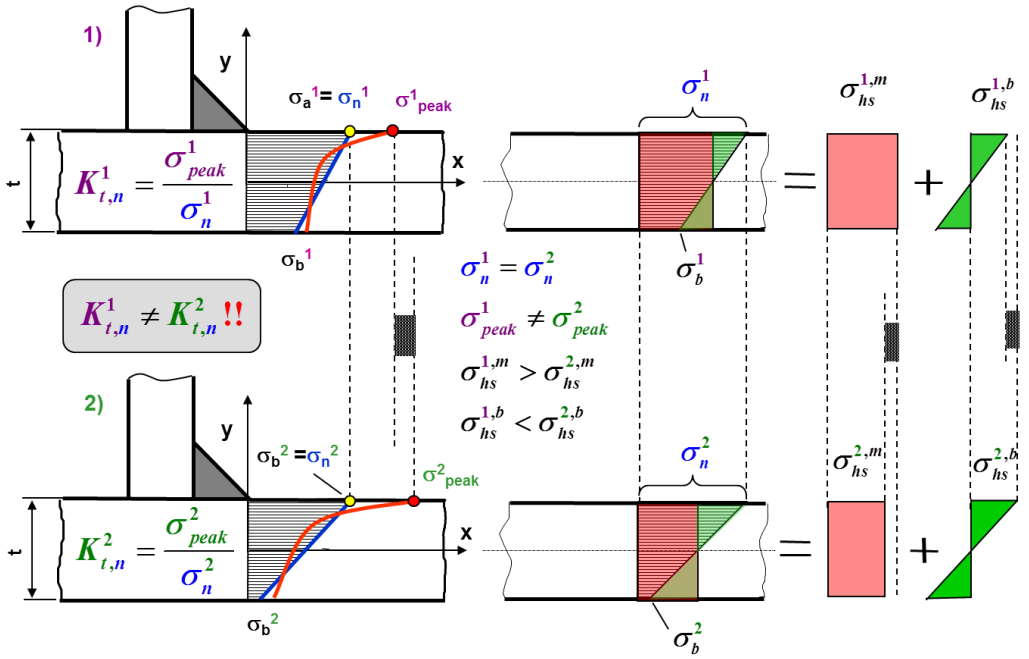

Figure 3-6: Limitation of the hot spot stress method

The statically equivalent linearized stress distribution can be characterized by two parameters, i.e. the magnitude of the hot spot stress, σ_{hs} and the slope. If the stress concentration factors, based on the hot spot stress, σ_{hs} as the reference (or nominal stress), are known then the finite element models can be used to determine only the hot spot stress at the weld toe and subsequently to determine the peak stress by using appropriate stress concentration factors. However there is a major challenge in using the hot spot stress method for some cases like the T-joint as shown in Figure 3-6. Two different load combinations could have the same nominal hot spot stress but different peak stress values because the stress concentration factor, $K_{t,n}$ not only depends on the

geometry but also on the mode of loading. The stress concentration factor $K_{t,n}$ depends on the membrane to bending stress ratio, $\sigma_{hs}^{m}/\sigma_{hs}^{b}$. Thus the hot spot stress alone is not sufficient to be used as reference stress for the determination of the load independent stress concentration factors as they are different even for the same geometry.

Due to these limitations with the nominal and the hot spot stress approaches, the local strain life method and the fractures mechanics method have been utilized in this work. The local strain life approach requires information about the peak stress at the weld toe σ_{peak} and the fracture mechanics approach requires the through-thickness stress distribution at the critical section, $\sigma\ (y)$, refer Figure 3-1. One of the main objectives of this work is to determine these stress quantities in an efficient manner, as required for fatigue life analysis.

3.2 Finite element analysis using 3D elements

One of the factors, which have dominating effect on the fatigue life of welded joints, is the stress concentration factor. The local stress approaches utilize the stress in the vicinity of the location of crack initiation. In order to obtain a precise stress by calculation, it is necessary to know the detailed information of local structural geometry. While the stress at cracked location is sometimes very sensitive to the local geometry, the structural modeling of the local geometry itself sometimes is highly uncertain. In addition, the local stress at cracked location cannot be sometimes evaluated without considering the entire structure behavior. Such areas need numerous efforts to obtain the precise stress data.

The 3D finite element modeling methods are becoming more feasible with the significant improvements in the computing power. Therefore it is possible to model complex and large structures using 3D finite elements such as the brick or tetrahedral elements. Two finite element techniques based on different types of 3D FE meshes can be used for stress analysis of the welded structures. One method is to use ‘fine’ FE mesh in the weld toe region and the second method could be based on using ‘coarse’ FE mesh in the entire domain, refer Figure 3-7 which shows the difference between these two meshing techniques.

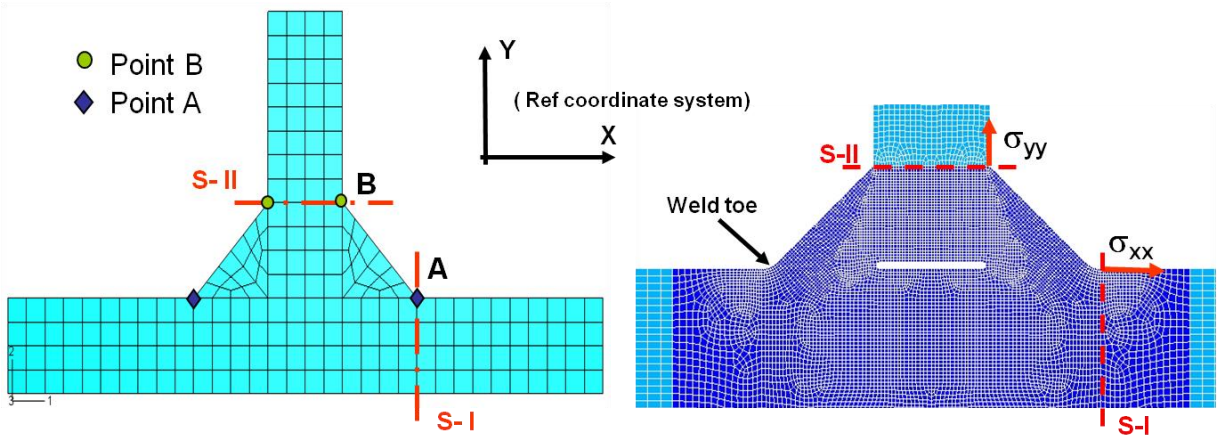

Figure 3-7: Coarse vs. fine mesh FE Model

To conduct fine mesh FE analysis, as the name indicates, the size of the smallest element adjacent to the weld toe line is highly critical and it should not be larger than one quarter of the weld toe radius, $\delta_{el} \leq 1/4\ r$. This means that the weld toe radius should be modeled with at least 4 elements. If the weld toe radius is 0.5mm, then the minimum finite element size which needs to be used in order to capture the stress gradient around the radius is 0.125mm. Use of such small element size could result in very large and complex FE models, especially if there are multiple sections with potential of crack initiation in the large scale welded structure. The local peak stress and the through-thickness stress distribution, as required for the strain-life and the fracture mechanics methods respectively, can be obtained directly from the 3D fine mesh FE analysis. However due to the large modeling time and even larger solving time, this method is not attractive in practice.

A more practical approach is to use 3D coarse mesh, which can accurately capture global geometry of the welded structure including welds, but excluding the micro geometrical features such as the weld toe radius. The coarse FE mesh is not capable of capturing information about stress concentration at the weld toe. Therefore it is not possible to determine the through thickness stress distribution directly from the 3D coarse mesh FE analysis. The stress concentration cannot be extracted from the 3D coarse mesh finite element analysis because the weld toe, weld root and other notch-like regions are modeled as sharp corners. On the other hand stress values at the sharp corner obtained from the coarse mesh FE analysis are highly inaccurate because the finite element size of

the coarse mesh is often larger than the high stress gradient region near the weld toe. Therefore in order to determine the stress concentration and the through thickness stress distribution based on the 3D coarse mesh FE analysis, a special post processing method is required.

3.3 The Proposed GR3 Methodology

Welded structures require an extremely fine mesh 3D FE models to capture the effect of weld micro geometrical features so that accurate information of the stress concentration and the stress distribution in the weld toe region can be obtained for fatigue life analyses. Appropriate 3D fine mesh FE models are prohibitively complex with very large number of finite elements if used for modeling of real 3D welded structures. Therefore, a special coarse mesh FE modeling technique is proposed, which allows for modeling the full scale 3D welded structures with coarse brick or tetrahedral finite elements along with a special post processing method named as GR3 methodology. 'GR' is named after the author of this thesis (R-Rakesh) and his PhD supervisor (G-Gregory) while the digit '3' signifies that it was 3rd attempt which was successful while working on this methodology development. Such an approach i.e. the proposed GR3 methodology represents the practical alternative for design engineers. The proposed methodology should help to model the complete welded structure with multiple hot spots, using relatively large 3D finite elements, allowing automatic FE mesh generation. Such a technique does not result in determining the stress concentration (peak stress) at the weld toe or the non-linear through-thickness stress distribution but it helps to determine the linearized hot spot membrane and the bending stresses, σ_{hs}^{m} and σ_{hs}^{b} , respectively. It is essential to estimate the correct values of σ_{hs}^{m} and σ_{hs}^{b} in the critical cross sections from any type of FE model as these values need to be the same as the actual ones. The proposed GR3 methodology helps to resolve this challenge for 3D coarse mesh FE modeling of the welded structures.

The proposed methodology establishes the procedures for the stress analysis of welded structures using solid-3D coarse mesh FE models and for post processing of the FE stress data to determine the local peak stress and the non-linear through-thickness stress distribution necessary for fatigue life evaluations. Several different types of weld joints, involving different levels of complexity in terms of geometry, shape, size, and loading

modes, have been used to demonstrate the validation and application of the proposed method.

In brief, the post processing procedure includes the stress linearization, subsequent determination of the local peak stress, σ_{peak} , and the non-linear through-thickness stress distribution (normal stress component), $\sigma_{xx}(y)$, by using the appropriate stress concentration factors and the generalized through thickness stress distribution expressions respectively. The details of the post processing procedure are covered in the later sections. The resultant stress information obtained from the post processing of the coarse mesh FE model data can be subsequently used as the base for the local strain life and the fracture mechanics analyses of fatigue life of weldments. The predicted peak stress and the through thickness stress distributions obtained from 3D coarse mesh FE models have been compared against the results obtained from 3D fine mesh FE models.

3.4 Evaluation of residual stress

There are at least two undesirable states which are created as a result of the welding process; the tensile residual stress and distortion of the welded structure. Design engineers are more concerned about the first one, whereas the manufacturing community is more concerned about the second. Presence of tensile residual stresses in the weld toe region can be detrimental to the fatigue life of welded structures. So it is critical to determine the welding residual stresses and account for their effect while determining the fatigue life of welded structures.

Although, extensive research has been done for the welding process simulation of simple joints, there has been little work on simulating the large structures. Welding process simulations are complex as many variables need to be considered. In the present work, a welding process simulation model, VrWeld from Goldak Technologies Inc., has been used to accurately capture the thermal-microstructure-stress changes during the welding process. The analysis accounts for transient thermal effects because of the localized, non-uniform and dynamic nature of the heat input as the part is being welded. The heat distribution, heating and cooling rates which affect the microstructure of the weld and the heat-affected-zone are accounted for. The thermal and microstructure history which, in turn, affects the stress distribution in the model are also accounted for. This model has the

capability to account for many variables. These include accurately defining the material properties, welding parameters, welding sequence and boundary conditions that include tack welds and constraints. It also provides the capability to create a mesh and define time stepping in a way that can accurately capture the thermal, microstructure and stress history of the welding process. The research has been carried out to determine an equation for the temperature dependent convection coefficient that can reduce the error in modeling an accurate transient temperature field, during heating and cooling of a welded structure which is the basic step in distortion and residual stress predictions, more details are covered in the paper presented by the author [65]. The model has been validated extensively for its prediction capabilities with the literature benchmark, experimental set up at lab scale and measurements from large real life welded structures [66]. This welding process simulation tool solves the coupled equations for the conservation of energy, mass and momentum for a structure being welded. Complex equations are solved by using the mathematics of transient non-linear FEM and the evolution of microstructure. The simulation model uses the Goldak's double ellipsoidal power density distribution of heat source model below the welding arc, which can accurately simulate different types of welding processes with shallow and deep penetration.

This model enables to simulate the transient 3D temperature field, the evolution of microstructure in low alloy steel welds, the transient 3D displacement, and the stress and strain in the structure as it is being welded. Inputs for the simulation include stereo-lithographic (STL) files for the parts being welded, the set of weld procedures and the weld path for each joint and temperature dependent material properties for the materials being welded and the boundary conditions. For thermal analysis the boundary conditions are chosen from prescribed temperatures, prescribed power density, prescribed thermal fluxes and convection cooling applied during the welding process. A detailed step by step procedure on how to set up the model and perform welding simulation analysis is shown in the flow chart in the Appendix B.

Residual stresses obtained from the welding process simulation model can be combined with the appropriate structural stresses obtained using the proposed 3D coarse mesh FE methodology, using the Neuber's rule as shown in section 2.5.1 and using the Kurihara's model as shown in section 2.6.1, to determine the fatigue life of welded structures.

3.5 Fatigue life estimation based on the 3D coarse mesh FE analysis

Simple 3D geometrical T-joint shown in Figure 3-8 was considered as the first object for the illustration of the proposed methodology. Such a simple joint can be analyzed using either a coarse or a fine finite element mesh. The weld toe is represented by a sharp corner if the coarse mesh FE model is used, as shown in Figure 3-9. To begin with, the coarse mesh FE analysis is not expected to deliver accurate results concerning the stress concentration and the non-linear through-thickness distribution, though benefit lies in the fact that relatively large size finite elements can be used for making the model relatively simple and computationally efficient. The smallest finite element size in the proposed method does not need to be less than 25% of the plate thickness 't' or the weld leg size 'h', i.e. $\delta_{el} \leq 0.25t$ or $\delta_{el} \leq 0.25h$.

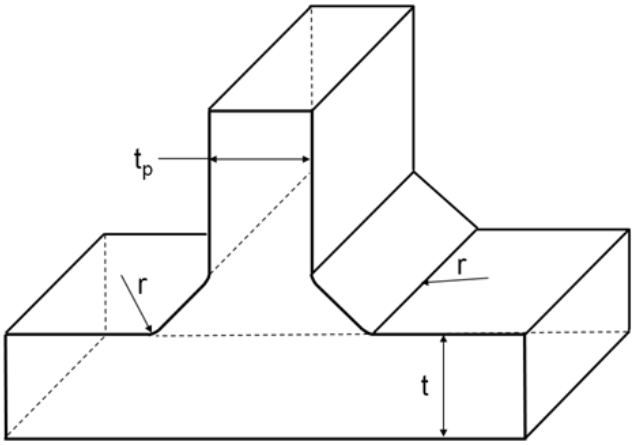

Figure 3-8: T-joint with the base plate thickness 't' and weld toe radius 'r'

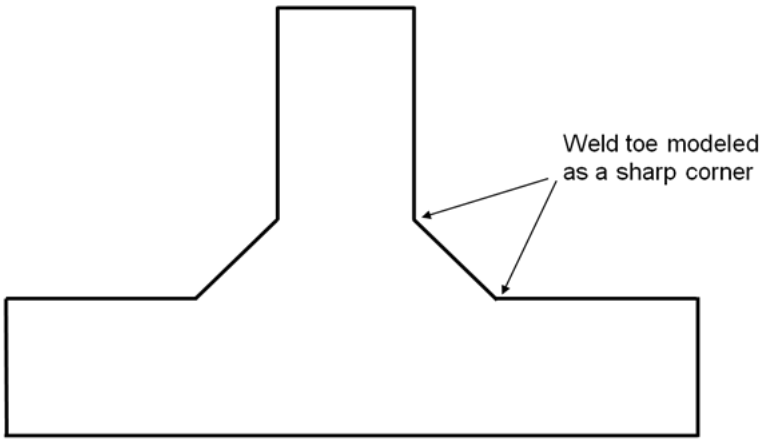

Figure 3-9: Weld toe modeled as sharp corner during coarse FE mesh modeling

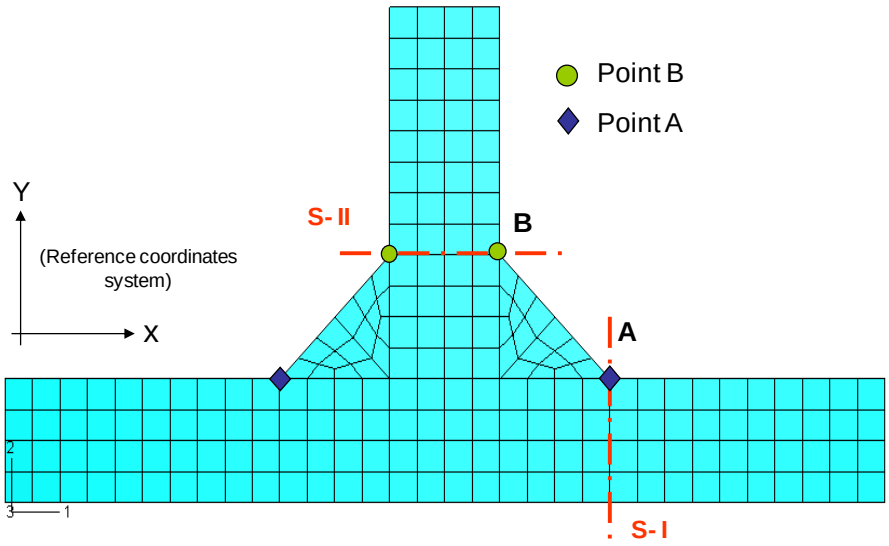

Figure 3-10: Fatigue crack intiation sites at critical weld toe cross sections

The cross sections S-I and S-II (Figure 3-10) represent the weld toe cross sections in the base plate and the attachment respectively. The cross sections S-I and S-II are located at the transition between the weld and the plate. Potential sites for fatigue crack initiation at the critical weld toe cross sections are denoted (Figure 3-10) by points A and B in both the base and the attachment plate respectively.

The transition points (points A and B) or the adjacent points experience the highest stress concentration. As described earlier, the normal stress component contributes mainly towards the fatigue performance of the welded joints. So for carrying out fatigue analysis of the base plate (if the critical cross section lies in base plate), the normal stress component, $\sigma_{xx}(y)$, in the base plate cross section S-I needs to be determined and likewise the normal stress component, $\sigma_{yy}(x)$, in the attachment plate cross section S-II is needed for the fatigue analysis of the attachment.

As per the local strain-life approach, the local peak stress amplitude and the mean stress of each stress cycle must be known to estimate the fatigue crack initiation life. The through thickness stress distribution and its fluctuations are necessary for fracture mechanics analyses. In order to determine these stresses from the FE analysis, it is necessary to correctly model all the weld micro-geometrical features but this result in a complex fine FE mesh with very large numbers of small size elements when applied to a

real full scale welded structure. Therefore the use of 3D coarse mesh FE model to analyze large engineering objects offers an attractive alternative. Basic steps to calculate the peak stress at weld toe and the through-thickness stress distribution at the critical section using the 3D coarse mesh FE stress analysis are discussed and summarized as follows.

1. The first step is to determine the distribution of the normal stress component in the critical cross section S-I or S-II shown in Figure 3-11. As mentioned earlier, it is required to extract normal stresses $\sigma_{xx}(y)$ in the cross section S-I for the fatigue analysis of the base plate and the normal stresses $\sigma_{yy}(x)$ in the cross section S-II for the fatigue analysis of the attachment.

2. Since the weld toe is modeled as a sharp corner in 3D coarse mesh FE procedures so the peak stress at this corner is highly inaccurate and cannot be used directly for fatigue life estimations. Instead, $\sigma_{\text{hs}}^{\text{m}}$ and $\sigma_{\text{hs}}^{\text{b}}$, the membrane and bending stress respectively in the plate cross section (Figure 3-12) are determined from the through-thickness coarse mesh FE stress distribution, $\sigma_{xx}(y)$ or $\sigma_{yy}(x)$.

3. The local peak stress, σ_{peak}, at the weld toe can be calculated using the below formula:

$$\sigma_{\text{peak}} = \sigma_{\text{hs}}^{\text{m}} K_{\text{t,hs}}^{m} + \sigma_{\text{hs}}^{\text{b}} K_{\text{t,hs}}^{b} \tag{3.7}$$

   More details concerning the membrane and bending stress concentration factors, $K_{\text{t,hs}}^{m}$ and $K_{\text{t,hs}}^{b}$, respectively are covered later.

4. Determine the through-thickness stress distribution in the analyzed cross-section using eqn. 3.8 [67]. If the critical cross section is section S-I, then the equation can be presented as follows:

$$\sigma_{xx}(y) = \left[\frac{K_{t,hs}^{m}\sigma_{hs}^{m}}{2\sqrt{2}}\ \frac{1}{G_m} + \frac{K_{t,hs}^{b}\sigma_{hs}^{b}}{2\sqrt{2}}\ \frac{1-2\left(\frac{y}{t}\right)^{0.89}}{G_b}\right]\left[\left(\frac{y}{r}+\frac{1}{2}\right)^{-\frac{1}{2}} + \frac{1}{2}\left(\frac{y}{r}+\frac{1}{2}\right)^{-\frac{3}{2}}\right] \tag{3.8}$$

   More details concerning parameters used in the equation above are explained later.

5. Carry out welding process simulation and determine the through-thickness residual stress distribution in the same critical plane as used for the determination of stress distribution induced by the external load.
6. Estimate the total life of the welded structure using the strain life and the fracture mechanics analyses.

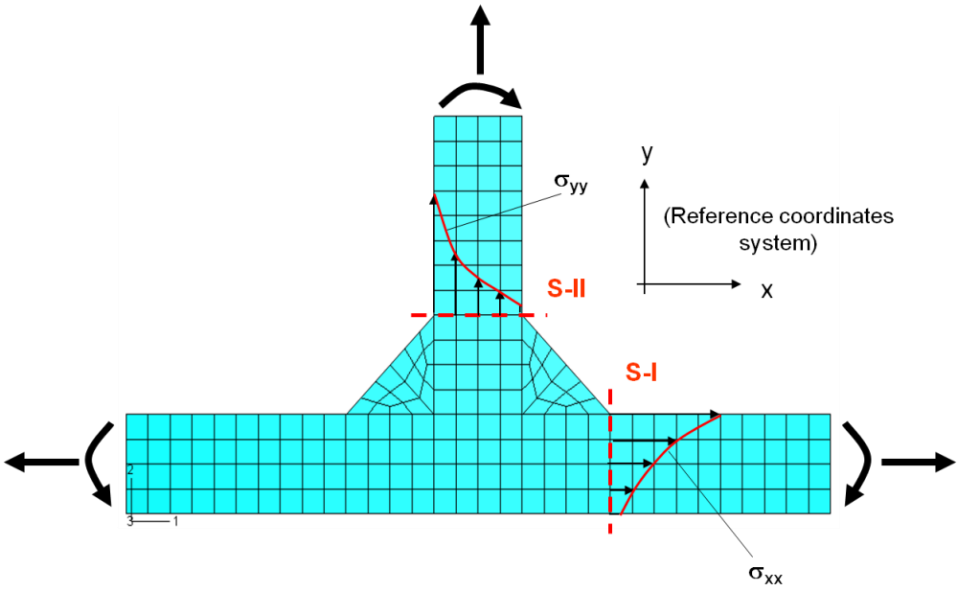

Figure 3-11: Normal stress components responsible for fatigue failure

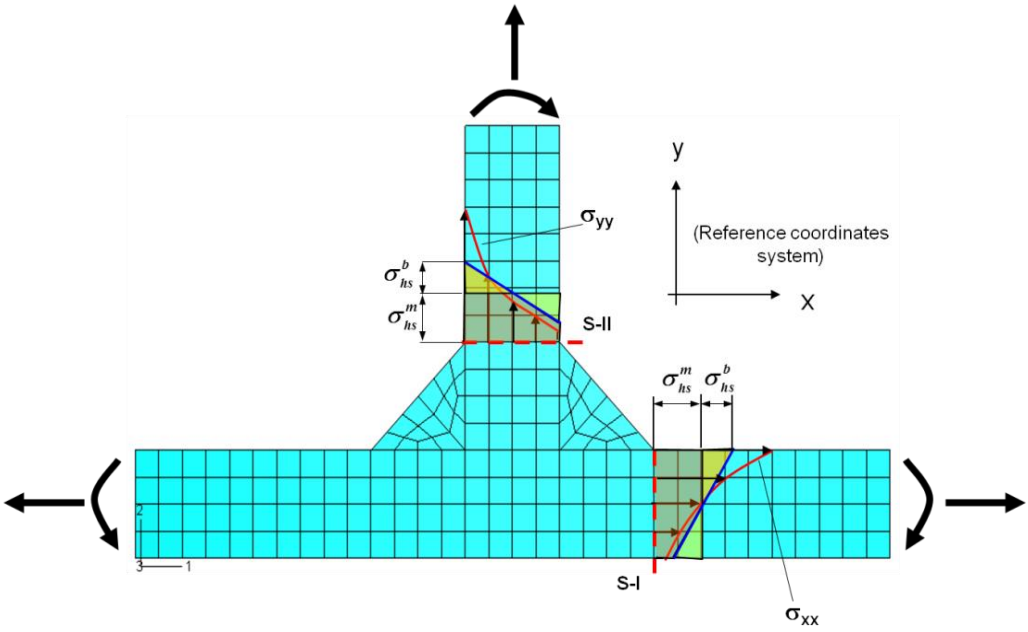

Figure 3-12: The mebrane and bending hot spot stress in the crtical cross section

To determine the peak stress and the stress distribution in the critical cross section based on the stress data obtained from the 3D coarse FE mesh model of analyzed welded joint, eqns. (3.7) and (3.8) are used. The peak stress at a sharp corner and the through thickness stress distribution obtained from the coarse FE mesh model cannot be directly used for the fatigue life analyses because of insufficient accuracy caused by the singularity at the weld toe. Although, the membrane and bending hot spot stresses determined using proper method (explained in next section) can be reasonably accurate because they are barely dependent on the finite element size. Further, combining the membrane and the bending stresses with appropriate stress concentration factors (eqn. 3.7) and Monahan's equations (eqn.3.8) can predict reasonably accurate peak stress and through-thickness stress distribution, which are needed for fatigue crack initiation and propagation life prediction respectively.

3.6 Determine membrane and bending hot spot stresses from 3D coarse mesh FEA

The membrane and bending hot spot stresses can be established by linearization of the discrete stress field obtained from the coarse mesh FE analysis (Figure 3-13). The linearized equivalent stress field is considered as linearly through the thickness distributed stress field having the same axial force and the same bending moment as the actual nonlinear stress field. The classical nominal stress σ_{n} differs from the hot spot stress σ_{hs} in the fact that the nominal stress represents an average stress over the complete cross section and its value is the same at any point along the weld toe line. The hot spot stress is obtained from the linearization of the actual non-linear stress field through the plate thickness and it varies along the weld toe line. To account for this fact that the hot spot stress varies along the weld toe line, the linearization is carried out locally over a small part of the cross section beneath selected critical point on the weld toe line, i.e. over an area 't $\times\Delta$z' at location (x=0, y=0, z=z_i), where the coordinate z=z_i locates the position along the weld toe. The axial force, P and the bending moment, M_b can be calculated by integrating the stress function σ(x=0, y, z) acting over the area 't $\times\Delta$z'.

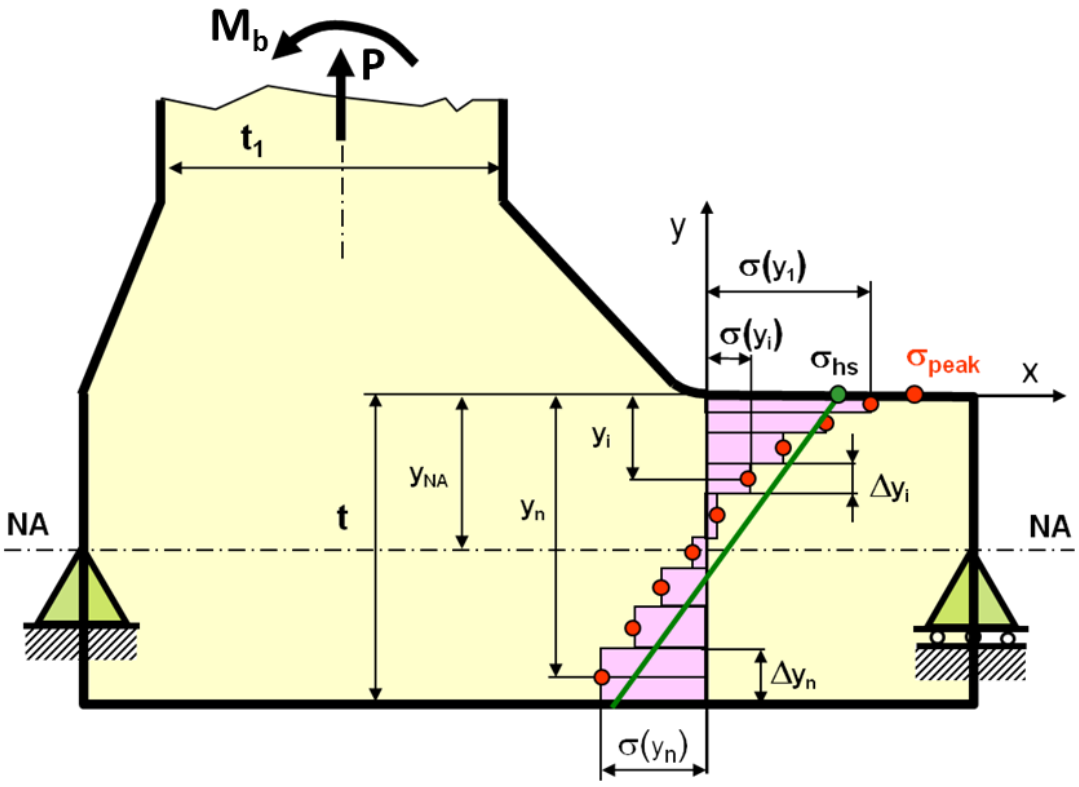

Figure 3-13: Through thickness discrete stress dstribution data

$$P = \int_{z=z_i}^{z=z_i+\Delta z} \int_{y=-t}^{y=0} \sigma(x=0,y,z)\, dy\, dz \tag{3.9}$$

$$M_b = \int_{z=z_i}^{z=z_i+\Delta z} \int_{y=-t}^{y=0} \sigma(x=0,y,z)\,(y_{NA}-y)\, dy\, dz \tag{3.10}$$

Where: y_{NA} is the coordinate of the neutral axis of the cross section 't ×Δz'

Mathematically, the linearization of the stress field needs to be carried out along the line at the critical cross section (x=0, y, z=z_i) and over the domain [y=0; y=t]. So theoretically at this cross section, width 'Δz' of the cross section approaches to zero and accordingly the stress $\sigma_{xx}(y)$ can be assumed as constant over such a small variation of co-ordinate 'z', i.e. it can be considered as a constant value (independent of z) along the weld toe line for such a small distance. This further means that the integration of the stress field along any line (x=0, y, z=z_i) does not involve integration with respect to the co-ordinate 'z' and therefore it can be assumed for convenience that 'Δz=1 unit' and perform the integration

only with respect to co-ordinate ‘y’. Therefore for the discrete stress distribution and for the co-ordinate system, shown in Figure 3-13 the axial force P and the bending moment M_b can be calculated from eqns. (3.11) and (3.12) respectively.

$$P = \int_{-t}^{0} \sigma\,(y)\, dy = \sum_{1}^{n} \frac{\sigma(y_i) + \sigma(y_{i+1})}{2} \, |y_i - y_{i+1}| \tag{3.11}$$

$$M_b = \int_{-t}^{0} \sigma\,(y)\,(y_{NA} - y)\, dy = \sum_{1}^{n} \sigma\,(y_i)\,(y_{NA} - y_i)\,\Delta y_i \tag{3.12}$$

From the finite element analysis, the stress field in the cross section of interest is usually given (Figure 3-13) in the form of a series of discrete points [$\sigma(y_i)$, y_i], i.e. nodal stresses and their coordinates. Therefore a numerical integration routine need to be applied in the form of appropriate summation of contributions from all nodal stress points. If the spacing (y_{i+1} - y_i) between subsequent nodal points is not too large the integration can be replaced, according to eqns. (3.11) and (3.12), by the summation of discrete increments. Unfortunately, such a simple integration technique (Figure 3-13), used extensively for development of the shell GY2 modeling method [68], is not sufficiently accurate when applied to coarse mesh FE stress data.

Therefore, a new numerical integration method has been developed which is mathematically exact and applies to both fine and coarse 3D FE mesh stress data. To start with, it is assumed in this method that simple finite elements with the linear shape function are used. Therefore the stress field between two subsequent nodal points can be represented (Figure 3-13) by a linear equation.

$$\sigma(y) = a_i y + b_i \tag{3.13}$$

Where: a_i and b_i are the parameters of the linear stress function valid for the range, $y_i \leq y \leq y_{i+1}$, i.e. between two adjacent nodal points.

The nodal stresses, (σ_i, σ_{i+1}), and their co-ordinates (y_i, y_{i+1}) respectively corresponding to two adjacent points can be used for the determination of parameters a_i and b_i of eq.(3.13).

$$a_i = \frac{\sigma_i - \sigma_{i+1}}{y_i - y_{i+1}} \quad and \quad b_i = \frac{\sigma_{i+1} y_i - \sigma_i y_{i+1}}{y_i - y_{i+1}} \tag{3.14}$$

Thus the integral (3.11) representing the force contributed by stresses acting over the interval, $y_i \leq y \leq y_{i+1}$, can be written as:

$$P = \int_{y_i}^{y_{i+1}} \sigma\,(y)\,dy = \int_{y_i}^{y_{i+1}} (a_i y + b_i)\,dy = \left|\frac{a_i y^2}{2} + b_i y\right|_{y_i}^{y_{i+1}}$$

$$= \frac{(\sigma_{i+1} + \sigma_i)(y_{i+1} - y_i)}{2} \qquad (3.15)$$

In order to determine the resultant force P acting over the entire thickness of the cross section all force contributions P_i need to be accounted for as follow:

$$\mathrm{P} = \sum_{1}^{\mathrm{n}} \mathrm{P_i} = \sum_{1}^{\mathrm{n}} \frac{(\sigma_{i+1} + \sigma_i)(y_{i+1} - y_i)}{2} \qquad (3.16)$$

Similar integration technique can be used for the determination of the bending moment M_b. First the bending moment $M_{b,i}$ contributing by the segment [y_i, y_{i+1}] needs to be calculated.

$$M_{b,i} = \int_{y_i}^{y_{i+1}} \sigma\,(y)\,(y_{NA} - y)\,dy = \int_{y_i}^{y_{i+1}} (a_i y + b_i)\,(y_{NA} - y)\,dy$$

$$= a_i \left(\frac{y_i^3 - y_{i+1}^3}{3}\right) - (a_i y_{NA} - b_i)\left(\frac{y_i^2 - y_{i+1}^2}{3}\right) - b_i y_{NA}\,(y_i - y_{i+1}) \qquad (3.17)$$

After substitution of eqn. (3.14) into eqn. (3.17) and rearrangement a general expression for the bending moment contributing by the segment [y_i, y_{i+1}] can be written as:

$$M_{b,i} = \frac{(\sigma_i - \sigma_{i+1})}{(y_i - y_{i+1})} \frac{(y_i^3 - y_{i+1}^3)}{3} - [(\sigma_i - \sigma_{i+1})y_{NA} - \sigma_{i+1} y_i + \sigma_i y_{i+1}] \frac{(y_i + y_{i+1})}{2}$$

$$- (\sigma_{i+1} y_i - \sigma_i y_{i+1}) y_{NA} \qquad (3.18)$$

In order to determine the resultant bending moment M_b acting over the entire thickness, t, all bending moments contributions, $M_{b,i}$ from all segments of the cross section need to be added together.

$$M_b = \sum_1^n M_{b,i} = \sum_1^n \frac{(\sigma_i - \sigma_{i+1})}{(y_i - y_{i+1})} \frac{(y_i^3 - y_{i+1}^3)}{3} - \sum_1^n [(\sigma_i - \sigma_{i+1}) y_{NA} - \sigma_{i+1} y_i + \sigma_i y_{i+1}] \frac{(y_i + y_{i+1})}{2} - \sum_1^n (\sigma_{i+1} y_i - \sigma_i y_{i+1}) y_{NA} \quad (3.19)$$

Then the membrane and bending hot spot stresses can be determined (Figure 3-13) using simple membrane and bending stress formulae.

$$\sigma_{hs}^m = \frac{P}{t} = \frac{1}{t} \sum_1^n \frac{(\sigma_{i+1} + \sigma_i)(y_{i+1} - y_i)}{2} \quad (3.20)$$

$$\sigma_{hs}^b = \frac{c.M_b}{I} = \frac{\frac{t}{2}.M_b}{\frac{t^3}{12}} = \frac{6.M_b}{t^2} = \frac{6}{t^2} \sum_1^n \frac{(\sigma_i - \sigma_{i+1})}{(y_i - y_{i+1})} \frac{(y_i^3 - y_{i+1}^3)}{3} - \frac{6}{t^2} \sum_1^n [(\sigma_i - \sigma_{i+1}) y_{NA} - \sigma_{i+1} y_i + \sigma_i y_{i+1}] \frac{(y_i + y_{i+1})}{2} - \frac{6}{t^2} \sum_1^n (\sigma_{i+1} y_i - \sigma_i y_{i+1}) y_{NA} \quad (3.21)$$

The purpose of the coarse FE mesh analysis is to determine the hot spot stresses σ_{hs}^m and σ_{hs}^b at specified point on the weld toe line. Therefore the linearized stress distribution, as mentioned earlier, is determined not over a small segment of the cross section but along the line [x=0, y, z=z_i] and the integration is carried out (Figure 3-13) only over the interval ($-t \leq y \leq 0$) along the y axis.

It is found that the average membrane stress determined from eqn. 3.20, applicable to piecewise stress distribution obtained from a coarse FE mesh model, resulted in very close approximation of the membrane stress and as such is proposed for calculating the membrane stress for both the coarse and fine 3D FE mesh stress data.

Unfortunately, the bending moment obtained by integrating (eqn. 3.21) the stress field over the entire domain ($-t \leq y \leq 0$) of the coarse FE mesh stress distribution is found to be highly inaccurate due to strong effect of the highest and very inaccurate stress value at the sharp corner present at the weld toe line. It is also known that FE stresses near a sharp corner are very mesh sensitive and therefore they cannot be used for the estimation of the bending moment. Therefore, extensive numerical and analytical studies have been carried out for the purpose of finding what part of the through thickness stress field is mesh independent.

Investigations led to the finding that the mid-thickness segment ($-0.75t \leq x \leq -0.25t$) of any through thickness stress distribution in any welded joint is the same regardless of the FE mesh resolution (fine or coarse). Several weld joint configurations are studied and one among them is the gusset weld joint as shown in Figure 3-14. Gusset plate is subjected to lateral force and the through-thickness stress distribution of the normal stress component through gusset plate thickness, $\sigma_{yy,}$ at the critical cross section shown in Figure 3-15 is chosen for the detailed analysis.

An example of the mesh independence of the mid-thickness stress field, mentioned above, is shown in Figure 3-16 where stress fields from a very fine and very coarse FE mesh are same in the mid-thickness segment of the cross section. Therefore the mid-thickness region ($-0.75t \leq x \leq -0.25t$) of the stress distribution is selected as the base for the estimation of the entire bending moment and the resulting bending hot spot stress acting at that location. Another interesting finding is that reducing the element size to half, i.e. increasing the number of elements from four to eight through the plate thickness of 4mm results into the same stress distribution through middle half thickness of plate. So this is the reason that it is not required to have element size of less than 0.25 times plate thickness as per the proposed method.

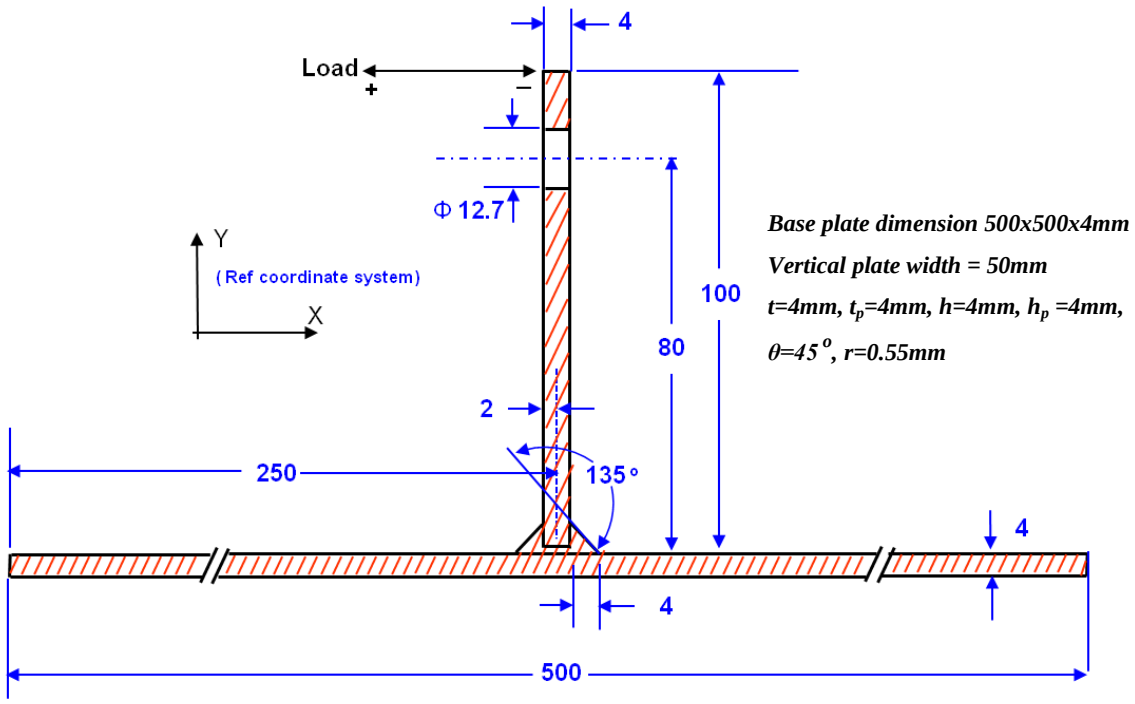

Figure 3-14: Geometry and dimensions of the gusset welded joint

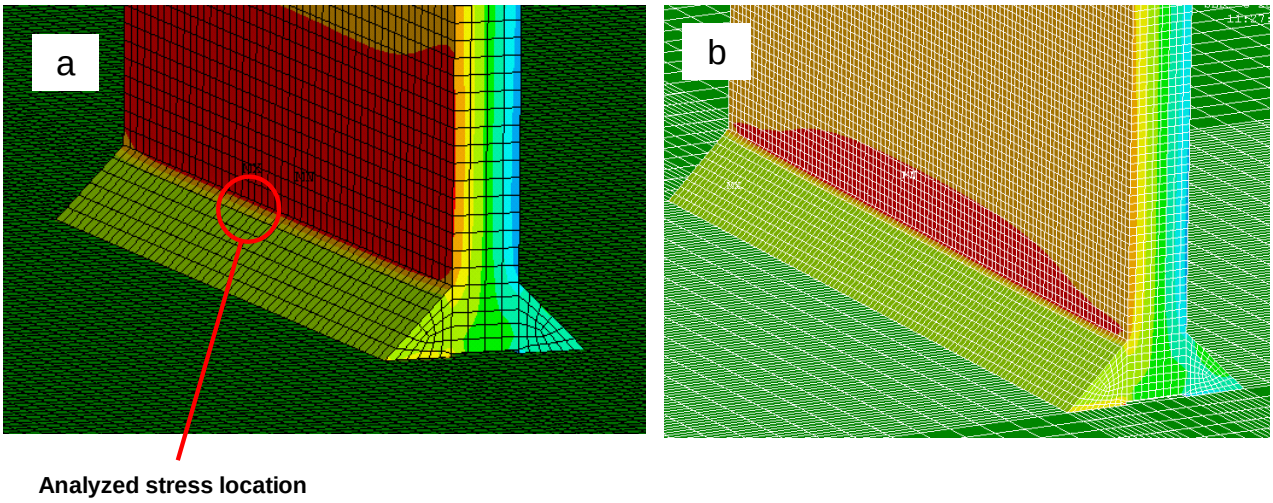

Figure 3-15: Coarse mesh FE models – (a) Four vs. (b) Eight elements per plate thickness

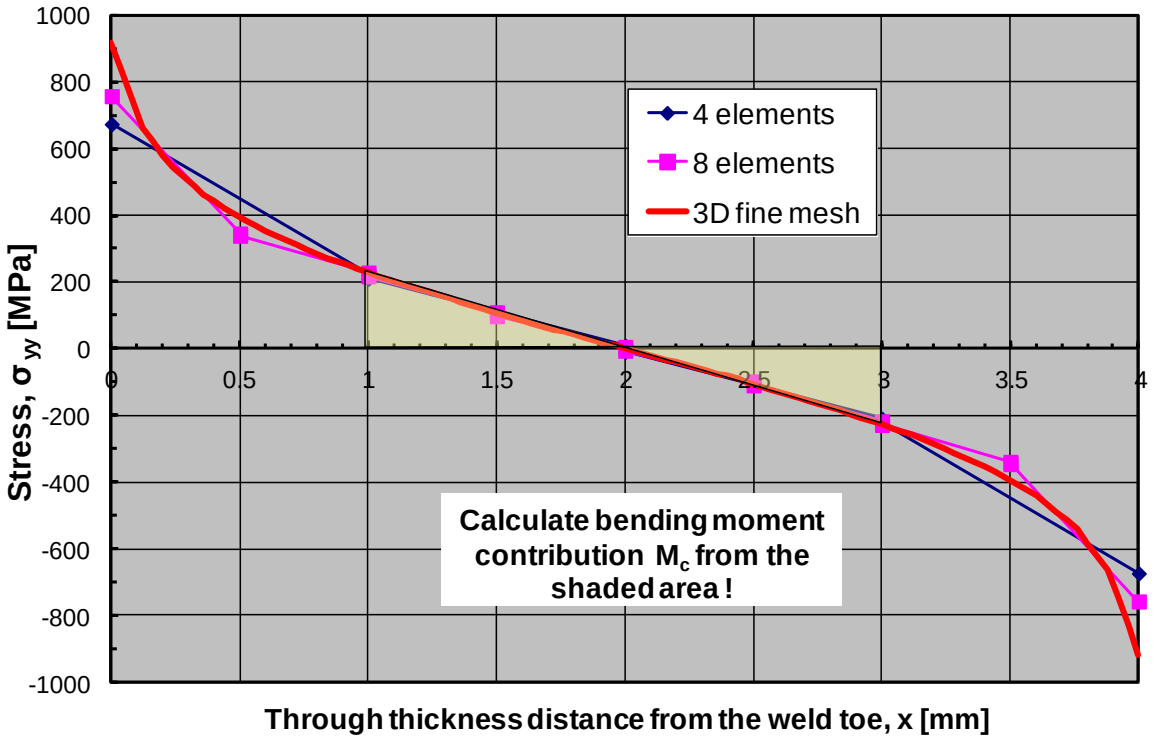

Figure 3-16: The through thickness stress distributions in the gusset plate under bending load: Mesh independent behavior of stress distribution can be observed in the middle part of the plate thickness

The bending moment contribution M_c can be obtained from the mid-thickness stress distribution using formulae in mechanics of materials, based on the decomposition of the linear stress distribution into appropriate rectangles and triangles (Figure 3-17) and using their areas and centroids. Then the bending moment is determined (for $\Delta z=1$) using the following expression.

$$M_c = \sigma_3 |x_3 - x_2| \frac{(x_3 - x_2)}{2} + \frac{(\sigma_3 - \sigma_2)|x_3 - x_2|}{2} \frac{2}{3}(x_3 - x_2) + \frac{\sigma_3 |x_3 - x_0|}{2} \frac{1}{3}(x_3 - x_0) + \frac{\sigma_4 |x_0 - x_4|}{2} \left[(x_3 - x_0) + \frac{2}{3}(x_0 - x_4)\right] \quad (3.22)$$

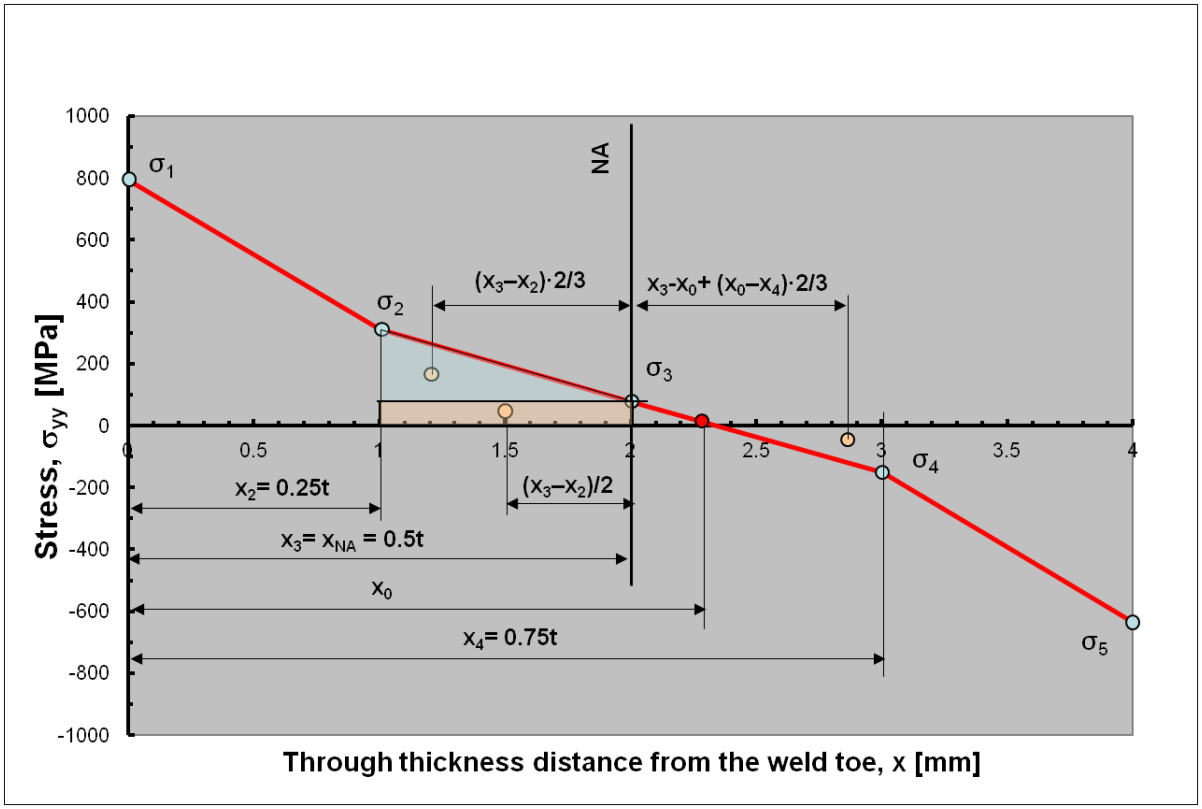

Figure 3-17: Bending moment calculation nomenclature based on through thickness stress distribution in the gusset plate under bending

The bending moment M_c is calculated with respect to the neutral axis $x = x_{NA}$ which coincides with the center line of the plate thickness. Expression (3.22) represents the integral (3.12) but limited to the domain of $0.25t \leq x \leq 0.75t$ and piecewise linear stress distribution between nodal points. Expression (3.22) might be sometimes inconvenient in practice because the analyst must find the co-ordinate x_0 where the stress diagram intersects the abscissa (Figure 3-17).

However, for a linear stress distribution between points x_2-x_3 and x_3-x_4 (Figure 3-17) the general technique in the form of eq. (3.17) can be applied with analytical integration over the domain limited to $0.25t \leq x \leq 0.75t$.

$$M_c = \int_{0.25t}^{0.75t} \sigma_{yy}(x)\,(x_{NA} - x)dx = \int_{x_2}^{x_4} \sigma_{yy}(x)\,(x_{NA} - x)dx \qquad (3.23)$$

The analysis presented below assumes that the FE mesh has only four finite elements per plate thickness. Therefore, there are only three stress point values within the integration domain, σ_2, σ_3, σ_4 and corresponding coordinates x_2, x_3, x_4. The integration of eqn. (3.23) can be done separately for the segment [x_2, x_3] and the segment [x_3, x_4]. The linear stress function in the interval [x_2: x3], coinciding with the finite element on the left hand side of the neutral axis, can be written in the form of the linear eqn. (3.24).

$$\sigma_{yy}(x) = a_1 x + b_1 \tag{3.24}$$

The parameters a_1 and b_1 can be determined (Figure 3-17) from known nodal stresses σ_2 at x_2 and σ_3 at x_3.

$$a_1 = \frac{\sigma_2 - \sigma_3}{x_2 - x_3} \ and \ b_1 = \frac{\sigma_3 x_2 - \sigma_2 x_3}{x_2 - x_3} \tag{3.25}$$

Thus the integral (3.23) can be written in the form:

$$M_{c1} = \int_{x2}^{x3} \sigma_{yy}(x)\,(x_{NA} - x)dx = \Delta z \int_{x_2}^{x_3} (a_1 x + b_1)\,(x_{NA} - x)dx$$

$$= \left[a_1 \frac{x_2^3 - x_3^3}{3} - (a_1 x_{NA} - b_1)\left(\frac{x_2^2 - x_3^2}{2}\right) - b_1 x_{NA}(x_2 - x_3)\right] \tag{3.26}$$

Similar set of equations can be written for the second (Figure 3-17) interval [x_3:x_4] adjacent to and being on the right hand side of the neutral axis (NA).

$$\sigma_{yy}(x) = a_2 x + b_2 \tag{3.27}$$

$$a_2 = \frac{\sigma_3 - \sigma_4}{x_3 - x_4} \ \text{and} \ b_2 = \frac{\sigma_4 x_3 - \sigma_3 x_4}{x_3 - x_4} \tag{3.28}$$

$$M_{c2} = \int_{x3}^{x4} \sigma_{yy}(x)\,(x_{NA} - x)dx = \Delta z \int_{x_3}^{x_4} (a_2 x + b_2)\,(x_{NA} - x)dx$$

$$= \left[a_2 \frac{x_3^3 - x_4^3}{3} - (a_2 x_{NA} - b_2)\left(\frac{x_3^2 - x_4^2}{2}\right) - b_2 x_{NA}(x_3 - x_4)\right] \tag{3.29}$$

The total contribution to the bending moment resulting from the mid-thickness stress distribution is the sum of bending moments M_{c1} and M_{c2}.

$$M_c = M_{c1} + M_{c2} \tag{3.30}$$

Now that the bending moment contribution from the mid thickness portion of stress distribution can be calculated accurately, the next challenge is to find the relationship between the bending moment M_c and the total bending moment M_b induced by the entire stress field acting at analyzed location underneath the weld toe. Extensive numerical studies of various welded joints have confirmed that the ratio of the, M_c, bending moment to the total one, M_b, is the same for all geometrical configurations of welded joints studied up to date.

$$\frac{M_c}{M_b} \cong 0.1 \quad with\ error\ of\ \pm 5\% \tag{3.31}$$

Therefore, it is proposed to determine the total bending moment, M_b, from eqn. (3.32).

$$M_b = 10\ M_c \tag{3.32}$$

Thus the bending moment can be determined from the coarse FE mesh (four elements per thickness) stress data using only nodal stresses σ_2, σ_3, and σ_4.

The bending hot spot stress, σ_{hs}^b, can then be finally determined from the general bending stress formula.

$$\sigma_{hs}^b = \frac{c\ M_b}{I} = \frac{\frac{t}{2}\ M_b}{\frac{t^3}{12}} = \frac{6\ M_b}{t^2} \tag{3.33}$$

Objective of the analysis is to determine the membrane, σ_{hs}^m , and bending, σ_{hs}^b , hot spot stresses at selected point along the weld toe line. Therefore, the linearized stress distribution (Figure 3-13) is determined not over a segment of the cross section but along the line [x=0, y, z=z_i].

The advantage of using eqn. 3.7 and eqn. 3.8 and the membrane and bending hot spot stresses, σ_{hs}^m and σ_{hs}^b respectively, lies in the fact that only two stress concentration factor expressions are necessary, $K_{t,hs}^m$ and $K_{t,hs}^b$, for all fillet welds in order to determine the peak stress and the through-thickness stress distribution at any location along the weld toe line. The membrane and bending hot spot stresses, σ_{hs}^m and σ_{hs}^b , respectively are on the other hand mesh independent and therefore they can be determined using relatively simple and coarse finite element mesh models.

Another advantage of using such an approach is that the peak stress and the through thickness stress distribution can be determined at any location along the weld toe line without any ambiguity associated with the classical definition of the nominal stress.

3.7 Determine stress concentration factors (SCF)

Fatigue crack initiation usually occurs at relatively high stress location such as at the weld toe due to high stress concentration present at that location. The simplest method to calculate local peak stresses at the weld toe is to use analytical formulas of stress concentration factors available in the literature for appropriate specified reference stress. This method is only good for theoretical cases as these stress concentration factors depend on given geometry and unidirectional load. But in reality weldments are subjected to complex loading condition, which makes it difficult to use the method described above. As per the structural stress concept appropriate stress concentration factors based on the hot spot reference stress, σ_{hs} can be used to determine the peak stress. However even for the same exact geometry the hot spot stress based stress concentrations factor values could be different for a tension versus a bending load case i.e. these are also load dependent.

The proposed method uses stress concentration factors which are classified based on the mode of loading and dependent mainly on the geometry. The peak stress at the weld toe σ_{peak} can be calculated based on geometrical unique stress concentration factors along with appropriately calculated membrane and bending stresses. Only accounting for the hot spot stress magnitude is not enough, but both the magnitude and gradient of the linearized hot spot stress through the thickness need to be accounted to determine the load independent, geometry unique stress concentration factors. Membrane (axial) and anti-symmetric bending stress obtained from linearization of the through thickness stress distribution helps to capture the stress gradient at the hot spot. Accordingly, two separate stress concentration factors for membrane and bending modes are used. An advantage of using two stress concentration factors lies in the fact that they are independent of load and unique for given geometry.

Further the weldments are also categorized as being geometrically non-symmetric or symmetric, i.e. symmetric with welds being symmetrically located at both sides of the

plate (Figure 3-18) and non-symmetric with only one weld on one side of the plate (Figure 3-19). Therefore different stress concentration factor formulas have to be used for geometrically identical non-symmetric and symmetric fillet welds. The most reliable are Japanese stress concentration factor expressions [69] also recommended by the International Institute of Welding.

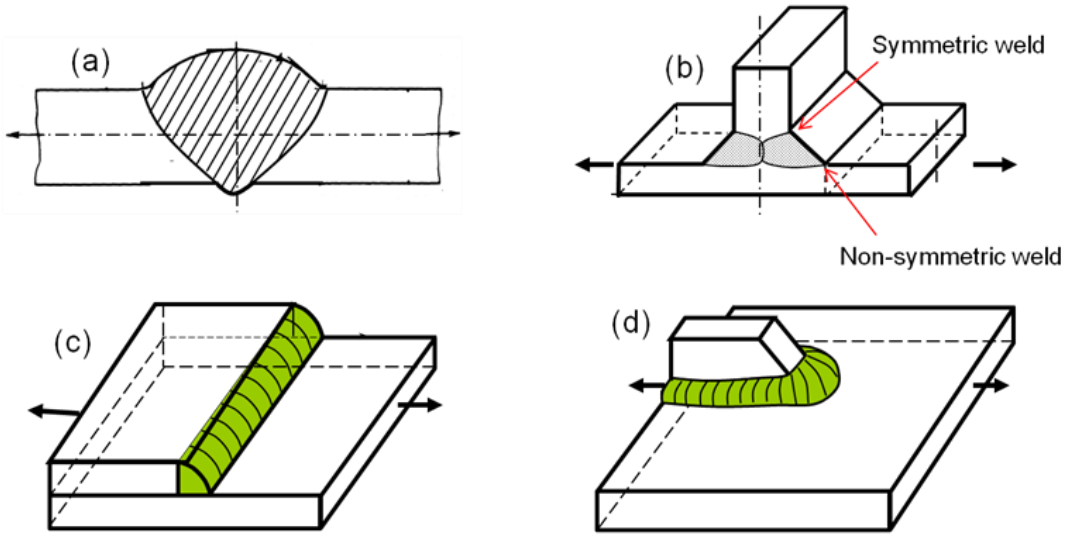

Figure 3-18: Examples of geometrically non-symmetric welded joints

(a) Butt joint (b) T-joint (c) Single lap joint (d) Gusset joint

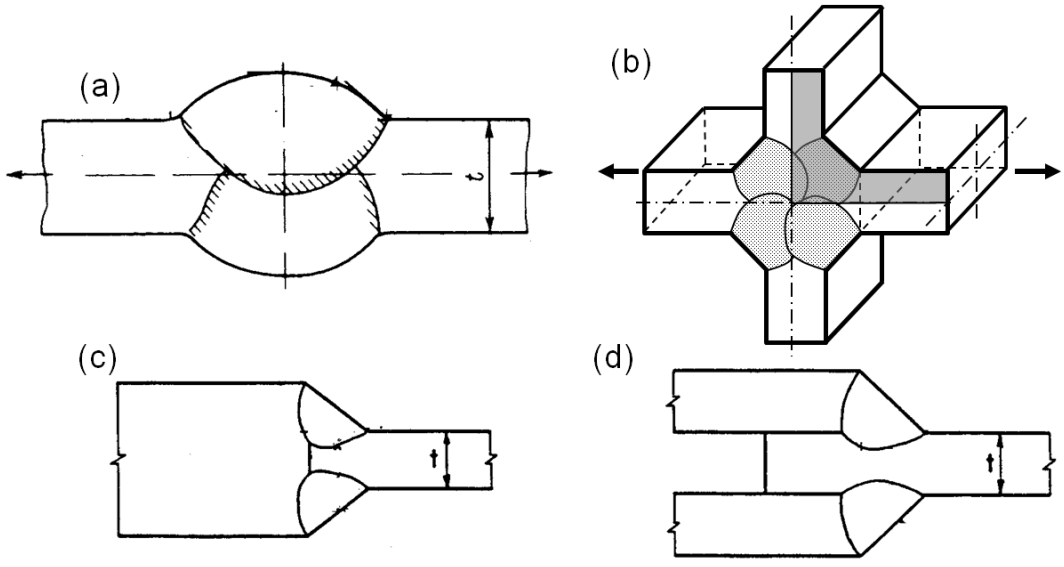

Figure 3-19: . Examples of geometrically symmetric welded joints

(a) Butt joint (b) Cruciform joint (c) Symmetric fillet welds (d) Double lap joint

3.7.1 Symmetric butt welds

In order to calculate the stress concentration factor at the weld toe point A of a symmetric butt weld (Figure 3-20), it is recommended to use the stress concentration expressions (3.34) and (3.35) for the axial and bending load respectively [69].

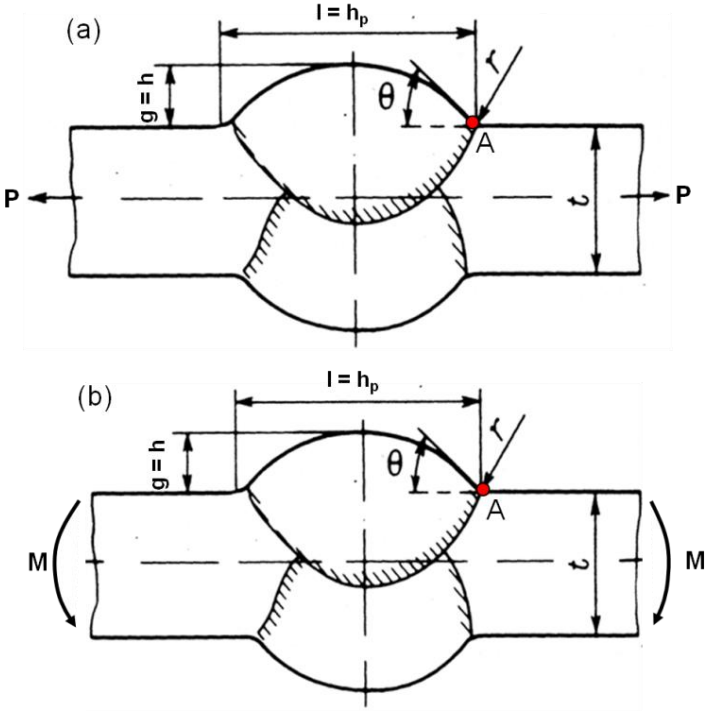

Figure 3-20: Symmetric butt weld under (a) axial load (b) bending load

$$K_{t,hs}^{m} = 1 + \frac{1 - \exp\left(-0.9\theta\sqrt{\frac{W}{2h}}\right)}{1 - \exp\left(-0.45\pi\sqrt{\frac{W}{2h}}\right)} X\ 2\left[\frac{1}{2.8\left(\frac{W}{t}\right) - 2} X\ \frac{h}{r}\right]^{0.65} \quad (3.34)$$

$$Where: W = t + 2h + 0.6h_p$$

$$K_{t,hs}^{b} = 1 + \frac{1 - exp\left(-0.9\theta\sqrt{\frac{W}{2h}}\right)}{1 - exp\left(-0.45\pi\sqrt{\frac{W}{2h}}\right)} X\ 1.5\sqrt{tanh\left(\frac{2r}{t}\right)}\ X\ tanh\left[\frac{\left(\frac{2h}{t}\right)^{0.25}}{1 - \frac{r}{t}}\right] X\left[\frac{0.13 + 0.65\left(1 - \frac{r}{t}\right)^{4}}{\left(\frac{r}{t}\right)^{\frac{1}{3}}}\right]$$

$$Where: W = t + 2h + 0.6h_p \quad (3.35)$$

Both expressions are valid for standard geometries with parameters: r/t = 0.025 - 0.35, g/t = 0.1 - 0.25, $\theta = (\pi/9) - (\pi/3.6) = 20^{o}\text{-}50^{o}$.

3.7.2 Symmetric fillet welds

In order to calculate the stress concentration factor at the weld toe point B of a symmetric fillet weld (Figure 3-21), it is recommended to use the stress concentration expressions (3.36) and (3.37) for the axial and bending load respectively [69]. It is critical that the meaning of the angle θ and dimension t_p should be consistent with the location of point B.

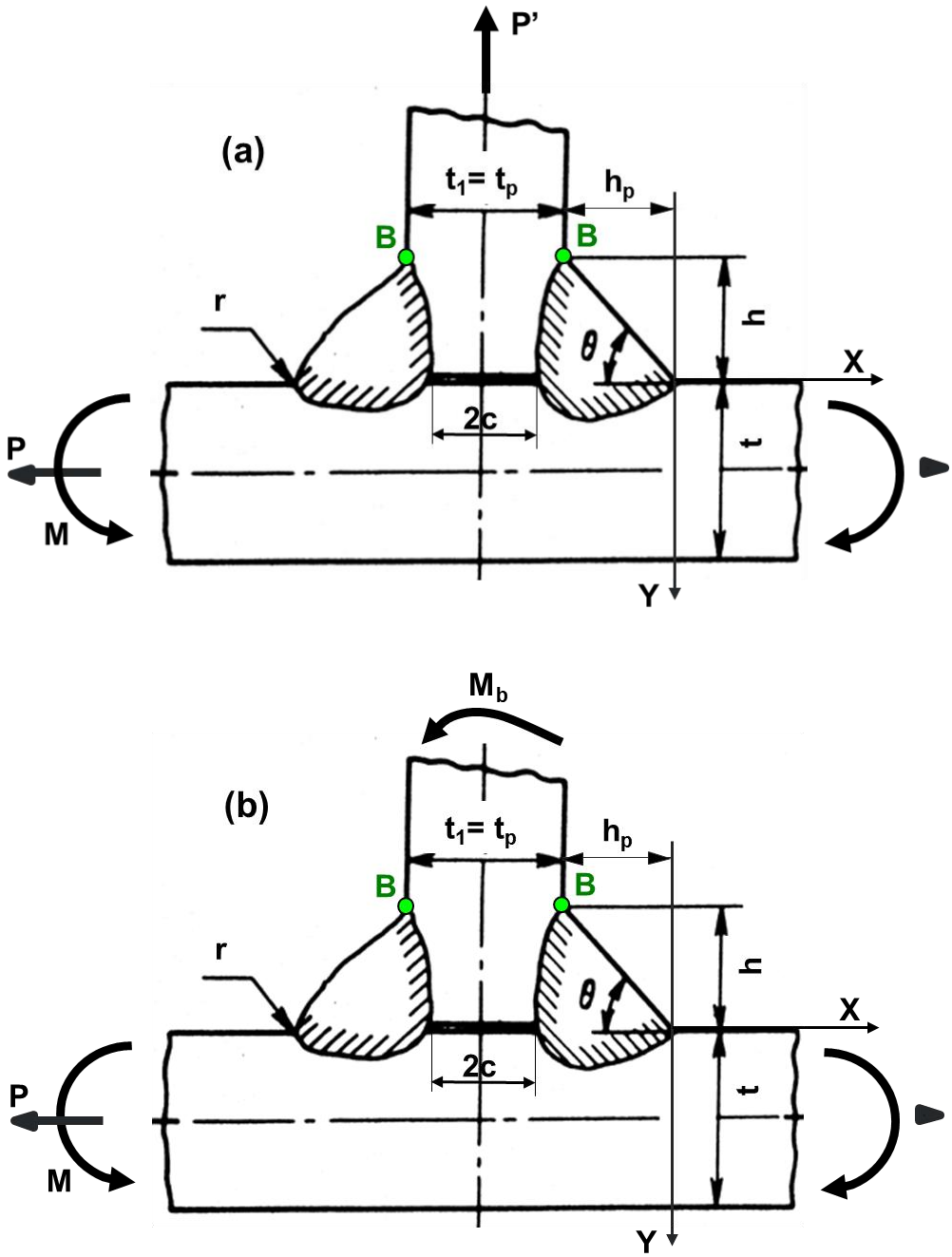

Figure 3-21: Symmetric fillet weld under (a) axial load (b) bending load

$$K_{t,hs}^{m} = \left\{ 1 + \frac{1 - exp\left(-0.9\left(\frac{\pi}{2} + \theta\right)\sqrt{\frac{W}{2h_p}} \right)}{1 - exp\left(-0.45\pi\sqrt{\frac{W}{2h_p}} \right)} X\ 2.2 \left[\frac{1}{2.8\left(\frac{W}{t_p}\right) - 2} X \frac{h_p}{r} \right]^{0.65} \right\} X$$

$$\left\{ 1 + 0.64 \frac{\left(\frac{2c}{t_p}\right)^2}{\frac{2h}{t_p}} - 0.12 \frac{\left(\frac{2c}{t_p}\right)^4}{\left(\frac{2h}{t_p}\right)^2} \right\};$$

$$where\ W = \left(t_p + 4h_p\right) + 0.3(t + 2h) \qquad (3.36)$$

$$K_{t,hs}^{b} = \left\{ 1 + \frac{1 - \exp\left(-0.9\left(\frac{\pi}{2} + \theta\right)\sqrt{\frac{W}{2h_p}} \right)}{1 - \exp\left(-0.45\pi\sqrt{\frac{W}{2h_p}} \right)} X \sqrt{\tanh\left(\frac{2t}{t_p + 2h_p} + \frac{2r}{t_p} \right)} \right\}$$

$$X\ \tanh\left[\frac{\left(\frac{2h_p}{t_p}\right)^{0.25}}{1 - \frac{r}{t_p}} \right] X \left[\frac{0.13 + 0.65\left(1 - \frac{r}{t_p}\right)^4}{\left(\frac{r}{t_p}\right)^{\frac{1}{3}}} \right] X \left\{ 1 + 0.64 \frac{\left(\frac{2c}{t_p}\right)^2}{\frac{2h}{t_p}} - 0.12 \frac{\left(\frac{2c}{t_p}\right)^4}{\left(\frac{2h}{t_p}\right)^2} \right\};$$

$$\text{where } W = \left(t_p + 4h_p\right) + 0.3(t + 2h) \qquad (3.37)$$

Both expressions have been validated for parameters: r/t_p = 0.025- 0.35, h_p/t_p = 0.5 - 1.0, $\theta = (\pi/9) - (\pi/3.6) = 20^o\text{-}50^o$.

3.7.3 Non-symmetric fillet welds

In order to calculate the stress concentration factor at the weld toe point A of a non-symmetric fillet weld (Figure 3-22), it is recommended to use the stress concentration expressions (3.38) and (3.39) for the axial and bending load respectively [69].

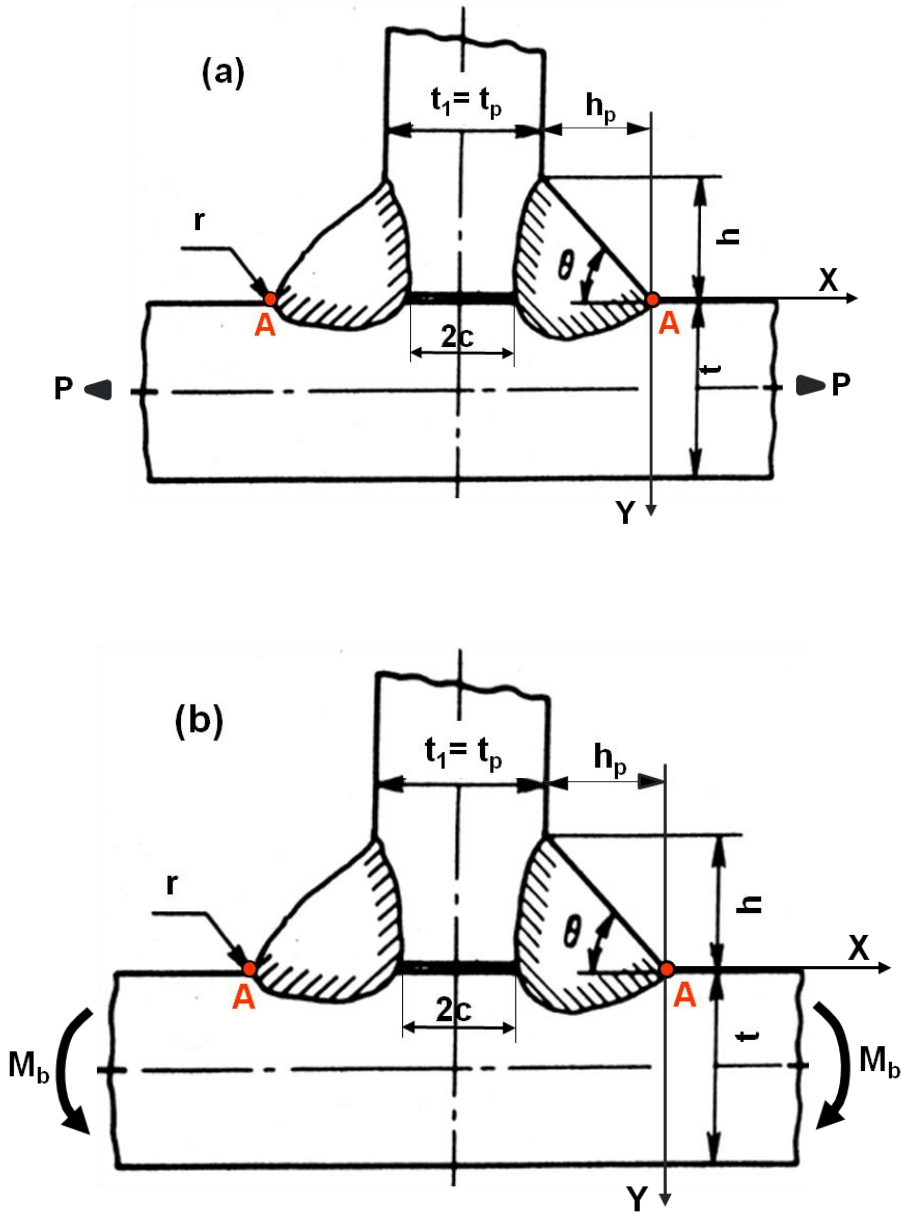

Figure 3-22: Non-Symmetric fillet weld under (a) axial load (b) bending load

$$K_{t,hs}^{m} = 1 + \frac{1 - \exp\left(-0.9\theta\sqrt{\frac{W}{2h}}\right)}{1 - \exp\left(-0.45\pi\sqrt{\frac{W}{2h}}\right)} X \left[\frac{1}{2.8\left(\frac{W}{t}\right) - 2} X \frac{h}{r}\right]^{0.65} \quad (3.38)$$

$$Where: W = (t + 2h) + 0.3(t_p + 2h_p)$$

$$K_{t,hs}^{b} = \left\{1 + \frac{1 - \exp\left(-0.9\theta\sqrt{\frac{W}{2h}}\right)}{1 - \exp\left(-0.45\pi\sqrt{\frac{W}{2h}}\right)} X\ 1.9 \sqrt{\tan\left(\frac{2t_p}{t + 2h} + \frac{2r}{t}\right)}\right\}$$

$$X\ \tanh\left[\frac{\left(\frac{2h}{t}\right)^{0.25}}{1 - \frac{r}{t}}\right] X \left[\frac{0.13 + 0.65\left(1 - \frac{r}{t}\right)^{4}}{\left(\frac{r}{t}\right)^{\frac{1}{3}}}\right];$$

$$\text{where } W = (t + 2h) + 0.3(t_p + 2h_p) \quad (3.39)$$

Both expressions have been validated for parameters: r/t_p = 0.025- 0.35, h_p/t_p = 0.5 - 1.0, $\theta = (\pi/9) - (\pi/3.6) = 20^o\text{-}50^o$.

3.8 Determination of the weld toe peak stress

The weld toe peak stress can be estimated using eqn. (3.7) which requires membrane and bending stresses determined using eqns. (3.20) and (3.33), along with the stress concentration factors for membrane and bending using eqns. (3.34) through (3.39), as applicable based on the geometry of the welded joint. The peak stress at the weld toe is needed to estimate the fatigue crack initiation life using the local strain life approach.

3.9 Determination of the through thickness stress distribution

The total fatigue life consists of the fatigue life crack initiation life and the fatigue crack propagation life. One of the critical pieces of information required for accurate fatigue crack growth analysis is the non-linear through-thickness stress distribution at the critical crack plane. Monahan [67] has derived a general expression for the through-thickness

stress distribution at a non-symmetric filet weld (Figure 3-22) as a function of stress concentration factors and the membrane and bending hot spot stress.

$$\sigma(y) = \left[\frac{K_{t,hs}^{m}\sigma_{hs}^{m}}{2\sqrt{2}}\frac{1}{G_m} + \frac{K_{t,hs}^{b}\sigma_{hs}^{b}}{2\sqrt{2}}\frac{1-2\left(\frac{y}{t}\right)^{0.89}}{G_b}\right]\left[\left(\frac{y}{r}+\frac{1}{2}\right)^{-\frac{1}{2}} + \frac{1}{2}\left(\frac{y}{r}+\frac{1}{2}\right)^{-\frac{3}{2}}\right] \quad (3.40)$$

Where:

$$G_m = 1 \qquad for\ \frac{y}{r} \leq 0.3$$

$$G_m = 0.06 + \frac{0.94\ exp(-E_m\,.\,T_m)}{1 + E_m^3 T_m^{0.8}.exp(-E_m\,.\,T_m^{1.1})}\ for\ \frac{y}{r} > 0.3$$

$$E_m = 1.05\ \theta^{0.18}\ \left(\frac{r}{t}\right)^{q}$$

$$q = -0.12\ \theta^{-0.62}$$

$$T_m = \frac{y}{t} - 0.3\frac{r}{t}$$

and

$$G_b = 1 \qquad for\ \frac{y}{r} \leq 0.4$$

$$G_m = 0.07 + \frac{0.93\ exp(-E_b\,.\,T_b)}{1 + E_b^3 T_b^{0.6}.exp(-E_b\,.\,T_b^{1.2})}\ for\ \frac{y}{r} > 0.4$$

$$E_b = 0.9\left(\frac{r}{t}\right)^{-\left(0.0026+\frac{0.0825}{\theta}\right)}$$

$$T_b = \frac{y}{t} - 0.4\frac{r}{t}$$

Equation (3.40) is valid over the entire thickness in the case of non-symmetric fillet welds and only over half the thickness in the case of symmetric fillet welds. Further the expression is valid for range of parameters.

$$\frac{\pi}{6} \leq \theta \leq \frac{\pi}{3} \quad and \quad \frac{1}{50} \leq \frac{r}{t} \leq \frac{1}{15} \quad and \quad 0 \leq y \leq t$$

An advantage in using such a through thickness stress distribution from un-cracked FE model lies in the fact that this helps to simulate fatigue crack growth behavior of any welded structure without the labor and time consuming extensive FE numerical analysis of cracked bodies. The through thickness stress distribution can be calculated by using stress concentration factors $K_{t,hs}^{m}$ and $K_{t,hs}^{b}$ and stresses σ_{hs}^{m} and σ_{hs}^{b} obtained from the 3D coarse mesh FE model described above by using Monahan eqn. (3.40).

3.10 Fatigue crack initiation and fatigue crack growth analysis

The fatigue crack initiation life (N_i) can be determined using the local strain life method as covered in section 2.5, accounting for the residual stress. The local strain life approach requires information about the peak stress at the weld toe, σ_{peak}, which can be determined using eqn. 3.7.

The fatigue crack propagation life (N_p) can be determined using the fracture mechanics method as covered in section 2.6, accounting for the residual stress. The fracture mechanics approach requires information about the non-linear through-thickness stress distribution at the critical section, $\sigma(y)$, which can be determined using eqn. 3.40.

The **total fatigue life (N_f)** can then be calculated as sum of the fatigue crack initiation life (N_i) and the fatigue crack propagation life (N_p).

Chapter 4 Validation of the Proposed Methodology

The proposed methodology has been validated through analysis of different weld joints representing variety of configurations in terms of the load and geometry combinations. At first, 3D coarse mesh FE analysis has been carried out for each selected weld joint with relatively large size finite elements, element size not significantly less than one quarter of the plate thickness (0.25t). As a next step, peak stress at the weld toe along with through thickness stress distribution at the critical section is calculated using the proposed GR3 method. Same stress values are obtained from 3D fine mesh FE analysis, which models the weld micro geometrical features in detail. To validate and to demonstrate the accuracy of the proposed methodology, the peak stress and the through-thickness stress distribution obtained according to the GR3 method are compared with those obtained from the fine FE mesh models. The commercial low carbon 1008 steel (plate) and ASTM A500 grade C (tube) steel materials were selected for preparing the welded test samples used for validation. The chemical, mechanical and fatigue properties for these steel grades are listed in Table 4-1, Table 4-2 and Table 4-3 respectively.

Table 4-1: Chemical composition (weight %)

	C	Mn	Si	P	S	Cr	Ni	B	Mo	Al
Low C 1008 steel	0.107	0.33	0.04	0.005	0.015	0.019	0.009	0.219	0.022	0.067
ASTM A500 Grade C steel	0.23	1.35		0.035	0.035					

Table 4-2: Mechanical Properties

	Low C 1008 steel	ASTM A500 Grade C steel
Monotonic yield strength, σ_{ys}	198 MPa	68.89 Ksi / 475 MPa
Ultimate tensile strength, σ_{uts}	351 MPa	79.0 Ksi / 545 MPa
Young's modulus, E	207447 MPa	29938 Ksi / 207000 MPa
Poisson's ratio, γ	0.3	0.3

Table 4-3: Fatigue parameters

	Low C 1008 steel	ASTM A500 Grade C steel
Fatigue strength coefficient (σ_f')	950.68 MPa	169.98 Ksi / 1172.1 MPa
Fatigue strength exponent (b)	-0.1319	-0.1197
Fatigue ductility coefficient (ε_f')	0.151	0.6488
Fatigue ductility exponent (c)	-0.4067	-0.5425
Cyclic strength coefficient (K')	1747.1 MPa	155.2 Ksi / 1070.0 MPa
Cyclic strain hardening exponent (n')	0.3219	0.1868

4.1 3D fine mesh FE reference models

The ideal method to validate the stress analysis results obtained using the proposed methodology would be to compare the same with the measured experimental stress/strain data. However the available experimental techniques (e.g. strain gauges etc.) do not have enough resolution to measure the stress/strain information at the weld toe. Hence, the validation of the proposed methodology has been done by comparing the results obtained from the GR3 method with that one obtained from the 3D fine mesh FE model. This validation approach was selected because of the fact that the weld micro geometrical features are accurately captured in the fine mesh FE model. The peak stress in the weld toe region and the stress distribution (gradient) through the thickness of critical section highly depend on the size of element used during FE analysis. In the case of 3D fine mesh FE model, the finite element size in the weld toe region (toe curvature also known as weld toe radius) is modeled at least one quarter of the weld toe or root radius, as applicable i.e. $\delta_{el} \leq r/4$. The 3D fine mesh FE model size becomes very large and requires high computational solving power. Model size can be optimized by modeling very small size elements ($\delta_{el} \leq r/4$) just within the region which is strongly affected by the weld toe radius. Usually it is sufficient to use very small size elements within the region of four weld toe radii, i.e. within an area of 4rx4r measured from the weld toe. Element size can be gradually increased as we go away from this region, helping to reduce the number of finite elements and at the same time can still accurately capture the stress gradient present at the weld toe and provide accurate results for the weld toe peak stress and the through thickness stress distribution. This is called as sub-structuring technique. However to

produce FE model with such a technique requires good skill and experience and still consumes significant time.

4.2 The Gusset weld joint – Symmetric welds

3D FE model becomes essential if the structure cannot be represented well by using 2D model. Gusset weld joint, one of the first joint selected for validation, shown in Figure 3-14 is an example of geometry which cannot be captured by 2D model and hence is modeled as 3D FE model as shown in Figure 4-1. The base plate is fixed at all the four corners, i.e. all degrees of freedom are constrained at each corner of the plate. The vertical attachment plate of the gusset joint is subjected to lateral out-of plane force P=1000N. 3D coarse mesh FE model is prepared with element size equal to one quarter of the plate thickness ($\delta_{el} < 0.25t$) i.e. four elements have been used through the thickness for 4mm thick plates.

Due to the applied boundary conditions and the lateral force, significant bending stresses are generated at the weld toe located at the bottom of the vertical attachment plate as shown by normal stress component, σ_{yy} plot in Figure 4-2. Weld toe location with highest stress value of normal stress component as shown in Figure 4-2 is selected for detailed analysis. The through thickness stress distribution is extracted from the section at this hot spot location and is shown in Figure 4-3.

Next, the membrane and the bending hot spot stresses are calculated as per the procedure described in section 3.6 utilizing the through thickness stress distribution obtained from the 3D coarse mesh FE model of the gusset joint. The membrane hot spot stress is determined as an average stress over the entire plate thickness (eqn. 3.20 and eqn. 4.1) including all nodal stresses shown in Figure 4-3.

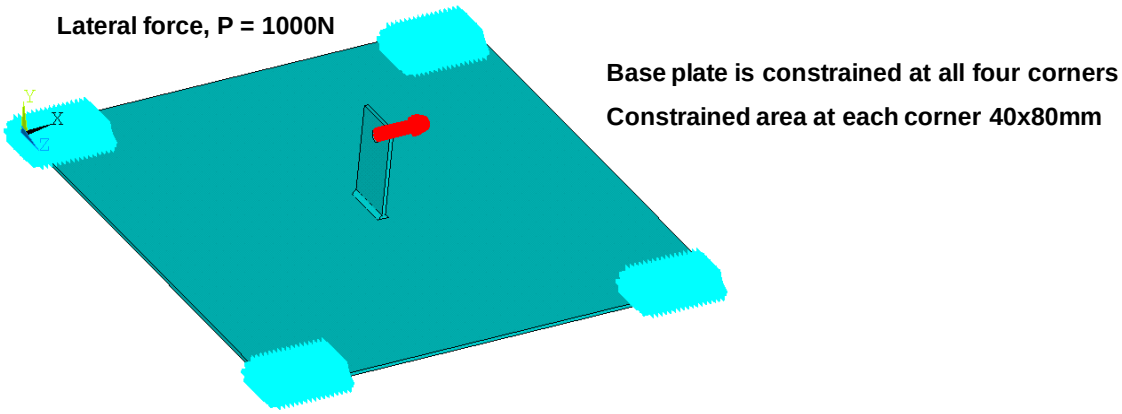

Figure 4-1: Gusset joint under out-of-plane bending load

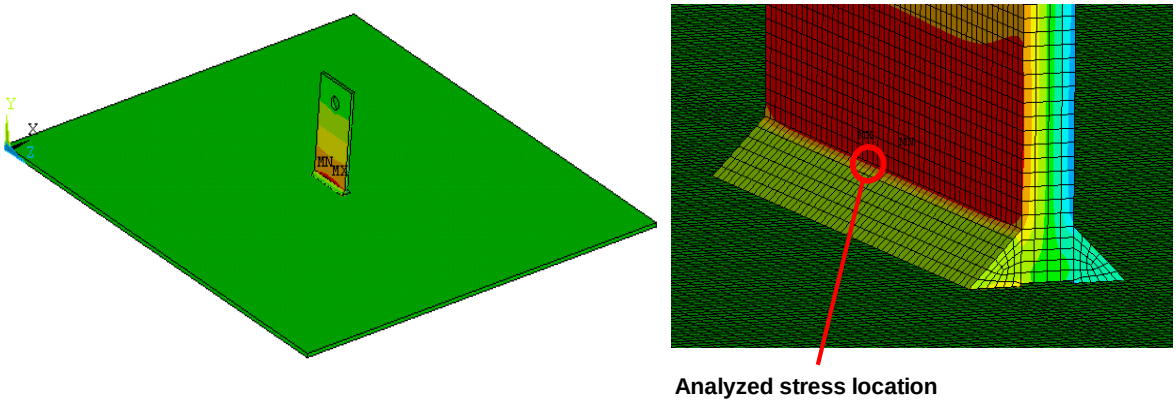

Figure 4-2: Normal stress component σ_{yy} plot and identified hot spot location at weld toe

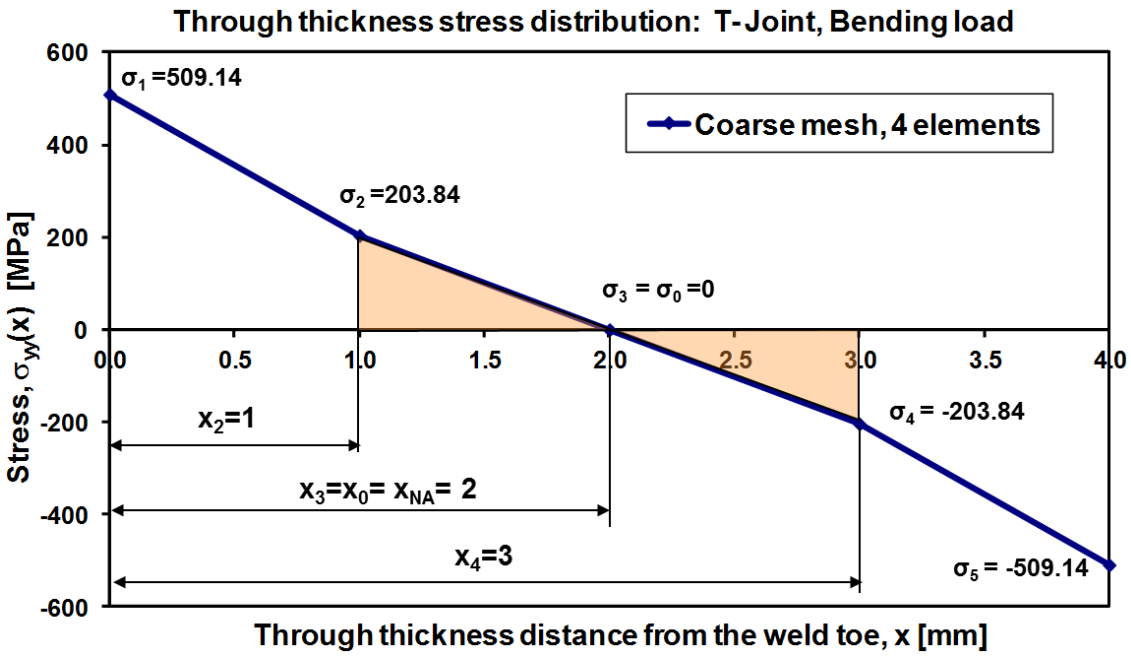

Figure 4-3: Through thickness stress distribution (nodal stresses) obtained from the 3D coarse mesh FE model - Symmetric weld gusset joint

$$\sigma_{hs}^{m} = \frac{1}{t}\left[\frac{(\sigma_2 + \sigma_1)(x_2 - x_1)}{2} + \frac{(\sigma_0 + \sigma_2)(x_0 - x_2)}{2} + \frac{(\sigma_4 + \sigma_0)(x_4 - x_0)}{2} + \frac{(\sigma_5 + \sigma_4)(x_5 - x_4)}{2}\right] \tag{4.1}$$

$$= \frac{1}{4}\left[\frac{(203.84 + 509.14)(1 - 0)}{2} + \frac{(0 + 203.84)(2 - 1)}{2} + \frac{(-203.84 + 0)(3 - 2)}{2} + \frac{(-509.14 - 203.84)(4 - 3)}{2}\right] = 0$$

As per the proposed method, the bending hot spot stress is calculated based on only the middle part of the coarse mesh stress distribution from Figure 4-3. At first, the bending moment contribution M_c is determined using the engineering method of eqn. (3.22).

$$M_c = \frac{\sigma_2 |x_0 - x_2|}{2}\frac{2}{3}(x_0 - x_2) + \frac{\sigma_4 |x_0 - x_4|}{2}\frac{2}{3}(x_0 - x_4)$$

$$= \frac{\sigma_2 |x_0 - x_2|(x_0 - x_2)}{3} + \frac{\sigma_4 |x_0 - x_4|(x_0 - x_4)}{3} \tag{4.2}$$

$$= \frac{203.84|2-1|(2-1)}{3} + \frac{-203.84|2-3|(2-3)}{3} = 135.89\ Nmm$$

The resultant bending moment M_b is calculated using eqn. 3.32 as follow:

$$M_b = 10\ M_c = 10 \times 135.89 = 1358.9\ Nmm \tag{4.3}$$

Finally, the hot spot bending stress is determined as in eqn. (4.4).

$$\sigma_{\text{hs}}^{\text{b}} = \frac{6\ M_b}{t^2} = \frac{6\ X\ 1358.9}{4^2} = 509.58\ MPa \tag{4.4}$$

Geometry unique stress concentration factors are calculated based on the geometry (dimensions) of the selected gusset weld joint (Figure 3-14) as demonstrated in Figure 3-21 and described in the form of eqns. (3.36) and (3.37) for the membrane and bending modes of loading respectively. The welds were made with only partial penetration and therefore it is assumed that there is a gap between the gusset and the base plate, of the size 2c=4 mm.

$$K_{\text{t,hs}}^{m} = 2.686 \text{ and } K_{\text{t,hs}}^{b} = 2.003 \tag{4.5}$$

The peak stress at the weld toe is subsequently calculated from eqn. (3.7).

$$\sigma_{\text{peak}} = \sigma_{\text{hs}}^{\text{m}}\ K_{\text{t,hs}}^{m} + \sigma_{\text{hs}}^{\text{b}}\ K_{\text{t,hs}}^{b} = 0 \times 2.686 + 509.58 \times 2.003 = 1020.72\ MPa \tag{4.6}$$

In addition, the bending moment M_c and subsequent parameters can easily be determined using (eqns. 3.26 through 3.33 and eqn. 3.7), when programmed in the excel spreadsheet. Stress distribution obtained from 3D coarse mesh FE analysis along with dimensions of the weld joint are the inputs needed for the excel macro to automatically calculate $M_c, M_b, \sigma_{hs}^{b}, \sigma_{hs}^{m}$ and finally σ_{peak} peak stress at weld toe. The advantage of using this excel macro lies in the fact than once the programming has been done for calculating the bending moment contribution M_c induced by any stress distribution around the neutral axis then no additional effort is required with the interpretation of eqn. 3.22.

The hot spot membrane and bending stresses along with the appropriate stress concentration factors have also been used for the determination of the through thickness stress distribution according to Monahan's eqn. 3.40 as shown in Figure 4-4.

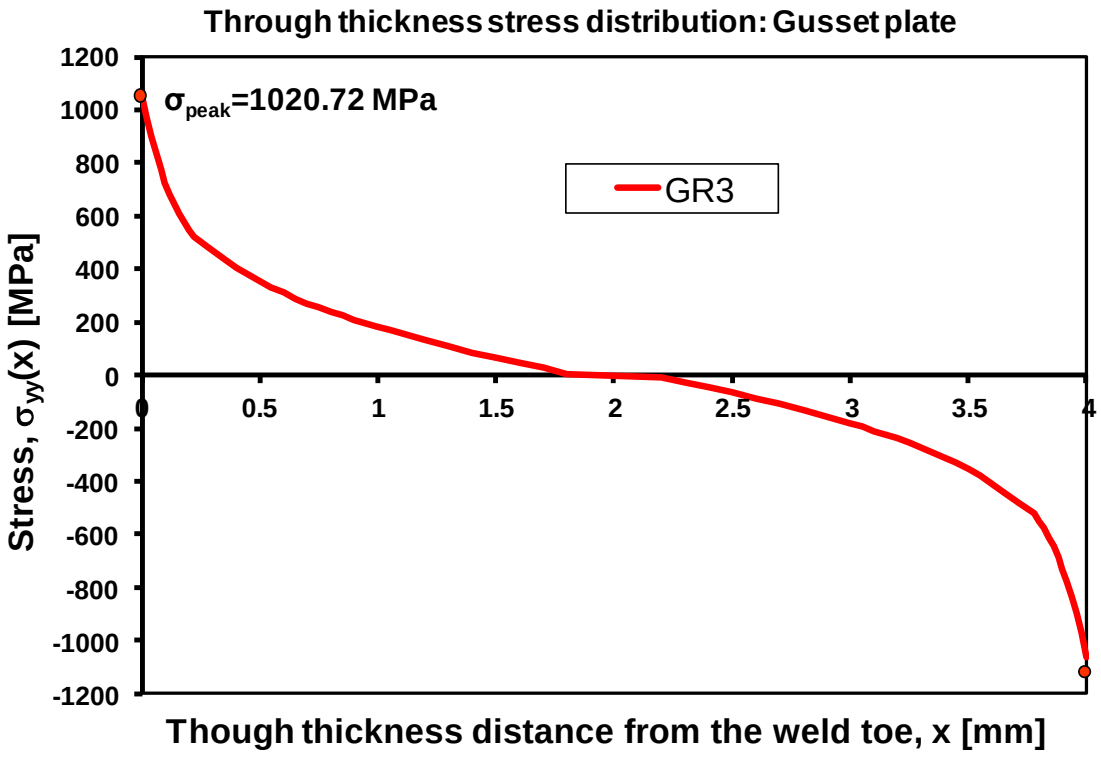

Figure 4-4: The through thickness stress distribution obtained from the coarse FE mesh model using GR3 method

4.2.1 Fine vs. Coarse mesh solid FE model

The validation of the proposed GR3 method along with its capability to produce accurate results has been demonstrated in this section by comparing results of 3D coarse mesh FE model from GR3 method against the results obtained from 3D fine mesh FE model for the gusset joint with symmetric welds. The same gusset weld joint under the same load configuration (Figure 3-14 and Figure 4-1) has been analyzed using very fine finite element mesh enabling appropriate modeling of the weld toe radius (Figure 4-5) and other micro-geometrical features. The through thickness stress distribution at the selected location (Figure 4-5) is plotted in Figure 4-6. In addition the predicted stress distribution according to the GR3 procedure has also been superposed.

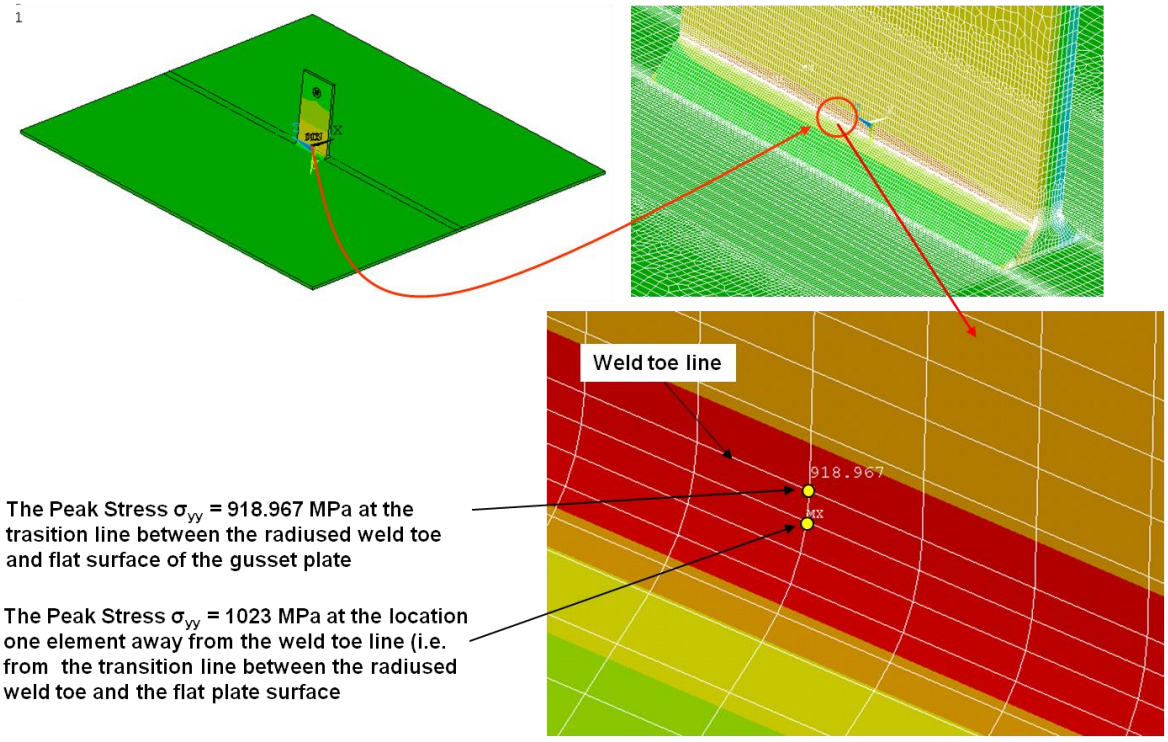

Figure 4-5: Details of the fine FE mesh model of the gusset welded joint

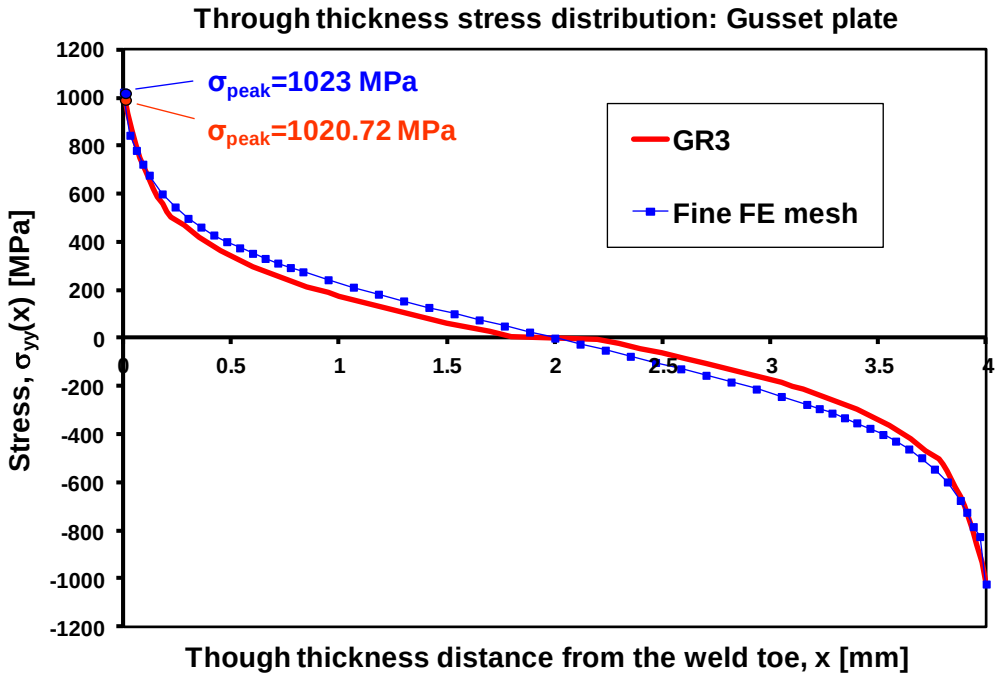

Figure 4-6: Comparison of through thickness stress distribution obtained from the coarse mesh FE model using the GR3 method and the fine FE mesh model

Figure 4-6 clearly shows that the profile of two stress distributions match each other very well proving that the coarse FE mesh procedure (GR3) can provide reliable stress information for reasonably accurate prediction of both the peak stress and the non-linear through-thickness stress distribution. The difference between the predicted GR3 peak stress (Figure 4-6) and that one obtained from the fine mesh FE model is less than 1%.

An alternative way of proving the validity of the proposed method is to compare the linearized stress distribution obtained from the GR3 method with that one resulting from the linearization of the fine mesh FE stress data. In order to find the linearized through thickness stress distribution it is sufficient to determine stresses on both sides of the plate.

$$\text{at } x = 0 \qquad \sigma_{hs}^{s1} = \sigma_{hs}^{m} + \sigma_{hs}^{b}$$

$$\text{at } x = t \qquad \sigma_{hs}^{s2} = \sigma_{hs}^{m} - \sigma_{hs}^{b} \tag{4.7}$$

The linearized stress (or the hot spot stress) on side 1 (s1) and side 2 (s2) for symmetric welds located on both sides of the gusset plate has been determined by using the coarse FE mesh stress data and the GR3 procedure as below:

$$\text{at } x = 0 \qquad \sigma_{hs}^{s1} = \sigma_{hs}^{m} + \sigma_{hs}^{b} = 0 + 509.58 = 509.58 \text{ MPa}$$

$$\text{at } x = 4 \qquad \sigma_{hs}^{s2} = \sigma_{hs}^{m} - \sigma_{hs}^{b} = 0 - 509.58 = -509.58 \text{ MPa} \tag{4.8}$$

Analogous stresses obtained by the linearization of the fine mesh FE stress data are:

$$\text{at } x = 0 \qquad \sigma_{hs}^{s1} = \sigma_{hs}^{m} + \sigma_{hs}^{b} = 0 + 584.86 = 584.86 \text{ MPa}$$

$$\text{at } x = 4 \qquad \sigma_{hs}^{s2} = \sigma_{hs}^{m} - \sigma_{hs}^{b} = 0 - 584.86 = -584.86 \text{ MPa} \tag{4.9}$$

A comparison of both linearized stress distributions plotted in Figure 4-7 shows that the difference between these two distributions is relatively small and the difference between those two linearized stresses is around 12%. It is interesting that this error has been compensated by the stress concentration expressions and the Monahan equation.

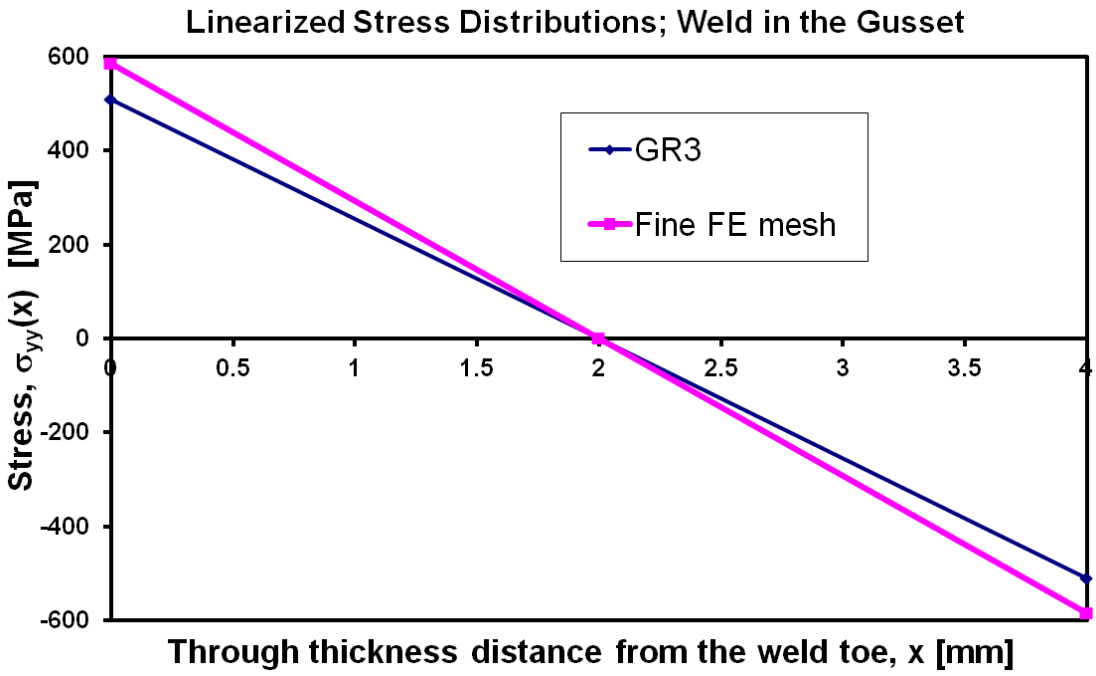

Figure 4-7: Linearized through thickness stress distributions in the gusset weld joint

4.3 The Gusset weld joint – Non symmetric weld

This section uses the same gusset weld joint as in the previous section for validation purpose but with a different loading mode (Figure 4-8), i.e. under the bending in-plane force P=1000 N applied to the gusset. However, the base plate is constrained in exactly the same manner i.e. all degrees of freedom are fixed at each corner of the plate. Based on the proposed method, near the weld toe region FE mesh (Figure 4-9) has finite element size equal to quarter of the plate thickness (δ_{el} < 0.25t). Extracted stress distribution through the thickness at the location marked in Figure 4-9 is shown in Figure 4-10.

Next, the membrane and the bending hot spot stresses are calculated as per the procedure described in section 3.6 utilizing the through thickness stress distribution obtained from the 3D coarse mesh FE model of the gusset joint with non-symmetric weld. The membrane hot spot stress is determined as an average stress over the entire plate thickness (eqn. 3.20 and eqn. 4.10) and all nodal stresses shown in Figure 4-10 are accounted during calculation.

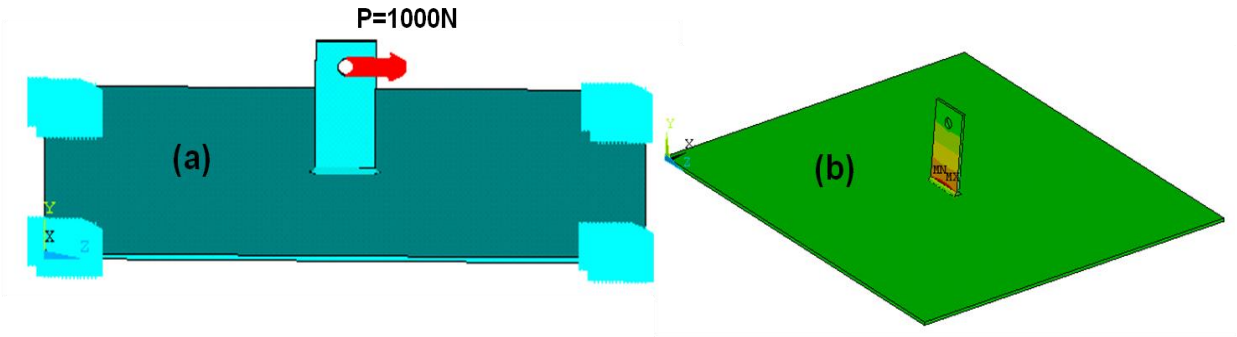

Base plate is constrained (zero displacement) at four corners. Constrained area at each corner 40x80mm

Figure 4-8: Gusset joint (a) under in-plane bending load (b) 3D FE model stress plot

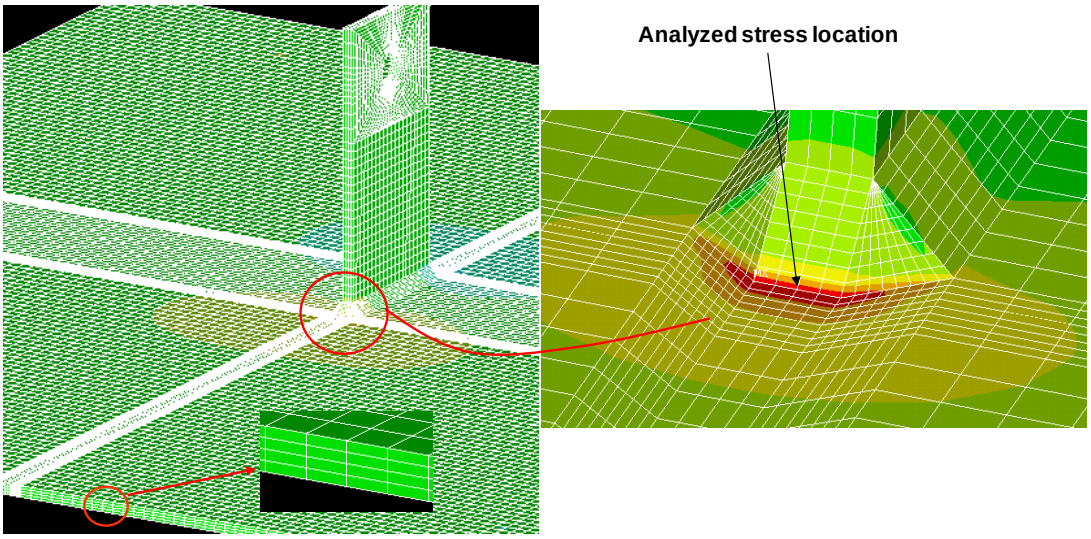

Figure 4-9: Identified hot spot location at weld toe from 3D coarse mesh analysis

$$\sigma_{hs}^{m} = \frac{1}{t}\left[\frac{(\sigma_2 + \sigma_1)(x_2 - x_1)}{2} + \frac{(\sigma_3 + \sigma_2)(x_3 - x_2)}{2} + \frac{(\sigma_4 + \sigma_3)(x_4 - x_3)}{2} + \frac{(\sigma_5 + \sigma_4)(x_5 - x_4)}{2}\right] \quad (4.10)$$

$$= \frac{1}{4}\left[\frac{(85.13 + 269.58)(1 - 0)}{2} + \frac{(-2.04 + 85.13)(2 - 1)}{2} + \frac{(-90.31 - 2.04)(3 - 2)}{2} + \frac{(-188.34 - 90.31)(4 - 3)}{2}\right]$$

$$= 8.35\ MPa$$

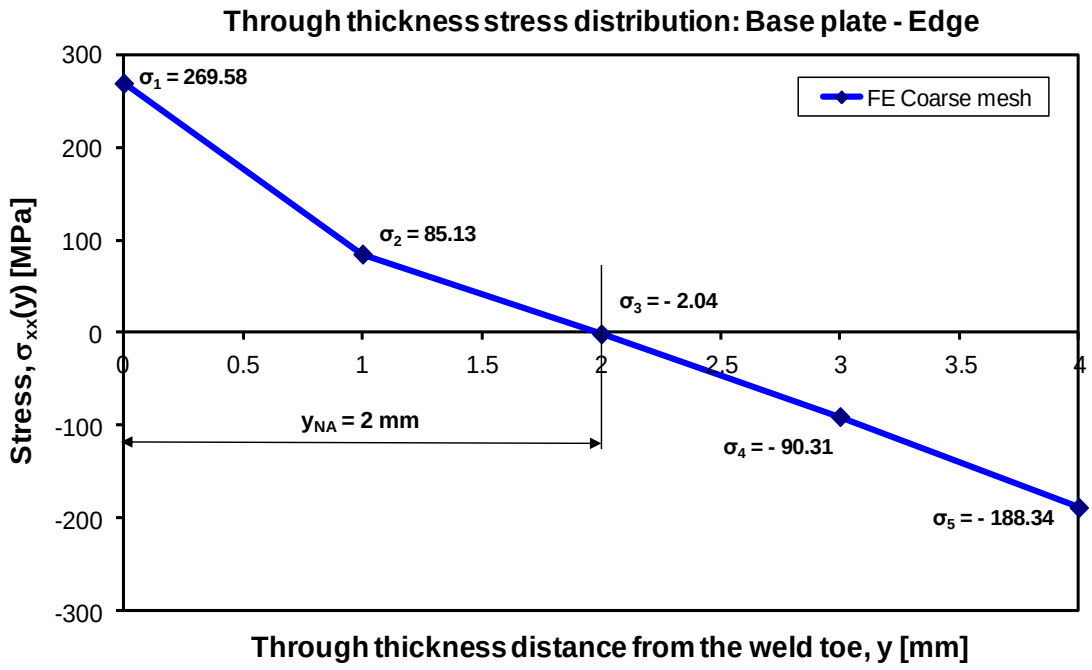

Figure 4-10: Through thickness stress distribution (nodal stresses) obtained from the 3D coarse mesh FE model – Non-symmetric weld gusset joint

As per the proposed method, the bending hot spot stress is calculated based on only the middle part ($1 \leq y \leq 3$ mm) of the coarse mesh stress distribution from Figure 4-10. At first, the bending moment contribution M_c is calculated using the excel macro using eqns. (3.26, 3.29, and 3.30).

M_c=58.48 Nmm

The resultant bending moment is calculated according to eqn. (3.32).

$$M_b = 10\, M_c = 10 \times 58.48 = 584.8 \text{ Nmm} \quad (4.11)$$

The hot spot bending stress is determined from eq. (3.33).

$$\sigma_{hs}^{b} = \frac{6\, M_b}{t^2} = \frac{6 \text{ X } 584.8}{4^2} = 219.3 \text{ MPa} \quad (4.12)$$

Geometry unique stress concentration factors are calculated based on the geometry (dimensions) of the selected gusset weld joint (Figure 3-14) as demonstrated in Figure 3-22 and described in the form of eqns. (3.38) and (3.39) for the membrane and bending modes of loading respectively. As recommended by Chattopadhyay [68], in the case of geometrical configurations as that one shown in Figure 4-8, assume the dimension 't_p' to

be equal to three weld legs (t_p=3h) if the real dimension t_p is greater than 3h. If the real dimension is t_p < 3h then the actual dimension t_p should be used in the estimation of the SCF. Therefore, the effective thickness of the attachment is calculated as tp=3x4=12 mm.

$$K^{m}_{t,hs} = 1.581 \quad \text{and} \quad K^{b}_{t,hs} = 2.166 \tag{4.13}$$

The peak stress at the weld toe is subsequently calculated using eqn. (3.7).

$$\sigma_{peak} = \sigma^{m}_{hs}\ K^{m}_{t,hs} + \sigma^{b}_{hs}\ K^{b}_{t,hs} = 8.35 \times 1.581 + 219.3 \times 2.166 = 488.38\ \text{MPa} \tag{4.14}$$

The hot spot membrane and bending stresses along with the appropriate stress concentration factors have also been used for the determination of the through thickness stress distribution according to Monahan's eqn. 3.40 as shown in Figure 4-11.

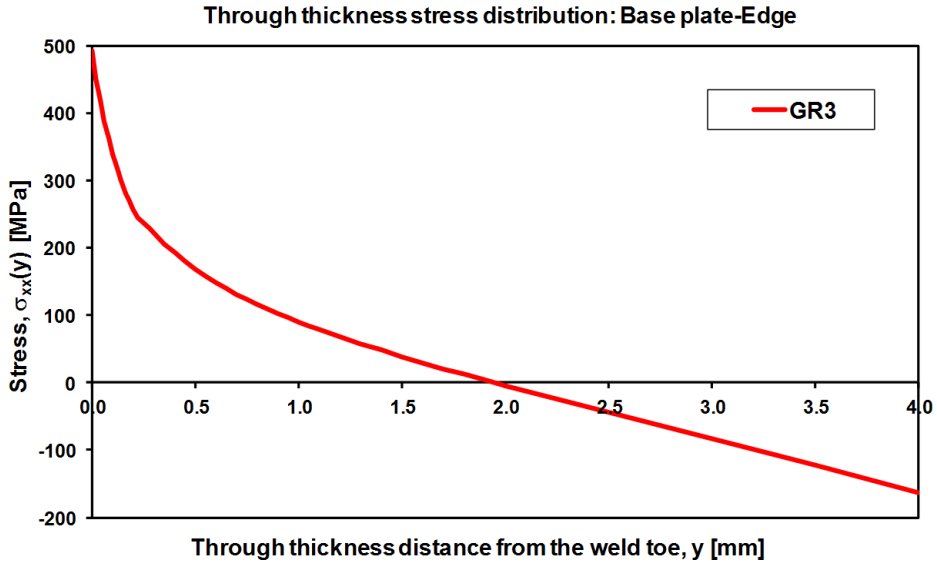

Figure 4-11: The through thickness stress distribution obtained from the coarse FE mesh model using GR3 method

4.3.1 Fine vs. Coarse mesh solid FE model

The validation of the proposed GR3 method along with its capability to produce accurate results has been demonstrated in this section by comparing results from 3D coarse mesh FE model using GR3 method against the results obtained from 3D fine mesh FE model for the gusset joint with non-symmetric welds. The same gusset weld joint under the same load configuration (Figure 3-14 and Figure 4-8) has been analyzed using very fine

finite element mesh enabling appropriate modeling of the weld toe radius (Figure 4-12) and other micro-geometrical features. The through thickness stress distribution at the selected location (Figure 4-9) is plotted in Figure 4-13. In addition the predicted stress distribution according to the GR3 procedure has been shown as well.

Figure 4-13 clearly shows that the profile of two stress distributions match each other very well proving that the coarse FE mesh procedure (GR3) can provide reliable stress information for reasonably accurate prediction of both the peak stress and the non-linear through-thickness stress distribution. The difference between the predicted GR3 peak stress of 488.38 MPa (Figure 4-13) and that one obtained from the fine mesh FE model, 420 MPa, is less than 14%.

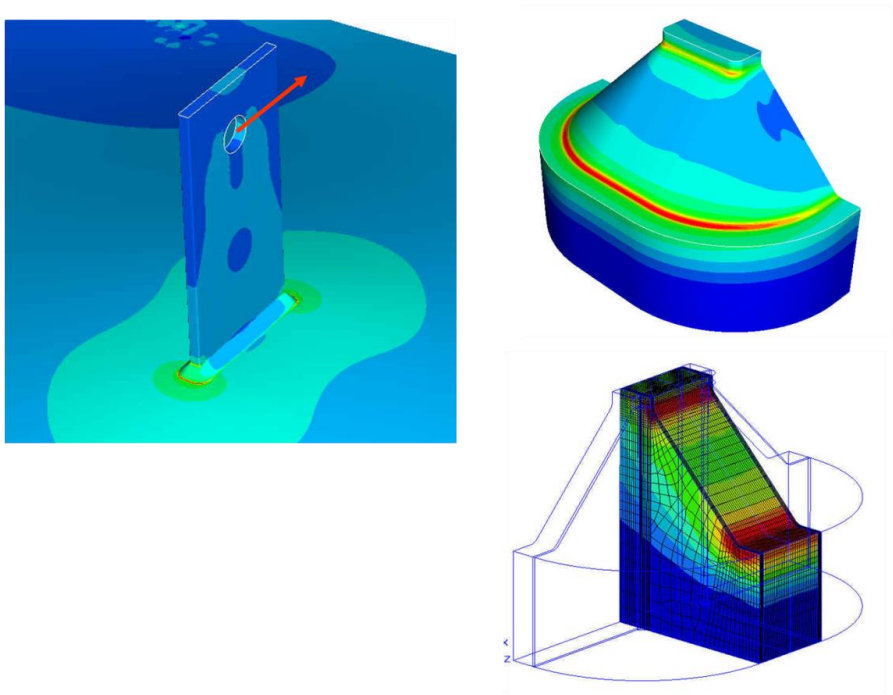

Figure 4-12: Details of the fine FE mesh model of the gusset edge fillet welded joint

An alternative way of proving the validity of the proposed method is to compare the linearized stress distribution obtained from the GR3 method with that one resulting from the linearization of the fine mesh FE stress data. In order to find the linearized through thickness stress distribution it is sufficient to determine stresses on both sides of the plate. The characteristic linearized stresses on both sides of the base plate determined using the coarse FE mesh stress data and the GR3 procedure are (refer eqn. 4.7):

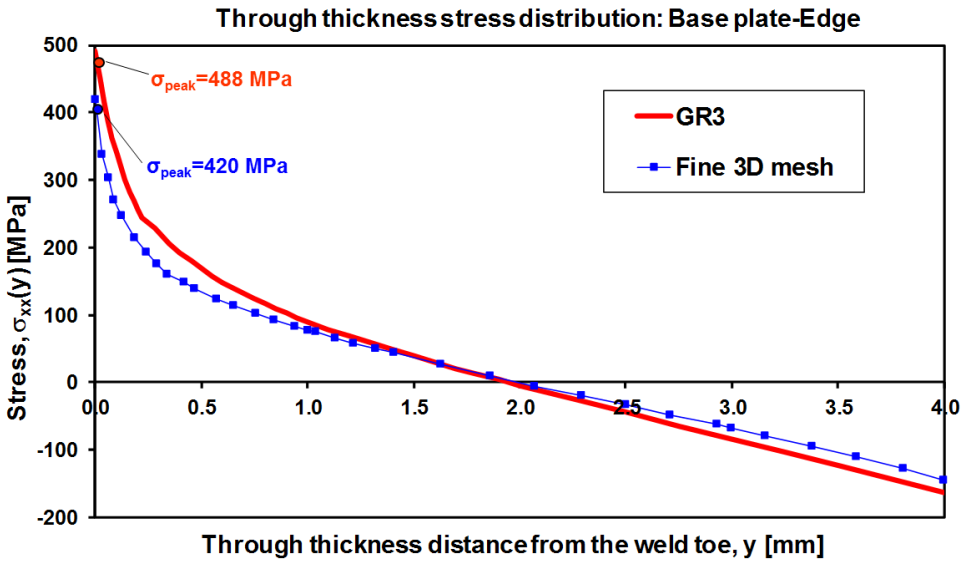

Figure 4-13: Comparison of through thickness stress distribution obtained from the coarse mesh FE model using the GR3 method and the fine FE mesh model of edge fillet weld gusset joint

$$\text{at } y = 0 \qquad \sigma_{hs}^{s1} = \sigma_{hs}^{m} + \sigma_{hs}^{b} = 8.35 + 219.30 = 227.65 \text{ MPa}$$

$$\text{at } y = 4 \qquad \sigma_{hs}^{s2} = \sigma_{hs}^{m} - \sigma_{hs}^{b} = 8.35 - 219.30 = -210.95 \text{ MPa} \qquad (4.15)$$

Analogous stresses obtained by the linearization of the fine mesh FE stress data are:

$$\text{at } y = 0 \qquad \sigma_{hs}^{s1} = \sigma_{hs}^{m} + \sigma_{hs}^{b} = 14.00 + 174.69 = 188.69 \text{ MPa}$$

$$\text{at } y = 4 \qquad \sigma_{hs}^{s2} = \sigma_{hs}^{m} - \sigma_{hs}^{b} = 14.00 - 174.69 = -160.69 \text{ MPa} \qquad (4.16)$$

A comparison of both linearized stress distributions plotted in Figure 4-14 shows that the difference between these two distributions at the weld toe position (y=0) is 18%. The difference is due to the fact that in this particular case the coarse and fine mid-thickness stress distributions are not the same unlike other cases. In this particular case the coarse mesh stresses in the mid-thickness region are higher (Figure 4-15) than those obtained from the fine 3D FE mesh analysis, which is probably because of the way the weld has been modeled at the edge in the coarse mesh FE model shown in Figure 4-9 (far different than reality). Therefore, the hot spot bending stresses are subsequently overestimated. It seems that the coarse mesh FE modeling in similar situations may need further studies by

improving the coarse mesh model to better capture the weld stiffness at macro level. Although it is interesting to note that the results are on the conservative side with the proposed method and the current coarse mesh model used in this research.

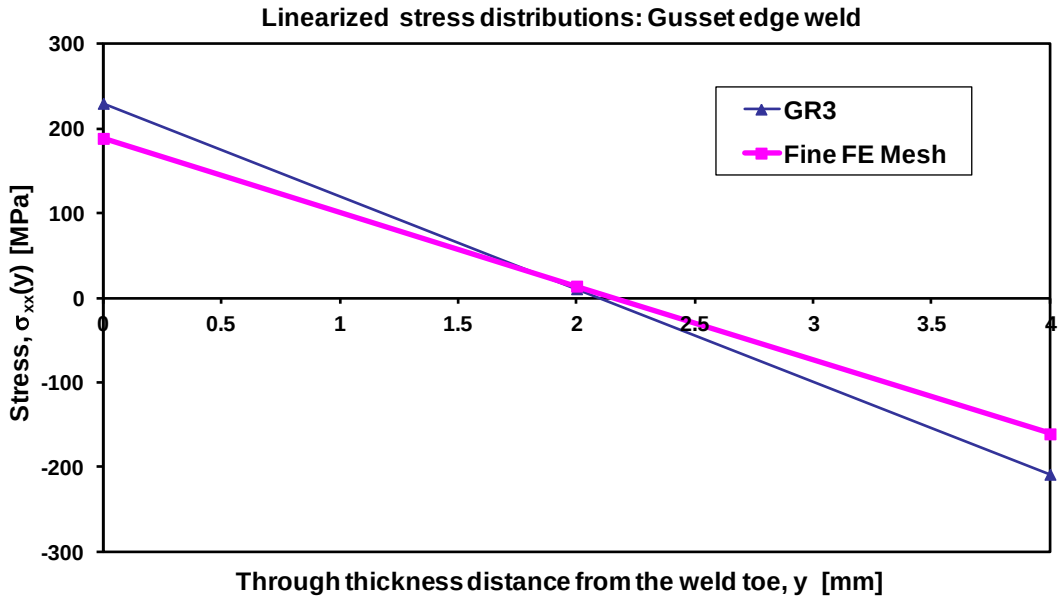

Figure 4-14: Linearized through thickness stress distributions in gusset edge weld joint

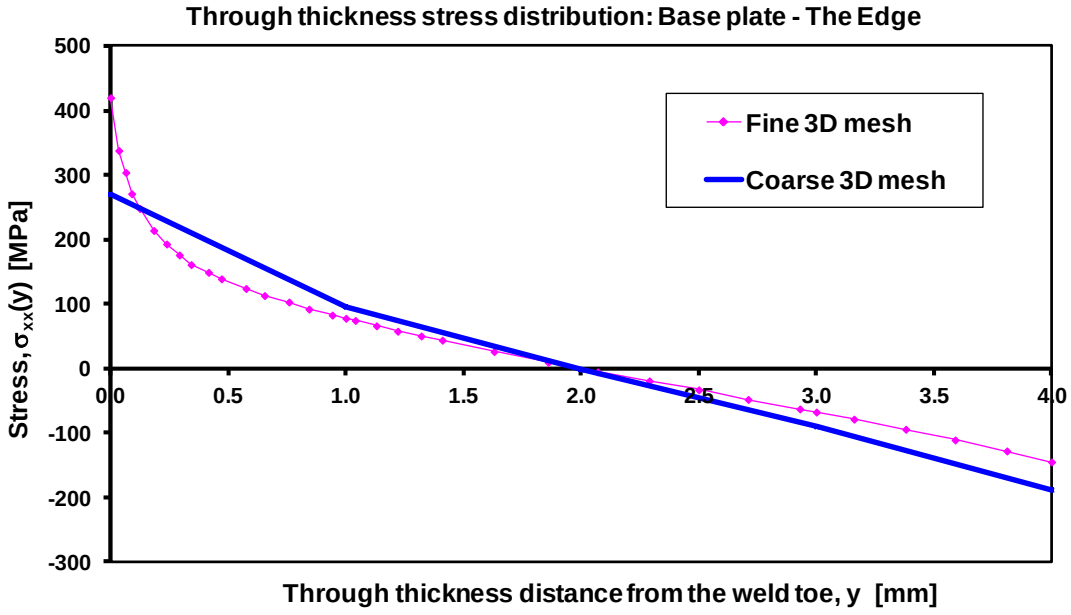

Figure 4-15: The coarse and fine FE through thickness stress distributions in the base plate of the gusset edge weld joint

4.4 The Tube-on-plate weld joint under axial load

This section uses the tube-on-plate weld joint for validation purpose under pure axial load (Figure 4-16), P_t=500 N, P_b=0 N applied to the tube. The base plate is constrained by fixing all degrees of freedom at each corner of the plate. Near the weld toe region FE mesh (Figure 4-17) has finite element size equal to one fifth of the plate thickness i.e. five elements per thickness have been used, as recommended in section 3.5 i.e. ($\delta_{el} \leq 0.25t$). Extracted stress distribution through the thickness from section S-I marked in Figure 4-17 is shown in Figure 4-18. Because five FE elements per thickness are used for the creation of the FE model, the stresses corresponding to co-ordinates y=0.25t and y=0.75t are not directly available from coarse mesh FE model and have been found by extrapolating the FE stress data as shown in Figure 4-18.

Next, the membrane and the bending hot spot stresses are calculated as per the procedure described in section 3.6 utilizing the through thickness stress distribution obtained from the 3D coarse mesh FE model. The membrane hot spot stress is determined as an average stress over the entire plate thickness (eqn. 3.20) and all nodal stresses shown in Figure 4-18 are accounted during calculation.

$$\sigma_{hs}^{m} = \frac{1}{t}\left[\begin{array}{c}\frac{(\sigma_2 + \sigma_1)(y_2 - y_1)}{2} + \frac{(\sigma_3 + \sigma_2)(y_3 - y_2)}{2} \\ + \frac{(\sigma_4 + \sigma_3)(y_4 - y_3)}{2} + \frac{(\sigma_5 + \sigma_4)(y_5 - y_4)}{2} + \frac{(\sigma_6 + \sigma_5)(y_6 - y_5)}{2}\end{array}\right] \quad (4.17)$$

$$= \frac{1}{6.25}\left[\begin{array}{c}\frac{(36.71 + 15.33)(1.25 - 0)}{2} + \frac{(4.64 + 15.33)(2.5 - 1.25)}{2} \\ + \frac{(-5.4 + 4.64)(3.75 - 2.5)}{2} + \frac{(-15.30 - 5.4)(5 - 3.75)}{2} \\ + \frac{(-25.93 - 15.3)(6.25 - 5)}{2}\end{array}\right] = 0.93\ MPa$$

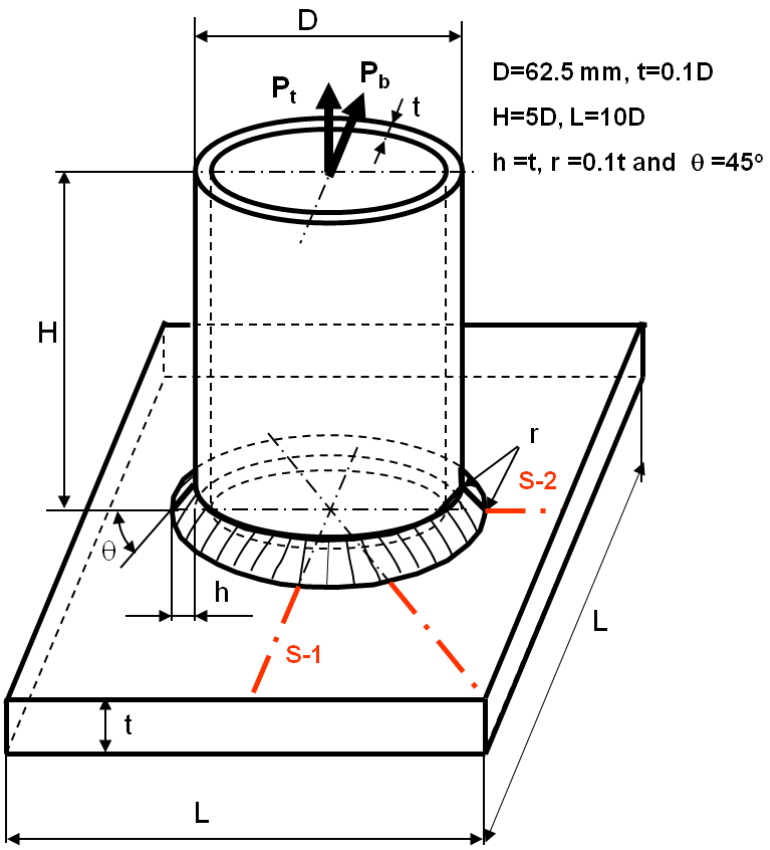

Figure 4-16: Geometry and dimensions of the tube on plate weld joint

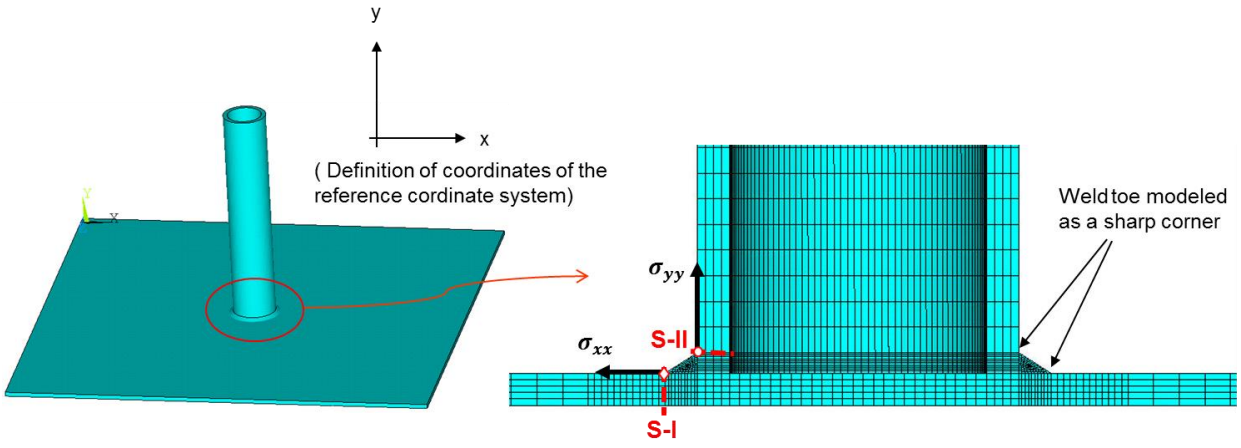

Figure 4-17: The coarse FE mesh model of the tube-on-plate welded joint (left picture) and cross sections of interest near the weld toe and stress notation (right picture)

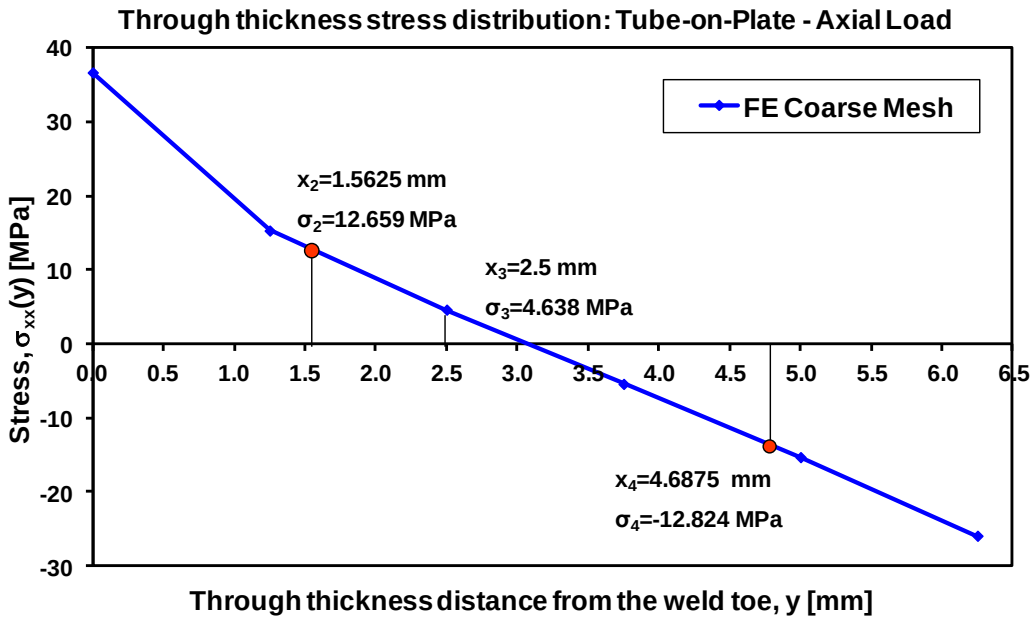

Figure 4-18: Through thickness stress distribution (nodal stresses) obtained from the 3D coarse mesh FE model – Tube on plate joint under axial load

As per the proposed method, the bending hot spot stress is calculated based on only the middle part ($1.5625 \leq x \leq 4.6875$ mm) of the coarse mesh stress distribution from Figure 4-18. At first, the bending moment contribution M_c is calculated using the excel macro using eqns. 3.26, 3.29, and 3.30.

$$M_c = 20.615 \text{ Nmm} \tag{4.18}$$

The resultant bending moment is calculated according to eqn. 3.32.

$$M_b = 10\, M_c = 10 \times 20.6157 = 206.157 \text{ Nmm} \tag{4.19}$$

The hot spot bending stress is determined from eqn. 3.33.

$$\sigma_{hs}^{b} = \frac{6\, M_b}{t^2} = \frac{6 \text{ X } 206.157}{6.25^2} = 31.67 \text{ MPa} \tag{4.20}$$

Geometry unique stress concentration factors are calculated based on the geometry (dimensions) of the selected weld joint (Figure 4-16) as demonstrated in Figure 3-22 and described in the form of eqns. (3.38) and (3.39) for the membrane and bending modes of loading respectively. The 't_p' dimension is assumed equal to the tube wall thickness, i.e. t_p =6.25 mm.

$$K_{t,hs}^{m} = 1.784 \quad \text{and} \quad K_{t,hs}^{b} = 2.203 \tag{4.21}$$

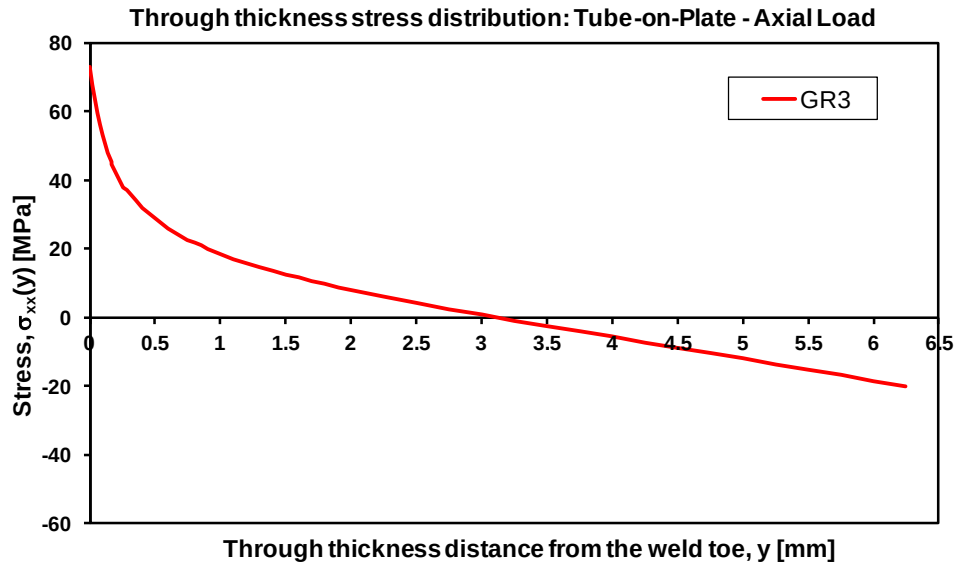

Figure 4-19: The through thickness stress distribution obtained from the coarse FE mesh model using GR3 method

The peak stress at the weld toe is subsequently calculated using eqn. 3.7.

$$\sigma_{peak} = \sigma_{hs}^{m} \, K_{t,hs}^{m} + \sigma_{hs}^{b} \, K_{t,hs}^{b} = 0.932 \times 1.784 + 31.665 \times 2.203 = 71.42 \text{ MPa} \tag{4.22}$$

The hot spot membrane and the bending stresses along with the appropriate stress concentration factors have also been used for the determination of the through thickness stress distribution according to Monahan's eqn. 3.40 as shown in Figure 4-19.

4.4.1 Fine vs. Coarse mesh solid FE model

The validation of the proposed GR3 method along with its capability to produce accurate results has been demonstrated in this section by comparing results from 3D coarse mesh FE model using GR3 method against the results obtained from 3D fine mesh FE model for the tube on plate joint under axial loading. The same weld joint under the same load configuration (Figure 4-16 and Figure 4-17) has been analyzed using very fine finite element mesh enabling appropriate modeling of the weld toe radius (Figure 4-20 and Figure 4-21) and other micro-geometrical features. The through thickness stress distribution at section S-I is plotted in Figure 4-22. In addition the predicted stress distribution according to the GR3 procedure has been shown as well.

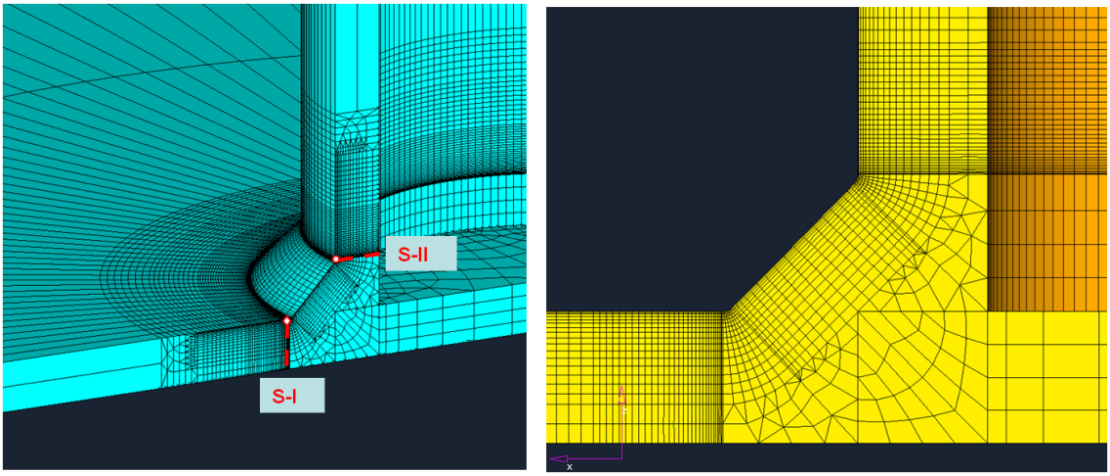

Figure 4-20: The fine FE mesh model of the Tube-on-Plate welded joint

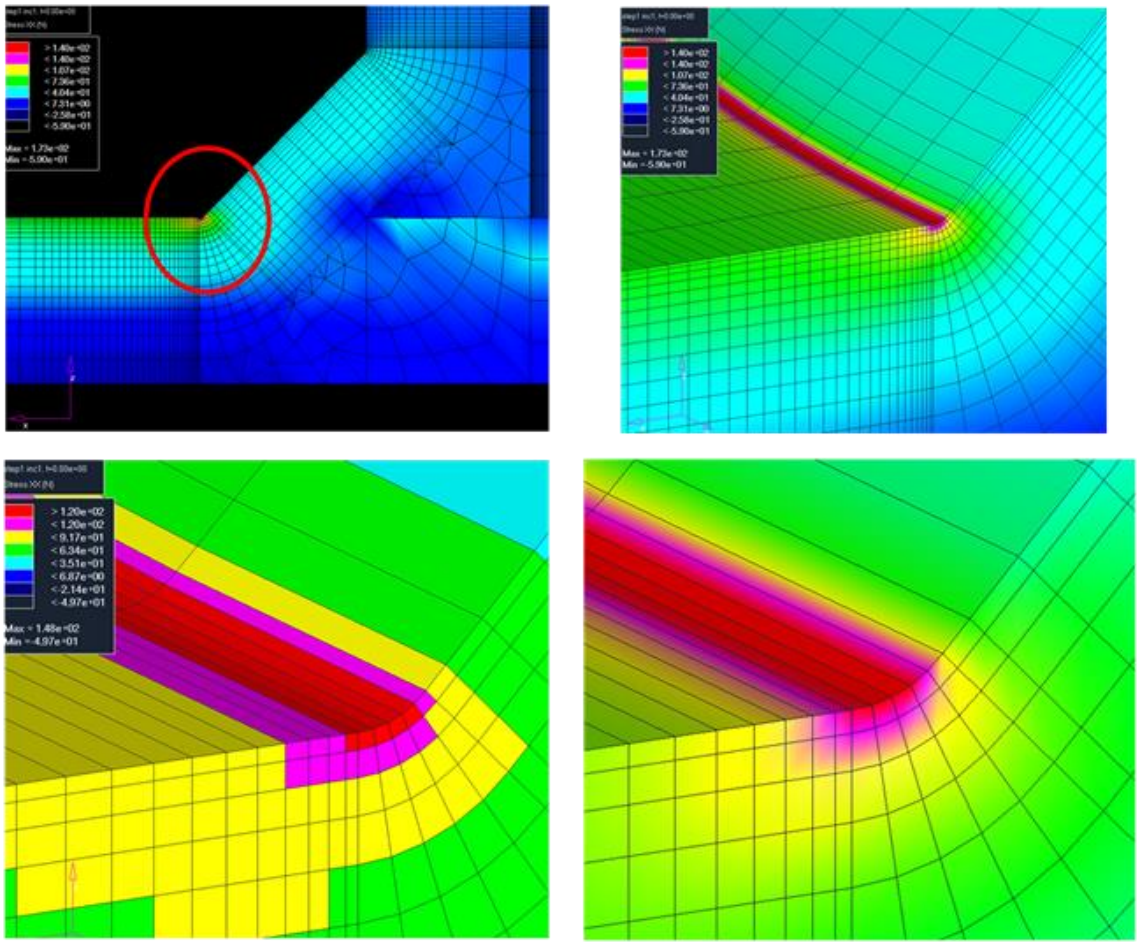

Figure 4-21: Details of the fine FE mesh model of the Tube-on-Plate welded joint

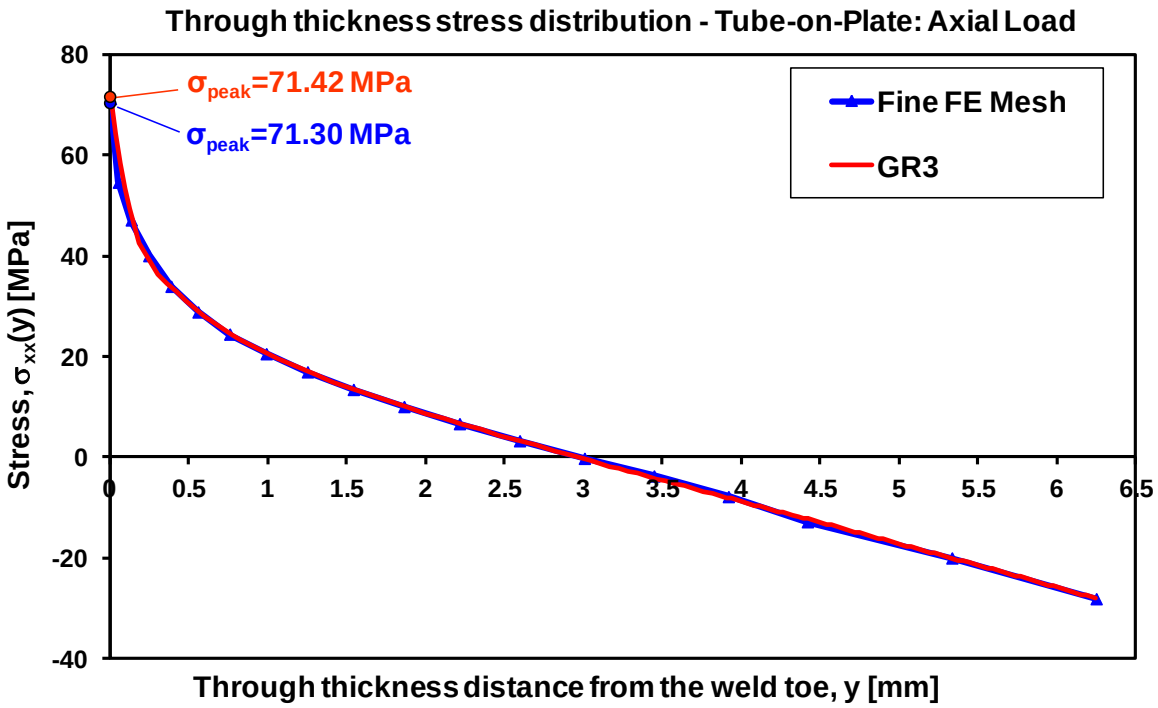

Figure 4-22: Comparison of through thickness stress distribution obtained from the coarse mesh FE model using GR3 method and fine FE mesh model of tube on plate joint

Figure 4-22 clearly shows that the profile of two stress distributions match each other very well proving that the coarse FE mesh procedure (GR3) can provide reliable stress information for reasonably accurate prediction of both the peak stress and the non-linear through-thickness stress distribution. The difference between the predicted GR3 peak stress of 71.42 MPa (Figure 4-22) and that one obtained from the fine mesh FE model, 71.3 MPa, is less than 1%.

An alternative way of proving the validity of the proposed method is to compare the linearized stress distribution obtained from the GR3 method with that one resulting from the linearization of the fine mesh FE stress data. In order to find the linearized through thickness stress distribution it is sufficient to determine stresses on both sides of the plate. The characteristic linearized stresses on both sides of the base plate determined using the coarse FE mesh stress data and the GR3 procedure are (eqn. 4.7):

$$\text{at } y = 0 \qquad \sigma_{hs}^{s1} = \sigma_{hs}^{m} + \sigma_{hs}^{b} = 0.93 + 31.67 = 32.60 \text{ MPa}$$

$$\text{at } y = 6.25 \qquad \sigma_{hs}^{s2} = \sigma_{hs}^{m} - \sigma_{hs}^{b} = 0.93 - 31.67 = -30.73 \text{ MPa} \qquad (4.23)$$

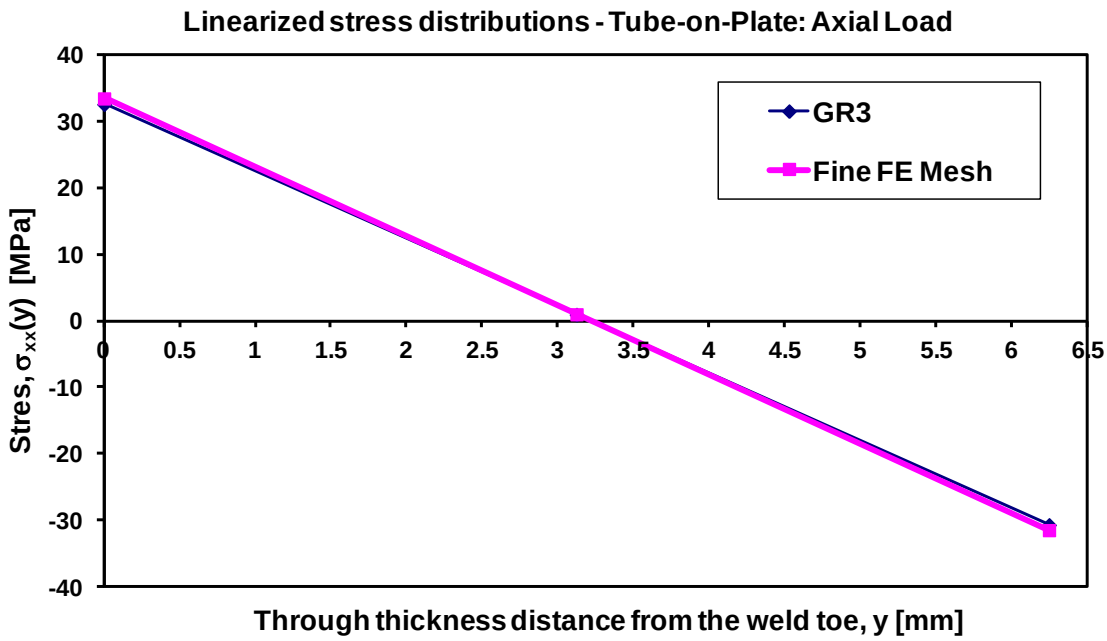

Figure 4-23: Linearized through thickness stress distributions in the tube on plate joint

Analogous stresses obtained by the linearization of the fine mesh FE stress data are:

$$\text{at } y = 0 \qquad \sigma_{hs}^{s1} = \sigma_{hs}^{m} + \sigma_{hs}^{b} = 0.98 + 32.50 = \quad 33.48 \text{ MPa}$$

$$\text{at } y = 6.25 \qquad \sigma_{hs}^{s2} = \sigma_{hs}^{m} - \sigma_{hs}^{b} = 0.98 - 32.50 = -31.52 \text{ MPa} \qquad (4.24)$$

A comparison of both linearized stress distributions plotted in Figure 4-23 shows that the difference between these two distributions at the weld toe position (y=0) is less than 3%.

4.5 The Tube-on-Plate weld joint under bending load

This section uses the same tube-on-plate weld joint as used in previous section for validation purpose under lateral bending load (Figure 4-16), P_b =1000 N, P_t=0 N applied to the tube. The base plate is constrained by fixing all degrees of freedom at each corner of the plate. Further, the same 3D coarse mesh finite element model as used in previous section (Figure 4-17) has been used but under the bending load conditions. Extracted stress distribution through the thickness from section S-I marked in Figure 4-17 is shown in Figure 4-24. Because five FE elements per thickness are used for the creation of the FE model the stresses corresponding to co-ordinates y=0.25t and y=0.75t are not directly available from coarse mesh FE model and have been found by extrapolating the FE stress data as shown in Figure 4-24.

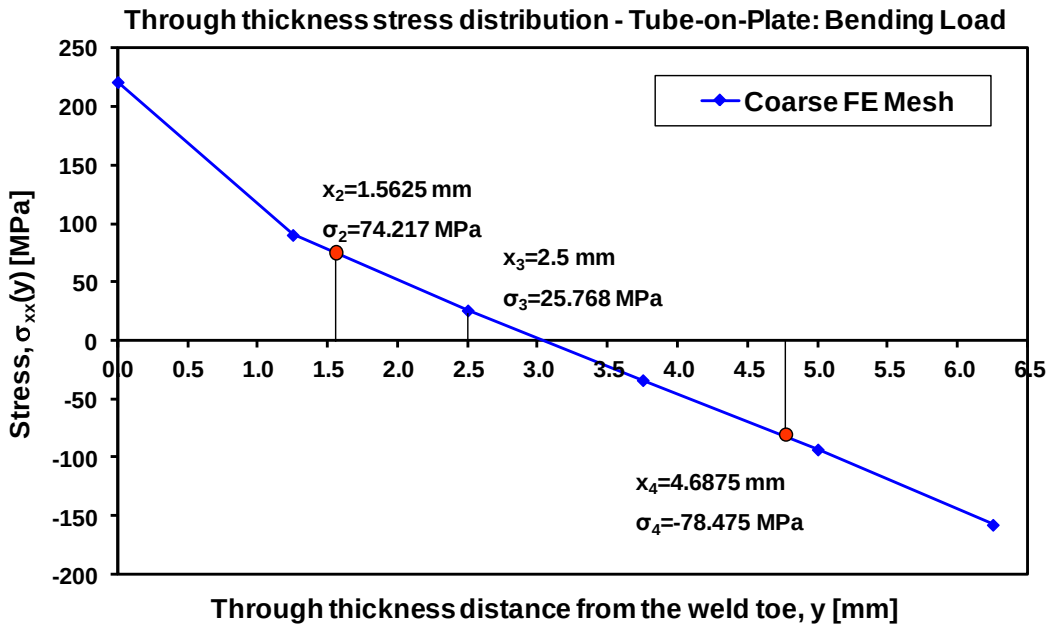

Figure 4-24: Through thickness stress distribution (nodal stresses) obtained from the 3D coarse mesh FE model – Tube on plate joint under bending load

Next, the membrane and the bending hot spot stresses are calculated as per the procedure described in section 3.6 utilizing the through thickness stress distribution obtained from the 3D coarse mesh FE model. The membrane hot spot stress is determined as an average stress over the entire plate thickness (eqn. 3.20) and all nodal stresses shown in Figure 4-24 are accounted during calculation.

$$\sigma_{hs}^{m} = \frac{1}{t}\left[\frac{(\sigma_2 + \sigma_1)(y_2 - y_1)}{2} + \frac{(\sigma_3 + \sigma_2)(y_3 - y_2)}{2} + \frac{(\sigma_4 + \sigma_3)(y_4 - y_3)}{2} + \frac{(\sigma_5 + \sigma_4)(y_5 - y_4)}{2} + \frac{(\sigma_6 + \sigma_5)(y_6 - y_5)}{2}\right] \quad (4.25)$$

$$= \frac{1}{6.25}\left[\frac{(90.37 + 221.25)(1.25 - 0)}{2} + \frac{(25.78 + 90.37)(2.5 - 1.25)}{2} + \frac{(-33.95 + 25.78)(3.75 - 2.5)}{2} + \frac{(-93.32 - 33.32)(5 - 3.75)}{2} + \frac{(-157.76 - 93.32)(6.25 - 5)}{2}\right] = 4.12\ MPa$$

As per the proposed method, the bending hot spot stress is calculated based on only the middle part (1.5625≤ x ≤4.6875 mm) of the coarse mesh stress distribution from Figure

4-24. At first, the bending moment contribution M_c is calculated using the excel macro using eqns. (3.26, 3.29, and 3.30).

M_c=123.401 Nmm (4.26)

The resultant bending moment is calculated according to eqn. 3.32.

$$M_b = 10\, M_c = 10 \times 123.401 = 1234.01 \text{ Nmm} \quad (4.27)$$

The hot spot bending stress is determined from eqn. 3.33.

$$\sigma_{hs}^{b} = \frac{6\, M_b}{t^2} = \frac{6 \text{ X } 1234.01}{6.25^2} = 189.54 \text{ MPa} \quad (4.28)$$

Geometry unique stress concentration factors are calculated based on the geometry (dimensions) of the selected weld joint (Figure 4-16) as demonstrated in Figure 3-22 and described in the form of eqns. 3.38 and 3.39 for the membrane and bending modes of loading respectively. The 't_p' dimension is assumed equal to the tube wall thickness, i.e. tp =6.25 mm.

$$K_{t,hs}^{m} = 1.784 \text{ and } K_{t,hs}^{b} = 2.203 \quad (4.29)$$

The peak stress at the weld toe is subsequently calculated using eqn. 3.7.

$$\sigma_{peak} = \sigma_{hs}^{m}\, K_{t,hs}^{m} + \sigma_{hs}^{b}\, K_{t,hs}^{b} = 4.123 \times 1.784 + 189.54 \times 2.203 = 424.92 \text{ MPa} \quad (4.30)$$

The hot spot membrane and the bending stresses along with the appropriate stress concentration factors have also been used for the determination of the through thickness stress distribution according to Monahan's eqn. 3.40 as shown in Figure 4-25.

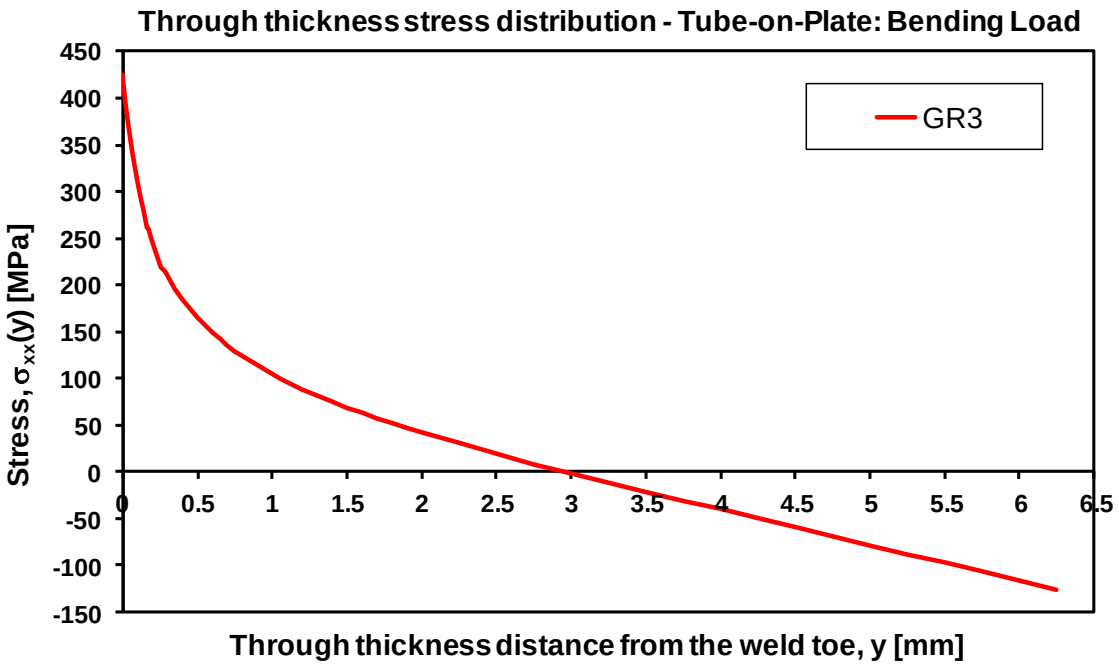

Figure 4-25: The through thickness stress distribution obtained from the coarse FE mesh model using GR3 method

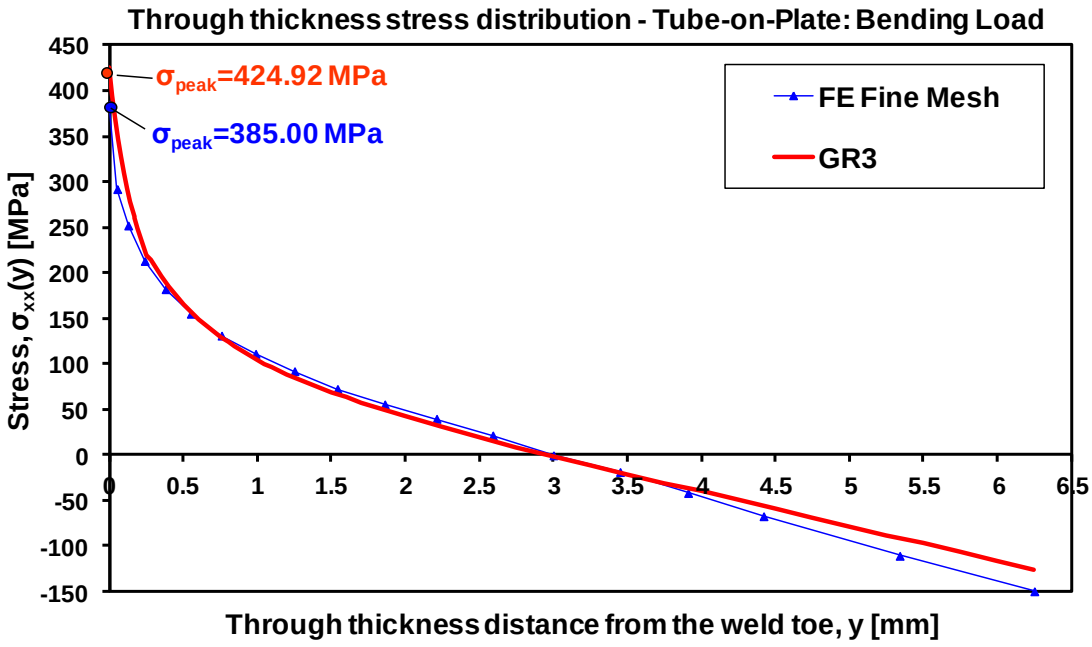

Figure 4-26: Comparison of through thickness stress distribution obtained from coarse mesh FE model using GR3 method and the fine FE mesh model of tube on plate joint

4.5.1 Fine vs. Coarse mesh solid FE model

The validation of the proposed GR3 method along with its capability to produce accurate results has been demonstrated in this section by comparing results from 3D coarse mesh FE model using GR3 method against the results obtained from 3D fine mesh FE model for the tube on plate joint under bending loading. The same weld joint under the same load configuration as the coarse FE model has been analyzed using very fine finite element mesh enabling appropriate modeling of the weld toe radius (Figure 4-20 and Figure 4-21) and other micro-geometrical features. The through thickness stress distribution at section S-I is plotted in Figure 4-26. In addition the predicted stress distribution according to the GR3 procedure has been shown as well.

Figure 4-26 clearly shows that the profile of two stress distributions match each other very well proving that the coarse FE mesh procedure (GR3) can provide reliable stress information for reasonably accurate prediction of both the peak stress and the non-linear through-thickness stress distribution. The difference between the predicted GR3 peak stress of 424.92 MPa (Figure 4-26) and that one obtained from the fine mesh FE model, 385.0 MPa, is less than 10%.

An alternative way of proving the validity of the proposed method is to compare the linearized stress distribution obtained from the GR3 method with that one resulting from the linearization of the fine mesh FE stress data. In order to find the linearized through thickness stress distribution it is sufficient to determine stresses on both sides of the plate. The characteristic linearized stresses on both sides of the base plate determined using the coarse FE mesh stress data and the GR3 procedure are (eqn. 4.7):

$$\text{at } y = 0 \qquad \sigma_{hs}^{s1} = \sigma_{hs}^{m} + \sigma_{hs}^{b} = 4.123 + 189.54 = \quad 193.67 \text{ MPa}$$

$$\text{at } y = 6.25 \qquad \sigma_{hs}^{s2} = \sigma_{hs}^{m} - \sigma_{hs}^{b} = 4.123 - 189.54 = -185.42 \text{ MPa} \qquad (4.31)$$

Analogous stresses obtained by the linearization of the fine mesh FE stress data are:

$$\text{at } y = 0 \qquad \sigma_{hs}^{s1} = \sigma_{hs}^{m} + \sigma_{hs}^{b} = 5.448 + 175.39 = \quad 180.94 \text{ MPa}$$

$$\text{at } y = 6.25 \qquad \sigma_{hs}^{s2} = \sigma_{hs}^{m} - \sigma_{hs}^{b} = 5.448 - 175.39 = -169.95 \text{ MPa} \qquad (4.32)$$

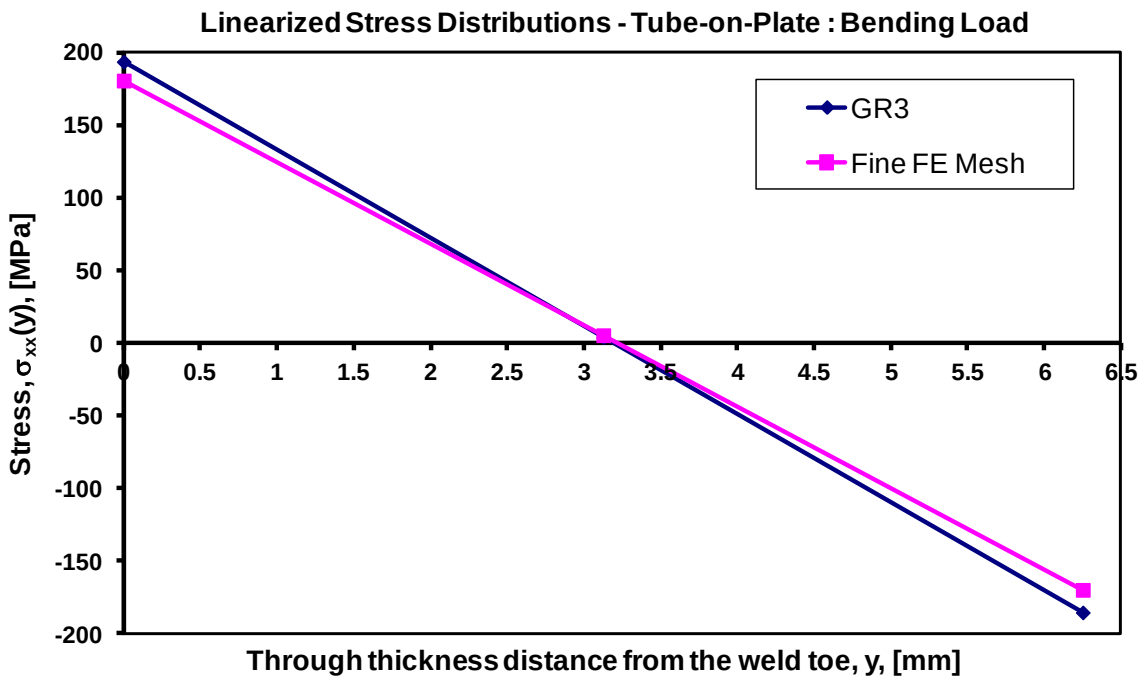

Figure 4-27: Linearized through thickness stress distributions in the tube on plate joint

A comparison of both linearized stress distributions plotted in Figure 4-27 shows that the difference between these two distributions at the weld toe position (y=0) is less than 7%.

4.6 The beam weldment under bending load

This section uses a beam weldment with various attachments welded to one side of the beam and subjected to four point bending load, for validation purposes. Details of the geometrical dimensions and the loading conditions are illustrated in Figure 4-28. Detail stress analysis is carried out in the region of the edge of the cover plate (lap joint) shown in Figure 4-29. The entire beam including the weld toe region of lap joint is modeled using coarse FE mesh (Figure 4-29) with tetrahedral elements of the size equal to one quarter of the wall thickness ($\delta_{el} < 0.25t$) across the tube wall thickness i.e. four elements across the tube wall thickness are used. Extracted stress distribution through the thickness from the hot spot location is shown in Figure 4-30.

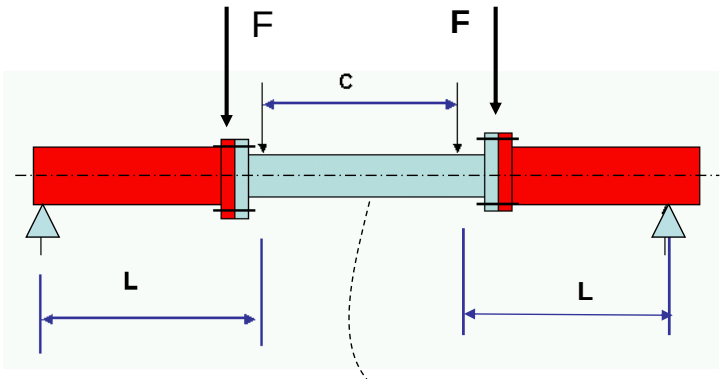

Loading :

2F= 2500 lbs (11120N), R=0.1

Fixture set up:

L=1437mm, total length= 3869mm

Component parameters:

C: 1854 mm
T-weld plate: 12.7mm thickness
Lap weld plate: 6.35mm thickness
Tube thickness: 6.35mm, 3x5 inch
Weld size: 6 mm
Weld toe radius: 0.5mm
Weld angle: θ = 45°

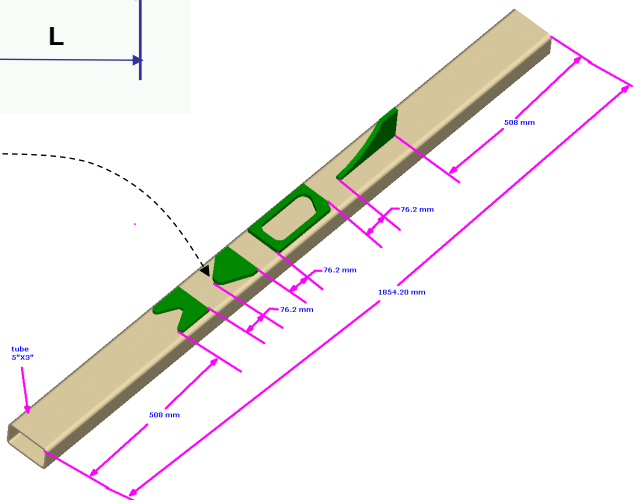

Figure 4-28: Geometry and dimensions of the beam weldment - Bending load

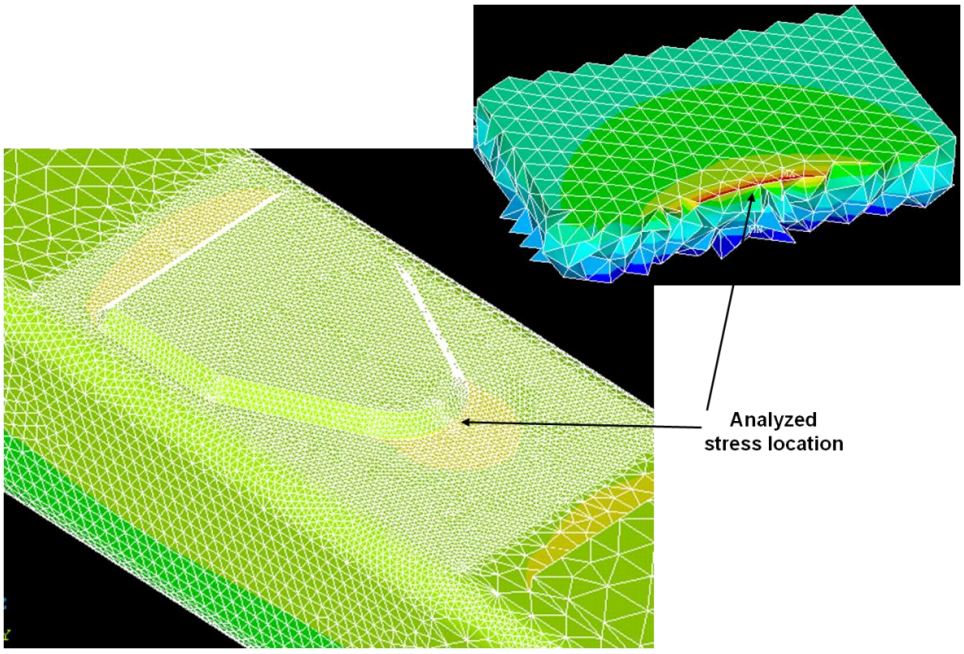

Figure 4-29: The coarse FE mesh model of the beam weldment and the analyzed stress location

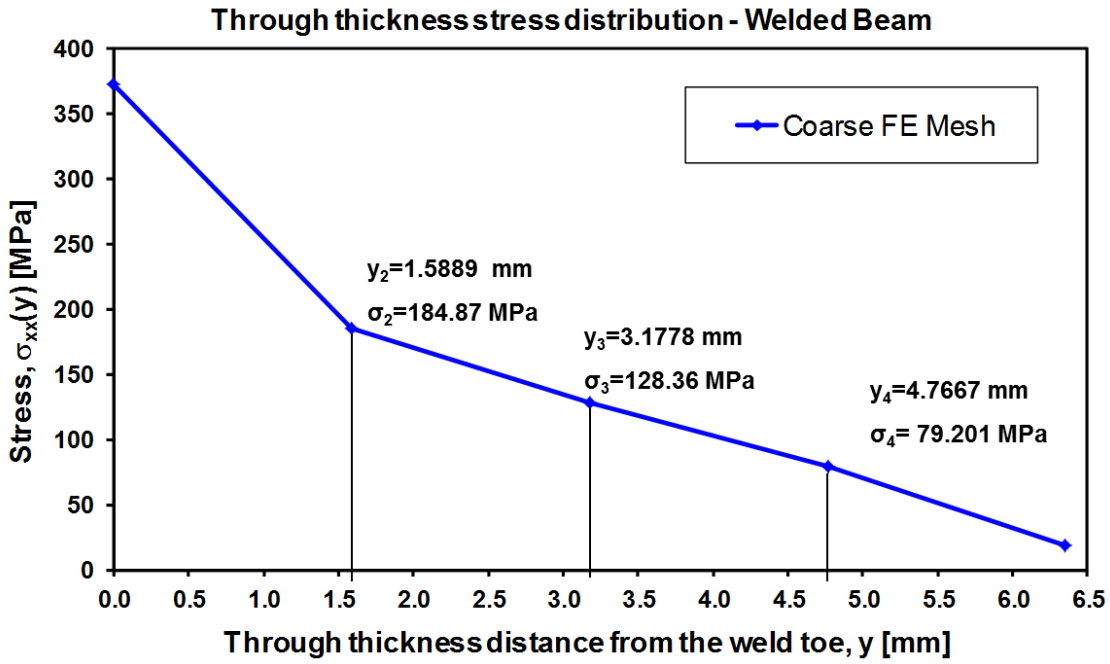

Figure 4-30: Through thickness stress distribution (nodal stresses) obtained from the 3D coarse mesh FE model – Beam weldment under bending load

Next, the membrane and the bending hot spot stresses are calculated as per the procedure described in section 3.6 utilizing the through thickness stress distribution obtained from the 3D coarse mesh FE model. The membrane hot spot stress is determined as an average stress over the entire plate thickness (eqn. 3.20) and all nodal stresses shown in the Figure 4-30 are accounted during calculation.

$$\sigma_{hs}^{m} = \frac{1}{t}\left[\frac{(\sigma_2 + \sigma_1)(y_2 - y_1)}{2} + \frac{(\sigma_3 + \sigma_2)(y_3 - y_2)}{2} + \frac{(\sigma_4 + \sigma_3)(y_4 - y_3)}{2} + \frac{(\sigma_5 + \sigma_4)(y_5 - y_4)}{2}\right] \tag{4.33}$$

$$= \frac{1}{6.35}\left[\frac{(184.87 + 372.86)(1.589 - 0)}{2} + \frac{(128.36 + 184.87)(3.178 - 1.589)}{2} + \frac{(79.20 + 128.36)(4.767 - 3.178)}{2} + \frac{(18.37 - 79.201)(6.35 - 4.767)}{2}\right] = 147.1\ MPa$$

As per the proposed method, the bending hot spot stress is calculated based on only the middle part (1.5889 ≤ x ≤ 4.7667 mm) of the coarse mesh stress distribution from Figure 4-30. At first, the bending moment contribution M_c is calculated using the excel macro using eqns. (3.26, 3.29, and 3.30).

M_c=87.7656 Nmm

The resultant bending moment is calculated according to eqn. 3.32.

$$M_b = 10\, M_c = 10 \times 87.7656 = 877.656\, Nmm \quad (4.34)$$

The hot spot bending stress is determined from eqn. 3.33.

$$\sigma_{\text{hs}}^{\text{b}} = \frac{6\, M_b}{t^2} = \frac{6\, X\, 877.656}{6.35^2} = 130.60\, MPa \quad (4.35)$$

The geometry unique stress concentration factors are calculated based on the geometry (dimensions) of the selected weld joint (Figure 4-28) as demonstrated in Figure 3-22 and described in the form of eqns. 3.38 and 3.39 for the membrane and bending modes of loading respectively. The 't_p' dimension is assumed equal to the three weld legs h, i.e. t_p =3x6=18 mm.

$$K_{\text{t,hs}}^{m} = 1.834 \text{ and } K_{\text{t,hs}}^{b} = 2.661 \quad (4.36)$$

The peak stress at the weld toe is subsequently calculated using eqn. (3.7).

$$\sigma_{\text{peak}} = \sigma_{\text{hs}}^{\text{m}}\, K_{\text{t,hs}}^{m} + \sigma_{\text{hs}}^{\text{b}}\, K_{\text{t,hs}}^{b} = 147.1 \times 1.834 + 130.6 \times 2.661 = 617.30\, MPa \quad (4.37)$$

The hot spot membrane and the bending stresses along with the appropriate stress concentration factors have also been used for the determination of the through thickness stress distribution according to Monahan's eqn. (3.40) as shown in Figure 4-31.

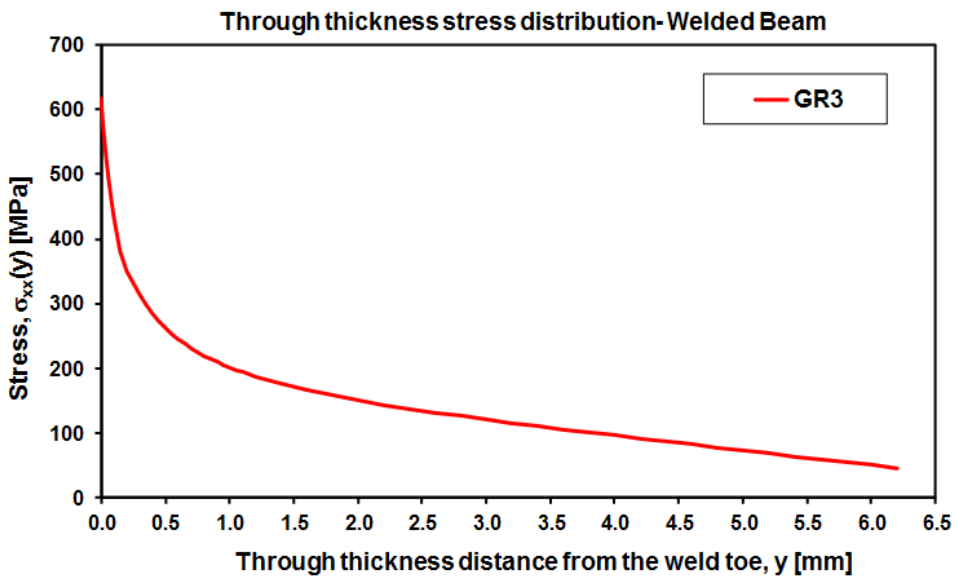

Figure 4-31: The through thickness stress distribution obtained from the coarse FE mesh model using GR3 method

4.6.1 Fine vs. Coarse mesh solid FE model

The validation of the proposed GR3 method along with its capability to produce accurate results has been demonstrated in this section by comparing results from 3D coarse mesh FE model using the GR3 method against the results obtained from 3D fine mesh FE model for the beam weldment under bending loading. The same weld joint under the same load configuration (Figure 4-28) has been analyzed using very fine finite element mesh enabling appropriate modeling of the weld toe radius (Figure 4-32 and Figure 4-33) and other micro-geometrical features. The through thickness stress distribution at same hot spot is plotted in Figure 4-34. In addition the predicted stress distribution according to the GR3 procedure has been shown as well.

Figure 4-34 clearly shows that the profile of two stress distributions match each other very well proving that the coarse FE mesh procedure (GR3) can provide reliable stress information for reasonably accurate prediction of both the peak stress and the non-linear through-thickness stress distribution. The difference between the predicted GR3 peak stress of 617.30 MPa (Figure 4-34) and that one obtained from the fine mesh FE model, 575.81 MPa, is less than 7%. This study further demonstrates that the proposed method is equally applicable with use of tetrahedron FE elements as with use of hex elements.

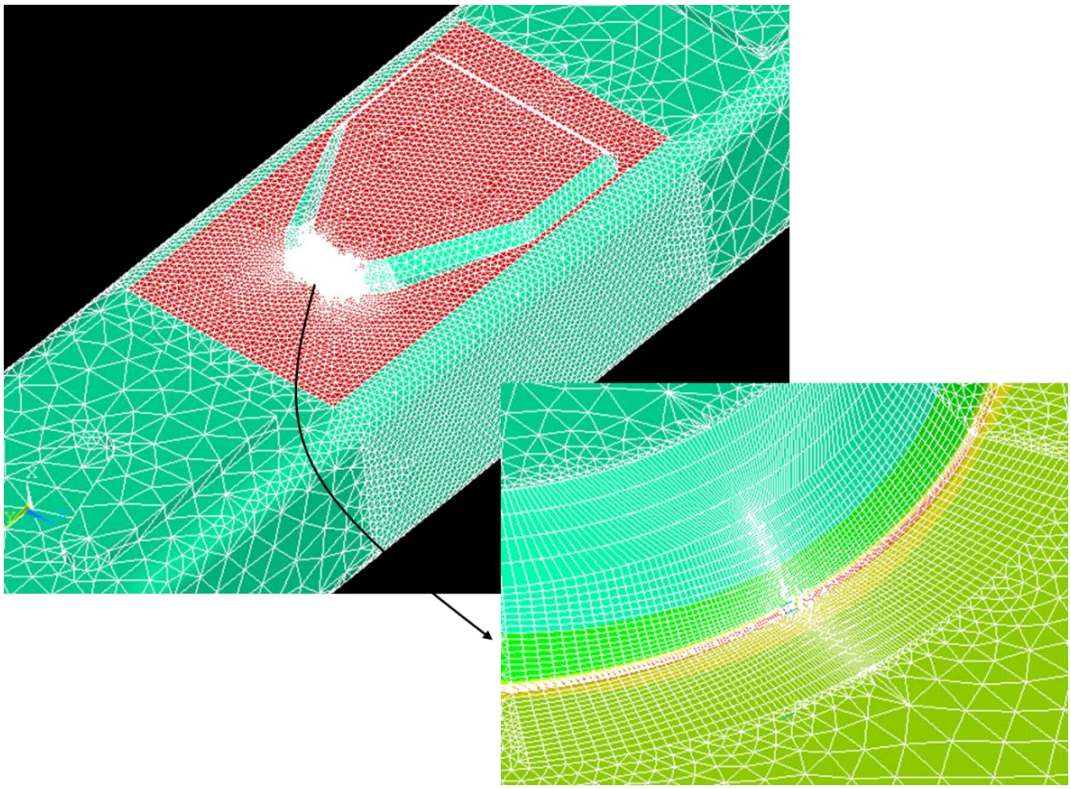

Figure 4-32: The fine FE mesh model of the beam weldment – lap joint details

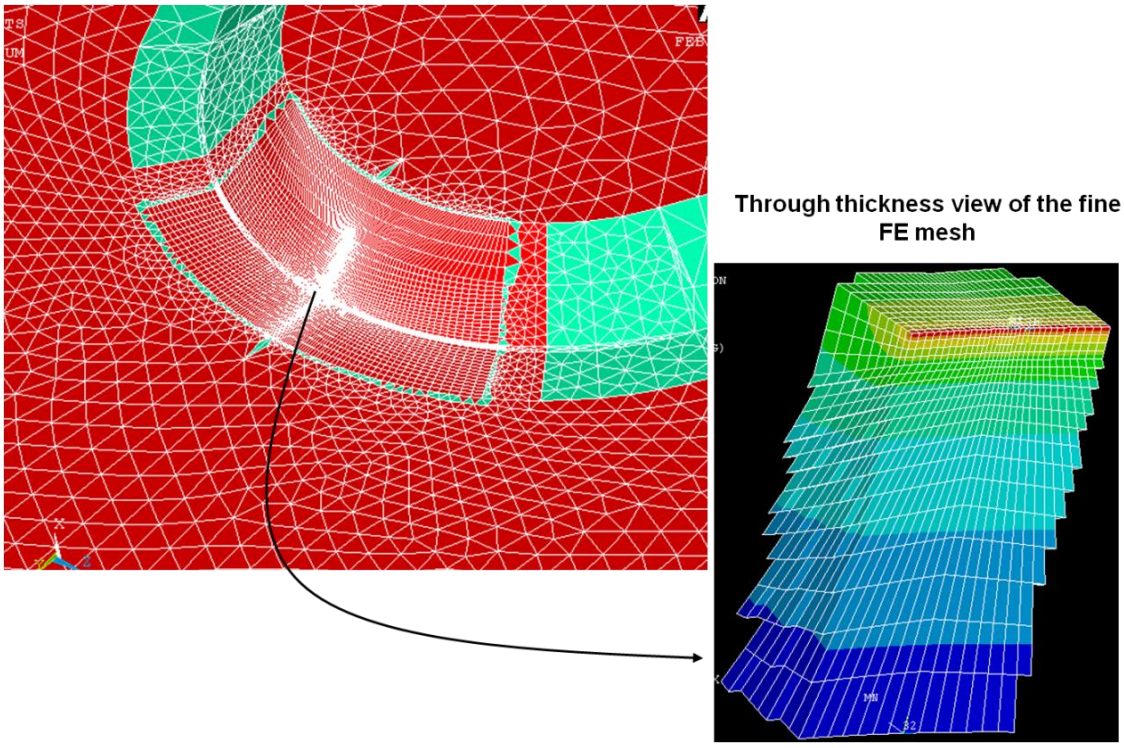

Figure 4-33: Details of the through thickness fine mesh FE model

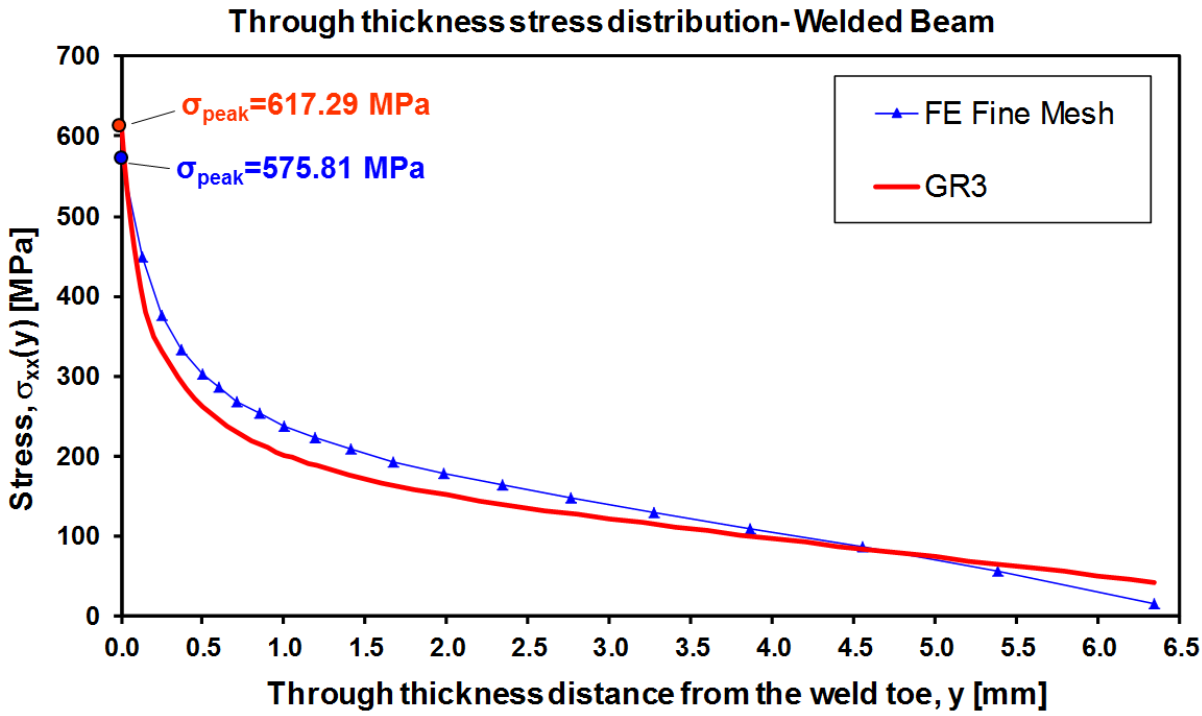

Figure 4-34: Comparison of through thickness stress distribution obtained from the coarse mesh FE model using the GR3 method and the fine FE mesh model of beam weldment

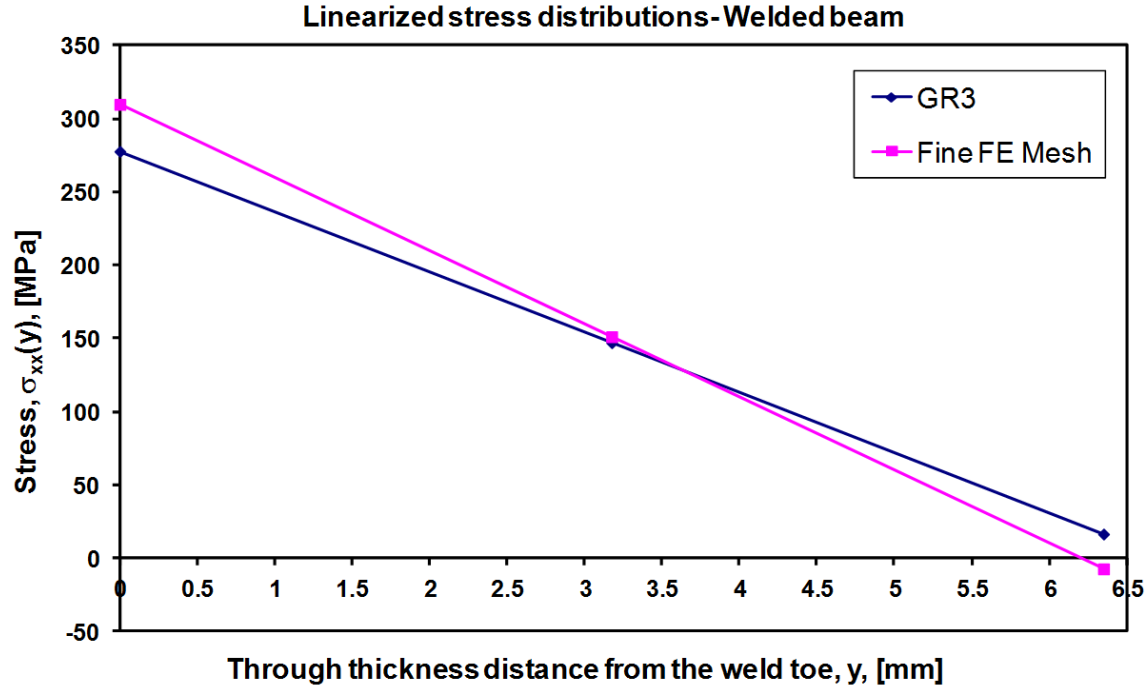

Figure 4-35: Linearized through thickness stress distributions in the beam weldment

An alternative way of proving the validity of the proposed method is to compare the linearized stress distribution obtained from the GR3 method with that one resulting from the linearization of the fine mesh FE stress data. In order to find the linearized through thickness stress distribution it is sufficient to determine stresses on both sides of the plate. The characteristic linearized stresses on both sides of the base plate determined using the coarse FE mesh stress data and the GR3 procedure are (eqn. 4.7):

$$\text{at } y = 0 \qquad \sigma_{hs}^{s1} = \sigma_{hs}^{m} + \sigma_{hs}^{b} = 147.1 + 130.6 = 277.7 \text{ MPa}$$

$$\text{at } y = 6.35 \qquad \sigma_{hs}^{s2} = \sigma_{hs}^{m} - \sigma_{hs}^{b} = 147.1 - 130.6 = 16.5 \text{ MPa} \qquad (4.38)$$

Analogous stresses obtained by the linearization of the fine mesh FE stress data are:

$$\text{at } y = 0 \qquad \sigma_{hs}^{s1} = \sigma_{hs}^{m} + \sigma_{hs}^{b} = 151.22 + 158.53 = 309.75 \text{ MPa}$$

$$\text{at } y = 6.35 \qquad \sigma_{hs}^{s2} = \sigma_{hs}^{m} - \sigma_{hs}^{b} = 151.22 - 158.53 = -7.30 \text{ MPa} \qquad (4.39)$$

A comparison of both the linearized stress distributions (Figure 4-35) shows that the difference between these two distributions at the weld toe position (y=0) is less than 10%.

4.7 The tubular welded structure subjected to torsion and bending load

This section uses a tubular welded structure subjected to simultaneous multiple loading modes such as bending and torsion, for validation purposes. Details of the geometrical dimensions and the loading conditions (P = 1 lb) are illustrated in Figure 4-36 and Figure 4-37. Detail stress analysis is carried out in the region shown in Figure 4-37. The entire weldment including the weld toe region of analyzed section is modeled using coarse FE mesh (Figure 4-38) with tetrahedral elements of the size equal to one third of the tube wall thickness ($\delta_{el} < 0.333t$) i.e. three elements across tube wall thickness are used. The reason to try little large finite element size in this case was to evaluate if this can still provide sufficient stress output data. Extracted stress distribution through the thickness from the hot spot location is shown in Figure 4-39. Because only three finite elements are used in the coarse FE mesh model an extrapolation technique is used (Figure 4-39) in order to determine stresses σ_2 and σ_4 at point y=0.25t and y=0.75t respectively. It is to be noted that the extrapolation concerns only the stress data from the middle part of the wall thickness, i.e. from the region of $0.25t \leq y \leq 0.75t$.

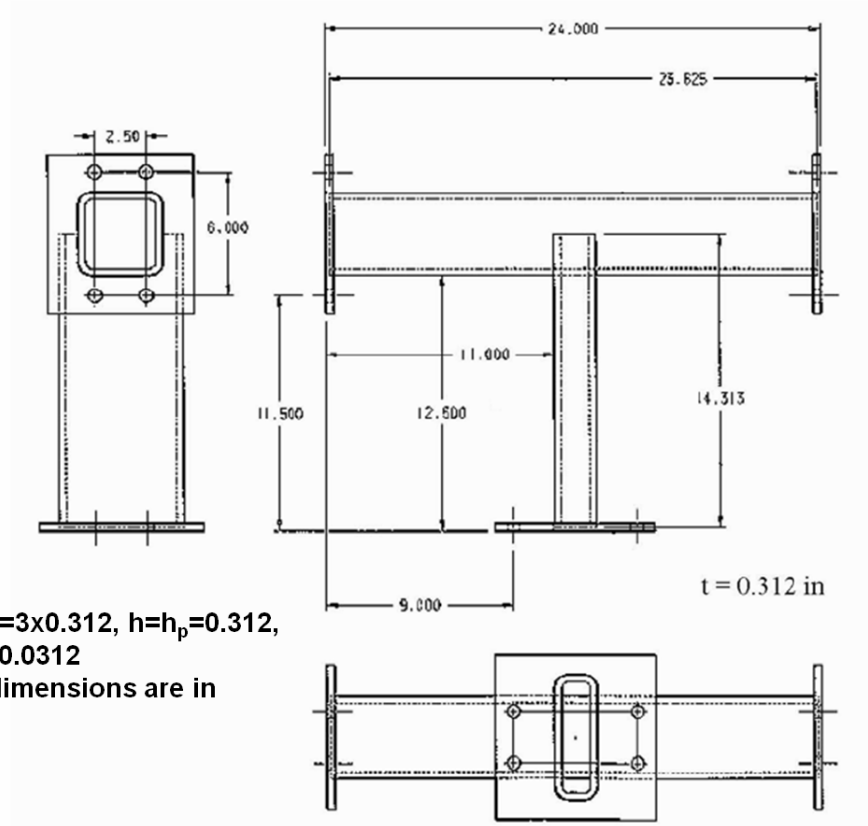

Figure 4-36: Geometry and dimensions of the considered tubular weldment

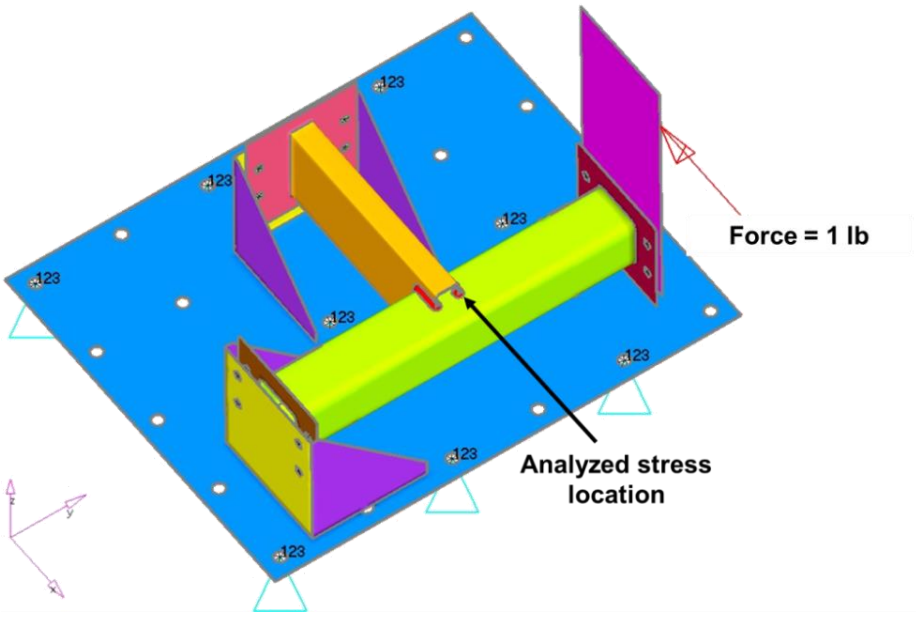

Figure 4-37: The coarse FE mesh model of the weldment and the analyzed stress location

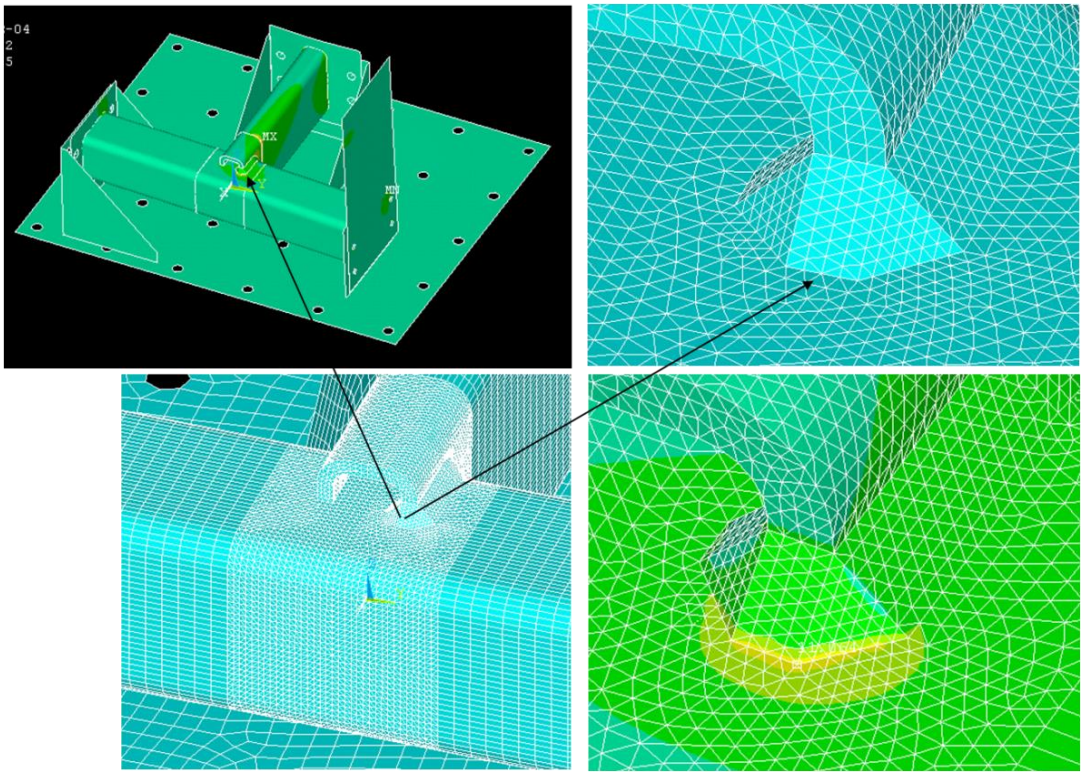

Figure 4-38: Details of the coarse mesh FE model and analysed section

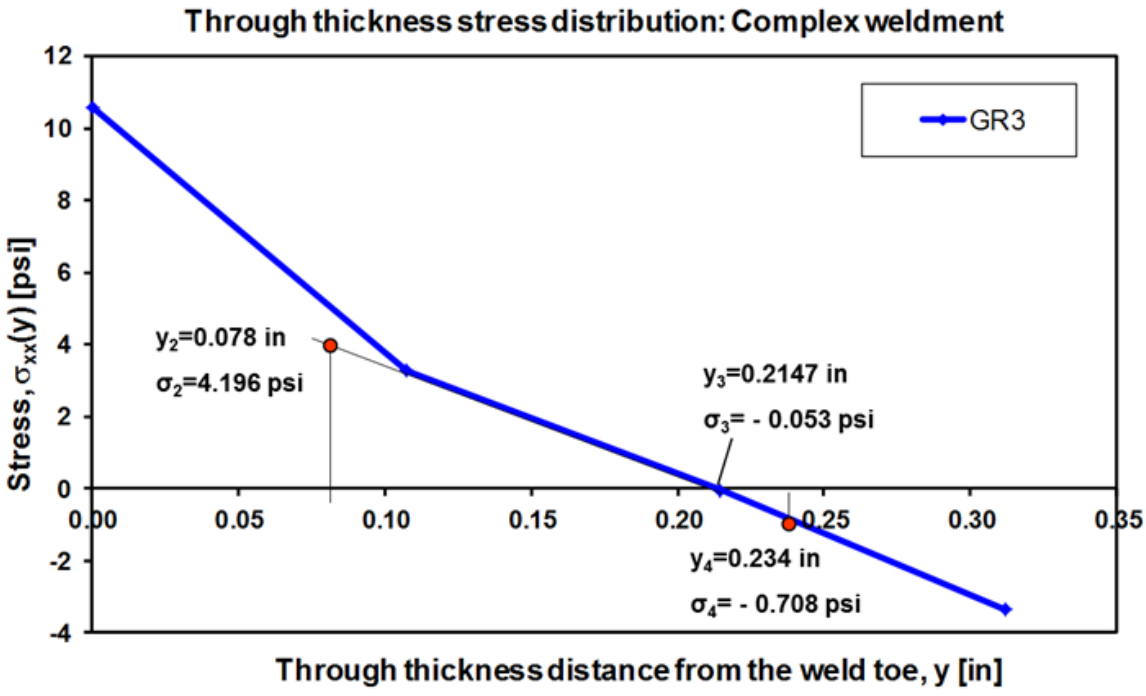

Figure 4-39: Through thickness stress distribution (nodal stresses) obtained from the 3D coarse mesh FE model - weldment under torsion and bending load

Next, the membrane and the bending hot spot stresses are calculated as per the procedure described in section 3.6 utilizing the through thickness stress distribution obtained from the 3D coarse mesh FE model. The membrane hot spot stress is determined as an average stress over the entire plate thickness (eqn. 3.20) and all nodal stresses shown in Figure 4-39 are accounted during calculation.

$$\sigma_{hs}^{m} = \frac{1}{t}\left[\frac{(\sigma_2 + \sigma_1)(y_2 - y_1)}{2} + \frac{(\sigma_3 + \sigma_2)(y_3 - y_2)}{2} + \frac{(\sigma_4 + \sigma_3)(y_4 - y_3)}{2}\right] \quad (4.40)$$

$$= \frac{1}{0.312}\left[\frac{(3.278 + 10.58)(0.1073 - 0)}{2} + \frac{(-0.05 + 3.28)(0.2147 - 0.1073)}{2} + \frac{(-3.36 - 0.053)(0.31 - 0.2147)}{2}\right] = 2.41\ psi$$

As per the proposed method, the bending hot spot stress is calculated based on only the middle part ($0.078 \leq y \leq 0.234$ in) of the coarse mesh stress distribution from Figure 4-39. At first, the bending moment contribution M_c is calculated using the excel macro using eqns. 3.26, 3.29 and 3.30.

M_c=0.0098494 lbs.in

The resultant bending moment is calculated according to eqn. 3.32.

$$M_b = 10\, M_c = 10 \times 0.0098494 = 0.098494 \text{ lbs.in} \quad (4.41)$$

The hot spot bending stress is determined from eqn. 3.33.

$$\sigma_{\text{hs}}^{\text{b}} = \frac{6\, M_b}{t^2} = \frac{6\, X\, 0.098494}{0.312^2} = 6.07\ psi \quad (4.42)$$

The geometry unique stress concentration factors are calculated based on the geometry (dimensions) of the selected weld joint (Figure 4-36) as demonstrated in Figure 3-22 and described in the form of eqns. 3.38 and 3.39 for the membrane and bending modes of loading respectively.

$$K_{\text{t,hs}}^{m} = 1.784 \text{ and } K_{\text{t,hs}}^{b} = 2.203 \quad (4.43)$$

The peak stress at the weld toe is subsequently calculated using eqn. (3.7).

$$\sigma_{\text{peak}} = \sigma_{\text{hs}}^{\text{m}}\ K_{\text{t,hs}}^{m} + \sigma_{\text{hs}}^{\text{b}}\ K_{\text{t,hs}}^{b} = 2.41 \times 1.784 + 6.07 \times 2.203 = 17.67\ psi \qquad (4.44)$$

The hot spot membrane and the bending stresses along with the appropriate stress concentration factors have also been used for the determination of the through thickness stress distribution according to Monahan's eqn. (3.40) as shown in Figure 4-40.

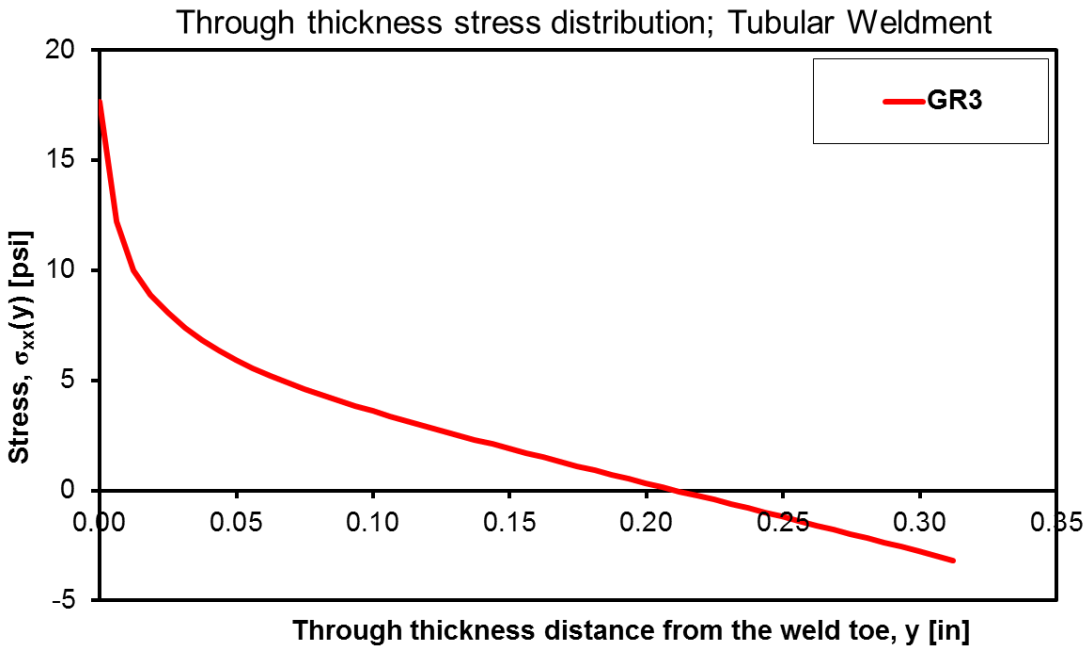

Figure 4-40: The through thickness stress distribution obtained from the coarse FE mesh model using GR3 method

4.7.1 Fine vs. Coarse mesh solid FE model

The validation of the proposed GR3 method along with its capability to produce accurate results has been demonstrated in this section by comparing results from 3D coarse mesh FE model using the GR3 method against the results obtained from 3D fine mesh FE model for the weldment under combined mode of loading. The same weld joint under the same load configuration (Figure 4-37) has been analyzed using very fine finite element mesh enabling appropriate modeling of the weld toe radius (Figure 4-41) and other micro-geometrical features. The through thickness stress distribution at same hot spot is plotted in Figure 4-42. In addition the predicted stress distribution according to the GR3 procedure has been shown as well.

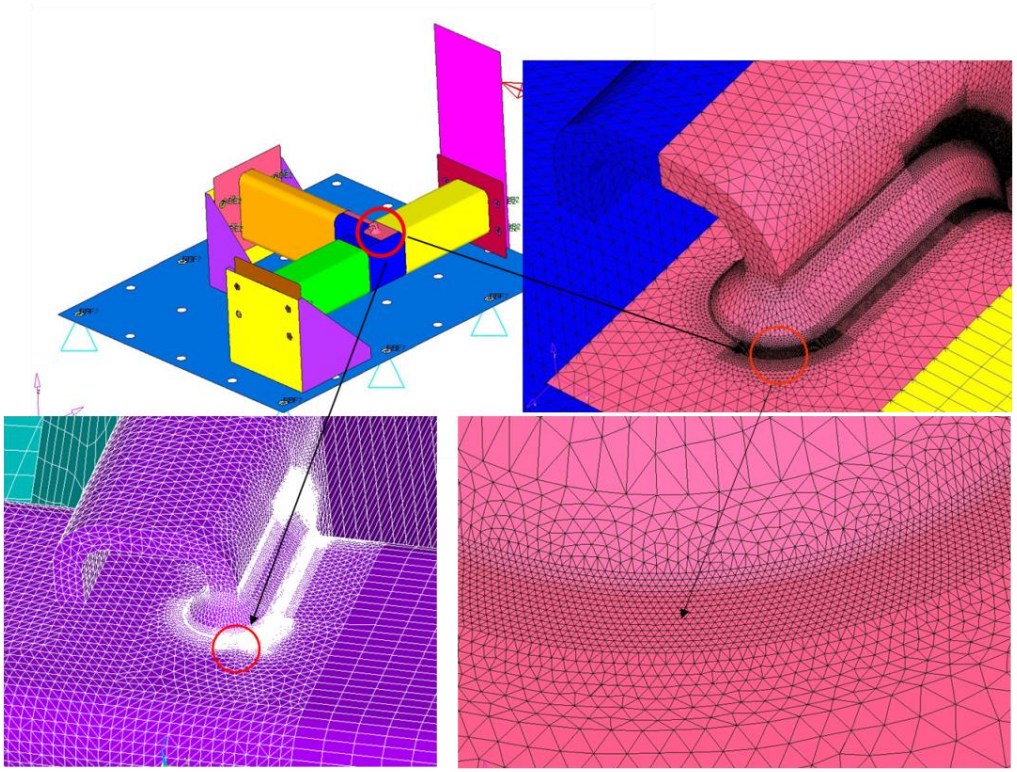

Figure 4-41: The fine FE mesh model of the weldment with focus on analysed section

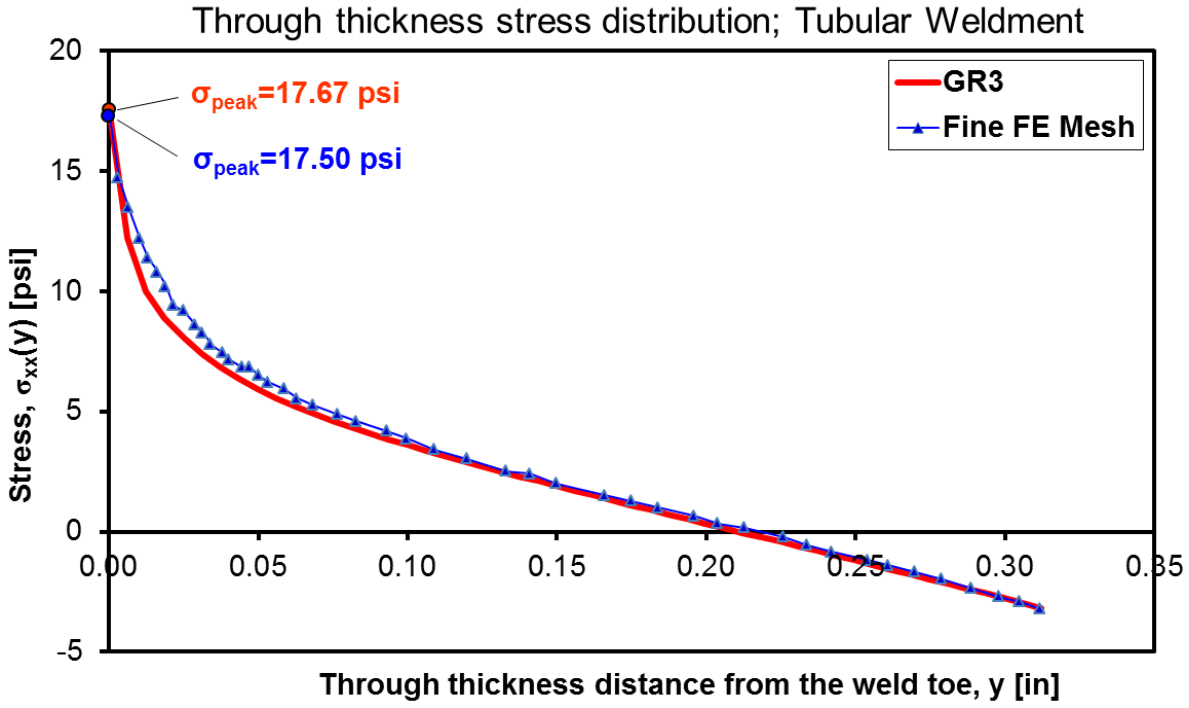

Figure 4-42: Comparison of through thickness stress distribution obtained from the coarse mesh FE model using the GR3 method and the fine FE mesh model

Figure 4-42 clearly shows that the profile of two stress distributions match each other very well proving that the coarse FE mesh procedure (GR3) can provide reliable stress information for reasonably accurate prediction of both the peak stress and the non-linear through-thickness stress distribution. The difference between the predicted GR3 peak stress of 17.67psi (Figure 4-42) and that one obtained from the fine mesh FE model, 17.50psi, is less than 1%. This study further confirms that the proposed method is equally applicable with the use tetrahedron FE elements as with the use of hex elements.

An alternative way of proving the validity of the proposed method is to compare the linearized stress distribution obtained from the GR3 method with that one resulting from the linearization of the fine mesh FE stress data. In order to find the linearized through thickness stress distribution it is sufficient to determine stresses on both sides of the plate. The characteristic linearized stresses on both sides of the base plate determined using the coarse FE mesh stress data and the GR3 procedure are (eqn. 4.7):

$$\text{at } y = 0 \qquad \sigma_{hs}^{s1} = \sigma_{hs}^{m} + \sigma_{hs}^{b} = 2.41 + 6.07 = 8.48 \text{ psi}$$

$$\text{at } y = 0.312 \quad \sigma_{hs}^{s2} = \sigma_{hs}^{m} - \sigma_{hs}^{b} = 2.41 - 6.07 = -3.66 \text{ psi} \tag{4.45}$$

Analogous stresses obtained by the linearization of the fine mesh FE stress data are:

$$\text{at } y = 0 \qquad \sigma_{hs}^{s1} = \sigma_{hs}^{m} + \sigma_{hs}^{b} = 2.59 + 6.74 = 9.33 \text{ psi}$$

$$\text{at } y = 0.312 \quad \sigma_{hs}^{s2} = \sigma_{hs}^{m} - \sigma_{hs}^{b} = 2.59 - 6.74 = -4.16 \text{ psi} \tag{4.46}$$

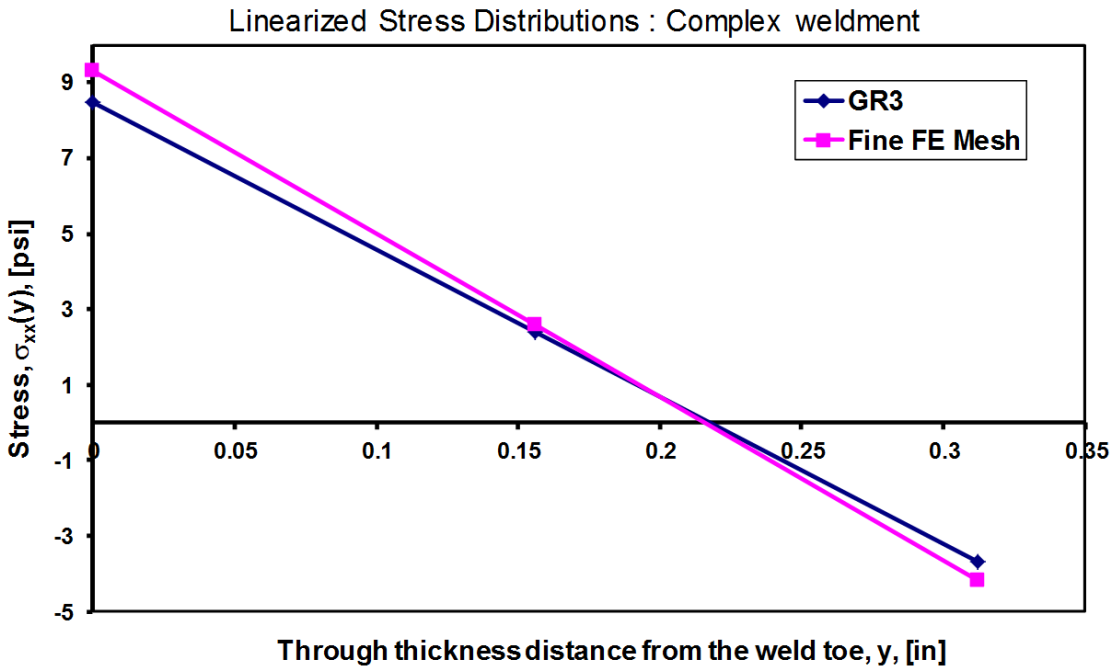

Figure 4-43: Linearized through thickness stress distributions in the weldment

A comparison of the linearized stress distributions plotted in Figure 4-43 shows that the difference between these two distributions at the weld toe position (y=0) is less than 10%.

4.8 Computational benefits of using the proposed methodology

This section shows the computational benefits from the use of proposed methodology using 3D coarse mesh FE models compared to 3D fine mesh FE reference models for the stress analysis of welded structures. The finite element modeling as well as the analysis was carried out using exactly the same hardware and software. The computer system with 64-bit operating system, Intel (R) Core i5 CPU@2.60GHZ and 16GB RAM was used for 3D coarse mesh as well as 3D fine mesh FE analysis of the six welded samples (shown in the earlier sections of this chapter). Table 4-4 shows comparison of the estimated peak stress at the critical weld toe location for the six welded samples, obtained using the proposed methodology with 3D coarse mesh FE analysis and the reference 3D fine mesh FE analysis. It can be seen that the estimated peak stress using the proposed methodology is in agreement with the similar peak stress data obtained using the reference 3D fine mesh FE analysis and is consistently found to be on the conservative side. Further, the Table 4-5 shows comparison of the modeling time and simulation time for the six welded

samples, while using the proposed methodology with 3D coarse mesh FE models and the reference 3D fine mesh FE models. It can be observed that minimum of 75% time savings for the model preparation and minimum of 67% time savings for the simulation was observed while using the proposed methodology. Hence it can be concluded that there is significant time savings while using the proposed methodology.

Table 4-4: Comparison of the modeling time and simulation time for the six welded specimens – 3D coarse mesh vs. 3D fine mesh FE models

Welded Joints - Selected for validation	**Peak stress prediction (MPa)**		
	3D fine	**3D coarse**	**% diff**
The Gusset weld joint – Symmetric welds	1023.0	1020.7	**0.2**
The Gusset weld joint – Non symmetric weld	420.0	488.0	**13.8**
The Beam weldment - Bending load	576.0	617.0	**7.1**
The Tubular welded structure - Torsion and bending load	121.0	131.0	**8.3**
The Tube-on-plate weld joint - Axial load	71.3	71.4	**0.1**
The Tube-on-Plate welded joint - Bending load	385.0	424.9	**10.4**

Table 4-5: Comparison of the modeling time and simulation time for the six welded specimens – 3D coarse mesh vs. 3D fine mesh FE models

Welded Joints - Selected for validation	**Modeling time (hrs)**			**Solving time (hrs)**		
	3D fine	**3D coarse**	**% diff**	**3D fine**	**3D coarse**	**% diff**
The Gusset weld joint – Symmetric welds	6	1	**83**	1.2	0.4	**67**
The Gusset weld joint – Non symmetric weld	13	2	**85**	1.7	0.5	**71**
The Beam weldment - Bending load	29	7	**76**	5.2	1.4	**73**
The Tubular welded structure - Torsion and bending load	36	9	**75**	6.1	1.5	**75**
The Tube-on-plate weld joint - Axial load	14	2	**86**	1.0	0.3	**70**
The Tube-on-Plate welded joint - Bending load	14	2	**86**	1.0	0.3	**70**

It should be noted that the major benefit of the proposed methodology lies in the fact that the proposed methodology helps to **efficiently** determine the **necessary and unique** stress quantities as required for the fatigue life analysis of **large size** welded structures subjected to **multiple modes** of cyclic loading, which is not feasible in the engineering practice using the 3D fine mesh FE analysis.

Chapter 5 Experimental and Numerical Fatigue Life Analysis

5.1 Introduction

In the previous chapter, the peak stress and the through-thickness stress distribution obtained using the proposed methodology from 3D coarse mesh FE models were compared against the similar data obtained from the accurate 3D fine mesh FE models for validation of the proposed methodology. The results from above mentioned verification confirmed the accuracy of the proposed methodology up to the stress analysis procedure, however in order to confirm that the proposed methodology provides sufficient information for the fatigue life analysis; validation has been done against the experimental fatigue life test data. The estimated fatigue life has been compared with the experimental data obtained from fatigue life testing of several welded joints.

This chapter mainly focuses on the fatigue life estimation (crack initiation and propagation life) based on the proposed methodology and comparison of the calculated fatigue lives with experimental data.

The fatigue life prediction program FALIN based on the local notch stress-strain approach was employed for the fatigue life prediction to crack initiation and the FALPR program was used to calculate the fatigue crack propagation life.

The total fatigue life (crack initiation and propagation) for each welded joint was calculated considering cases with and without the presence of residual stresses. As discussed in the sections 2.5.1 and 2.6.1, the effect of residual stress on the crack initiation life has been considered by adjusting the mean stress while calculation of the fatigue crack initiation life and in the fatigue crack propagation analysis by adjusting the stress intensity factor range according to the Kurihara's crack tip closure model.

Detailed procedure with step by step calculations is shown for the first case-study of gusset weld joint with symmetric welds. For rest of the three case studies only the final results are presented as the procedure followed is exactly the same for all the case studies.

5.2 Experimental Fatigue Testing

Fatigue testing was conducted using an Instron 50kN hydraulic linear actuator equipped with a 50kN load cell to apply a cyclic load to the test sample. The testing was controlled by an Instron 8801 controller. All experiments have been carried out under the load control conditions and the crack length 2c, visible on the surface, is measured versus the number of applied load cycles. A displacement limit of +1 mm beyond the stabilized displacement was set to shut the test down when this was exceeded. This was used as a method for crack detection as well as for safety. Cracks were detected visually with a five power magnifying glass. The samples were painted with high contrast paint to aid in the visual detection of cracks. The number of cycles and the size of the crack were noted. The number of cycles were recorded when the displacement limit was triggered i.e. when the displacement of the actuator increased to 1mm. The experimental fatigue life data is obtained for four structural components chosen for the validation : The gusset welded joint with symmetric welds subjected to out of plane load, the gusset welded joint with asymmetric welds subjected to in plane load, the beam weldment under four point bending load and the complex tubular welded structure subjected to bending and torsion load. All of these welded samples were tested under constant amplitude cyclic loading, at two different load levels. More details for each of these experiments are covered in the subsequent sections.

5.3 The Gusset weld joint – Symmetric welds

As covered in Chapter 3, the total fatigue life estimation requires analysis of the initiation and propagation lives of fatigue cracks. The resultant fatigue life is determined by summation of the crack initiation life predicted using the strain-life method and the crack propagation life predicted using the fracture mechanics approach. In order to compare the predicted fatigue lives with the experimental data, two series of tests have been carried out. The first one was conducted at the cyclic load of ±308 N and the other at ±468 N. The sample used for fatigue test experiments is shown in the Figure 5-1. The tested welded joints (specimens) were made of 1008 steel alloy 4mm thin sheets. The base plate had a square shape with dimension of 500 mm by 500mm and the vertical plate had dimension of 100 mm by 50mm. The dimensions of the sample are shown in Figure 3-14.

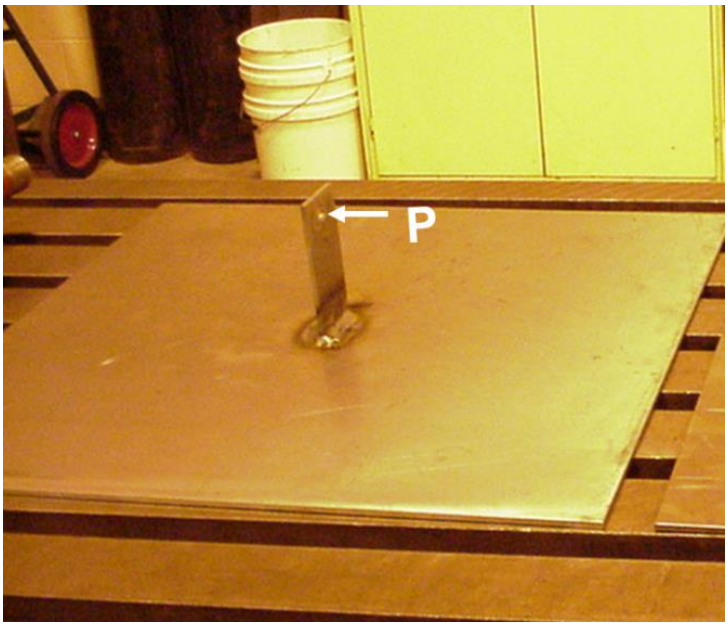

Figure 5-1: Welded specimen - gusset weld joint with symmetric welds

The samples were manually welded using gas metal arc welding process. The samples were initially tack welded before doing the full welding. A simple weld fixture to hold the tack welded sample was used to allow the full welds to be performed in the 2F welding position. The welding was performed using 1.2mm ER70S-6 weld wire with 90% Ar and 10% CO_2 shielding gas mixture. The spray mode of metal transfer was used with these weld process parameters: wire feed speed – 7.8 m/min, current – 259 A, voltage – 23V and travel speed – 0.45 m/min.

For the experimental fatigue testing, the samples were clamped in the fixture at four locations (approximate clamping area of 40 by 80 mm at each corner) and the cyclic load was applied through the hole in the vertical plate (see Figure 4-1 and Figure 5-1). The sample was put on two 50.8 mm square boxes. There was 50.8 mm spacing between the boxes and the test specimen was mounted at the edges at four places. More than 10 samples were welded and tested under fatigue loading, however as this was one of the first studies; data is presented for the 6 samples which were successful completed. Three samples were tested at the lower load level of 308N and the rest of them were tested at higher load level of 468N. The experimental fatigue lives obtained are listed in Table 5-1. The numbers of load cycles are given as a function of the crack length (2c) measured on the plate surface. The crack depth is only an estimate.

Table 5-1: Experimental fatigue crack growth data (2c-N) for the gusset weld joint with symmetric welds

Sample #	**1**	**2**	**3**	**4**	**5**	**6**
Load (N)	308	468	468	308	468	308
First detected crack length (mm)	3 to 4	3 to 4	3 to 4	3 to 4	4 to 5	3.0
Number of cycles (cycles)	347,000	15,510	14,131	533,675	13,900	156,200
Crack length (mm)						5.0
Cycle count						224,560
Crack length (mm)					6.0	6.0
Cycle count					17,141	231,802
Crack length (mm)					6.5	6.5
Cycle count					18,684	322,650
Crack length (mm)					7.0	7.0
Cycle count					30,527	331,054
Crack length (mm)						8.0
Cycle count						629,456
Crack length (mm)					15.0	
Cycle count					40,896	
Crack length (mm)					24.5	
Cycle count					53,150	
Crack length (mm)					25.0	
Cycle count					57,800	
Crack length (mm)					26	
Cycle count					64,155	
Crack length (mm)					35.0	
Cycle count					72,288	

Next, the numerical calculations have been carried out for estimation of fatigue life for the gusset weld joint with symmetric welds as per the proposed methodology.

The peak stresses and the through thickness stress distributions induced by the applied load levels are obtained by scaling the GR3 model stress data shown in Figure 4-4 and the simulated stress distributions are presented in Figure 5-2 and Figure 5-3.

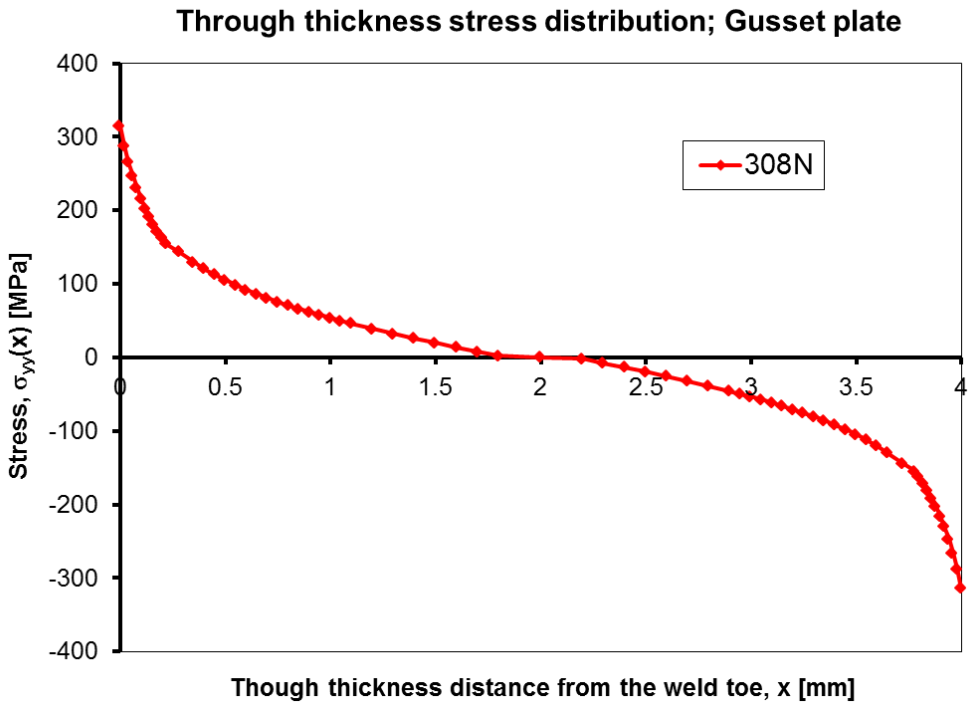

Figure 5-2: Simulated GR3 based through-thickness stress distribution in the critical cross section of the gusset weld joint with symmetric welds (F=308 N)

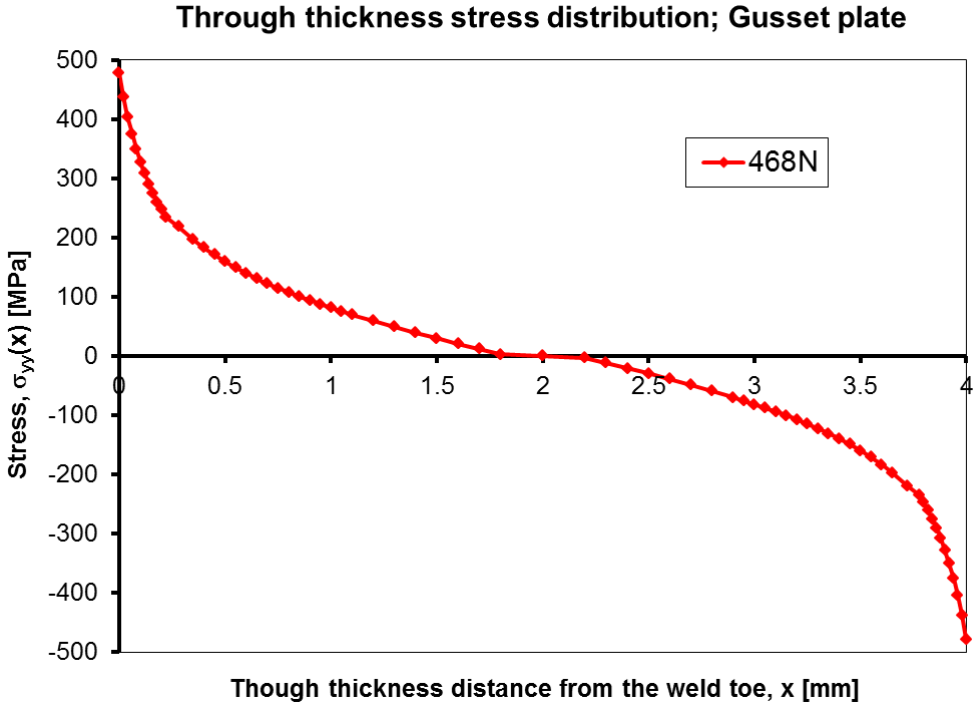

Figure 5-3: Simulated GR3 based through-thickness stress distribution in the critical cross section of the gusset weld joint with symmetric welds (F=468 N)

For each load case, the fatigue lives were determined with and without accounting for the presence of residual stress. Using the welding process simulation model explained in section 3.4, residual stresses have been estimated for this joint. Residual stress plot for the normal stress component σ_{zz} is shown in Figure 5-4 and the through thickness residual stress distribution extracted at the critical section (same as used for extracting the stress distribution induced by applied loads, see Figure 5-5) is shown in Figure 5-6. The residual stress was measured at the weld toe in the plate surface using XRD method and was found to be 99MPa, which is quite close to the residual stress obtained using weld simulation.

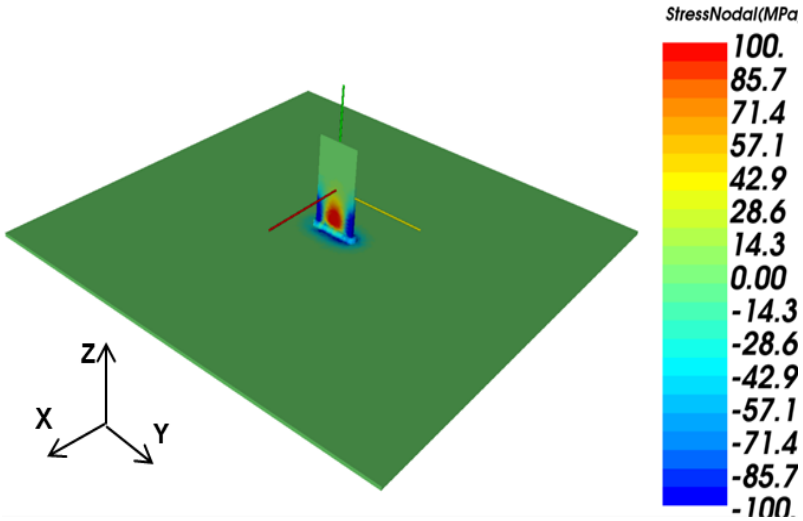

Figure 5-4: Residual stress plot (σ_{zz} component) obtained from the welding process simulation of the gusset weld joint with symmetric welds

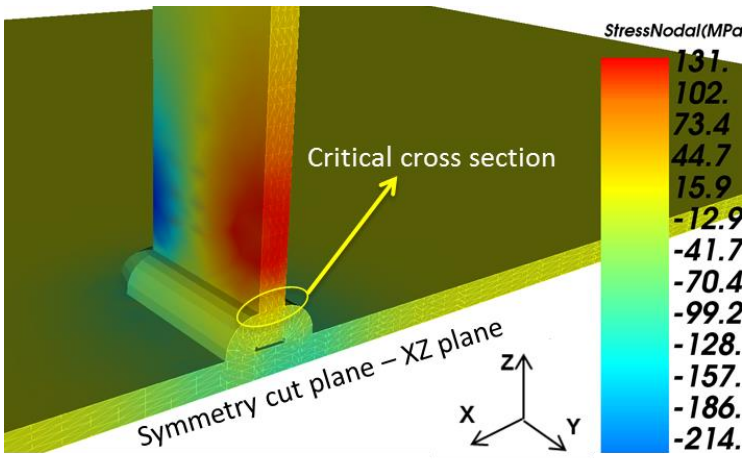

Figure 5-5: Closer view of the symmetry cut plane (XZ) of the gusset weld joint with symmetric welds showing the residual stress plot (σ_{zz} component)

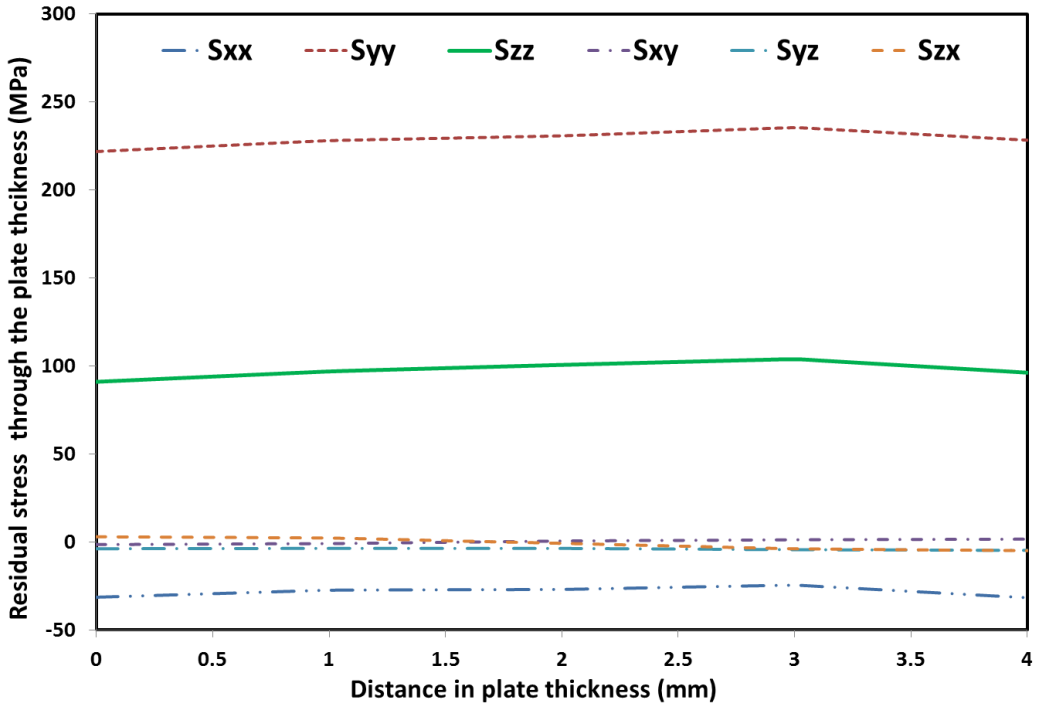

Figure 5-6: Simulated through the thickness residual stress distribution in the critical cross section of the of the gusset weld joint with symmetric welds

5.3.1 Fatigue crack initiation life estimation

The fatigue crack initiation life is predicted using the strain-life method coded into the FALIN software. The procedure is covered in sections 2.5 and 3.10. The elasto-plastic stresses and strains at the weld toe are calculated for each load cycle based on the Neuber's rule and the material Ramberg-Osgood stress strain curve per eqn. 2.2 and eqn. 2.3. These strains and stresses and the Smith, Watson, and Topper (SWT) strain-life eqn. 2.11 are used for calculating the fatigue life to crack initiation. The fatigue life calculations are based on the material properties listed in Table 4-2 and Table 4-3 for 1008 steel. The input and output data, the simulated stress-strain response at the weld toe and the estimated fatigue lives to crack initiation are shown in Figure 5-7 through Figure 5-11. It is noticeable (see Table 5-2 and Table 5-3) that the residual stress had profound effect on the fatigue crack initiation life. The analysis indicates that the tensile residual stress at the weld toe may decrease the fatigue crack initiation life approximately by a factor of 2.

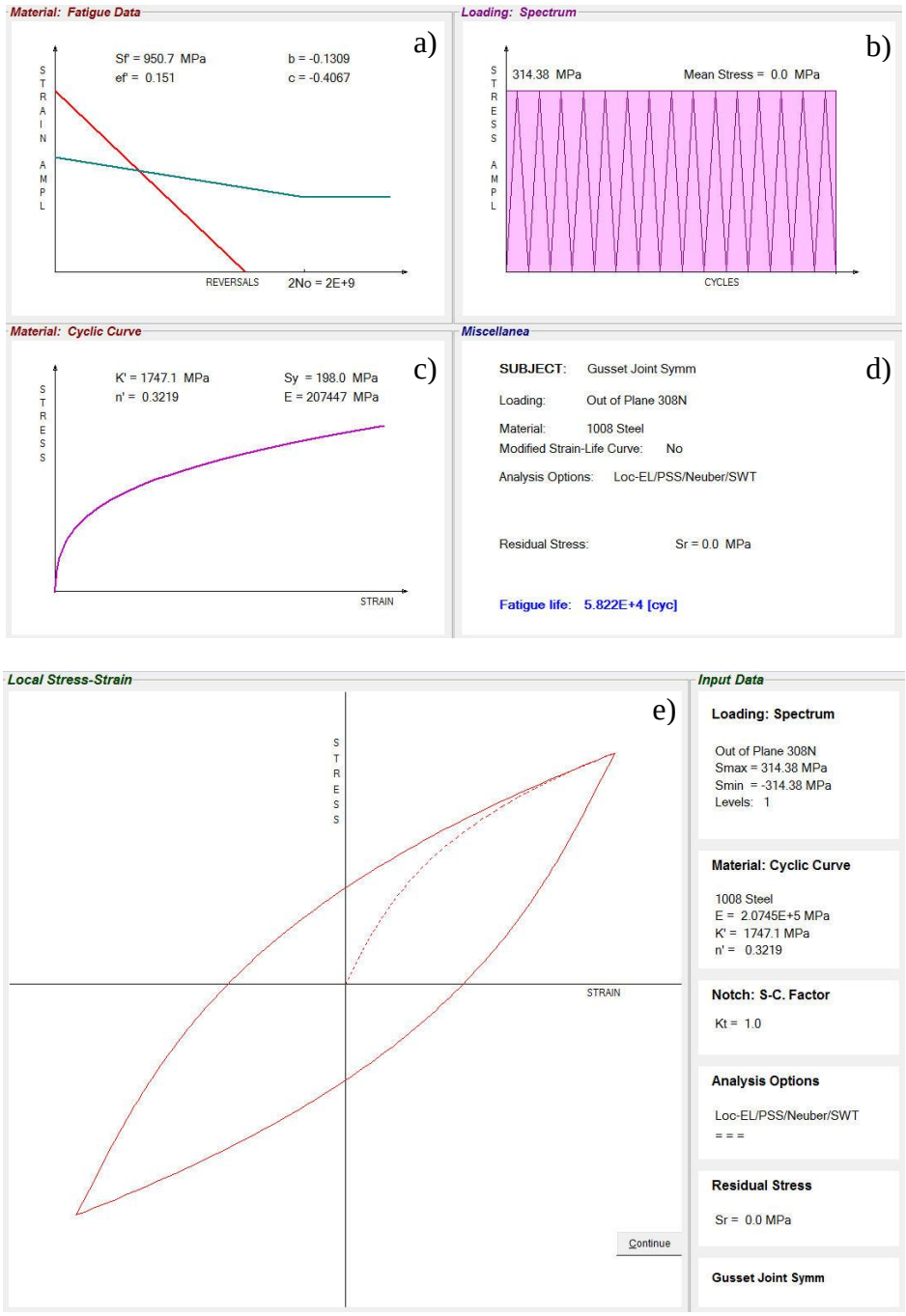

Figure 5-7: The input data and calculated fatigue crack initiation life for the gusset weld joint with symmetric welds F=308 N and the material stress-strain response at the weld toe (without residual stress). a) Manson-Coffin curve, b) Weld toe peak stress history, c) The Ramberg-Osgood curve, d) The output data, e) Simulated stress-strain material response at the weld toe

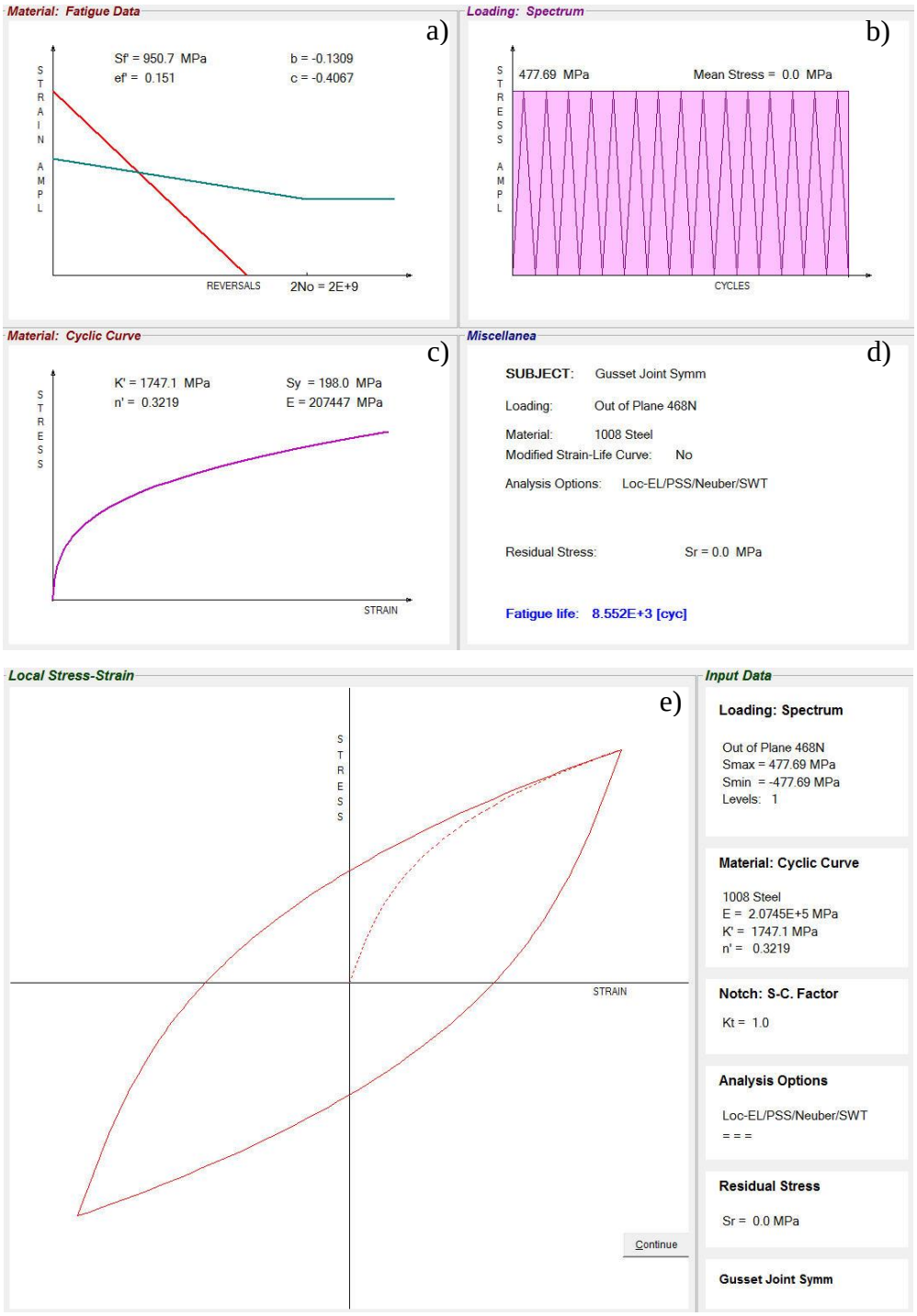

Figure 5-8: The input data and calculated fatigue crack initiation life for gusset weld joint with symmetric welds F=468 N and the material stress-strain response at the weld toe (without residual stress). a) Manson-Coffin curve, b) Weld toe peak stress history, c) The Ramberg-Osgood curve, d) The output data, e) Simulated stress-strain material response at the weld toe

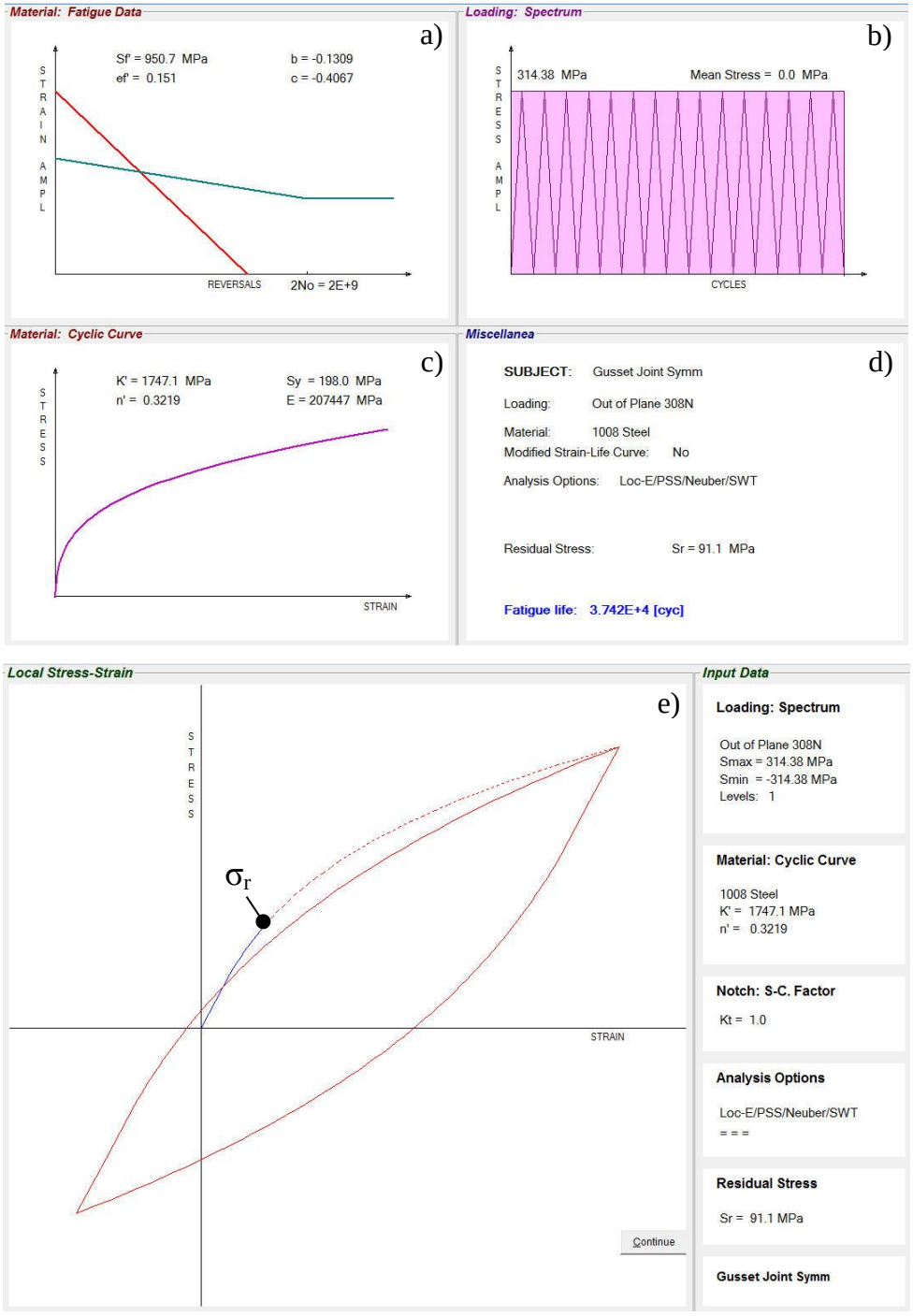

Figure 5-9: The input data and calculated fatigue crack initiation life for the gusset weld joint with symmetric welds F=308 N and the material stress-strain response at the weld toe (with residual stress). a) Manson-Coffin curve, b) Weld toe peak stress history, c) The Ramberg-Osgood curve, d) The output data, e) Simulated stress-strain material response at the weld toe

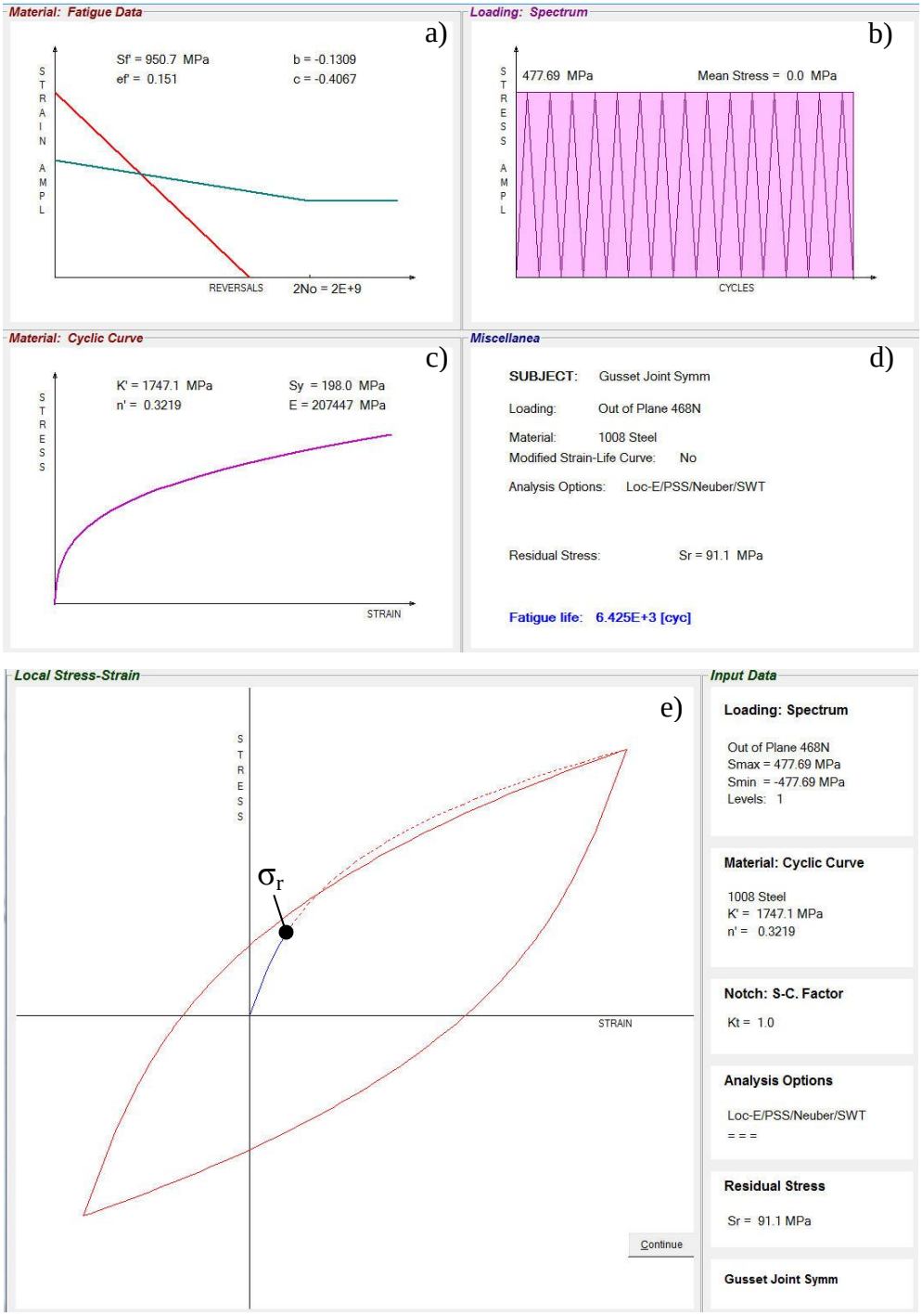

Figure 5-10: The input data and calculated fatigue crack initiation life for the gusset weld joint with symmetric welds F=468 N and the material stress-strain response at the weld toe (with residual stress). a) Manson-Coffin curve, b) Weld toe peak stress history, c) The Ramberg-Osgood curve, d) The output data, e) Simulated stress-strain material response at the weld toe

5.3.2 Fatigue crack propagation life estimation

The second part of the fatigue life analysis is concerned with the fatigue crack growth behavior and fracture mechanics. The fatigue crack growth analysis is carried out using the FALPR software package enabling the calculation of stress intensity factors and fatigue crack growth increments. The crack size at the end of the initiation period is estimated not to be greater than 0.5mm in depth. The observed initial cracks were semi-elliptical in shape with a length of 3.5 mm (Figure 2-8) measured on the surface, i.e. a/c=0.286. The semi-elliptical surface crack in a finite thickness plate is assumed to be the appropriate model for subsequent fatigue crack growth analysis.

The fatigue crack growth analysis of planar semi-elliptical cracks requires determination of stress intensity factors along the crack front. However, in the case of semi-elliptical cracks, it is sufficient to determine the stress intensity factor at only two points, i.e. the deepest and surface point along the crack front. The stress intensity factors for the actual crack shape (a/c) and depth, a, are calculated using the weight function method described in section 2.6. The through-thickness stress distribution based on the GR3 data induced by external load and the through-thickness residual stress distribution (σ_{zz} component as shown in Figure 5-6) have been used for the determination of stress intensity factors. The crack increments induced by subsequent stress cycles are calculated by using Paris fatigue crack growth expression (eqn. 2.13) valid for R=0 with parameters:

m = 3.720 and C = 1.95 x 10^{-12} for ΔK in [MPa$\sqrt{}$m] and da/dN in [m/cycle].

The threshold stress intensity range and the critical stress intensity factor for the tested material are:

$\Delta K_{th} = 3.5\ MPa\sqrt{m}$ at $R = 0$ and $K_C = 80\ MPa\sqrt{m}$.

It should be noted that the crack is not growing with the same rate in all directions. Therefore the crack increments at the deepest point and that one in the plate surface have been determined for each cycle. Both the crack depth and the crack aspect ratio (a/c) have updated after each load cycle. The fatigue crack growth predictions have been carried out with and without the residual stress effect.

The input data used in the FALPR software, the predicted crack depth growth versus the number of cycles, the stress intensity factor versus the number of cycles and the fatigue crack growth lives are presented in Figure 5-11 through Figure 5-18. The fatigue test experiments as well as the fatigue crack growth calculations were carried out until the crack reached approximate depth of a_f = 3.2mm.

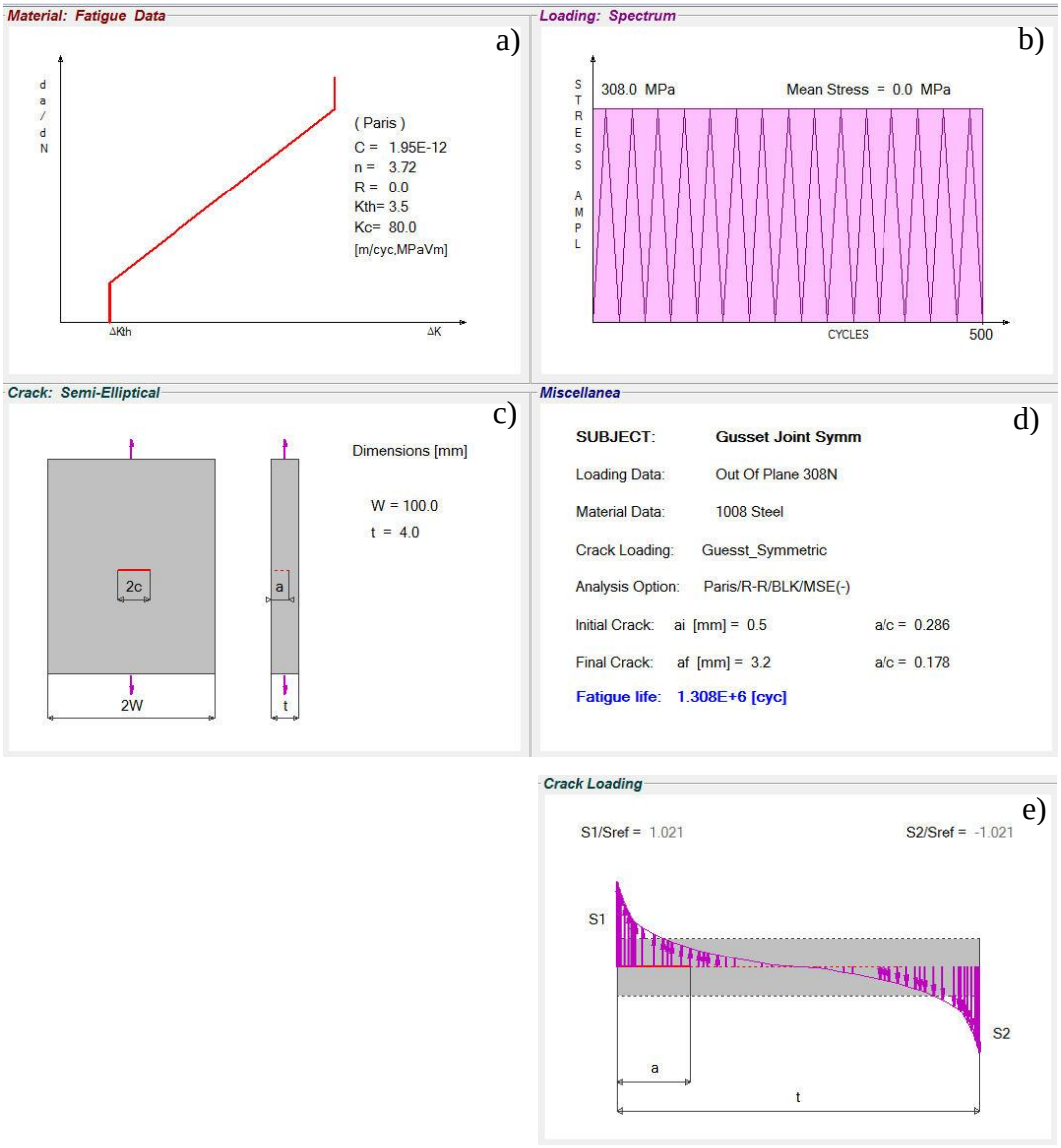

Figure 5-11: The input data for the fatigue crack growth analysis of the gusset weld joint with symmetric welds F=308 N (without residual stress). a) The Paris fatigue crack growth curve, b) The peak stress history, c) The crack model, d) The output data, e) The normalized through thickness stress distribution induced by the applied load.

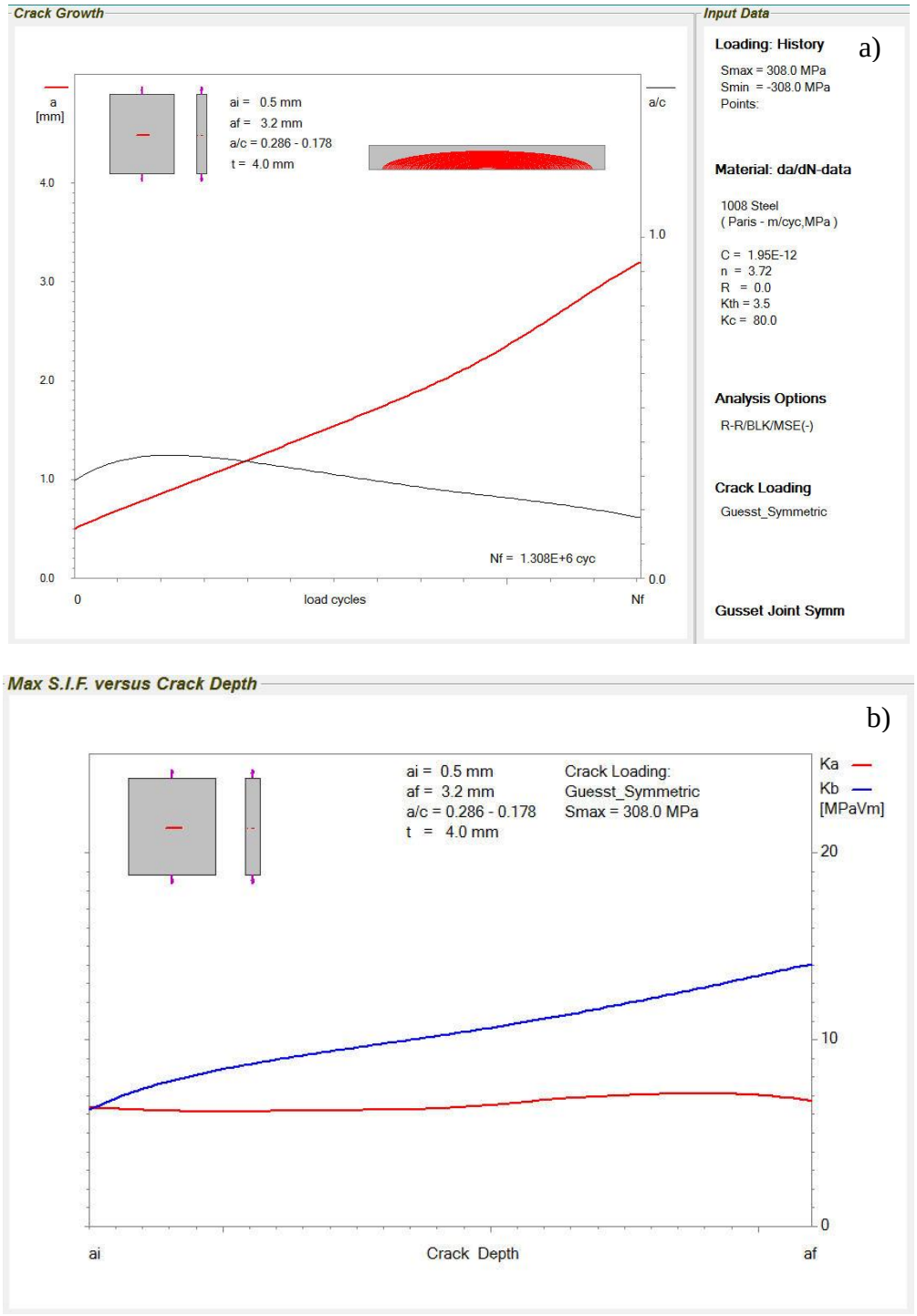

Figure 5-12: a) The crack depth versus the number of applied load cycles (a-N) diagram. b) The stress intensity factor versus the crack depth (K-a) diagram; Gusset weld joint with symmetric welds F=308 N (without residual stress)

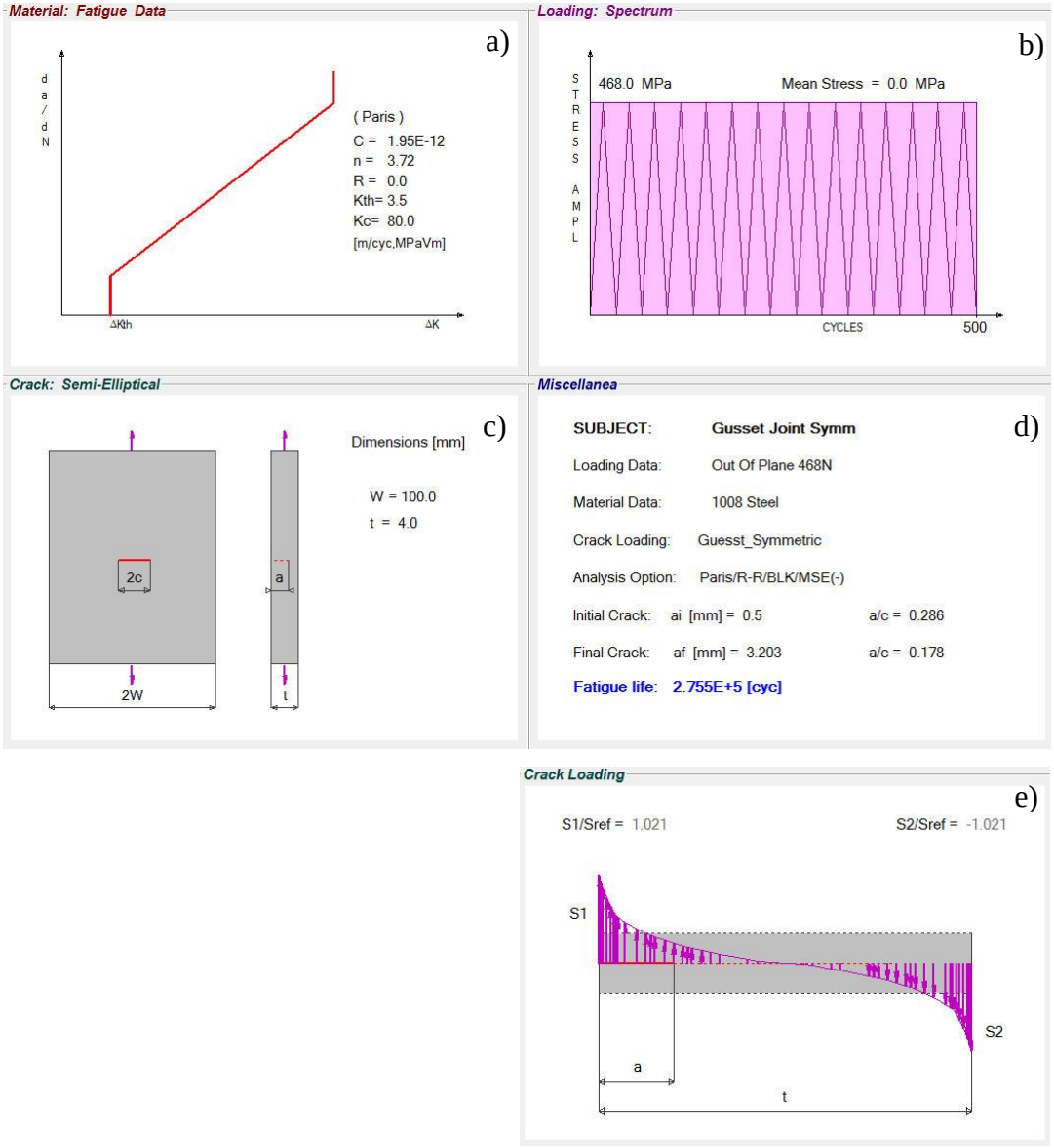

Figure 5-13: The input data for the fatigue crack growth analysis of the gusset weld joint with symmetric welds F=468 N (without residual stress). a) The Paris fatigue crack growth curve, b) The peak stress history, c) The crack model, d) The output data, e) The normalized through thickness stress distribution induced by the applied load.

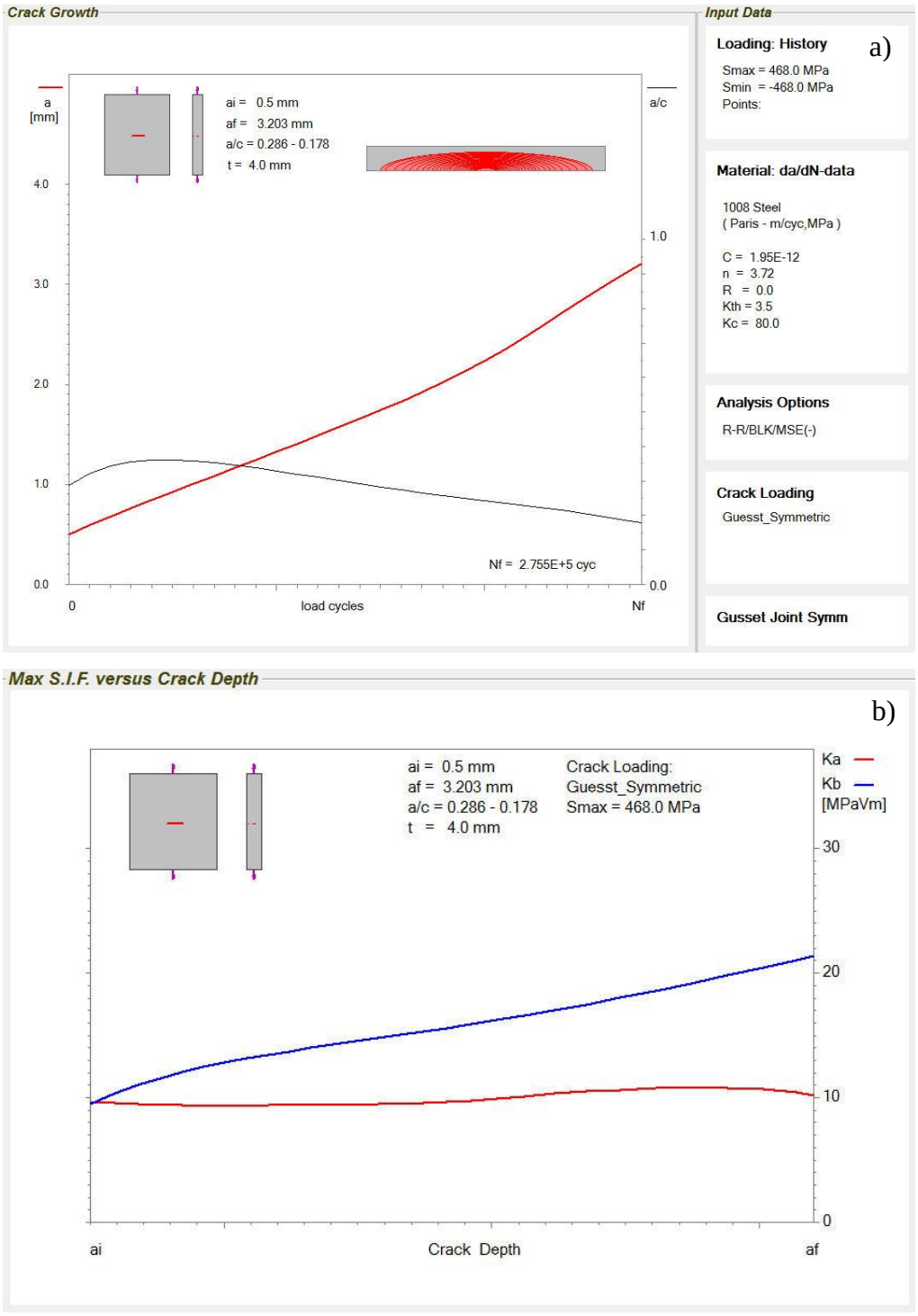

Figure 5-14: a) The crack depth versus the number of applied load cycles (a-N) diagram. b) The stress intensity factor versus the crack depth (K-a) diagram; Gusset weld joint with symmetric welds F=468 N (without residual stress)

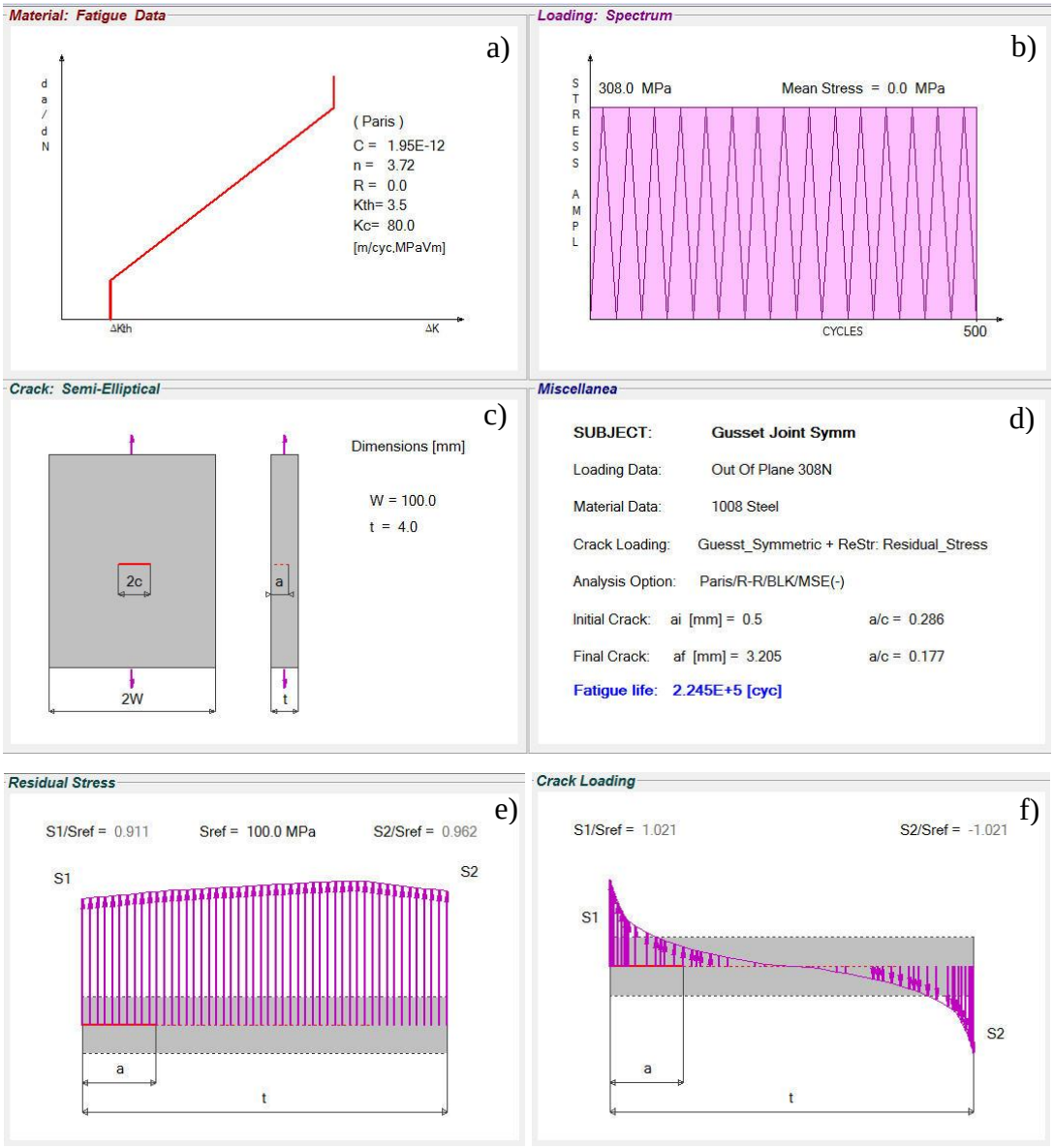

Figure 5-15: The input data for the fatigue crack growth analysis of the T-Joint subjected to out of plane load F=308 N (with residual stress). a) The Paris fatigue crack growth curve, b) The peak stress history, c) The crack model, d) The output data, e) Residual through thickness stress distribution, f) The normalized through thickness stress distribution induced by the applied load.

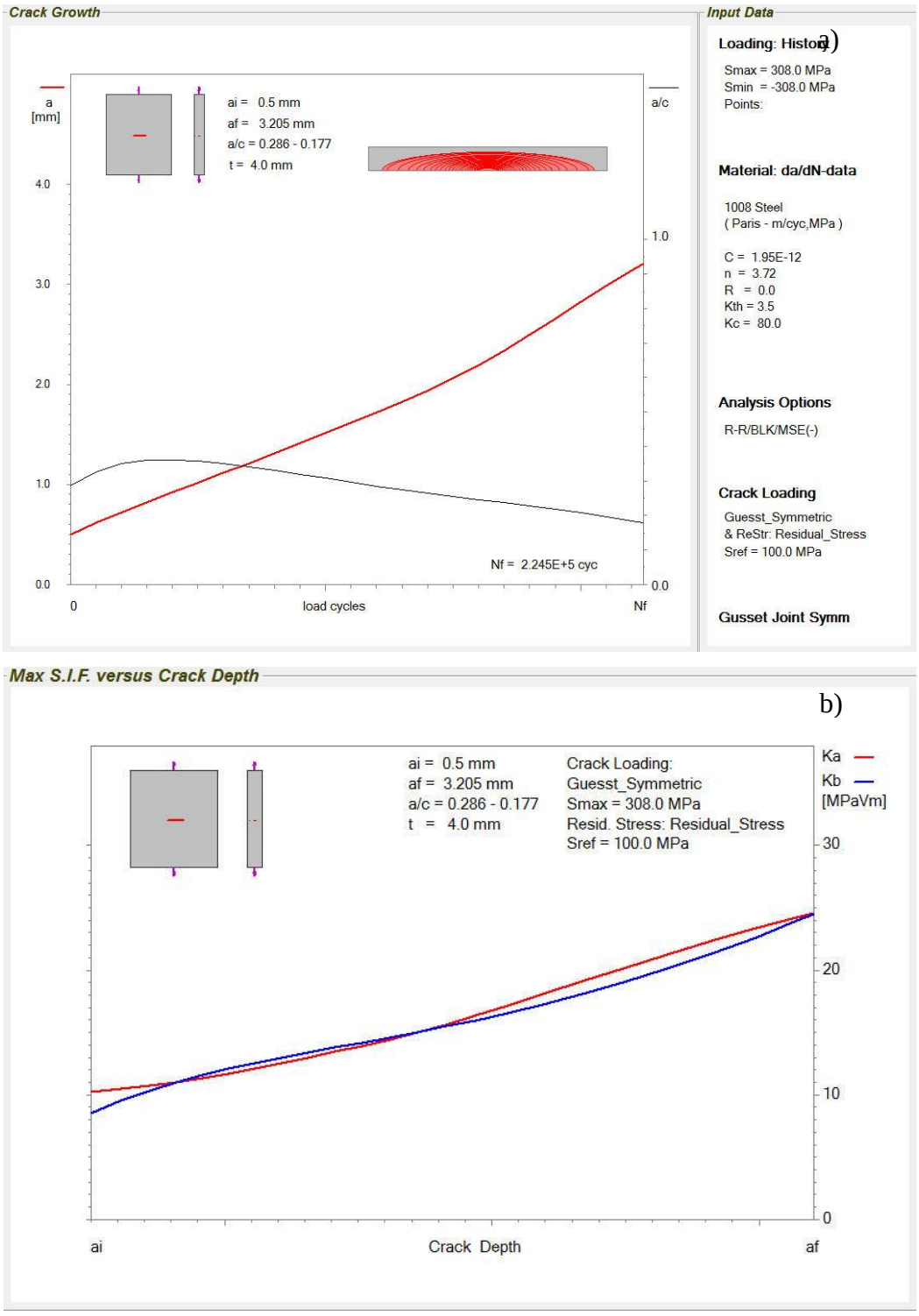

Figure 5-16: a) The crack depth versus the number of applied load cycles (a-N) diagram. b) The stress intensity factor versus the crack depth (K-a) diagram; T-Joint subjected to the out of plane load F=308 N (with residual stress).

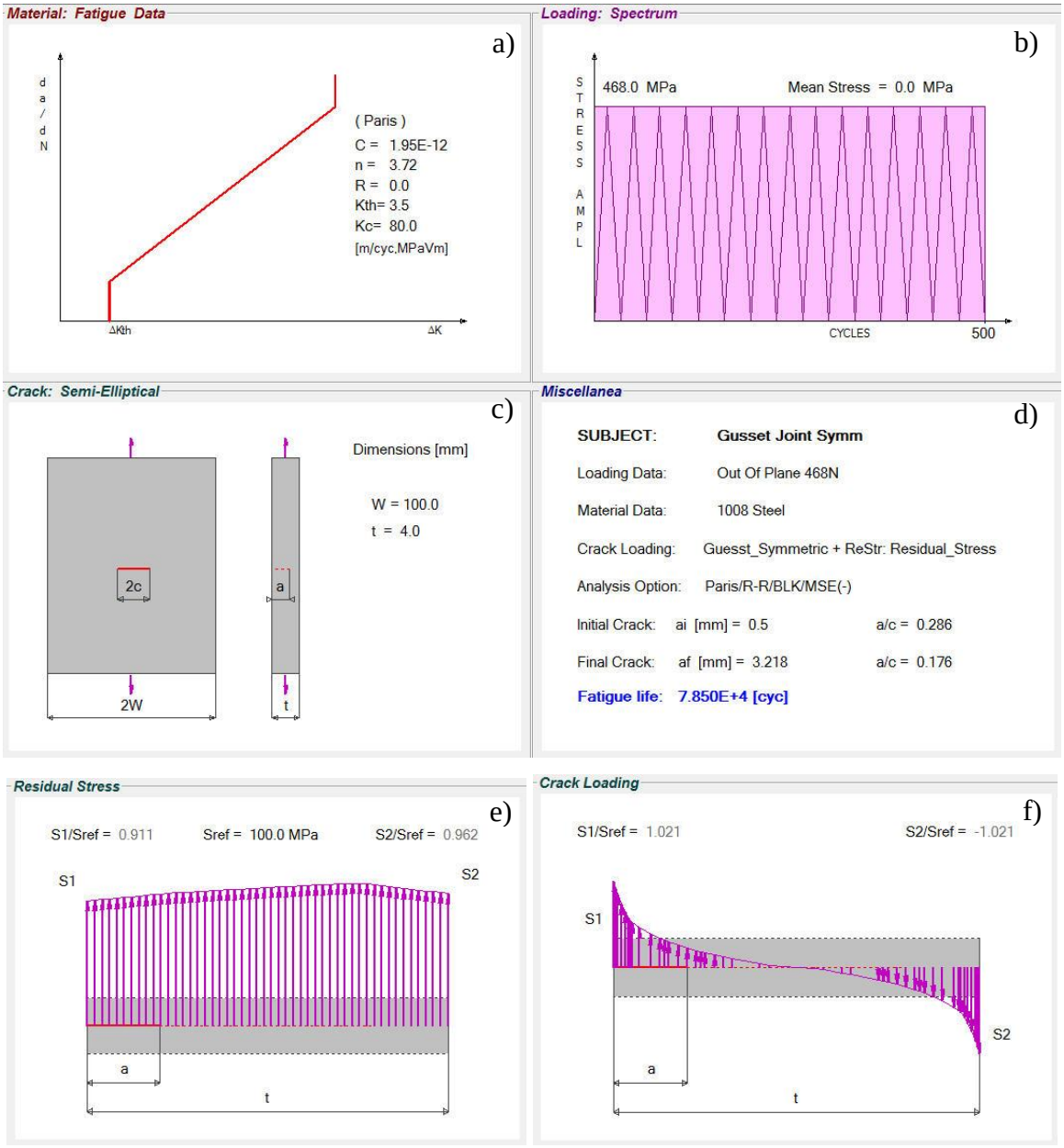

Figure 5-17: The input data for the fatigue crack growth analysis of the T-Joint subjected to out of plane load F=468 N (with residual stress). a) The Paris fatigue crack growth curve, b) The peak stress history, c) The crack model, d) The output data, e) Residual through thickness stress distribution, f) The normalized through thickness stress distribution induced by the applied load.

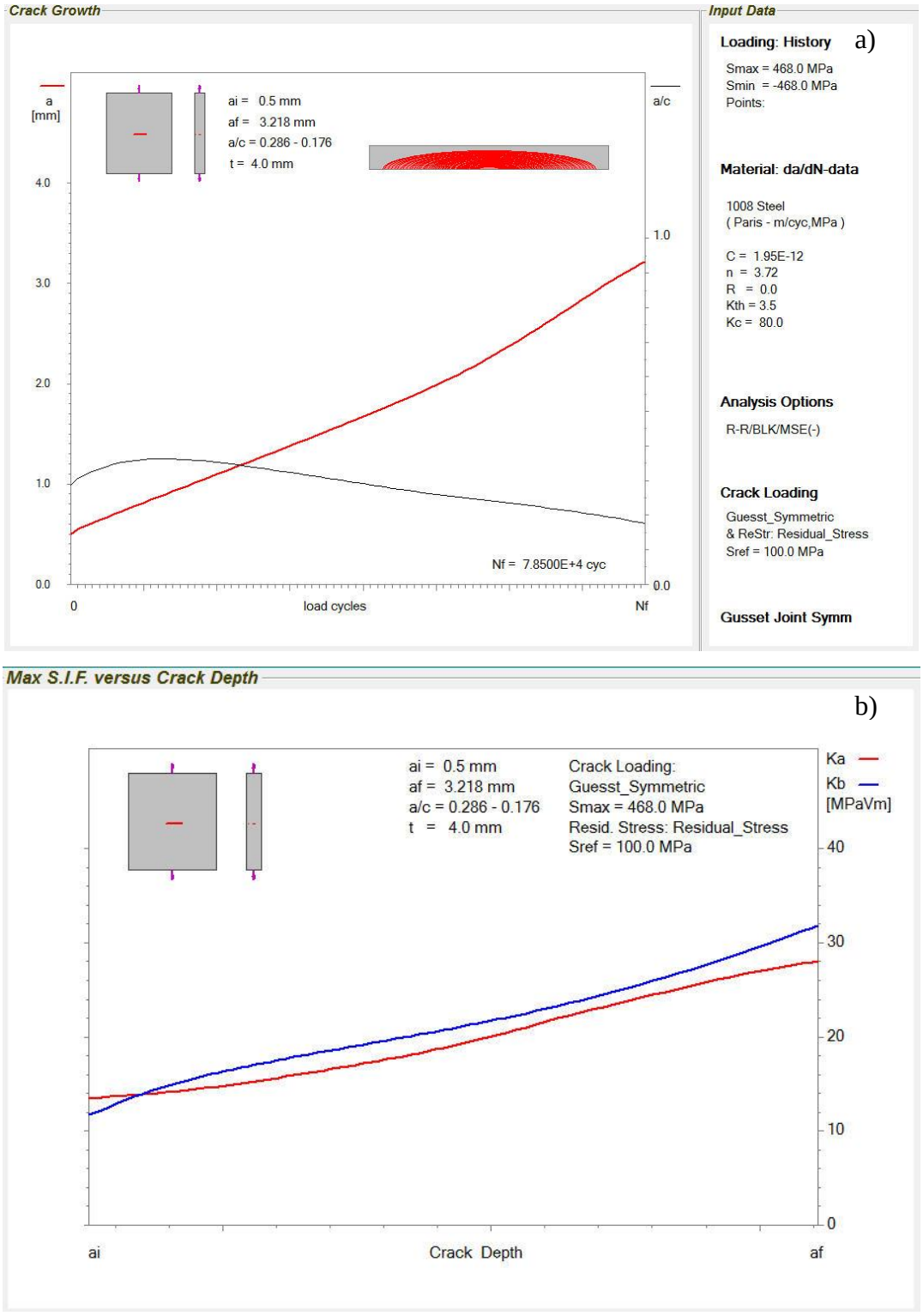

Figure 5-18: a) The crack depth versus the number of applied load cycles (a-N) diagram. b) The stress intensity factor versus the crack depth (K-a) diagram; T-Joint subjected to the out of plane load F=468 N (with residual stress).

5.3.3 The Total Fatigue Life

The total fatigue life (N_f) of the gusset weld joint with symmetric welds is determined as a sum of the fatigue crack initiation life (N_i) and the fatigue crack propagation life (N_P). The fatigue crack propagation life period is calculated for the initial crack depth $a_i = 0.5mm$ and final crack depth $a_f = 3.2mm$. The number of cycles as a function of the crack depth, a, and the crack aspect ratio, a/c, are determined by numerical integration of the Paris crack growth expression.

The calculated fatigue lives are summarized in Table 5-2 and Table 5-3.

Table 5-2: Summary of estimated fatigue lives for the gusset weld joint with symmetric welds (F=308 N)

Residual Stress (MPa)	N_i (Cycle) $a_i = 0.5mm$ 2c = 3.5 mm	N_p (Cycle) $a_f = 3.2mm$ 2c = 36.1 mm	N_i/N_p	N_f (Cycle)	N_i/N_f
$\sigma_r = 0$	58220	1308000	0.045	1366220	0.043
$\sigma_r = 91.1$	37420	224500	0.167	261920	0.143

Table 5-3: Summary of estimated fatigue lives for the gusset weld joint with symmetric welds (F=468 N)

Residual Stress (MPa)	N_i (Cycle) $a_i = 0.5mm$ 2c = 3.5 mm	N_p (Cycle) $a_f = 3.2mm$ 2c = 36.5 mm	N_i/N_p	N_f (Cycle)	N_i/N_f
$\sigma_r = 0$	8552	275500	0.031	284052	0.031
$\sigma_r = 91.1$	6425	78500	0.082	84925	0.076

According to the data above the ratios of the crack initiation to the crack propagation life and the crack initiation life to the total fatigue life are very low indicating that majority of the fatigue life of the analyzed weldment was spent on propagating the crack from its initial crack size a_i to final one a_f.

The calculated fatigue lives in terms of the number of load cycles are plotted as a function of the predicted surface crack length (2c) and they are shown in Figure 5-19 and Figure 5-20. The experimental fatigue lives are also shown in these figures.

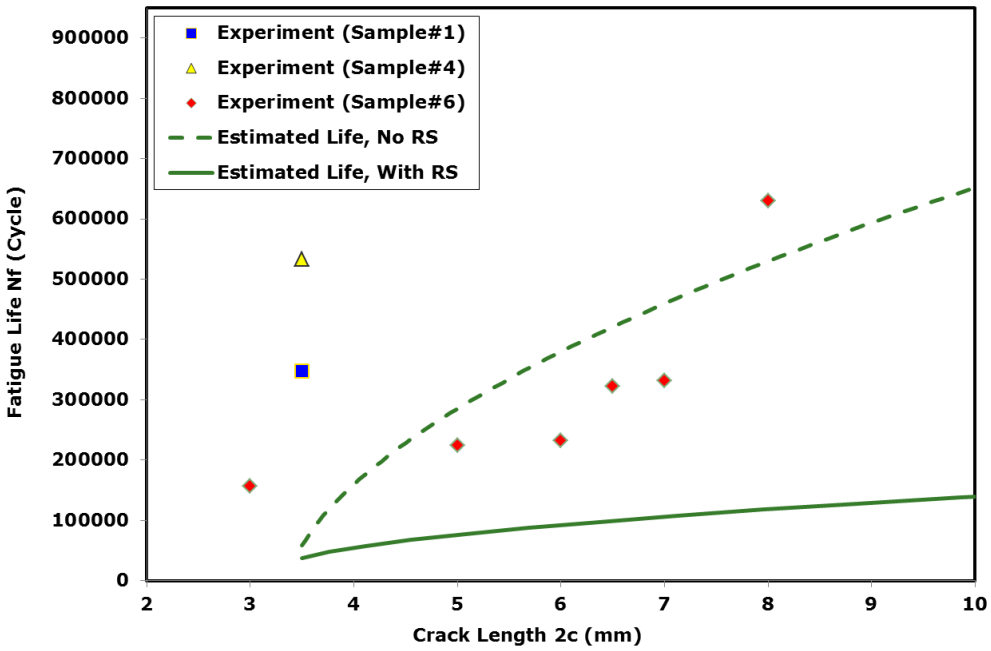

Figure 5-19: Comparison of calculated total fatigue lives and the experimental fatigue data for the gusset weld joint with symmetric welds (F = 308 N). Note: With RS means including the residual stress effect, No RS means excluding the residual stress effect.

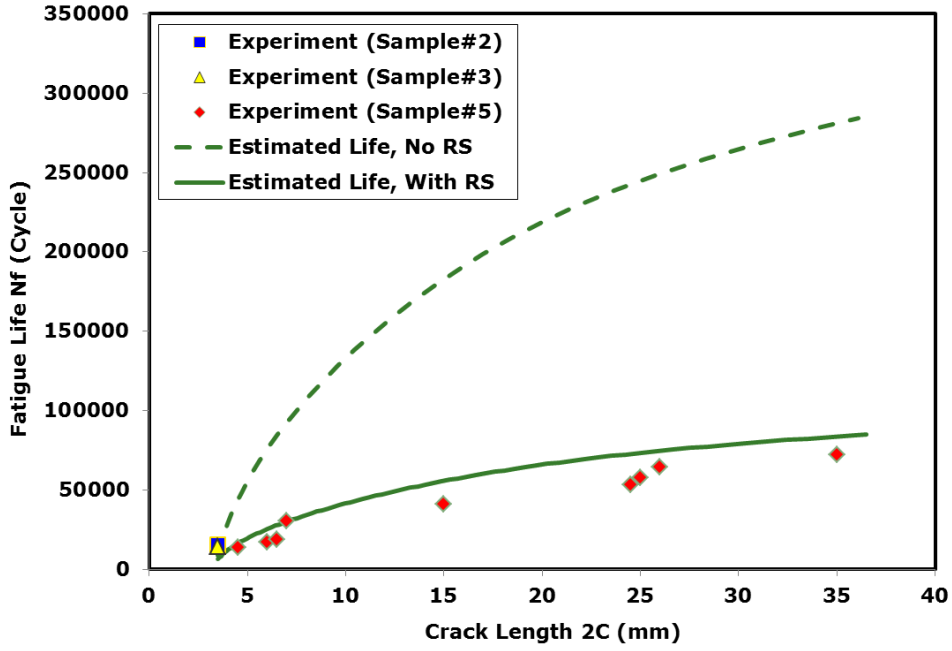

Figure 5-20: Comparison of calculated total fatigue lives and the experimental fatigue data for the gusset weld joint with symmetric welds (F = 468 N). Note: With RS means including the residual stress effect, No RS means excluding the residual stress effect.

The calculated fatigue lives (Figure 5-19 and Figure 5-20) and the experimental lives are generally in good agreement for both the low and high load levels. The cracks were located (as shown in Figure 5-21) in the region of estimated maximum stress in the gusset. The effect of the residual stress indicates the necessity of considering the residual stress contribution while estimating the fatigue lives of weldments.

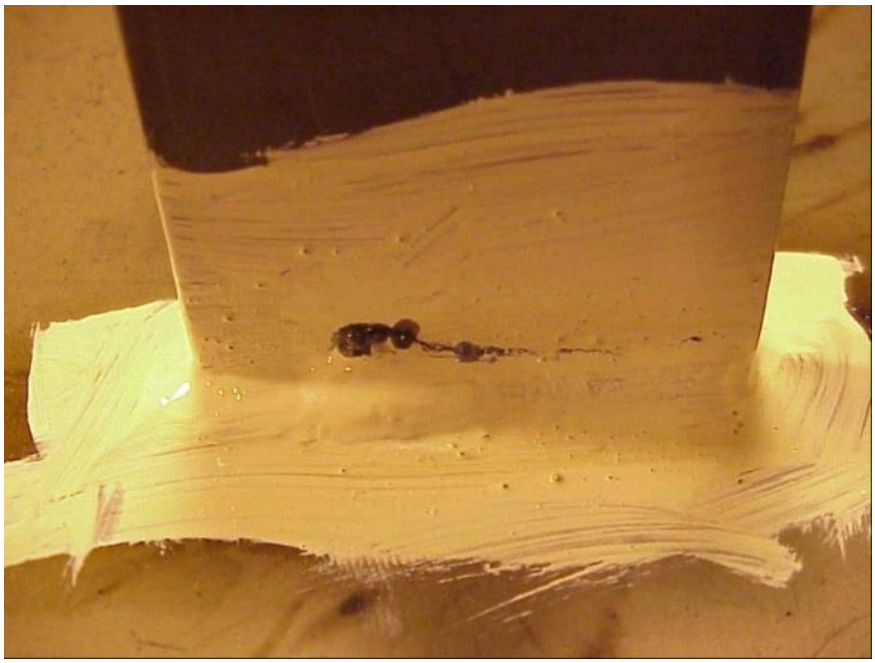

Figure 5-21: Fatigue location of fatigue cracks in the vertical attachment; gusset weld joint with symmetric welds (F=468 N). Cracks located in the region of predicted maximum stress

5.4 The Gusset weld joint – Non symmetric weld

In order to compare the predicted fatigue lives with the experimental data for the gusset weld joint with non-symmetric fillet welds, two series of fatigue tests have been carried out. The first one was conducted at the fully reversed load of 1320 N and the other at 2000 N. The welded sample along with the fatigue test set up arrangement is shown in the Figure 5-22. The tested welded joints (specimens) were made of 1008 steel alloy 4mm thin sheets. The base plate had a square shape with dimension of 500 mm by 500mm and the vertical plate had dimension of 100 mm by 50mm. The geometry of the sample is shown in Figure 3-14.

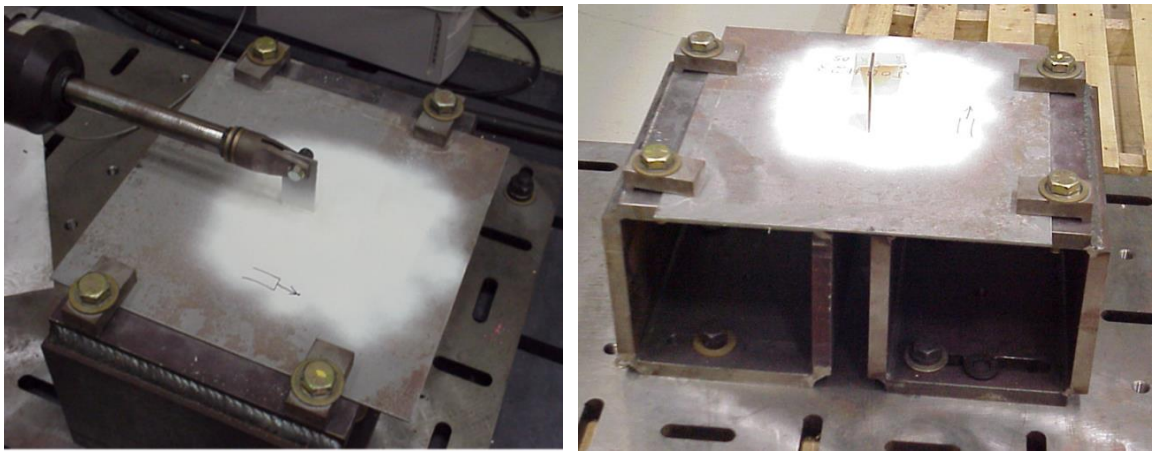

Figure 5-22: Welded specimen and the fatigue test setup arrangement - gusset weld joint with non-symmetric welds

The samples were manually welded using gas metal arc welding process. The samples were initially tack welded before doing the full welding. A simple weld fixture to hold the tack welded sample was used to allow the full welds to be performed in the 2F welding position. The welding was performed using 1.2mm ER70S-6 weld wire with 90% Ar and 10% CO_2 shielding gas mixture. The spray mode of metal transfer was used with these weld process parameters: wire feed speed – 7.8 m/min, current – 259 A, voltage – 23V and travel speed – 0.45 m/min.

For the experimental fatigue testing, the samples were clamped in the fixture at four locations (approximate clamping area of 40 by 80mm at each corner) and the cyclic load was applied through the hole in the vertical plate (see Figure 5-22). The sample was put on two 50.8 mm square boxes. There was 50.8 mm spacing between the boxes and the test specimen was mounted at the edges at four places. Around 10 such samples were welded and tested under fatigue loading and the data is presented for the 8 samples which were successful completed. Six samples were tested at the lower load level of 1320N and the rest of them were tested at higher load level of 2000N.

The experimental fatigue lives obtained are listed in Table 5-4. The numbers of load cycles are given as a function of the crack length (2c) measured on the plate surface. The crack depth is only an estimate.

Table 5-4: Experimental fatigue crack growth data (2c-N) for the gusset weld joint with non-symmetric welds

Sample #	**RE2**	**RE3**	**11**	**15**	**16**	**17**	**18**	**19**
Load (N)	1320	1320	2000	1320	1320	1320	1320	2000
First detected crack length (mm)	5.5	5.5	4.5	7.0	4.0	4.0	6.5	11.5
Number of cycles (cycles)	28777	46726	2196	66774	464500	117516	683500	4288
Crack length (mm)	-	-	10.0	8.5	-	-	-	-
Cycle count	-	-	2500	103825	-	-	-	-
Crack length (mm)	-	-	16.0	10.0	6.0	6.0	13.4	20.0
Cycle count	-	-	4600	211631	1190502	230096	797116	8369

Next, the numerical calculations have been carried out for estimation of fatigue life for the gusset weld joint with non-symmetric welds as per the proposed methodology.

The peak stresses and the through thickness stress distributions induced by the applied load levels are obtained by scaling the GR3 model stress data shown in Figure 4-11 and the simulated stress distributions are presented in Figure 5-23 and Figure 5-24.

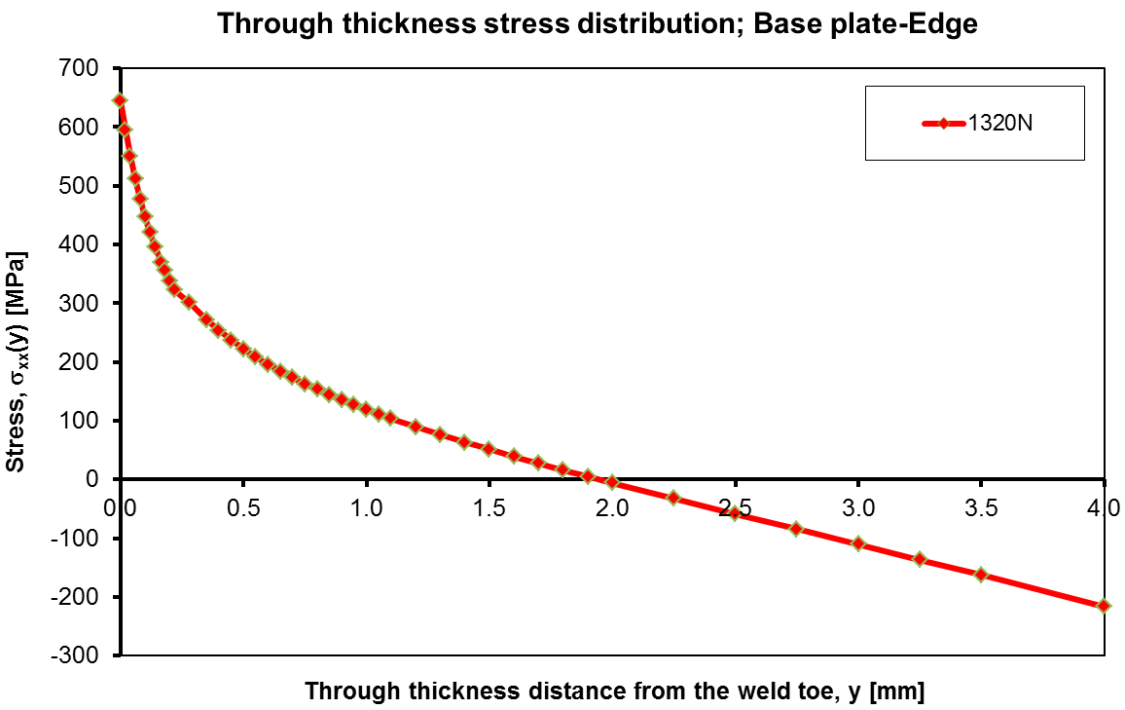

Figure 5-23: Simulated GR3 based through-thickness stress distribution in the critical cross section of the gusset weld joint with non-symmetric welds (F=1320 N)

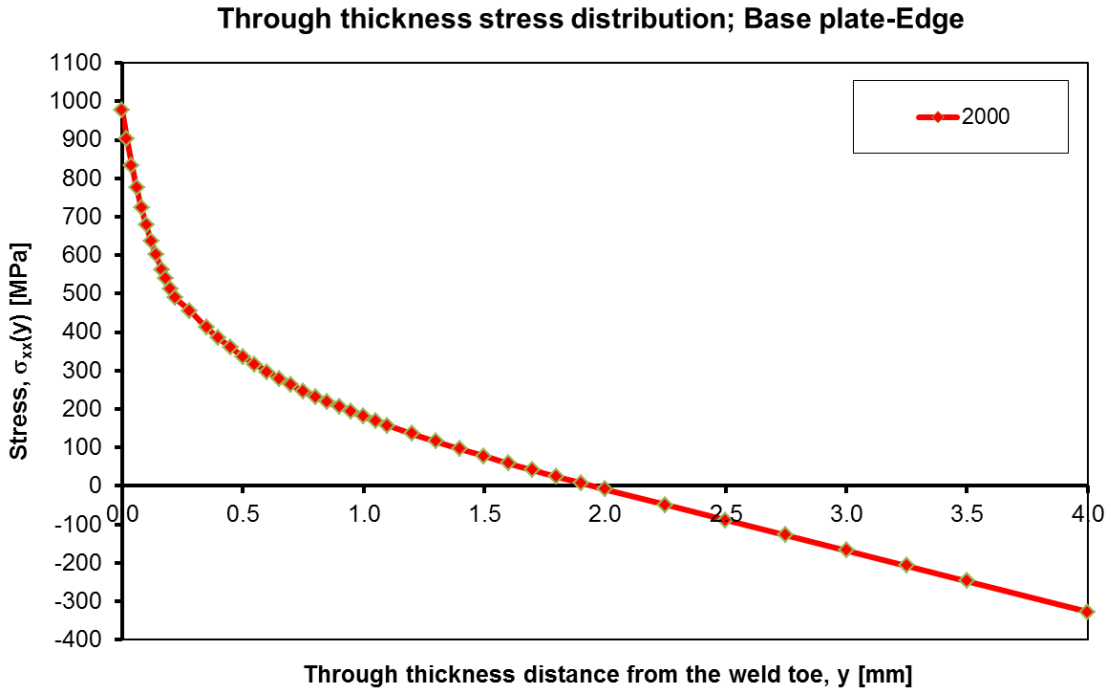

Figure 5-24: Simulated GR3 based through-thickness stress distribution in the critical cross section of the gusset weld joint with non-symmetric welds (F=2000 N)

Fatigue lives are calculated for each load case with and without accounting for the presence of the residual stress. Using welding process simulation model, the residual stresses were estimated for this joint and the through thickness residual stress distribution for the normal stress component extracted at the critical section (same as used for extracting the stress distribution induced by the external loads) is shown in Figure 5-25. The residual stress was measured in the plate surface using XRD method and was found to be 100MPa, which is quite close to the residual stress at the weld toe obtained using weld simulation.

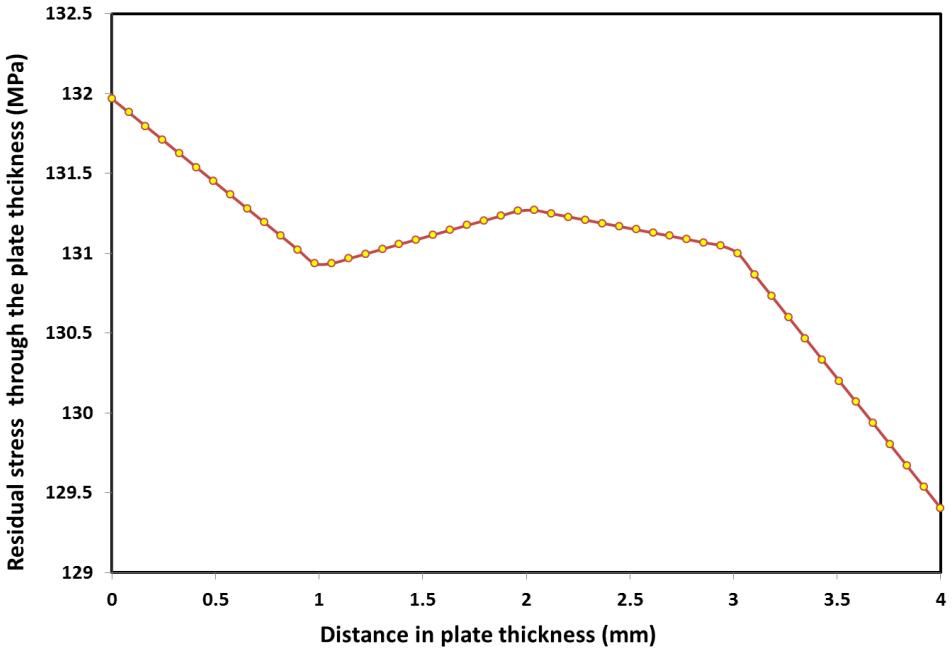

Figure 5-25: Simulated through the thickness residual stress distribution in the critical cross section of the of the gusset weld joint with non-symmetric welds

5.4.1 Fatigue crack initiation life estimation

The fatigue crack initiation life is estimated using the strain-life method coded into the FALIN software. The fatigue life calculations are based on the material properties listed in Table 4-2 and Table 4-3 for 1008 steel.

It is noticeable (see Table 5-5 and Table 5-6) that the residual stress had profound effect on the fatigue crack initiation life. The analysis indicates that the tensile residual stress at the weld toe may decrease the fatigue crack initiation life approximately by a factor of 2.

5.4.2 Fatigue crack propagation life estimation

The fatigue crack growth analysis was carried out using the FALPR software package. The crack size at the end of the initiation period, i.e. the initial crack for the fatigue crack growth analysis, was estimated as not to be greater than 0.5 mm in depth. The observed cracks were semi-elliptical in shape with a length of approximately 3.5 mm (Figure 2-8) on the surface, i.e. the initial crack aspect ratio was a/c=0.286. The planar semi-elliptical surface crack in a finite thickness plate (Figure 5-11c) was assumed to be the appropriate model for the fatigue crack growth predictions up to the final crack length 2c ≈ t, i.e. 2c ≈ 4-5mm. The planar crack model assumed in the analysis was not adequate to analyze cracks wrapping around the gusset plate edge. Therefore the analysis of the crack growth carried out for the cracks initiated at the gusset plate edge and presented below was valid up to the final crack length of approximately 2c < 5mm.

5.4.3 The Total Fatigue Life

The total fatigue life (N_f) of the T-welded joint subjected to in plane load was determined as a sum of the fatigue crack initiation life (N_i) and the fatigue crack propagation life (N_P). The fatigue crack propagation life period was calculated for the initial crack depth $a_i = 0.5\ mm$ and the final crack depth $a_f = 3.2\,mm$.

The calculated fatigue lives are summarized in Table 5-5 and Table 5-6.

Table 5-5: Summary of estimated fatigue lives for the gusset weld joint with non-symmetric welds (F=1320 N)

Residual Stress (MPa)	N_i (Cycle) $a_i = 0.5mm$ 2c = 3.5 mm	N_p (Cycle) $a_f = 3.2mm$ 2c = 36.1 mm	N_i/N_p	N_p (Cycle)	N_i/N_f
$\sigma_r = 0$	2344	84064	0.028	86408	0.027
$\sigma_r = 131.9$	1877	7265	0.258	9142	0.205

Table 5-6: Summary of estimated fatigue lives for the gusset weld joint with non-symmetric welds (F=2000 N)

Residual Stress (MPa)	N_i (Cycle) $a_i = 0.5mm$ 2c = 3.5 mm	N_p (Cycle) $a_f = 3.2mm$ 2c = 36.5 mm	N_i/N_p	N_p (Cycle)	N_i/N_f
$\sigma_r = 0$	419	17920	0.023	18339	0.023
$\sigma_r = 131.9$	359	2172	0.165	2531	0.141

According to the data above the ratios of the crack initiation to the crack propagation life and the crack initiation life to the total fatigue life were very low indicating that majority of the fatigue life of the analyzed weldment was spent on propagating the crack from its initial crack size a_i to final one a_f.

The calculated fatigue lives in terms of the number of load cycles are plotted as a function of the predicted surface crack length (2c) and they are shown in Figure 5-26 and Figure 5-29. The experimental fatigue lives are also shown in these figures.

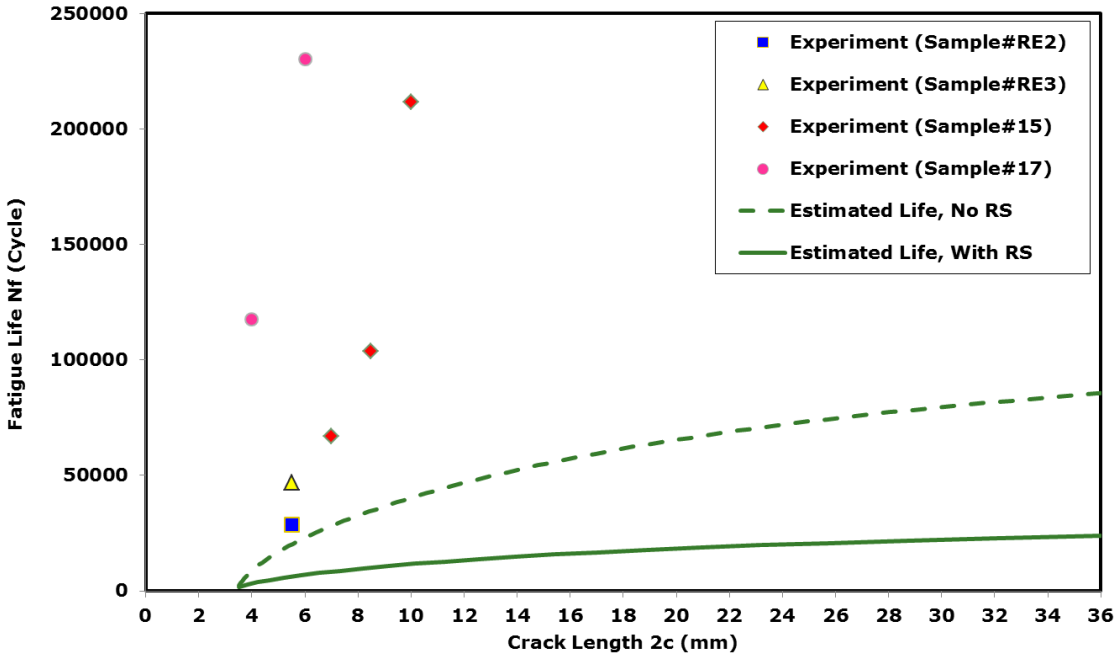

Figure 5-26: Comparison of calculated total fatigue lives and the experimental fatigue data; T-Joint specimen subjected to fully reversed in plane load F = 1320 N. Note: With RS means including the residual stress effect, No RS means excluding the residual stress effect

It is apparent (Figure 5-26) that the analysis based on the GR3 model stress data resulted in conservative under-prediction of fatigue lives by factor of 3 to 5. This is due to the fact that it was assumed in the fatigue crack growth analysis that the crack would be planar (i.e. grow in one plane normal to the gusset plane) from its initial to the final size. However, in reality fatigue cracks are following the weld toe line, i.e. they started from the edge of the gusset, propagated around the edge and growing later parallel to the gusset plate into the low stress region (See Figure 5-27). Therefore, almost all cracks got arrested after their tips moved along the plate sides a few millimeters away from the gusset edge. Therefore the applied crack model was valid for estimating the crack growth up the length of 2c=t (gusset thickness). After reaching the size t=2c the cracks went around the edge and they grew very slow or they were arrested. Therefore the fatigue life estimation are valid up to reaching the crack length of 2c = t= 4 mm. Unfortunately, the fatigue lives corresponding to the crack length of 2c ≈ 4mm were in most cases not recorded.

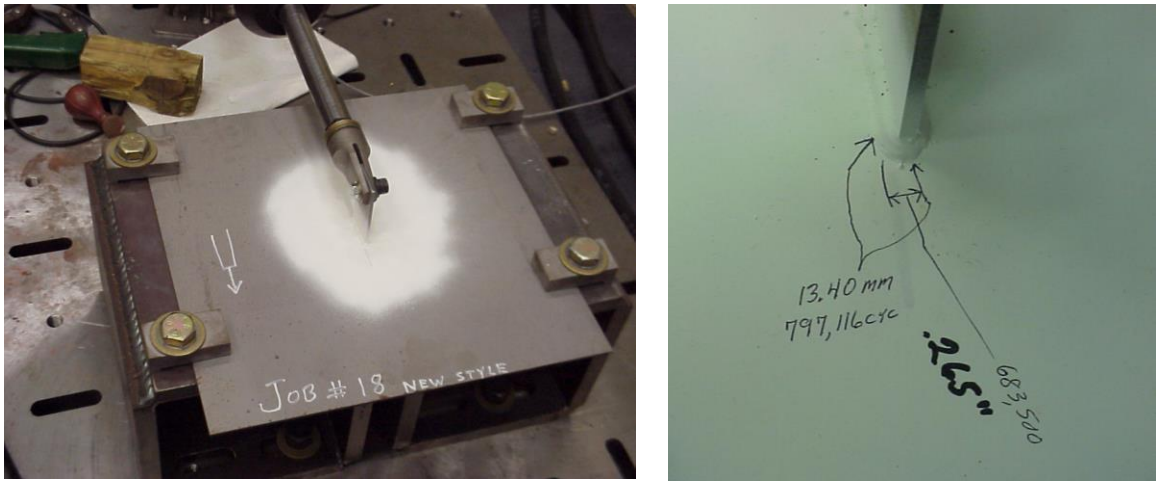

Figure 5-27: Fatigue crack in the base plate located in the region of estimated maximum stress (sample#18). Gusset joint with non-symmetric welds (F=1320 N)

The other source of error for the under-prediction of the fatigue crack initiation lives might have come from the overestimation of stresses at the gusset edge (see Figure 4-13 and Figure 4-14). One of the attributing facts is that in the real weld samples, weld was smoothly wrapped around the edge, whereas in the 3D coarse mesh FEA model weld was modeled with several sharp corners especially near the edge of the gusset.

Unfortunately, even there was a variation found in the test samples due to the differences in welding technique used for producing these samples (See Figure 5-28). Some samples had the continuous welds which were nicely wrapped around the edge (Sample#16 and #18), few other samples had the welds deposited at the gusset edge using a tack weld option causing weld starts and stops at the corners resulting in higher SCF (sample#15), while the remaining few samples did not even had the weld deposit around the gusset edge (sample#RE3). Effect of this variation in the weld geometry due to different welding practices, is reflected in the experimental fatigue test results (see Table 5-4). The test samples with the nicely wrapped weld around the gusset edge, without any start or stop at the corners, showed higher fatigue life compared to other samples with improperly wrapped welds. This finding brings out an important aspect about the quality and workmanship of welds, which becomes significantly important especially for the structural welds subjected to fatigue loading. Any change in the welding process, technique or skill of the operator could have large impact on the fatigue life variability.

Though the data was limited but better estimation was achieved in the case of high load level (Figure 5-29) where the total fatigue lives were less dependent on the accuracy of prediction of the crack initiation life.

The effect of the residual stress, shown in Figure 5-26 and Figure 5-29 indicates the necessity of including the residual stress effect into the analysis of fatigue lives of weldments.

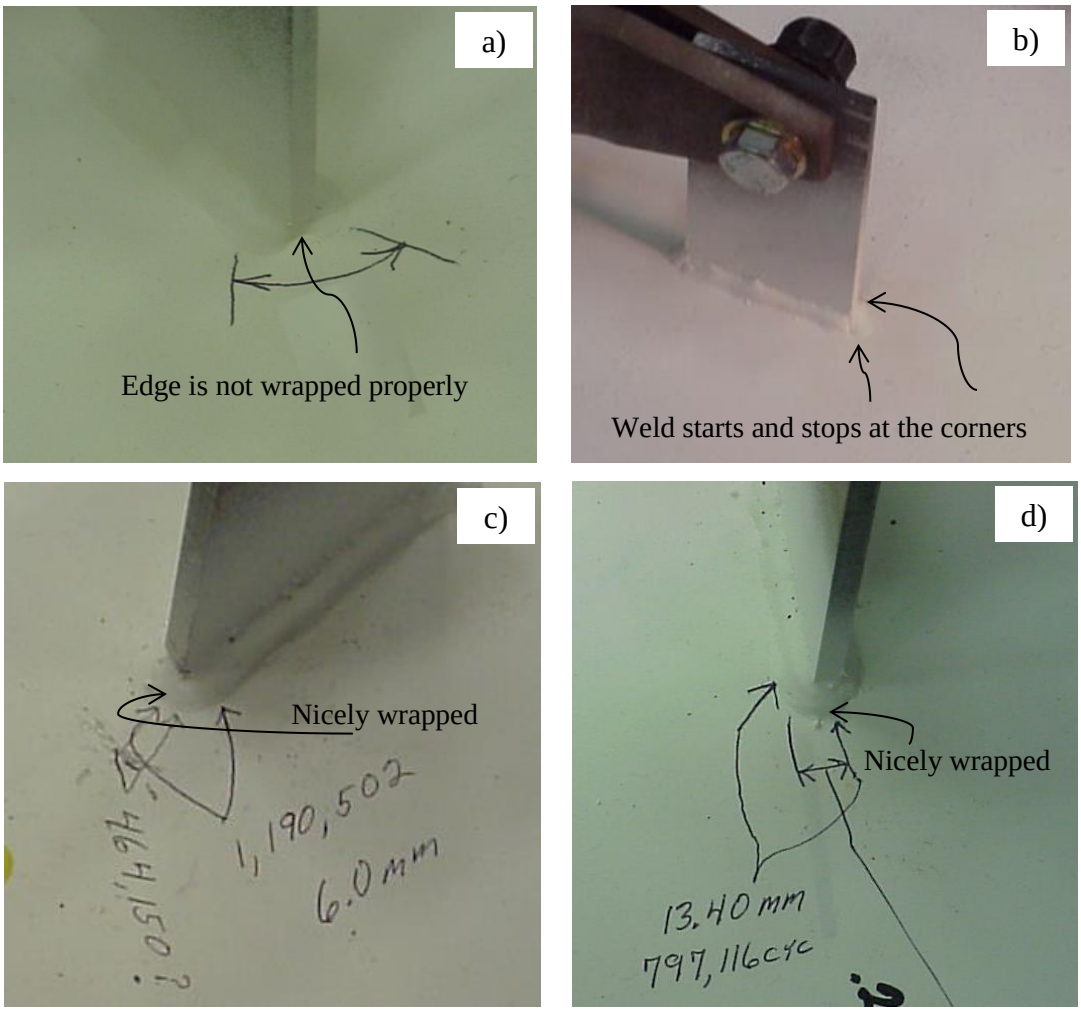

Figure 5-28: Manufacturing variability in the welded samples (a) Weld deposit missing around the gusset edge (Sample RE#3) (b) Weld deposit at the gusset edge using tack weld, causing weld starts and stops at the corners (Sample#15) (c) Nicely wrapped weld around the edge with no starts and stops in the corners (Sample#16) (d) Another sample with nicely wrapped weld around the edge (Sample#18)

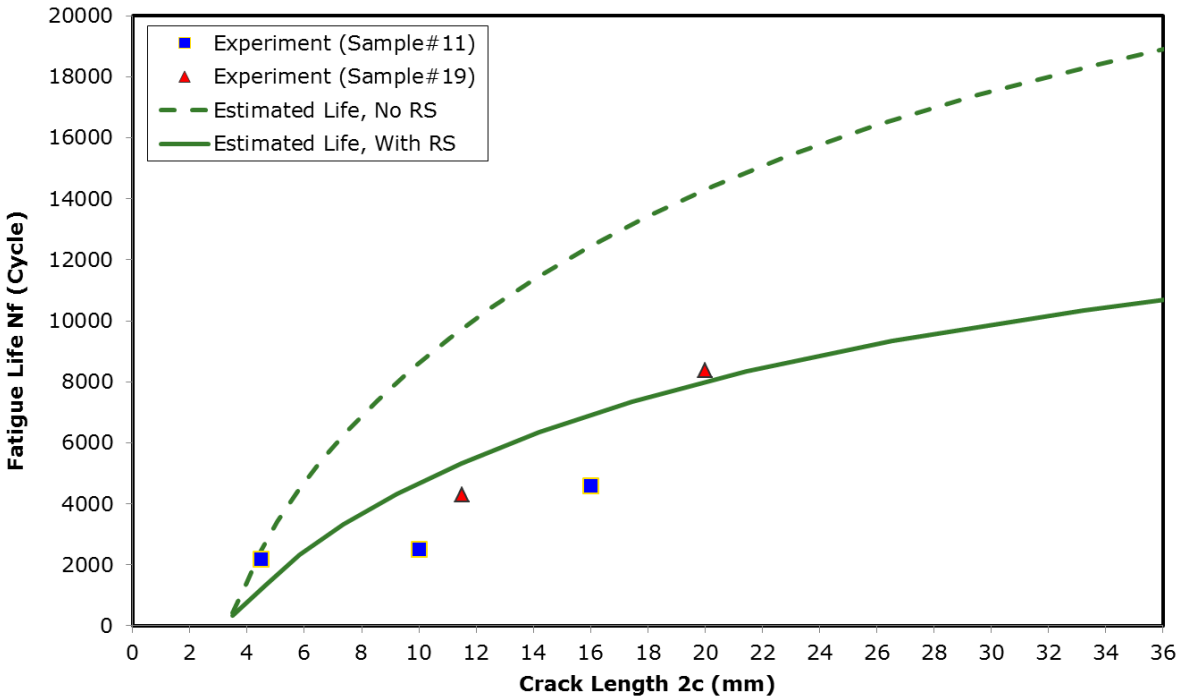

Figure 5-29: Comparison of calculated total fatigue lives and the experimental fatigue data; T-Joint specimen subjected to fully reversed in plane load F = 2000 N. Note: With RS means including the residual stress effect, No RS means excluding the residual stress effect.

It should be noted that the fatigue cracks detected in experiments are located, as estimated, in the region of maximum peak stress, i.e. at the weld toe near the gusset plate edge (see Figure 5-27 and Figure 5-28).

The fatigue cracks were growing into the base plate thickness and along the weld toe line in the plate surface. Due to high stress at the weld toe (Figure 4-11) cracks were growing faster on the surface (along the weld toe line) than into the thickness. Therefore the shape of final cracks was reaching relatively low aspect ratio.

5.5 The beam weldment under bending load

In order to compare the predicted fatigue lives with the experimental data for the beam weldment, two series of fatigue tests have been carried out at 2500lbs and 1600lbs at R=0.1. The tested welded joints (specimens) were made of ASTM A500 Grade C steel alloy for the tube material and 1008 steel alloy for the attachment plates. The tube had a thickness of 6.35mm and the cross-section was 127 mm by 76.2 mm. The cover plate had

a thickness of 6.35 mm as well. The geometry of the overall welded sample is shown in Figure 5-30. The fatigue test set up arrangement is shown in the Figure 5-31 and Figure 5-32.

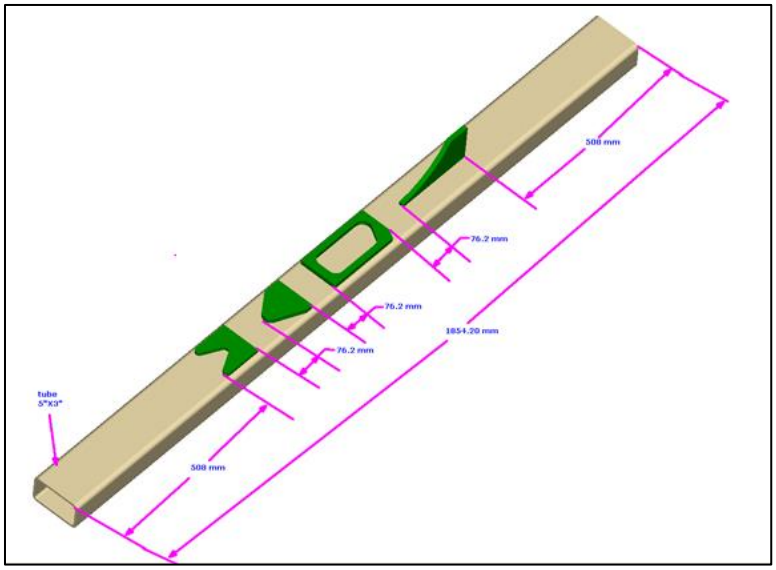

Figure 5-30: Geometrical details of the welded specimen – beam weldment

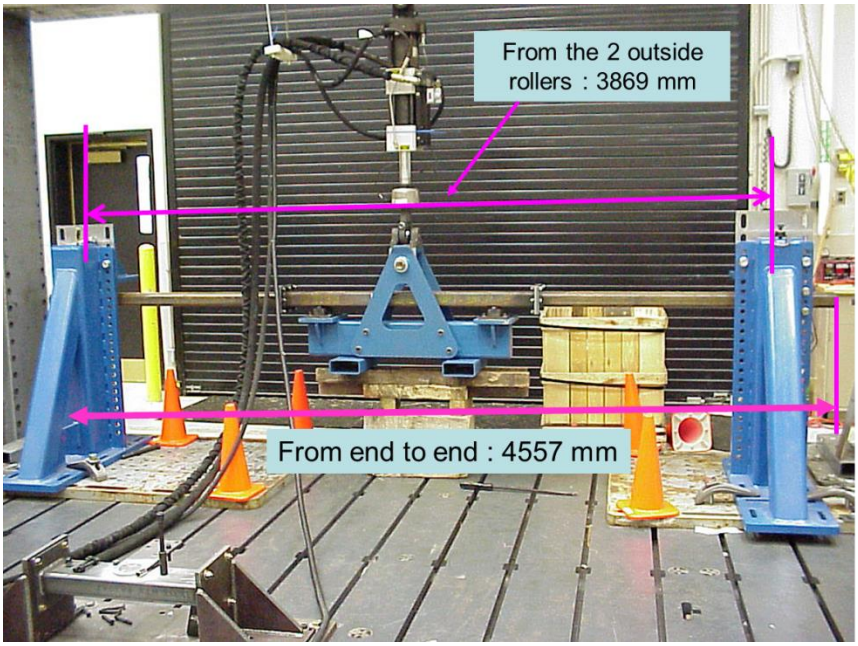

Figure 5-31: The fatigue test setup arrangement – beam weldment

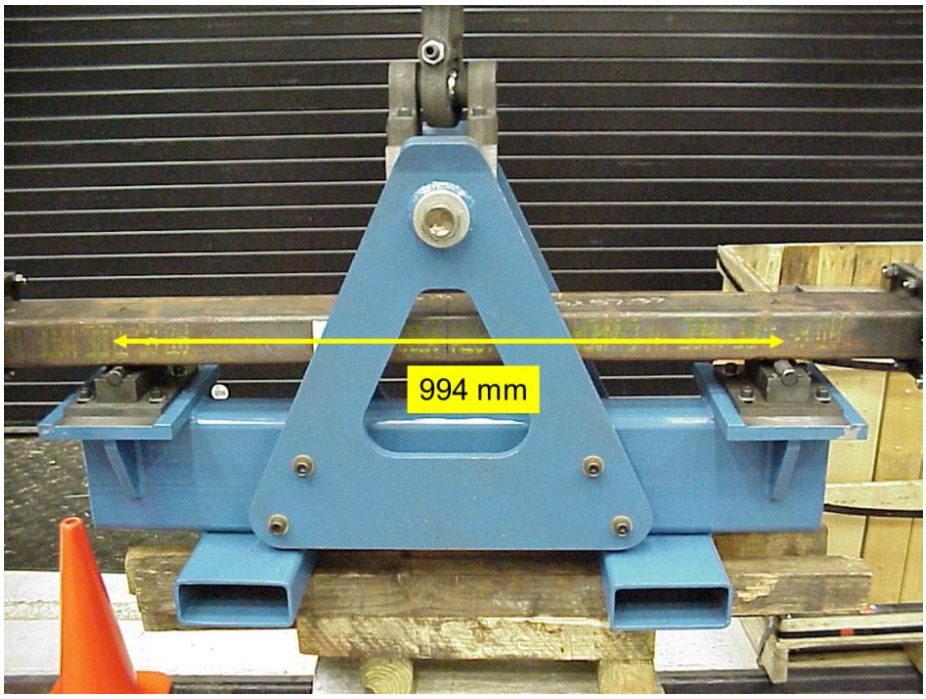

Figure 5-32: The fatigue test setup arrangement (closer view of the inside roller locations) – beam weldment

The samples were manually welded using gas metal arc welding process. The samples were initially tack welded before doing the full welding. A simple weld fixture to hold the tack welded sample was used to allow the full welds to be performed in the 2F welding position. The welding was performed using 1.2mm ER70S-6 weld wire with 90% Ar and 10% CO_2 shielding gas mixture. The spray mode of metal transfer was used with these weld process parameters: wire feed speed – 11.8 m/min, current – 321 A, voltage – 25 V and travel speed – 0.58 m/min.

For the experimental fatigue testing, the samples were subjected to four point pure bending load case as they were held in the fixture at the two end locations (see Figure 5-31) and the cyclic load was applied at the two inner locations (see Figure 5-32). Around 5 such samples were welded and tested under fatigue loading and the data is presented for these samples. Three samples were tested at the lower load level of 1600lbs and the rest of them were tested at higher load level of 2500lbs.

The experimental fatigue lives obtained are listed in the Table 5-7. The numbers of load cycles are given as a function of the crack length (2c) measured on the surface. The crack depth is only an estimate.

Table 5-7: Experimental fatigue crack growth data (2c-N) for the beam weldment

Sample #	**8**	**9**	**11**	**13**	**14**
Load (lbs)	2500	2500	1600	1600	1600
First detected crack length (mm)	3.0	10.5	9.3	10.3	7.8
Number of cycles (cycles)	150000	123469	572366	304299	232105
Crack length (mm)	4.0	-	33.8	-	-
Cycle count	159000	-	696987	-	-
Crack length (mm)	32.1	-	-	-	-
Cycle count	196997	-	-	-	-

Next, the numerical calculations have been carried out for the estimation of fatigue life for the beam weldment as per the proposed methodology.

The simulated peak stresses and the through thickness stress distributions obtained by using the GR3 model for the applied load level of 2500lbs is shown in Figure 4-31 and is reproduced in Figure 5-33. The scaled simulated stress distribution for the load level of 1600lb is presented in Figure 5-34.

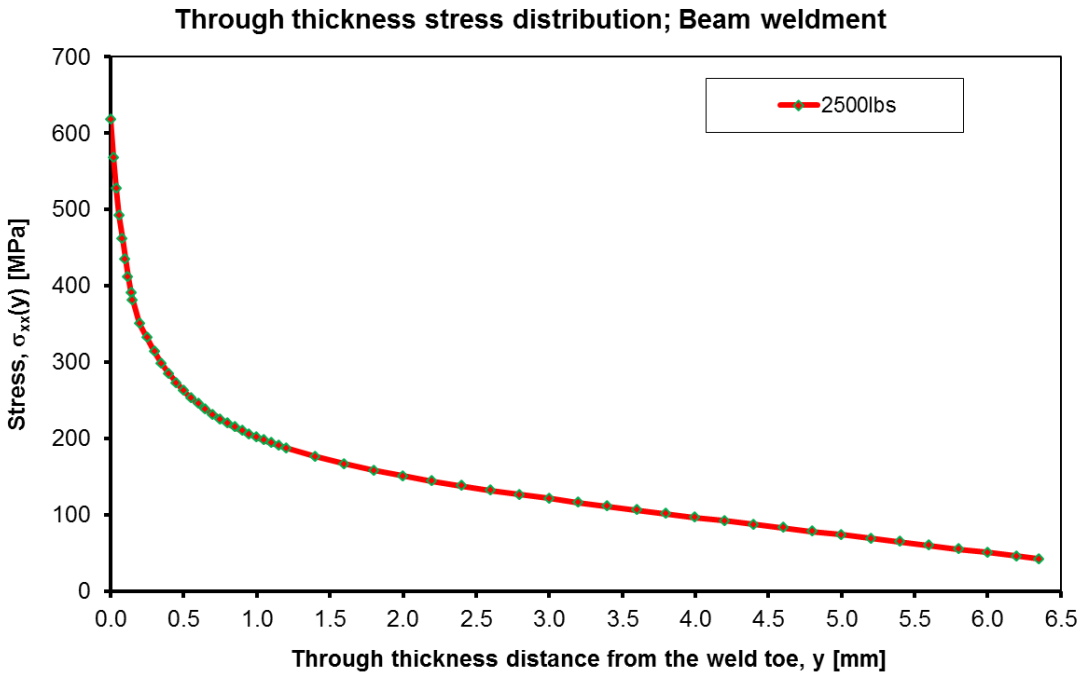

Figure 5-33: Simulated GR3 based through-thickness stress distribution in the critical cross section of the beam weldment (2F=2500 lbs)

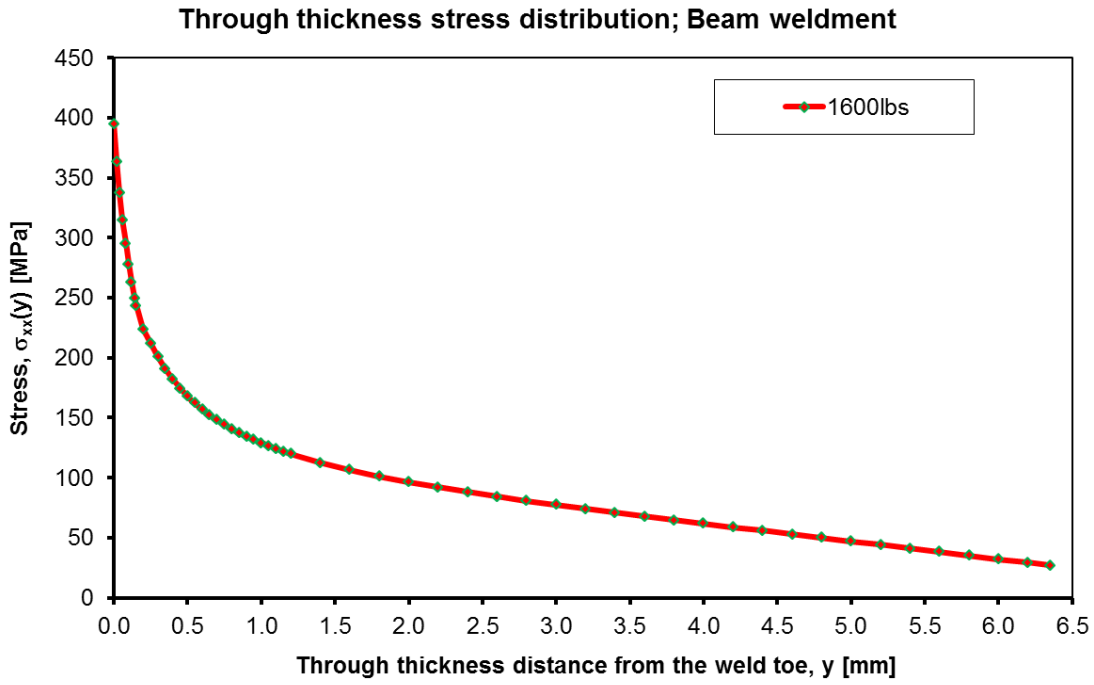

Figure 5-34: Simulated GR3 based through-thickness stress distribution in the critical cross section of the beam weldment (2F=1600 lbs)

Fatigue lives are calculated for each load case with and without accounting for the presence of the residual stress. Using welding process simulation model, the residual stresses were estimated for this joint and the through thickness residual stress distribution for the normal stress component extracted at the critical section (same as used for extracting the stress distribution induced by the external loads) is shown in Figure 5-35. The residual stress was not measured using XRD for the beam weldment.

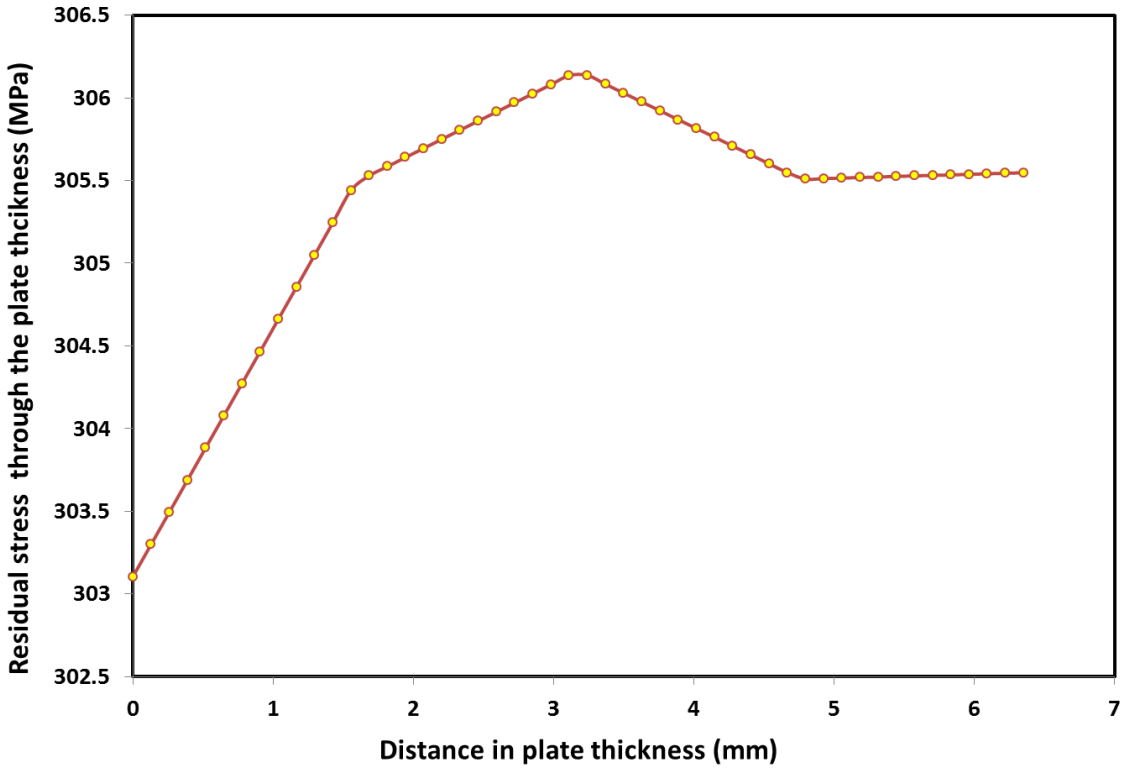

Figure 5-35: Simulated through the thickness residual stress distribution in the critical cross section of the beam weldment

5.5.1 Fatigue crack initiation life estimation

The fatigue crack initiation life is predicted using the strain-life method coded into the FALIN software. The fatigue life calculations are based on the material properties listed in Table 4-2 and Table 4-3 for ASTM A500 Grade C steel.

It is noticeable (see Table 5-8 and Table 5-9) that the residual stress had profound effect on the fatigue crack initiation life. The analysis indicates that the tensile residual stress at the weld toe may decrease the fatigue crack initiation life approximately by a factor of 3.

5.5.2 Fatigue crack propagation life estimation

The fatigue crack growth analysis is carried out using the FALPR software package. The crack size at the end of the initiation period, i.e. the initial crack for the fatigue crack growth analysis, was estimated as not to be greater than 0.5 mm in depth. The observed cracks were semi-elliptical in shape with a length of approximately 3.0 mm (Figure 2-8) on the surface, i.e. the initial crack aspect ratio was a/c=0.333. The planar semi-elliptical

surface crack in a finite thickness plate was assumed to be the appropriate model for the fatigue crack growth predictions up to the final crack length 2c ≈ t, i.e. 2c ≈ 6-7mm. The planar crack model assumed in the analysis was not adequate to analyze cracks wrapping around the edge of the cover plate. Therefore the analysis of the crack growth carried out for the cracks initiated at the edge of cover plate and presented below was valid up to the final crack length of approximately 2c < 7mm.

The crack increments induced by subsequent stress cycles are calculated by using Paris fatigue crack growth expression (eqn. 2.13) valid for R =0.1 with parameters:
m = 3.02 and C = 5.18 x 10^{-12} for ΔK in [MPa√m] and da/dN in [m/cycle].
The threshold stress intensity range and the critical stress intensity factor for the tested material are:

$\Delta K_{th} = 3.5\ MPa\sqrt{m}$ at $R = 0$ and $K_C = 80\ MPa\sqrt{m}$.

5.5.3 The Total Fatigue Life

The total fatigue life (N_f) of the beam weldment is determined as sum of the fatigue crack initiation life (N_i) and the fatigue crack propagation life (N_P). The calculated fatigue lives are summarized in Table 5-8 and Table 5-9.

Table 5-8: Summary of estimated fatigue lives for the beam weldment (2F=2500lbs)

Residual Stress (MPa)	N_i (Cycle) $a_i = 0.5mm$ 2c = 3.0 mm	N_p (Cycle) $a_f = 5.08mm$ 2c = 28.4 mm	N_i/N_p	N_f (Cycle)	N_i/N_f
$\sigma_r = 0$	113600	155459	0.731	269059	0.422
$\sigma_r = 303.1$	63610	56500	1.126	120110	0.529

Table 5-9: Summary of estimated fatigue lives for the beam weldment (2F=1600lbs)

Residual Stress (MPa)	N_i (Cycle) $a_i = 0.5mm$ 2c = 3.0 mm	N_p (Cycle) $a_f = 5.08mm$ 2c = 28.4 mm	N_i/N_p	N_f (Cycle)	N_i/N_f
$\sigma_r = 0.0$	906700	598000	1.516	1504700	0.602
$\sigma_r = 303.1$	330800	216500	1.528	547300	0.604

According to the data above the ratios of the crack initiation to the crack propagation life and the crack initiation life to the total fatigue life are quite high indicating that majority of the fatigue life of the analyzed weldment was spent for the crack initiation.

The calculated fatigue lives in terms of the number of load cycles are plotted as a function of the predicted surface crack length (2c) and they are shown in Figure 5-36 and Figure 5-37. The experimental fatigue lives are also shown in these figures.

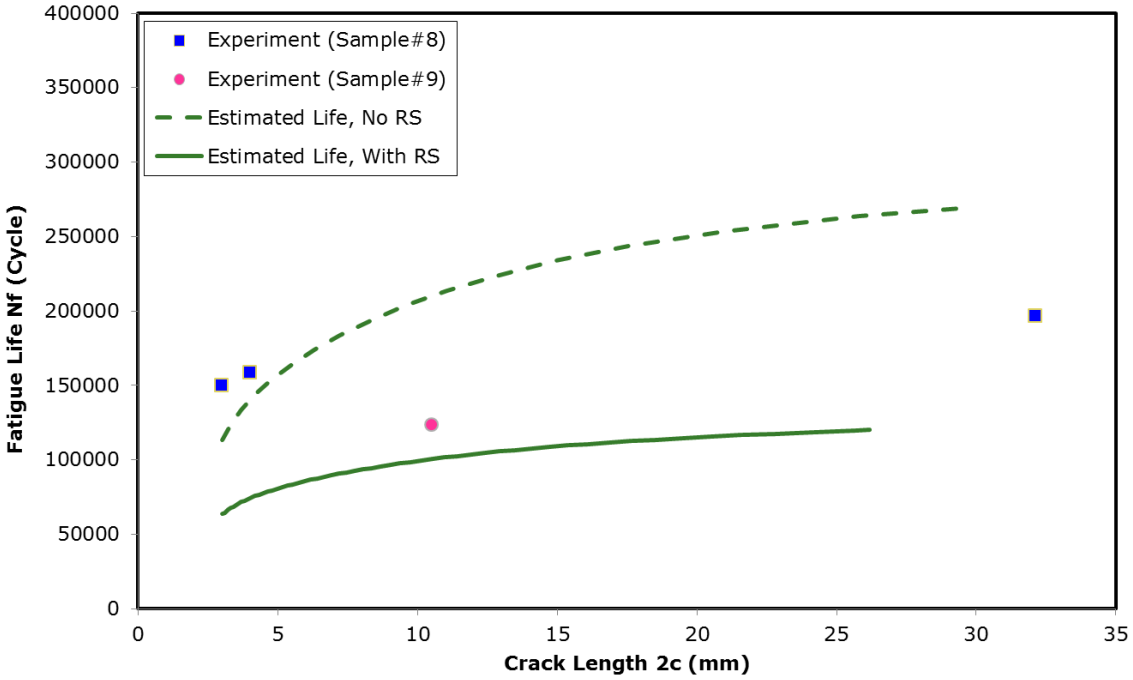

Figure 5-36: Comparison of calculated total fatigue lives and the experimental fatigue data; Beam weldment 2F = 2500lbs. Note: With RS means including the residual stress effect, No RS means excluding the residual stress effect.

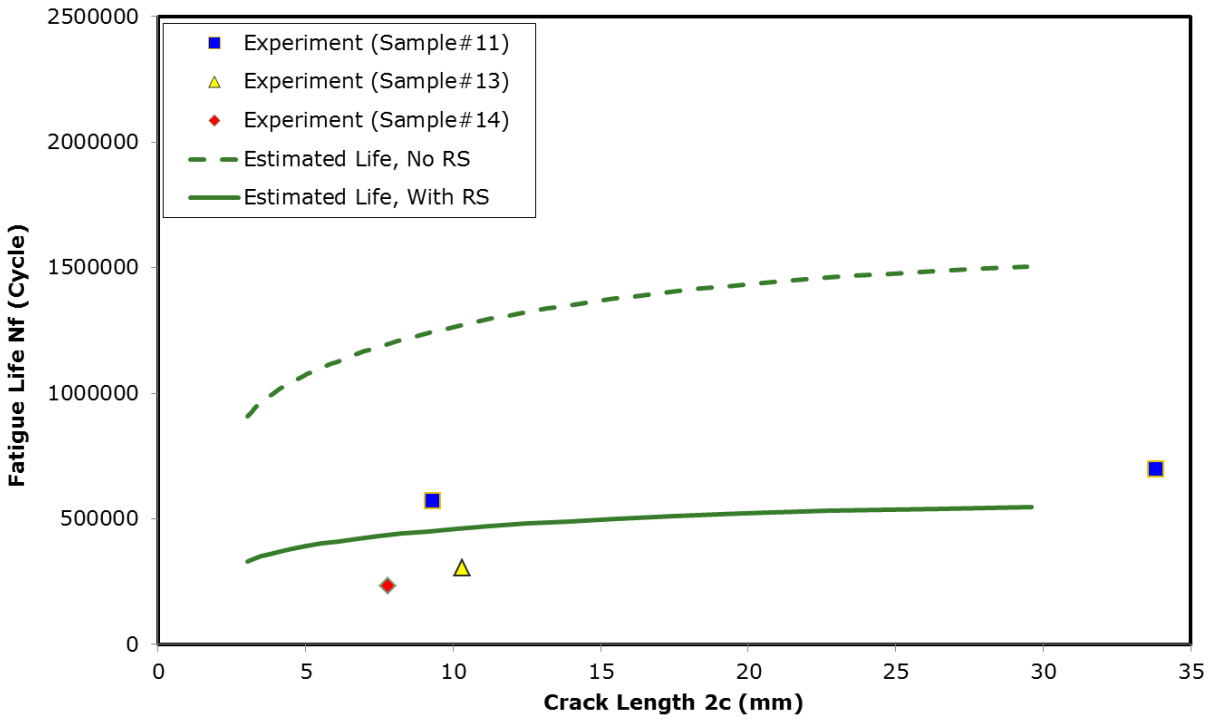

Figure 5-37: Comparison of calculated total fatigue lives and the experimental fatigue data; Beam weldment 2F = 1600lbs. Note: With RS means including the residual stress effect, No RS means excluding the residual stress effect.

The calculated fatigue lives (Figure 5-36 and Figure 5-37) and the experimental lives are generally in good agreement for both the low and high load levels. The effect of the residual stress, shown in Figure 5-36 and Figure 5-37 indicates the necessity of including the residual stress effect into the analysis of fatigue lives of weldments.

It should be noted that the fatigue cracks detected in experiments are located, as estimated, in the region of maximum peak stress, i.e. at the weld toe near the middle of edge (see Figure 5-38).

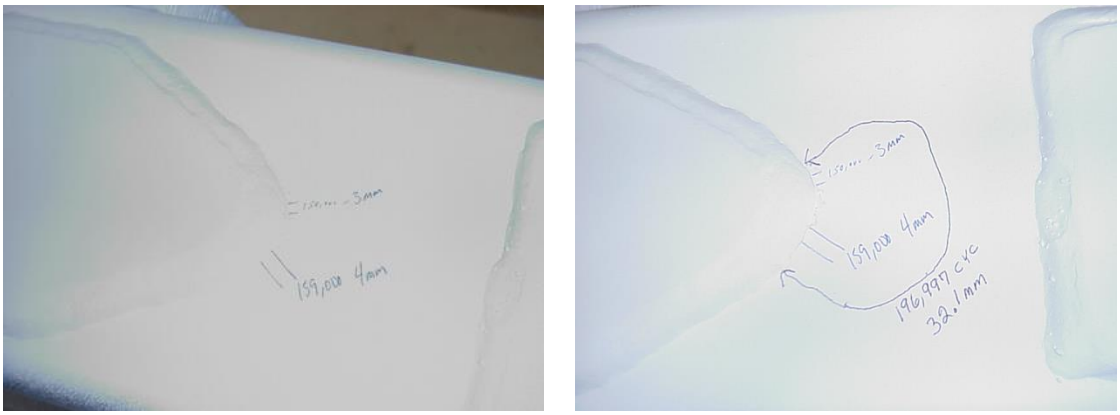

Figure 5-38: Fatigue crack in the base plate located in the region of estimated maximum stress (sample#8). Beam Weldment (2F=2500 lbs).

The fatigue cracks were growing into the base plate thickness and along the weld toe line in the plate surface. Due to high stress at the weld toe (Figure 4-31) cracks were growing faster on the surface (along the weld toe line) than into the thickness. Therefore the shape of final cracks was reaching relatively low aspect ratio.

5.6 The complex tubular welded structure under torsion and bending load

In order to compare the predicted fatigue lives with the experimental data for the tubular welded joint with complex geometry, two series of fatigue tests have been carried out at fully reversed cyclic loads of 3000lbs and 4000lbs. The tested welded joints (specimens) were made of ASTM A500 Grade C steel alloy for the tube material and 1008 steel alloy for the connecting plates. Within the same welded sample, two different tube sizes were used each with a thickness of 0.312 in and the cross-sections of 2 in by 6 in and 4 in by 4 in. All of the connecting plates had thickness of 0.1875 in. The geometry and dimensions of the overall welded sample is shown in Figure 4-36. The fatigue test set up arrangement is shown in the Figure 5-39.

Figure 5-39: The fatigue test setup arrangement – tubular weldment

The samples were manually welded using gas metal arc welding process. The samples were initially tack welded before doing the full welding. A simple weld fixture to hold the tack welded sample was used to allow the full welds to be performed in the 2F welding position. The welding was performed using 1.2mm ER70S-6 weld wire with 90% Ar and 10% CO_2 shielding gas mixture. The spray mode of metal transfer was used with these weld process parameters: wire feed speed – 11.8 m/min, current – 321 A, voltage – 25 V and travel speed – 0.58 m/min.

For the experimental fatigue testing, the samples were subjected to a combination of the torsion and bending load case. The base plate of the welded sample was fixed at the 8 different hole locations using M8 bolts and the fully-reversed cyclic load was applied at the end of the vertical plate attached to one side of the tube (see Figure 5-39). Around 9 such samples were welded and tested under fatigue loading and the data is presented for these samples. Two samples were tested at the lower load level of 3000lbs and the rest of them were tested at higher load level of 4000lbs.

The experimental fatigue lives obtained are listed in Table 5-10. The numbers of load cycles are given as a function of the crack length (2c) measured on the tube surface. The crack depth is only an estimate.

Table 5-10: Experimental fatigue crack growth data (2c-N) for the complex weldment

Sample #	**Load (lbs)**						
9	3000	Crack length (in)	1.5				
		Cycle count	267000				
13	3000	Crack length (in)	0.75	1	1.25	1.5	
		Cycle count	72525	84844	96670	175235	
11	4000	Crack length (in)	0.25	0.63	0.74	1.25	
		Cycle count	21000	59529	166218	316205	
12	4000	Crack length (in)	0.75	1	3		
		Cycle count	28000	48131	134907		
14	4000	Crack length (in)	0.75	1.06			
		Cycle count	22000	60000			
15	4000	Crack length (in)	0.44	0.84	1.5		
		Cycle count	10691	26149	31611		
16	4000	Crack length (in)	0.75	1	1.3	1.5	
		Cycle count	10292	30793	35100	40893	
17	4000	Crack length (in)	0.75	1	1.5		
		Cycle count	12085	14853	37507		
18	4000	Crack length (in)	0.25	0.38	0.44	0.62	1.5
		Cycle count	9550	12195	18332	19354	26537

Next, the numerical calculations have been carried out for the estimation of fatigue life for the beam weldment as per the proposed methodology.

The simulated peak stresses and the through thickness stress distributions induced by the applied load levels are obtained by scaling the GR3 model stress data shown in Figure 4-40 and the scaled simulated stress distributions for the load levels of 3000lbs and 4000lbs are presented in Figure 5-40 and Figure 5-41.

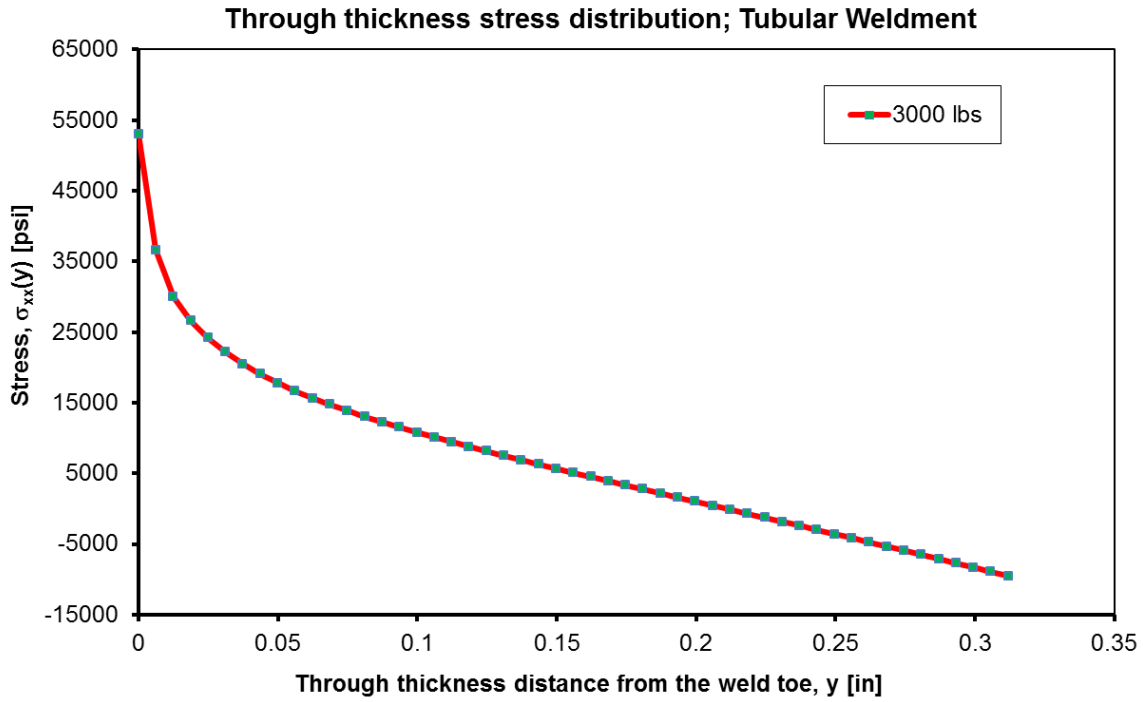

Figure 5-40: Simulated GR3 based through-thickness stress distribution in the critical cross section of the complex tubular weldment (F=3000 lbs)

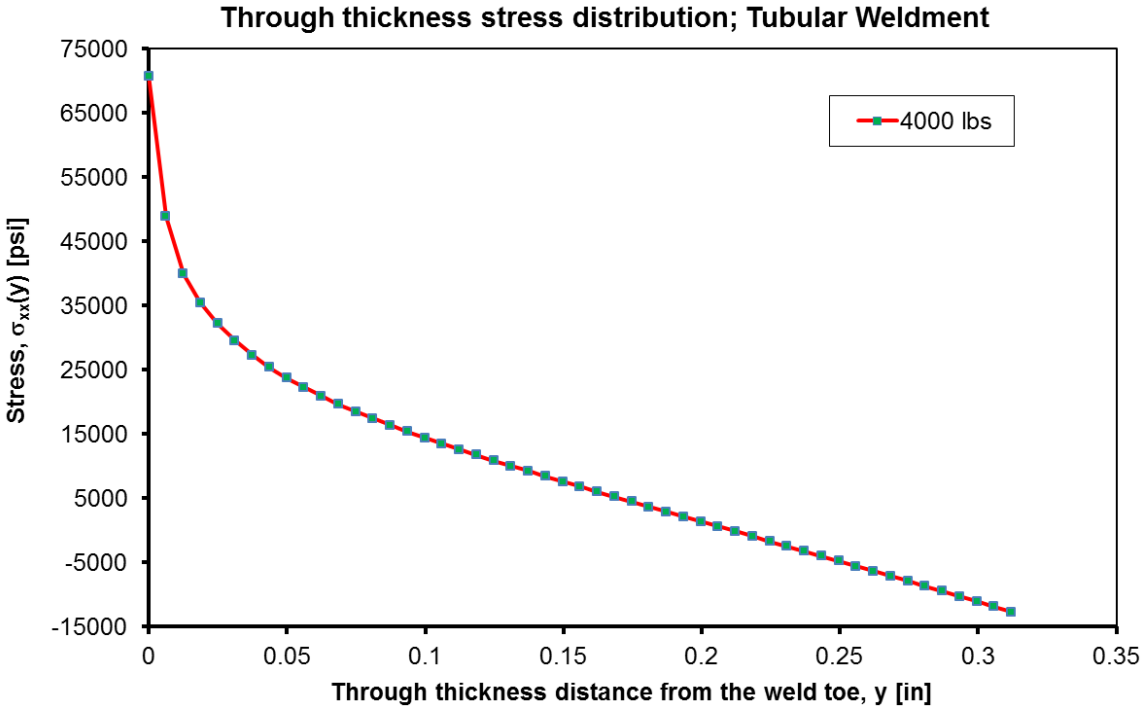

Figure 5-41: Simulated GR3 based through-thickness stress distribution in the critical cross section of the complex tubular weldment (F=4000 lbs)

Fatigue lives are calculated for each load case with and without accounting for the presence of the residual stress. Using welding process simulation model, the residual stresses were estimated for this joint and the through thickness residual stress distribution for the normal stress component extracted at the critical section (same as used for extracting the stress distribution induced by the external loads) is shown in Figure 5-42. The residual stress was measured in the tube surface using XRD method (Figure 5-43) and was found to be 45ksi, which is quite close to the residual stress at the weld toe obtained using weld simulation.

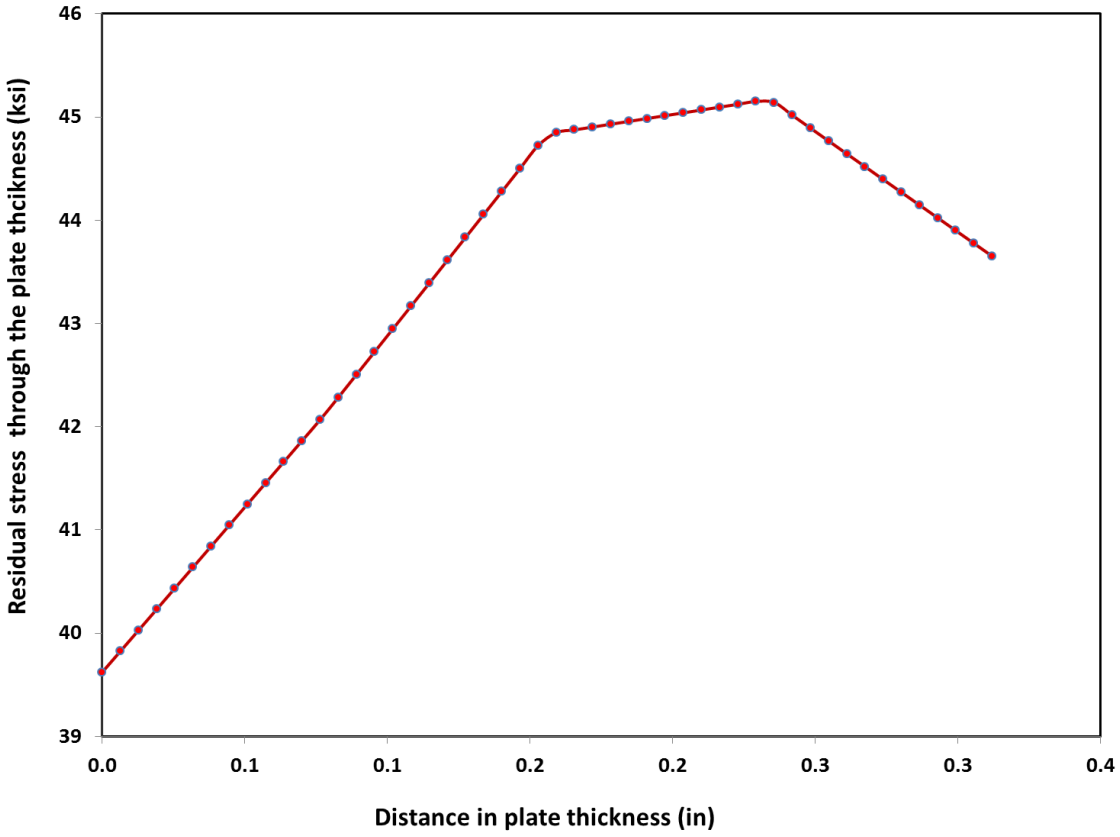

Figure 5-42: Simulated through the thickness residual stress distribution in the critical cross section of the complex tubular weldment

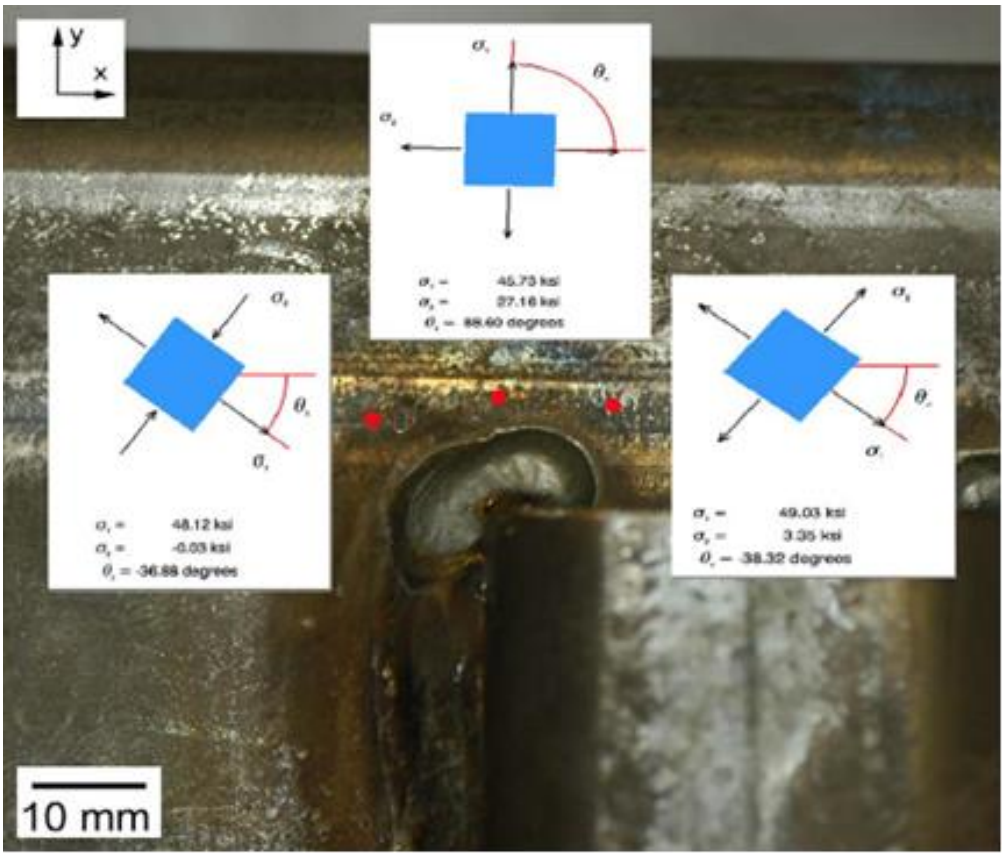

Figure 5-43: The residual stresses in the profile surface plane; complex tubular weldment subjected to torsional and bending loads

5.6.1 Fatigue crack initiation life estimation

The fatigue crack initiation life is predicted using the strain-life method coded into the FALIN software. The fatigue life calculations are based on the material properties listed in Table 4-2 and Table 4-3 for ASTM A500 Grade C steel.

It is noticeable (see Table 5-11 and Table 5-12) that the residual stress had profound effect on the fatigue crack initiation life. The analysis indicates that the tensile residual stress at the weld toe may decrease the fatigue crack initiation life approximately by a factor of 3.

5.6.2 Fatigue crack propagation life estimation

The fatigue crack growth analysis is carried out using the FALPR software package. The crack size at the end of the initiation period, i.e. the initial crack for the fatigue crack

growth analysis, was estimated as not to be greater than 0.02 *in* in depth. The observed cracks were semi-elliptical in shape with a length of approximately 0.14 *in* (Figure 2-8) on the surface, i.e. the initial crack aspect ratio was a/c=0.286. The planar semi-elliptical surface crack in a finite thickness plate was assumed to be the appropriate model for the fatigue crack growth predictions up to the final crack length 2c ≈ t, i.e. 2c ≈ 0.312 *in*.

The crack increments induced by subsequent stress cycles are calculated by using Paris fatigue crack growth expression (eqn. 2.13) valid for R=0 with parameters:
m = 3.02 and C = 2.97364 x 10^{-10} for ΔK in [Ksi√in] and da/dN in [in/cycle].
The threshold stress intensity range and the critical stress intensity factor for the tested material are:

$\Delta K_{th} = 3.19\ ksi\sqrt{in}$ at $R = 0$ and $K_C = 72.81\ ksi\sqrt{in}$.

5.6.3 The Total Fatigue Life

The total fatigue life (N_f) of the tubular weldment is determined as a sum of the fatigue crack initiation life (N_i) and the fatigue crack propagation life (N_P).

The calculated fatigue lives are summarized in Table 5-11 and Table 5-12.

Table 5-11: Summary of estimated fatigue lives for the tubular weldment (F=3000lbs)

Residual Stress (ksi)	$\boldsymbol{N_i}$ (Cycle) $a_i = 0.02\,in$ 2c = 3.5 mm	$\boldsymbol{N_p}$ (Cycle) $a_f = 0.2497\,in$ 2c = 47.9 mm	$\boldsymbol{N_i / N_p}$	$\boldsymbol{N_f}$ (Cycle)	$\boldsymbol{N_i / N_f}$
$\sigma_r = 0.0$	80680	668000	0.121	748680	0.108
$\sigma_r = 39.6$	37420	82000	0.456	119420	0.313

Table 5-12: Summary of estimated fatigue lives for the tubular weldment (F=4000lbs)

Residual Stress (ksi)	$\boldsymbol{N_i}$ (Cycle) $a_i = 0.02\,in$ 2c = 3.5 mm	$\boldsymbol{N_p}$ (Cycle) $a_f = 0.2497\,in$ 2c = 47.7 mm	$\boldsymbol{N_i / N_p}$	$\boldsymbol{N_f}$ (Cycle)	$\boldsymbol{N_i / N_f}$
$\sigma_r = 0.0$	22140	280000	0.079	302140	0.073
$\sigma_r = 39.6$	13060	38419	0.339	51479	0.254

According to the data in the tables the ratios of the crack initiation to the crack propagation life and the crack initiation life to the total fatigue life are quite low indicating that majority of the fatigue life of the analyzed weldment was spent on propagating the crack from its initial crack depth $a_i = 0.02\ in$ to the final one $a_f = 0.2497\ in$.

The calculated fatigue lives in terms of the number of load cycles are plotted as a function of the predicted surface crack length (2c) and they are shown in Figure 5-44 and Figure 5-45. The experimental fatigue lives are also shown in these figures.

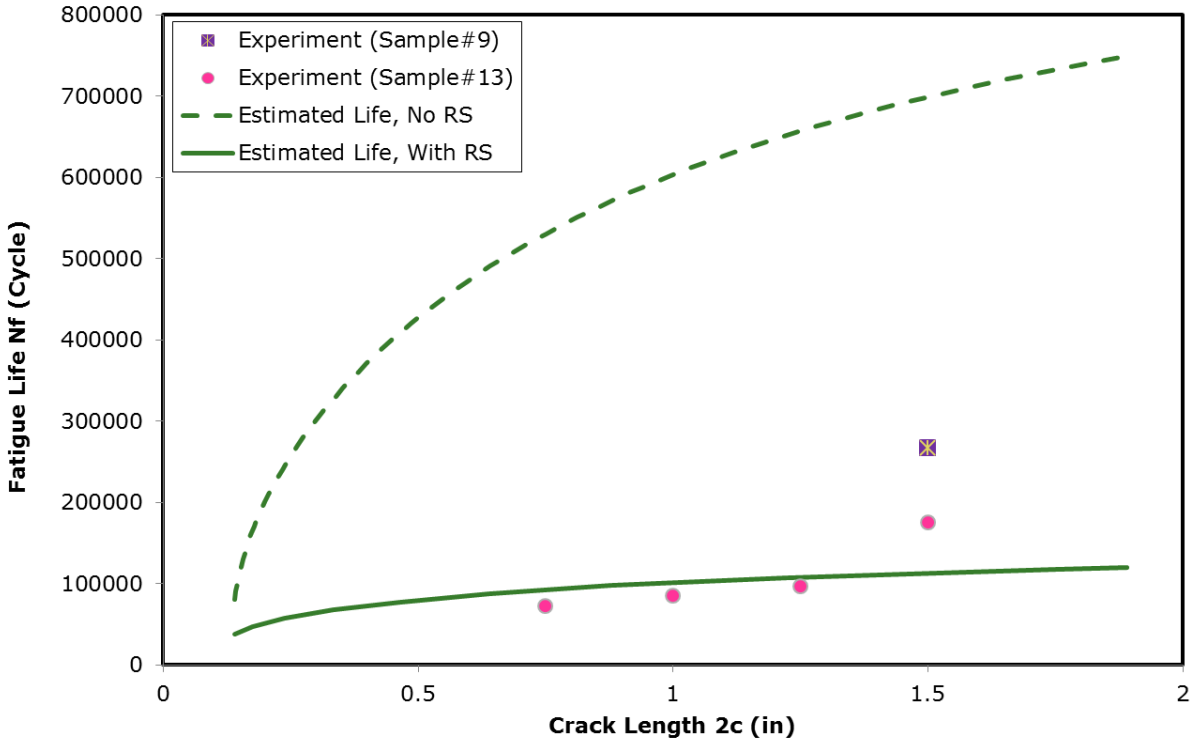

Figure 5-44: Comparison of calculated total fatigue lives and the experimental fatigue data; Complex tubular weldment F = 3000lbs. Note: With RS means including the residual stress effect, No RS means excluding the residual stress effect.

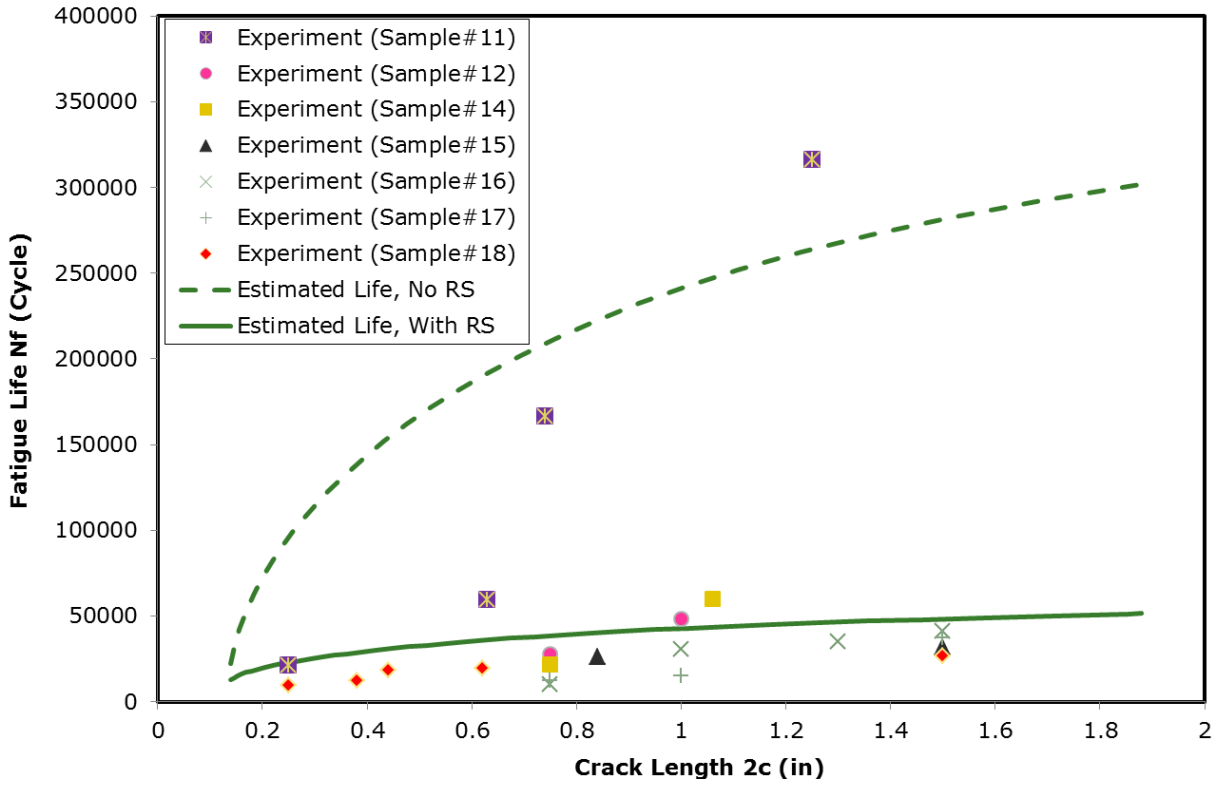

Figure 5-45: Comparison of calculated total fatigue lives and the experimental fatigue data; Complex tubular weldment F = 4000lbs. Note: With RS means including the residual stress effect, No RS means excluding the residual stress effect

The predicted fatigue lives as shown in Figure 5-44 and Figure 5-45 and the experimental lives are in good agreement. The effect of the residual stress, shown in Figure 5-44 and Figure 5-45 indicates the necessity of including the residual stress effect into the analysis of fatigue lives of weldments.

It should be noted that the fatigue cracks detected in experiments are located, as estimated, in the region of maximum peak stress, i.e. at the weld toe near the edge of wrapped corner, see Figure 5-46 and Figure 5-47.

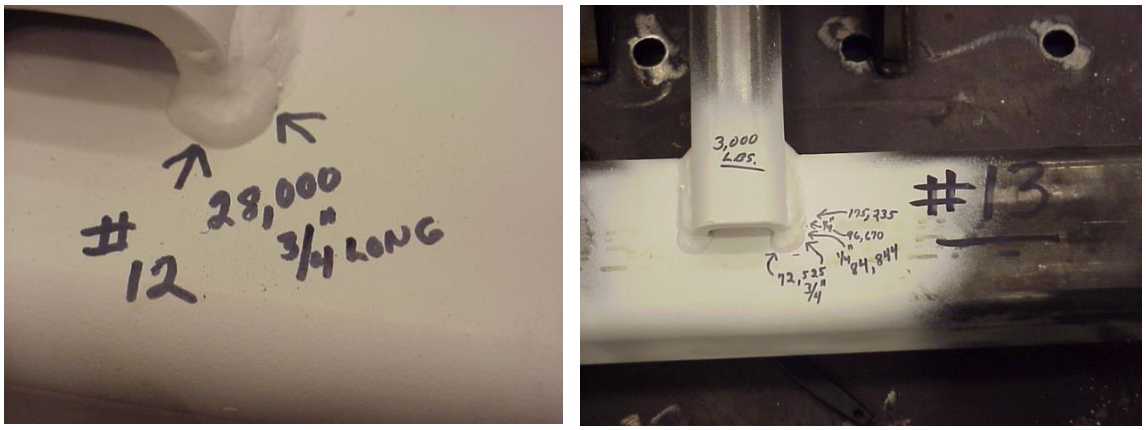

Figure 5-46: Fatigue crack in the base tube located in the region of estimated maximum stress (Sample#12 and Sample#13) of Tubular Weldment.

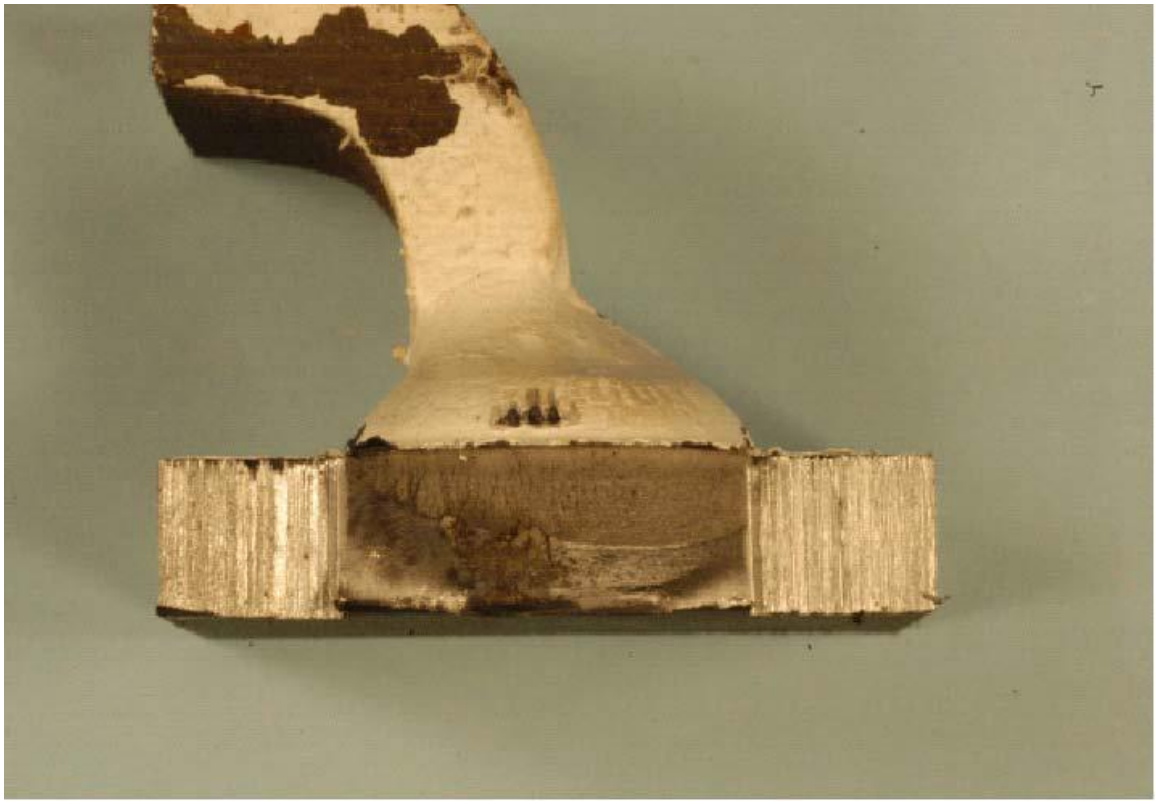

Figure 5-47: Fatigue crack in the wall of the square tube located in the region of estimated maximum stress of Tubular Weldment (F=3000 lbs).

5.7 Total Fatigue Life Concept

As per this concept *the total fatigue life* can be modeled as fatigue growth of cracks starting either from the weld toe or weld root rather than first calculating crack initiation life up to some arbitrary initial crack size. Only the crack propagation approach can be used for total life prediction with the initial crack size selected as a small crack characteristic for a given material, i.e. being dependent only on the material. The weight function method is very useful to calculate required stress intensity factors. Cruciform weld joint has been selected for demonstration of this concept as well as for validation of the proposed GR3 model.

5.7.1 Cruciform joint and welding defects

Welded structures contain occasionally defects, either built in during fabrication or created in service. When welded structures are subjected to cyclic stresses, fatigue cracks start propagating from these defects to a critical size. The weld defects or the stress concentration due to geometrical changes in welded joint reduce unfortunately their fatigue lives. The effect from welding defects such as of the lack of penetration flaw and misalignment on fatigue life of cruciform welded joints made of low alloy steel has been studied experimentally and numerically. It is found that two locations of fatigue fracture are possible under cyclic tension loading, depending on the relative magnitude of the misalignment. In absence of misalignment, all fatigue failures occurred as a result of fatigue growth of cracks emanating from weld root. In the presence of misalignment the fatigue life is found to be dependent on the fatigue growth of cracks growing from the weld toe.

Most contemporary practical fatigue design codes for welded joints are based on experimentally produced nominal stress vs. number of stress cycles (S-N) curves, which classify welds into specific ranges of geometrical severity depending on the geometry and load configuration. However, welding defects such as the lack of penetration, porosity and misalignment may reduce the fatigue life and shift the 'weakest' section of the joint from the internal defect (weld root) to the external discontinuity (weld toe). As a result the fatigue life of a weldment with defects may be different from that one given by the code. In order to quantify those effects several failure configurations needs to be analyzed

before the fatigue life can be reliably estimated. The weakest section usually exhibits the shortest fatigue life and as a result it determines the fatigue life of the entire welded joint. The identification of the potential location of the failure and the fatigue life of the joint can be based on the comparison of fatigue lives determined for various fatigue crack locations and load configurations. For this reason the effect of the lack of penetration flaw and misalignment on fatigue lives of welded cruciform joints have been studied experimentally and theoretically. The techniques based on the fracture mechanics and fatigue crack growth analysis have been used in this study.

5.7.1.1 **Material and geometrical configurations**

The tested weld joints (specimens) were made of low alloy steel plate, 8mm thick. The chemical composition and mechanical properties of this steel, denoted 15G2ANb, are given in Table 5-13 and Table 5-14 respectively. The weldments (see Figure 5-48) were mechanically cut from previously manually welded plates of 360 mm wide and 368 mm long. Each specimen was then machined and a piece of material of thickness 2e was welded to each end of the specimen in order to enable easy installation in the testing machine grips of specimens with misalignments. Two series, each comprising of 7 to 10 specimens, were prepared and tested. All specimens were tested under the stress ratio of R=0.5. The first series of specimens had no misalignment and they were denoted as having the relative misalignment of 2e/t=0. The second series of specimens had the relative misalignment of 2e/t=1. Each specimen was tested until the final failure under different amplitude load level.

Table 5-13: Chemical composition of 15G2ANb low alloy steel (weight %)

C	Mn	Si	P	S	Cr	Ni	Cu	Mo	V	N	AI
0.18	1.6	0.4	0.04	0.04	0.3	0.3	0.3	0.1	0.1	0.06	0.02

Table 5-14: Mechanical Properties of the 15G2ANb low alloy steel

---

Monotonic yield strength, σ_{ys} = 370 MPa

Ultimate strength, σ_{uts} = 570 MPa

Intrinsic initial flaw, $\rho^* = 2 \cdot 10^{-5}$ m

Paris equation constants obtained at R=0.5, three pieces;

$C_1 = 1.68^{x}10^{-18}$ $m_1 = 13.15$

$C_2 = 2.00^{x}10^{-15}$ $m_2 = 7.5$

$C_3 = 5.00^{x}10^{-12}$ $m_3 = 3.4$

For ΔK in [MPa$\sqrt{m}$] and da/dN in [m/cycle].

ΔK_{th} = 2 MPa$\sqrt{m}$

K_c = 90 MPa$\sqrt{m}$

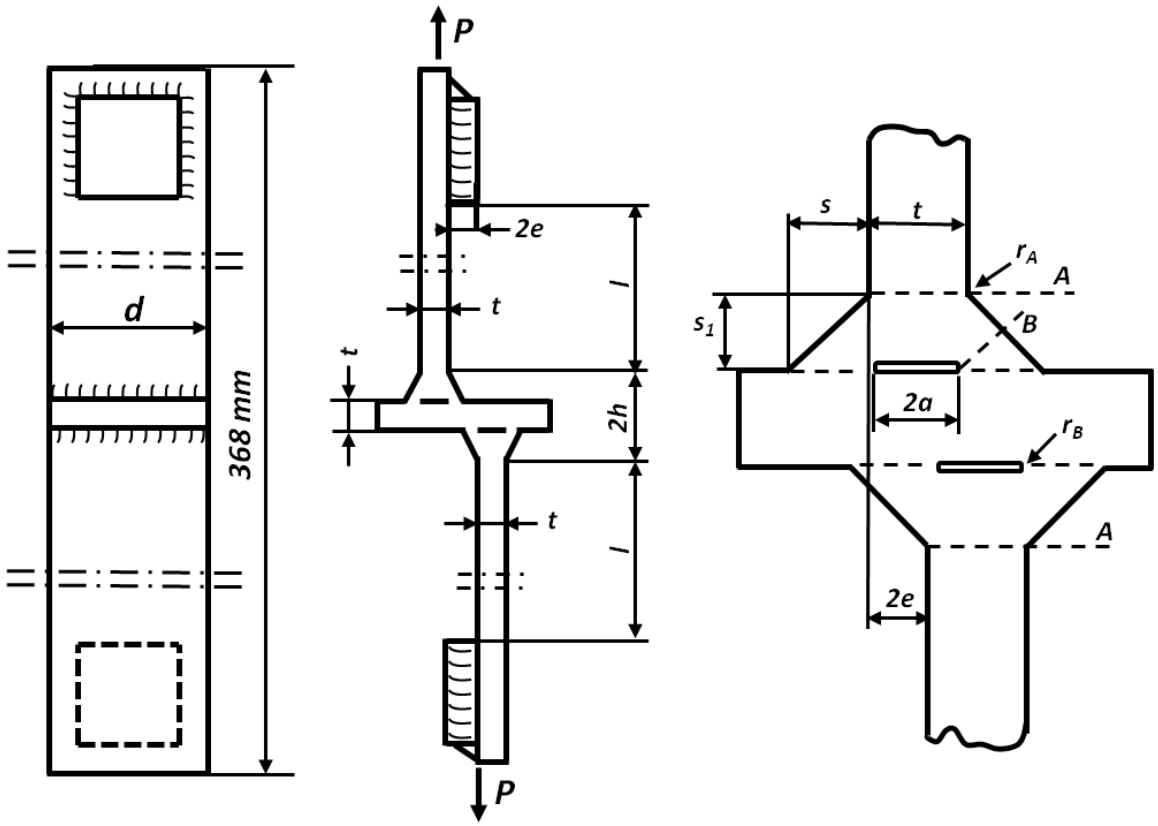

Figure 5-48: Specimen geometry and dimensions: (a) general geometry, (b) details of the weld geometry

Several specimens, chosen at random, were also sliced and the radii 'r_A' of the weld toe and those at the weld root 'r_B' were measured. The distribution of the weld toe radii r_A was close to the Weibull distribution with the most frequent value being r_A=0.8 mm. The most frequent value of the root radius has been found to be r_B=0.1 mm. The average length of the non-penetrating flaw was 2a=7.9 mm. The other dimensions shown in Figure 5-48 were as follows: h = 12.3 mm, d = 40 mm, l=130 mm, s = 7.8 mm, s_1 = 8.3 mm and t = 8 mm.

The three pieces of fatigue crack growth curve as shown in Figure 5-49 are taken from the data generated by Prof Glinka earlier. The near threshold fatigue crack growth data and the intrinsic initial flaw size ρ* are estimated according to the model described in reference [70].

5.7.2 Fatigue crack modeling and calculation of fatigue lives

The estimation of the fatigue life of a weldment is usually divided into two stages: the fatigue crack initiation and the fatigue crack propagation period. Unfortunately, there is no in practice clear distinction between the crack initiation stage and the following crack growth period. This distinction is in most cases arbitrary. However, microscopic observations indicate that small fatigue cracks start growing from almost the first loading cycle. Therefore it might be possible to determine the fatigue life of a weldment using only the crack propagation theory without splitting the process into the initiation and propagation stages. It should be noted that due to the project schedules, there was a significant time gap (more than 1 year) between the experimental fatigue testing of the specimens and when the specimens were actually welded. Therefore, a reasonable assumption was made that residual stresses from welding process were already relaxed during this time period.

One of important element of such a philosophy is the choice of the initial crack size which should be a material property, i.e. it should be independent of the geometry and loading. Such a parameter is established in the UniGrow fatigue crack growth methodology [70] and approximate value of this parameter can be established from the expression 5.1.

$$\Delta\sigma_{th} = \frac{1.633\ \Delta K_{th}}{\sqrt{2\pi\rho^*}} \tag{5.1}$$

Where: $\Delta\sigma_{th}$ - is the fatigue limit and ΔK_{th} - is the fatigue threshold.

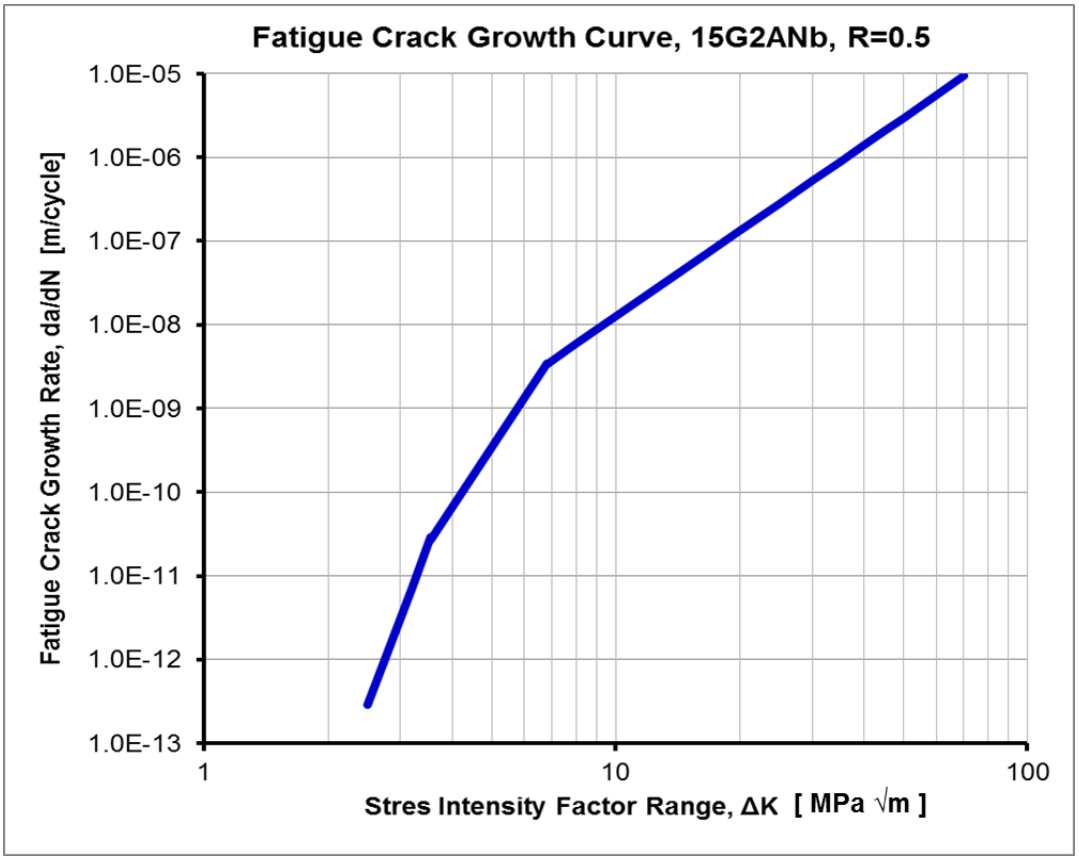

Figure 5-49: Piecewise fatigue crack growth curve da/dN-ΔK

The fatigue crack propagation life N of a weldment can be subsequently calculated by integrating the Paris equation (eqn. 2.13).

The Paris equation must be integrated from the initial crack size of ρ* until the final crack size of a_f.

$$N = \int_{\rho^*}^{a_f} \frac{da}{(\Delta K)^m} \tag{5.2}$$

Special care must be taken while calculating the stress intensity factor ΔK for small cracks in weldments because of complex geometry and highly nonlinear stress

distribution in the potential crack plane. Therefore the weight function technique has been used for calculating required stress intensity factors.

5.7.2.1 **Calculation of Stress Intensity Factors**

Experimental observations indicate that majority of the total fatigue live of welded joints are spent on propagating semi-elliptical surface cracks emanating either form the weld toe (section A, Figure 5-48) or from the weld root (section B, Figure 5-48). Therefore the weight function as demonstrated earlier in Figure 2-8 for a semi-elliptical crack in a finite thickness plate is used for subsequent calculations.

Schematic stress distributions and appropriate crack models used for the analysis are shown in Figure 2-9. In both cases, the same weight function for a semi-elliptical crack is used, for both the crack in the weld toe section and that one in the weld throat plane. The stress distributions in sections A and B (Figure 5-48 and Figure 2-9) are obtained from 3D fine mesh finite element analysis. Same has also been obtained using 3D coarse mesh to validate the proposed GR3 method at the weld toe. It is to note that the stress analysis needs to be carried out only once and for the un-cracked body. The product of the stress distribution $\sigma(x)$ and the weight function $m(x,a)$ needs to be integrated over the entire crack surface area.

5.7.2.2 **Stress distributions in critical cross sections**

It is obvious that in the case of weldments with a misalignment certain amount of bending will be generated in the specimen under the tensile or compressive axial load. On the other hand the bending moment is linearly dependent on the amount of misalignment. Therefore, only two finite element stress analyses needed to be carried out; one for pure axial load and the second one for pure bending load. The stress distribution in section A and/or B induced by the combination of the actual axial load and the misalignment are obtained by superposition and appropriate scaling of the fundamental stress distributions obtained earlier for pure axial and bending load.

There were, as mentioned earlier, tested two groups of specimens. The first group included specimens with no misalignment (2e/t=0). Stress distributions in section A (toe) and B (root) obtained with help of the finite element method for specimens with no misalignment are shown in Figure 5-50 and Figure 5-51 respectively. Both stress

distributions have been scaled (normalized) with respect to the average membrane (axial) stress σ_m^A in the cross section A (see Figure 5-48 and Figure 2-9).

$$\sigma_m^A = \frac{P}{d\,t} \tag{5.3}$$

In the case of specimens without any misalignment there is no bending induced during the application of the axial load P and therefore the stress distribution (Figure 5-50) in section A is symmetrical.

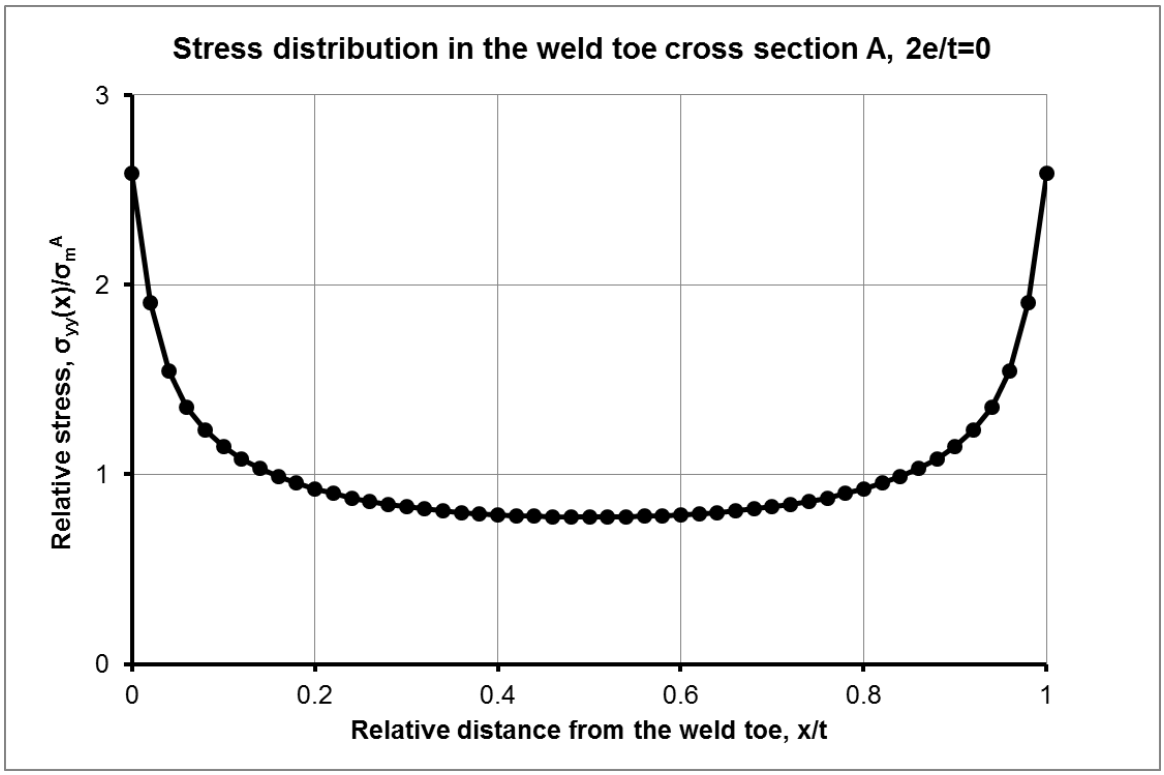

Figure 5-50: Stress distribution in the cross section A, 2e/t=0

The stress distribution in section B is found (Figure 5-51) to be decreasing with the distance from the weld root. Section B is chosen to be in the 45^o plane as that plane is close to the plane of maximum normal stress $\sigma_{yy}(x)$ and close to the crack plane found in tested specimens.

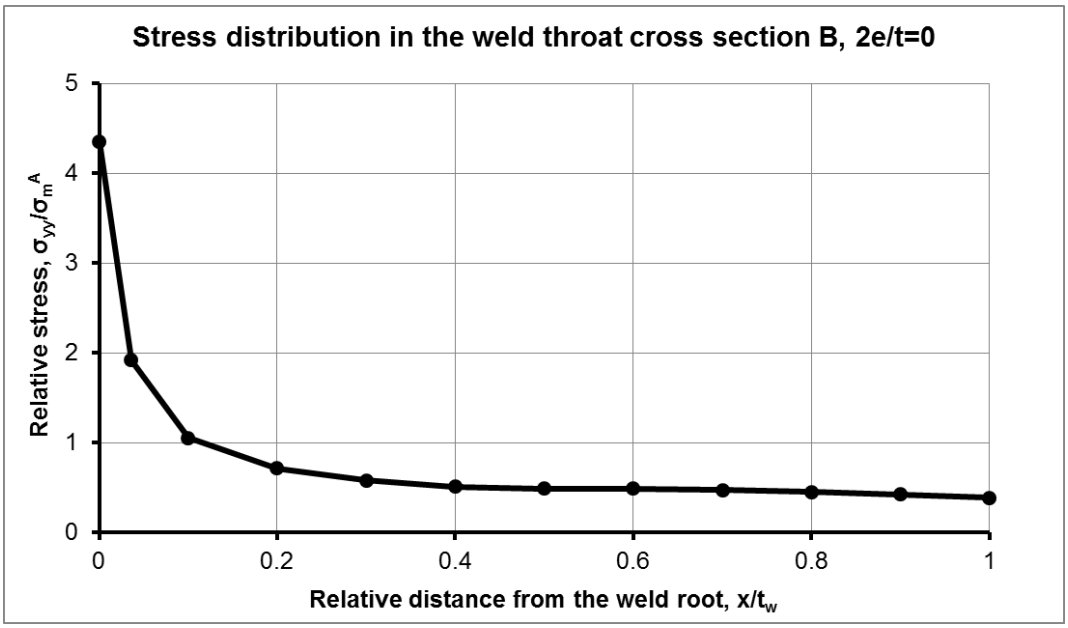

Figure 5-51: Stress distribution in the cross section B, 2e/t=0

In the case of specimens with misalignment 2e/t=1 the stress distribution in section A is (Figure 5-52) non-symmetrical with the majority of tensile stresses on one side of the thickness due to the superposition of membrane and bending stresses.

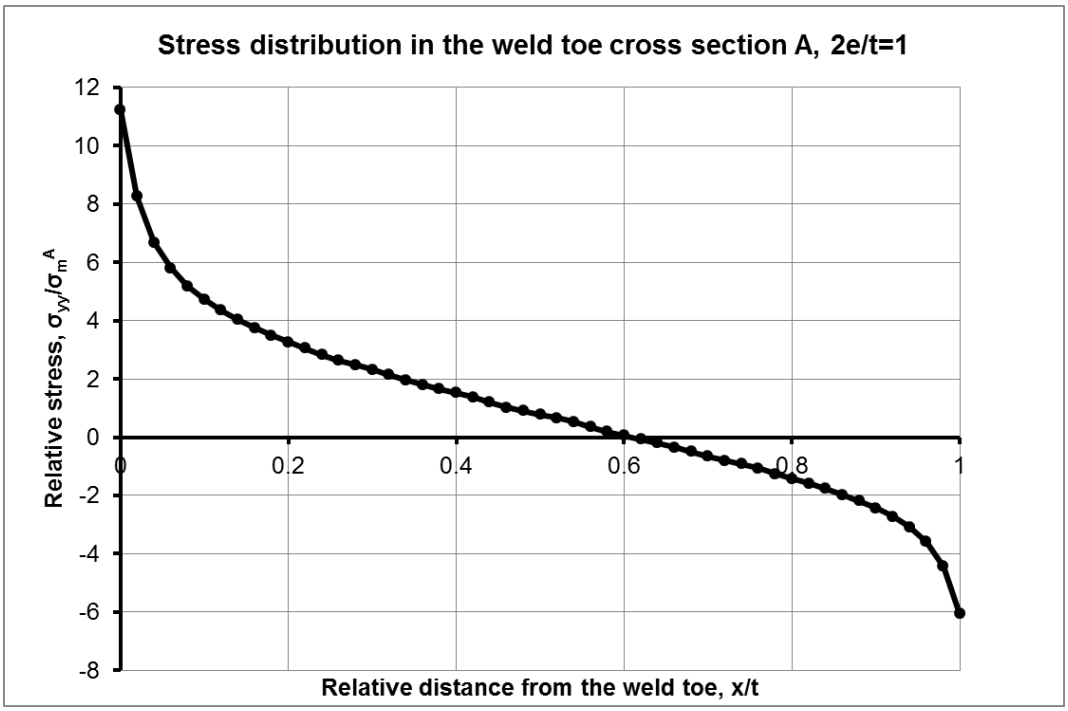

Figure 5-52: Stress distribution in the cross section A, 2e/t=1

It should be noted that the bending stress at the weld toe is approximately 4.35 times greater than the simultaneous membrane stress, σ_m^A. Therefore even small amount of misalignment may significantly increase stresses at the weld toe.

However, the bending action in the weld root section B induced by the misalignment is not as significant as in the case of the weld toe section A. Comparison of stress distributions shown in Figure 5-51 and Figure 5-53 indicate that the presence of the relative misalignment of the magnitude of 2e/t=1 resulted in the increase of the weld root stress by factor of 1.87.

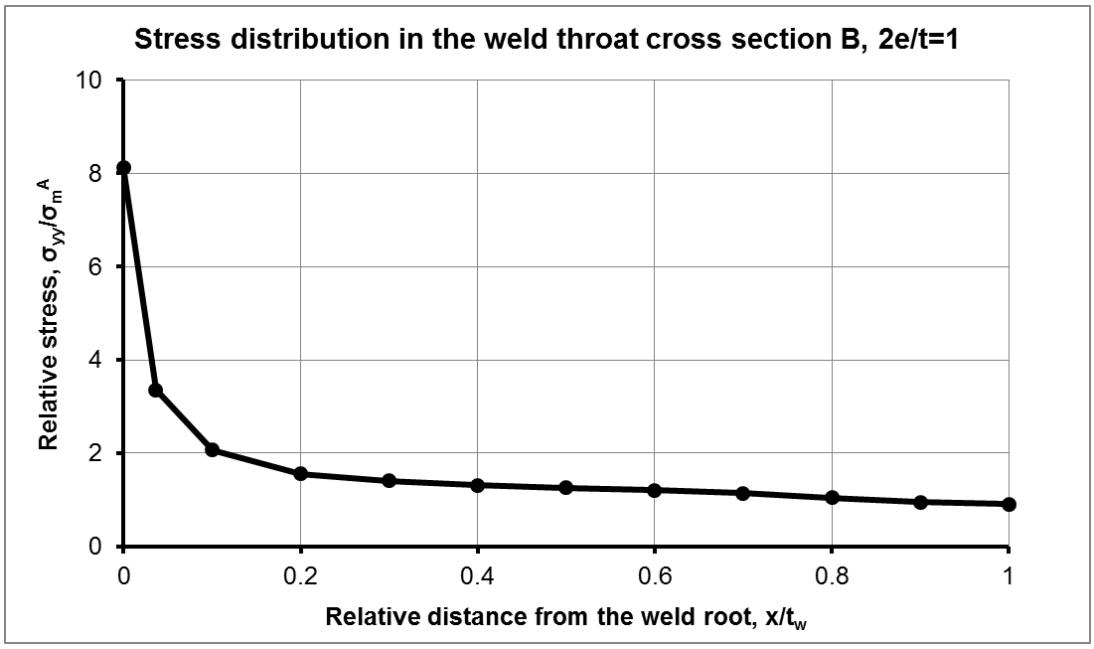

Figure 5-53: Stress distribution in the cross section B, 2e/t=1

These through thickness stress distributions along with the weight functions, eqns. 2.16 and 2.17, are subsequently used for the calculation of stress intensity factor at the surface point B and the deepest point A. The stress intensity factors K_A and K_B are computed in the form of integrals, eqns. 2.18 and 2.19, respectively.

5.7.2.3 **Fatigue crack growth analysis**

The fatigue crack growth analysis is carried out using the software package, FALPR enabling the calculation of stress intensity factors based on the weight function method and the determination of subsequent fatigue crack growth increments generated by subsequent load cycles. The observed fatigue cracks were semi-elliptical in shape. The

initial depth is assumed to be $a_0=\rho^*=2^x10^{-5}$ m and the aspect ratio a/c=0.25. Observations of small fatigue cracks in weldments indicate that early fatigue cracks in weldments most often have the aspect ratio 0.2<a/c<0.3. The final crack depth in the weld toe section A is assumed a_f=0.8t and in the case of root cracks the final crack size is $a_f = 0.8t_w$. The 80% of the thickness final crack is dictated by the maximum validity of the weight function (eqns. 2.16 and 2.17). The final crack size c_f or/and the final aspect ratio a_f/c_f are not defined because of the unknown final shape of the crack.

The stress intensity factor ranges ΔK_A and ΔK_B and crack increments Δa and Δc at point A and B (Figure 2-9) respectively are calculated simultaneously on cycle by cycle basis. It is found that the crack is not growing with the same rate in both directions. Therefore crack increments at the deepest point A and those at the surface point B (Figure 2-9) are determined separately for each cycle.

$$\Delta a_i = C\left(\Delta K_{A,i}\right)^m$$

$$\Delta c_i = C\left(\Delta K_{B,i}\right)^m \tag{5.4}$$

The instantaneous crack dimension ‘a’ and ‘c’ and the crack aspect ratio (a/c) are updated after each loading cycle and the current dimensions a_N and c_N and the shape (a_N/c_N) are determined by summing up all crack increments after the application of N loading cycles.

$$a_N = a_0 + \sum_1^N \Delta a_i$$

$$c_N = c_0 + \sum_1^N \Delta c_i \tag{5.5}$$

As a result of the applied procedure the crack growth and the crack shape evolution are simulated at the same time. An example of the simulated crack growth and shape evolution is shown in Figure 5-54. It is interesting to note that the crack initially grows faster into the depth direction (direction of a) in spite of decreasing stress and after reaching certain depth it started growing faster on the surface. This example indicates that the crack growth simulation can’t be carried out, as it is frequently done in practice, assuming constant aspect ratio a/c=const.

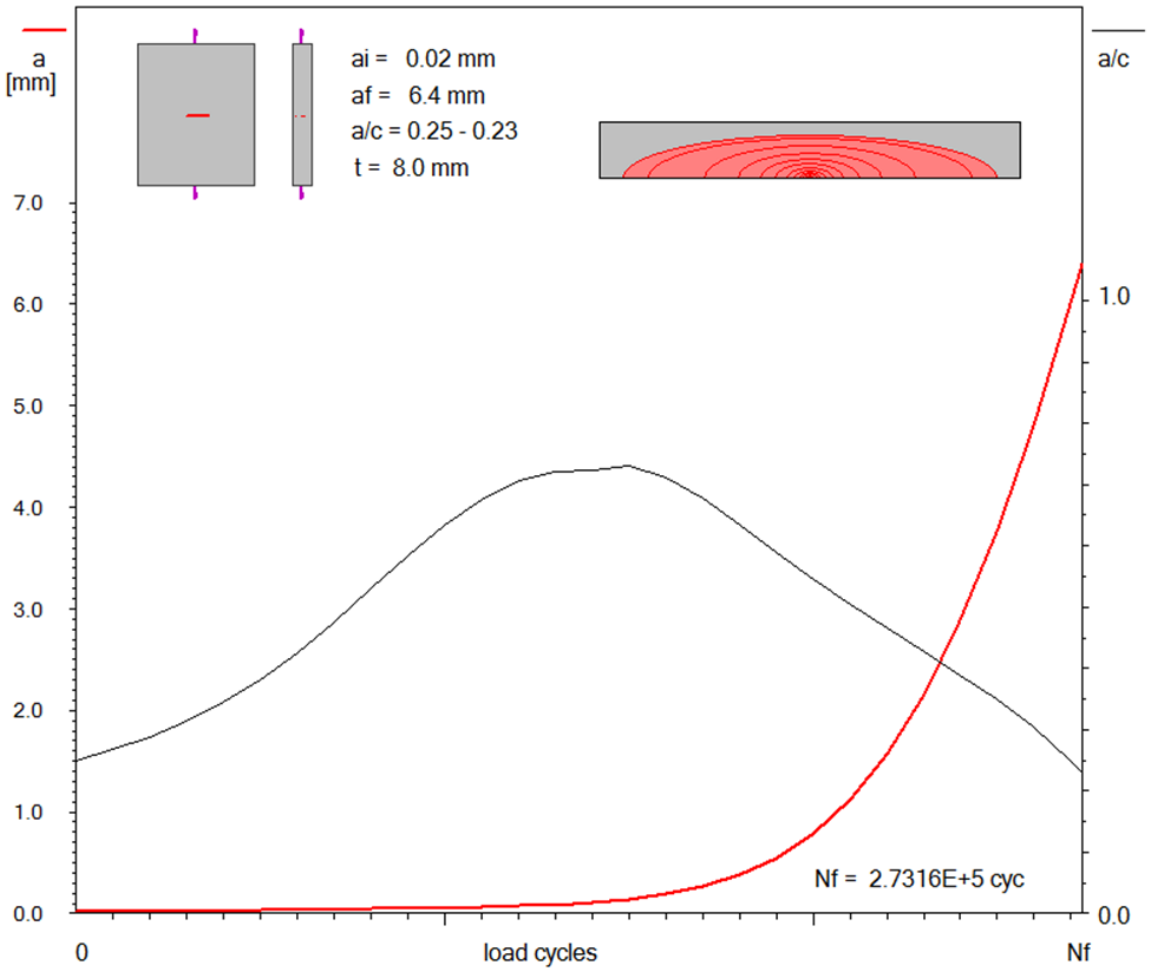

Figure 5-54: The fatigue crack growth and the fatigue crack aspect ratio evolution in the toe cross section A; 2e/t=1, $\Delta\sigma_m^A$ = 48.1 MPa, R=0.5

The fatigue crack growth analyses has been carried out at the stress ratio R=0.5 and at the same stress magnitudes $\Delta\sigma_m^A$ as in the experiments. The experimental and simulated data sets are presented in terms of the membrane stress $\Delta\sigma_m^A$ versus the number of cycles to failure N, i.e. in terms of $\Delta\sigma_m^A$ vs. N. The fatigue lives are determined for the same reference stress range $\Delta\sigma_m^A$ for both the toe and the root cross section. The comparison of experimental and simulated fatigue lives for specimens with no misalignment (2e/t=0) and with misalignment (2e/t=1) are shown in Figure 5-55 and Figure 5-56 respectively.

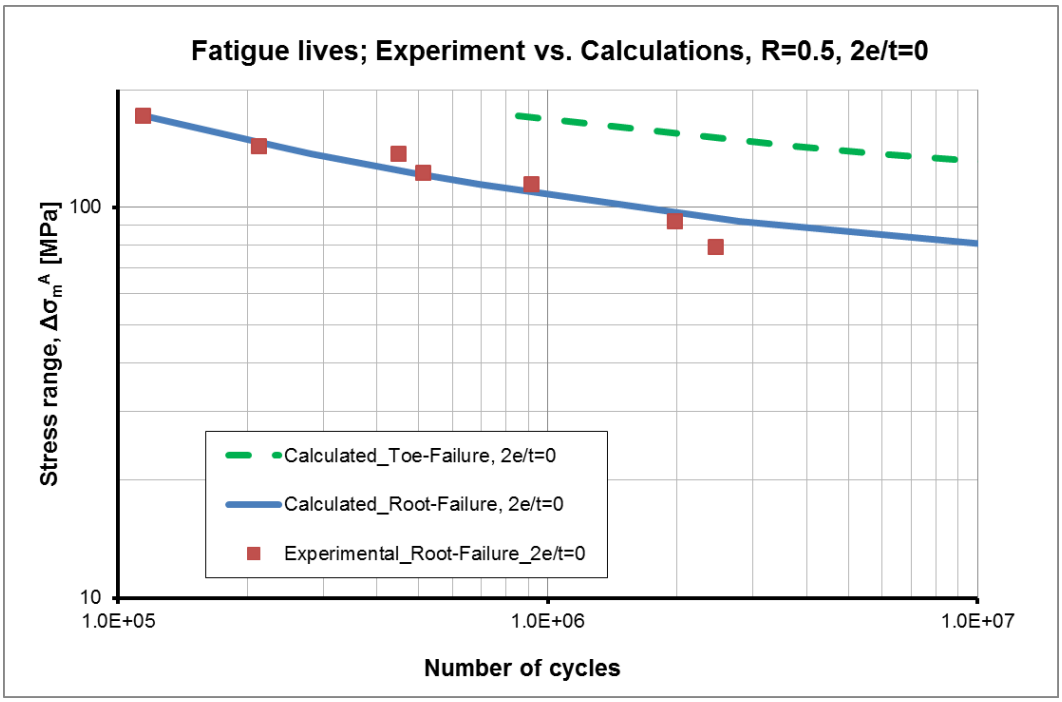

Figure 5-55: Experimental and simulated fatigue lives for specimens without misalignments 2e/t=0, R=0.5

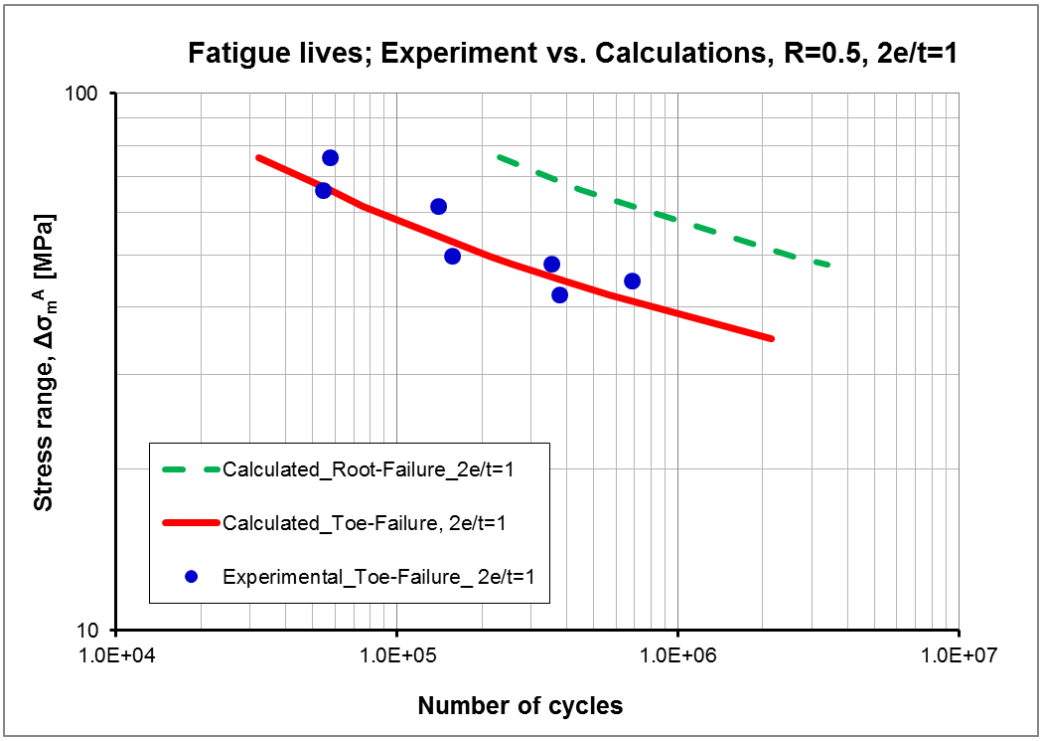

Figure 5-56: Experimental and simulated fatigue lives for specimens with relative misalignment of 2e/t=1, R=0.5

In the case of specimens with no misalignment shorter simulated lives are obtained for cracks in the weld root section and they are closer to experimental fatigue lives also resulted from failure in the weld throat section. It means that the shortest simulated fatigue live among those obtained for several crack locations indicate the most probable location of the final failure. On the other hand all specimens with the relative misalignment of 2e/t=1 failed in experiment in the weld toe section A. Shorter simulated fatigue lives are also obtained for cracks in section A confirming the conclusions that the shortest simulated live indicates also the most probable location of the final fatigue failure.

5.7.3 Fine vs. Coarse mesh solid FE model

Validation of GR3 method along with its capability to produce accurate results has been demonstrated in this section by comparing results of 3D coarse mesh FE model from GR3 method against the results obtained from 3D fine mesh FE model for the cruciform joint (Figure 5-48). The same cruciform weld joint under the same load configurations has been analyzed using coarse FE model, not capturing weld micro features (Figure 5-57) as well as using very fine finite element mesh enabling appropriate modeling of the weld toe radius (Figure 5-58) and other micro-geometrical features. Two load cases of the cruciform weld joint with no misalignment (2e/t=0) are presented here, one under pure axial load of 10kN and another under pure bending load of 1kN. The through thickness stress distribution at the crack weld toe location for axial and bending load cases are plotted in Figure 5-59 (a) and (b) respectively. In addition the predicted stress distributions according to the GR3 procedure have also been superposed.

These figures clearly show that the profile of two stress distributions match each other very well for both the load cases, proving that the coarse FE mesh procedure (GR3) can provide reliable stress information for reasonably accurate prediction of both the peak stress and the non-linear through-thickness stress distribution. The difference between the predicted GR3 peak stress (Figure 5-59) and that one obtained from the fine mesh FE model is found to be less than 7% and 10% for axial and bending load cases respectively, moreover results from GR3 model are on the conservative side for both of the load cases. Further as the fine mesh FE model results have been already been validated against

experimental data in section 5.7.2.3 justifies that results from coarse mesh using GR3 model can provide convincingly accurate results.

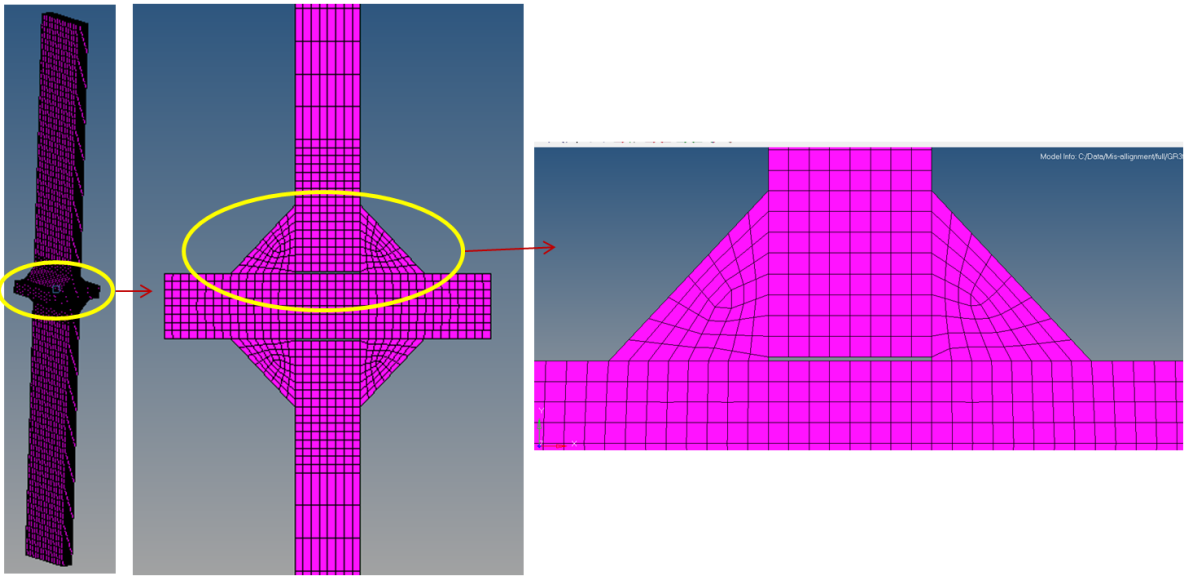

Figure 5-57: 3D coarse mesh FE model of cruciform joint, 2e/t=0

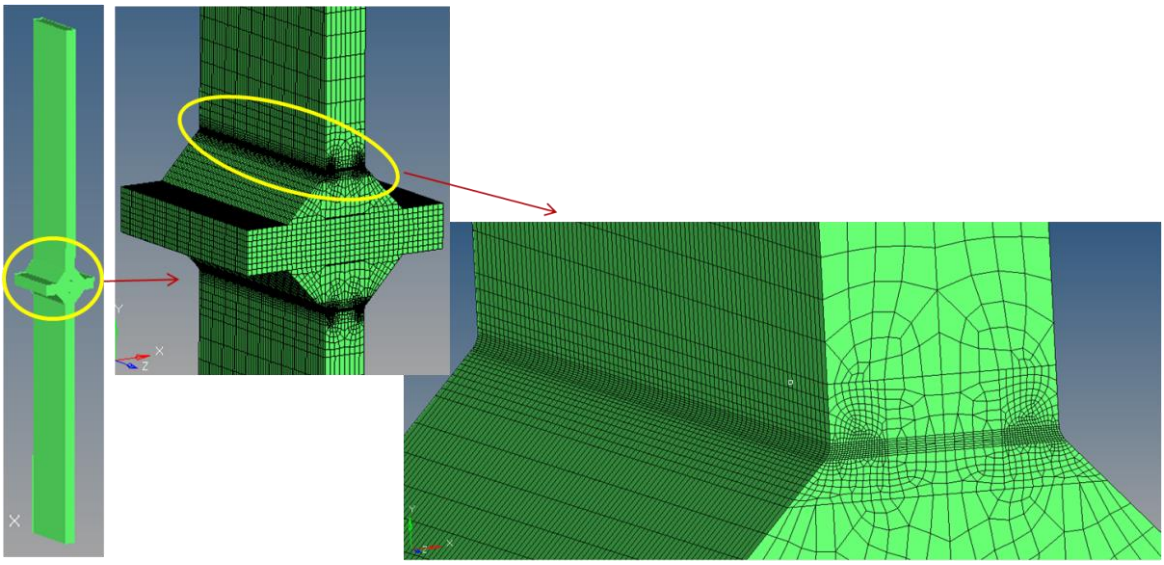

Figure 5-58: 3D FE model with fine mesh at weld toe of cruciform joint, 2e/t=0

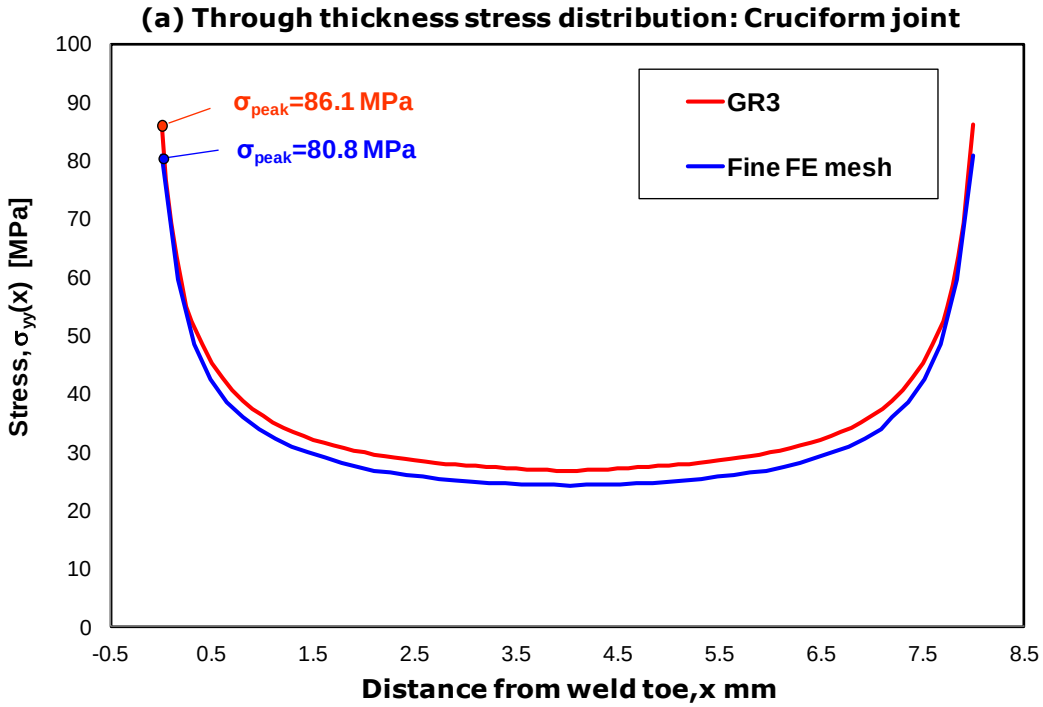

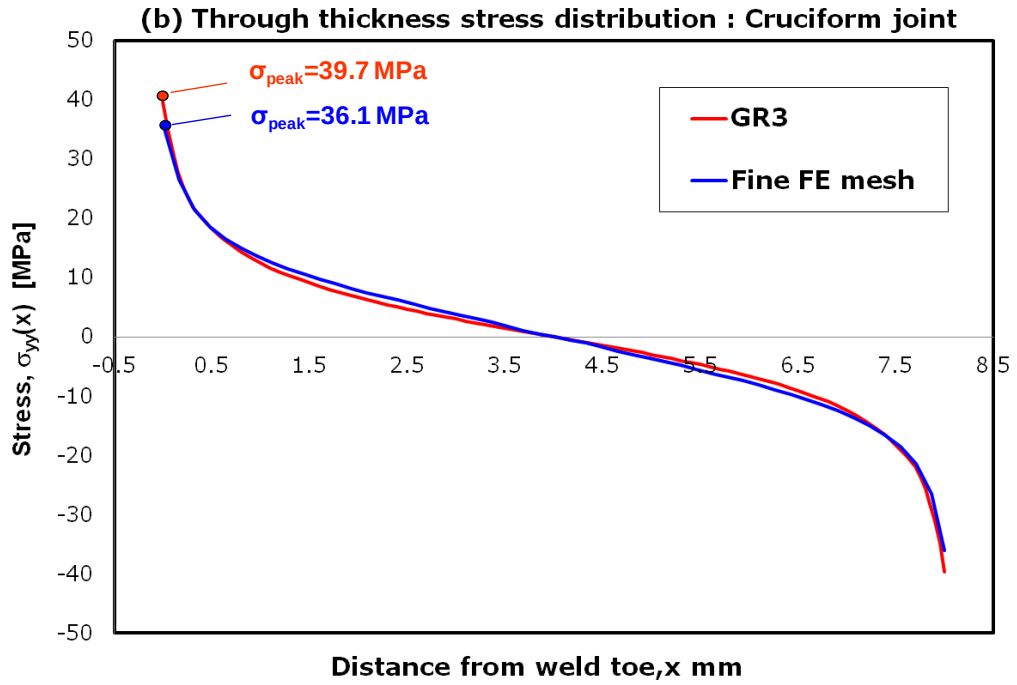

Figure 5-59: Comparison of through thickness stress distribution obtained from the coarse mesh FE model using GR3 method and fine FE mesh model of cruciform joint under (a) Pure axial load – 10kN (b) Pure bending load – 1kN

5.7.4 Summary

It has been shown that estimation of fatigue lives of welded joints can be successfully carried out by considering the fatigue process as a fatigue crack growth from the initial intrinsic crack size of $a_0 = \rho^*$ until the final crack a_f. Such an approach enables avoiding somewhat arbitrary division of the fatigue process into the crack initiation and propagation and to concentrate on using only one methodology, i.e. the fracture mechanics theory. In order to carry out the analysis detail information about the stress distribution in the potential crack plane is required, which can be obtained easily from 3D coarse mesh FE model using GR3 model. The advantage is that the stress analysis needs to be carried out only once and for an un-cracked configuration. The stress intensity factors can be determined in such cases by the weight function method and therefore appropriate weight function solution is needed.

The fatigue crack growth analysis needs to be carried out for several crack locations and the shortest estimated fatigue life is associated with the future location of the final failure. The method enables efficient estimation of the effect of various welding defects such as the lack of penetration flaw, misalignment and the detail geometry of the weld. The approach makes it also possible to simulate the crack shape evolution throughout the life of the weldment what might be of some value for the NDI inspectors.

5.8 Conclusions

Based on the various case studies presented in this chapter, it can be concluded that in general good agreement has been found between the calculated fatigue lives and the experimental lives for several different joint types subjected to different loading configurations, under low and high load levels. Hence, it can be further concluded that the stress analysis data obtained using the proposed GR3 methodology can be used for the estimation of fatigue lives of welded joints and structures. Further it was shown that the effect of the residual stress indicates the necessity of including the residual stress effect into the analysis of fatigue lives of weldments.

Chapter 6 Future Work

6.1 Introduction

Based on the findings during several investigations carried out during this research work, few recommendations can be made for the future work. These recommendations are briefly mentioned here while the details are covered later.

1. It might be possible to improve upon the proposed methodology by using an alternative approach to obtain the hot spot bending stress. As per the proposed GR3 methodology, hot spot bending stress is determined based on the appropriately scaled bending moment obtained using the mid-thickness stress distribution data from 3D coarse mesh FE model. Only the mid-thickness stress distribution data is used as a base to determine the bending moment while the remaining portion of the through thickness stress distribution obtained from 3D coarse mesh FE model is ignored. In the case of 3D coarse mesh FE analysis mainly the stress data point at the sharp weld toe corner is inaccurate due to the singularity issue at that location. So it might be possible to determine the hot spot bending stress using an alternative method, which could utilize the entire through-thickness stress distribution as obtained from 3D coarse mesh FE analysis except the stress data point at the sharp weld toe corner. The stress data point at the sharp weld toe corner can be obtained using the conventional hot spot structural stress method as shown in Figure 2-2. Eventually the hot spot bending stress can be determined using the bending moment based on the through-thickness stress distribution data obtained from 3D coarse mesh FE model, except the stress data point at the sharp weld toe corner which can be obtained using traditional hot spot stress method. The remaining steps towards fatigue life estimation could stay the same as per the proposed GR3 methodology. This new approach of obtaining the hot spot bending stress has a potential for enhancing the proposed GR3 methodology and can be named as *Hybrid GR3 methodology* because this approach is a combination of the proposed GR3 methodology and the conventional hot spot stress method.

2. In the proposed methodology, nodal-averaged FE technique has been used for extracting the through thickness stress distribution data from 3D coarse mesh FE model. It might be possible to improve upon the proposed methodology by utilizing the through thickness stress distribution data obtained using different FE averaging techniques from the 3D coarse mesh FE model. Basic objective is increase the accuracy for determination of the hot spot membrane and bending stress.
3. Few limitations have been observed in the proposed methodology for certain applications. One of the limitations is coming from the stress concentration factors which are valid for the certain range of weld geometry parameters as specified in section 3.7. Other limitation is that it could be difficult to apply the methodology directly for the situations where the fatigue crack initiation is from root of the weld (e.g. in the case of plug welds or the tube on plate joint subjected to pure torsional load). Further, as the proposed methodology is based on the strain life and the fracture mechanics methods, one of the major limitations with the local strain life approach is the ambiguity associated with the crack size at the end of crack initiation life. It might be possible to determine the total fatigue life by only using the fatigue crack propagation approach with the initial crack size selected as a small crack characteristic for a given material, i.e. being dependent only on the material.

Some initial work has also been carried out on these future proposals and the findings are covered in the next sections.

6.2 The Hybrid GR3 Methodology for determining the hot spot bending stress

As per the proposed *Hybrid GR3 methodology*, the hot spot bending stress can be determined using the bending moment based on the entire through-thickness stress distribution data obtained from 3D coarse mesh FE model, except the stress data point at the sharp weld toe corner which can be determined using the traditional hot spot stress method. The benefit of using this new hybrid approach lies in the fact that the scaling factor of 10 for the bending moment is no more required, as used in the proposed GR3 methodology.

The gusset joint with symmetric welds from Section 4.2 has been selected for demonstration of this concept. The through-thickness stress distribution data as extracted from 3D coarse mesh FE model of this joint is shown in Figure 4-3 and the same is shown by blue curve in Figure 6-1. The through-thickness stress distribution as obtained from 3D coarse mesh FE model but the stress data points at the sharp weld toe croners replaced with the stress values obtained using the conventional hot spot stress method i.e. obtained using the hybrid GR3 method, is shown by green curve in the Figure 6-1.

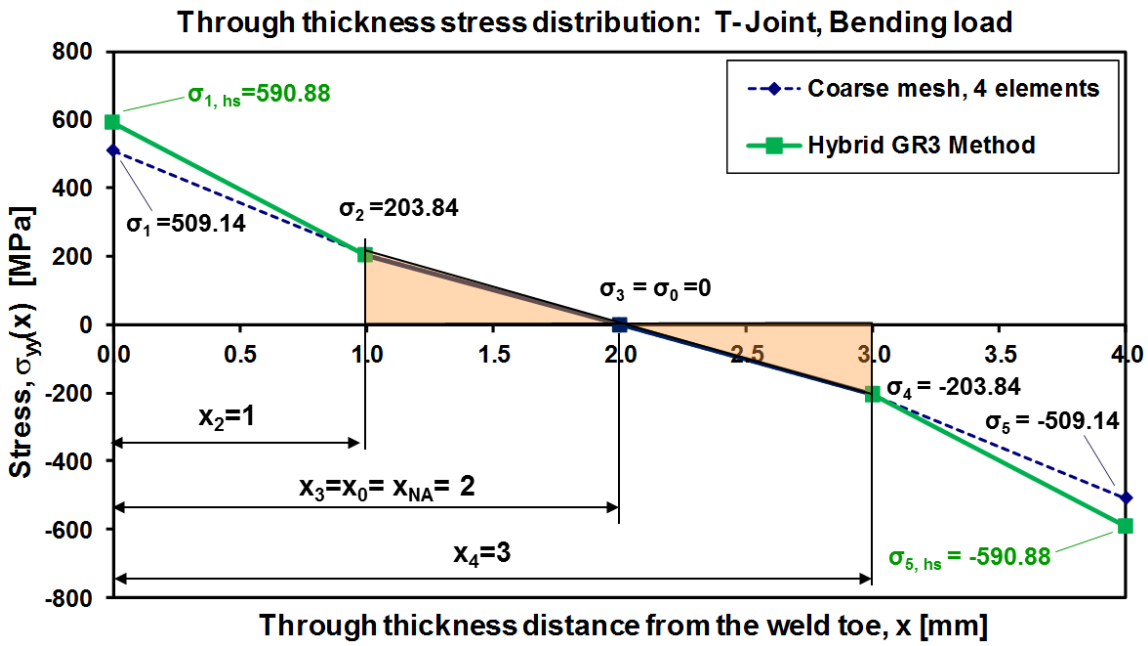

Figure 6-1: The through-thickness stress distribution - As obtained from 3D coarse mesh FE model (blue curve) and obtained using Hybrid GR3 method (green curve) for the gusset joint with symmetric welds

Based on the through thickness stress distribution obtained using the Hybrid GR3 method and using eqn. 3.19, eqn. 3.20, and eqn. 3.21, bending moment, membrane stress and bending stresses are calculated as below:

$$M_b = 1392.42 \text{ Nmm} \tag{6.1}$$

$$\sigma_{hs}^{m} = 0 \text{ MPa} \tag{6.2}$$

$$\sigma_{hs}^{b} = \frac{6\, M_b}{t^2} = 522.16 \text{ MPa} \tag{6.3}$$

The peak stress at the weld toe is calculated using eqn. 3.7 and same SCF's as previously calculated from eqn. 4.5:

$$\sigma_{peak} = \sigma_{hs}^{m} K_{t,hs}^{m} + \sigma_{hs}^{b} K_{t,hs}^{b} = 0 \times 2.686 + 522.16 \times 2.00 = 1045.93 \text{ MPa} \qquad (6.4)$$

The hot spot membrane and bending stresses determined using the stress distribution obtained from the Hybrid GR3 method along with the appropriate stress concentration factors have also been used for the determination of the through thickness stress distribution according to Monahan's eqn. 3.40 and is shown by green curve in Figure 6-2, along with the similar stress distributions obtained from 3D fine mesh model and 3D coarse mesh model using GR3 method.

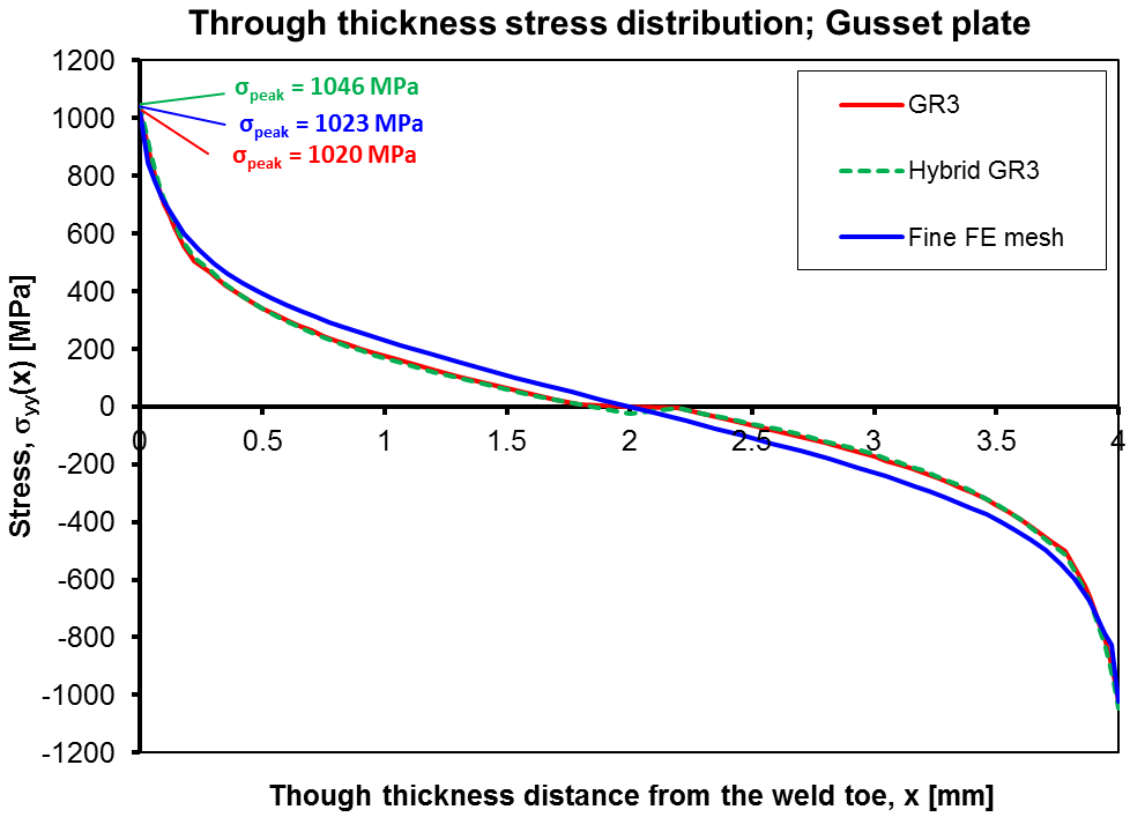

Figure 6-2: Through thickness stress distributions - Symmetric weld gusset joint

Figure 6-2 clearly shows that the profile of stress distribution obtained using the Hybrid GR3 method matches quite well with the similar stress distributions obtained using GR3 method as well as using 3D fine mesh FE model. This indicates that the new coarse FE mesh procedure (Hybrid GR3) can also provide reliable stress information for reasonably

accurate prediction of both the peak stress and the non-linear through-thickness stress distribution. So the Hybrid GR3 method could be a promising alternate approach for determining the hot spot bending stress, but more detailed investigation of this method is recommended by analyzing various joint types under different loading conditions.

6.3 Different FE stress data averaging techniques

In the case of finite element analysis, the FE solver internally evaluates the stresses for each element in the model at specific locations inside the element (also called as Gaussian or Quadrature points). These points form the basis of numerical integration schemes used in various finite element codes. The subsequent stresses obtained at the gaussian points inside each element are extrapolated to the nodes of the element. Several different extrapolation or FE averaging techniques are available for the nodal stress output data. Nodal averaged and nodal un-averaged are the two commonly used FE averaging techniques. As the name indicates, in the case of nodal averaged FE technique, stress data at the nodes is the averaged values of stresses at each node. The value shown at the node is the average of the stresses from the gaussian points of each element that it belongs to. In the case of nodal un-averaged FE technique, stress data at the nodes is obtained by ignoring the stresses from the gaussian points of the connected elements.

In the proposed GR3 methodology nodal averaged stress data has been used. It might be possible to improve upon the proposed methodology by utilizing the nodal un-averaged FE stress data. Basically the idea is that stress data for the nodes located at the sharp weld toe corner could be obtained by ignoring the stresses from the gaussian points of connecting elements as shown in Figure 6-3.

The gusset joint with symmetric welds from Section 4.2 has been selected for demonstration of this concept. The through-thickness stress distribution data as extracted from 3D coarse mesh FE model of this joint using nodal averaged FE technique is shown in Figure 4-3 and same is shown by the blue curve in Figure 6-4. The through-thickness stress distribution obtained from the same 3D coarse mesh FE model using nodal un-averaged FE technique is shown by the green curve in the Figure 6-4.

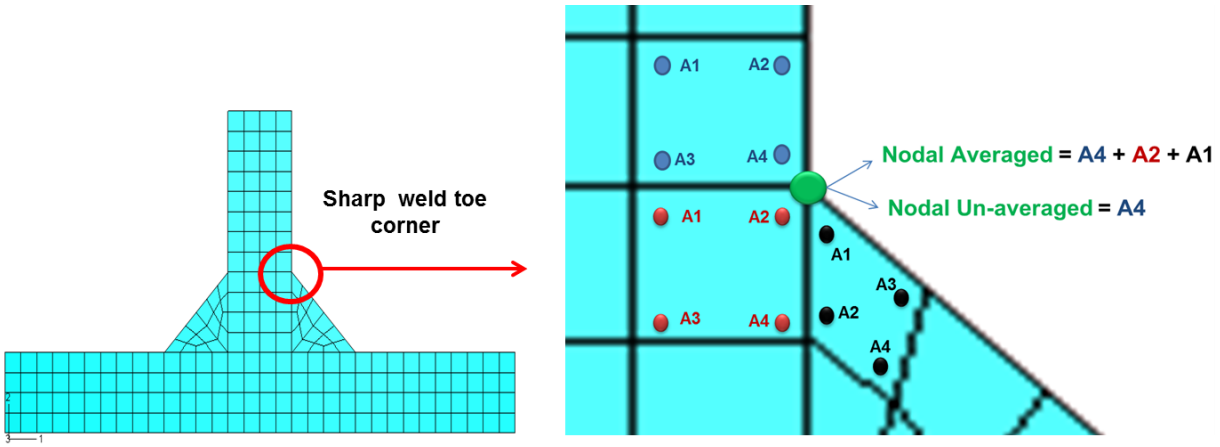

Figure 6-3: Coarse mesh FE model (on left) and enlarged view of the finite elements near the sharp weld toe corner showing different FE averaging techniques (on right), where A1, A2, A3 and A4 are the stress values at the gaussian points inside each element.

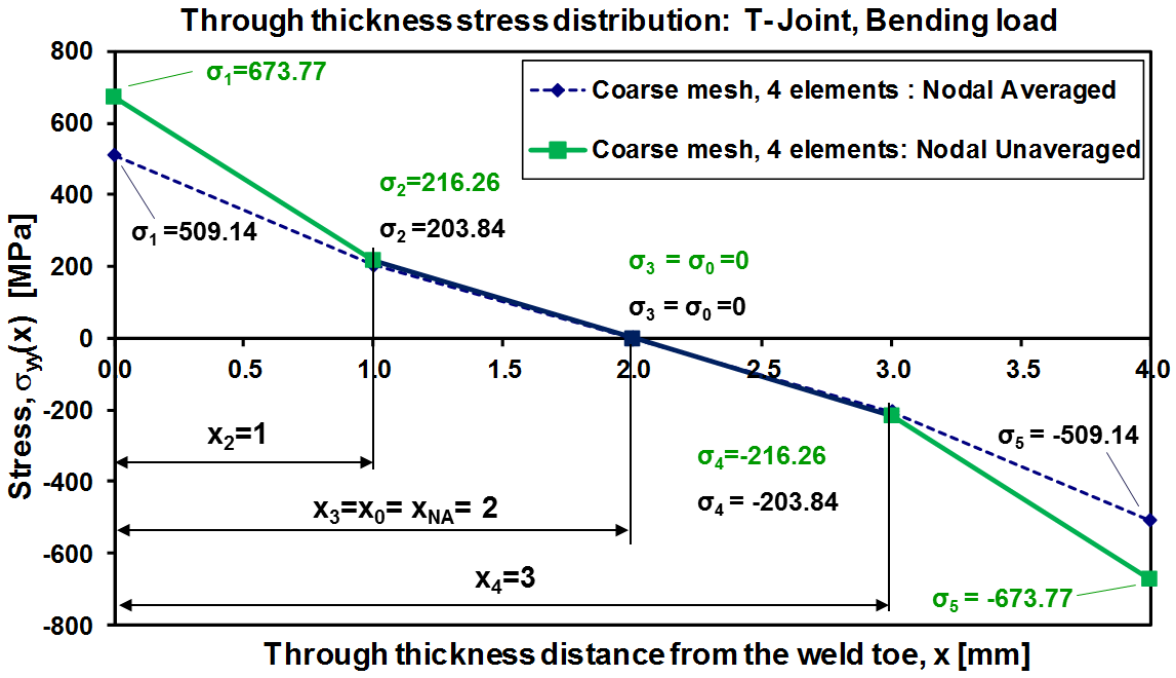

Figure 6-4: The through-thickness stress distribution obtained from 3D coarse mesh FE model obtained using nodal averaged FE technique (blue curve) vs. obtained using nodal un-averaged FE technique (green curve) for the gusset joint with symmetric welds

Based on the stress distribution obtained using nodal un-averaged FE technique and using eqn. 3.19, eqn. 3.20, and eqn. 3.21, bending moment, membrane stress and bending stresses are calculated as below:

$$M_b = 1555.43 \text{ Nmm} \tag{6.5}$$

$$\sigma_{hs}^{m} = 0.0 \text{ MPa} \tag{6.6}$$

$$\sigma_{hs}^{b} = \frac{6\, M_b}{t^2} = 583.29 \text{ MPa} \tag{6.7}$$

One of the ways of testing the validity of this new method is to compare the linearized stress distribution obtained from the new method using nodal unaveraged FE technique with that one resulting from the linearization of the fine mesh FE stress data (see Figure 4-7). In order to find the linearized through thickness stress distribution it is sufficient to determine stresses on both sides of the plate.

The characteristic linearized stresses on both sides of the base plate determined using the coarse FE mesh nodal-unaveraged stress data are (refer eqn. 4.7):

$$\text{at } x = 0 \qquad \sigma_{hs}^{s1} = \sigma_{hs}^{m} + \sigma_{hs}^{b} = 0.0 + 583.29 = 583.29 \text{ MPa}$$

$$\text{at } x = 4 \qquad \sigma_{hs}^{s2} = \sigma_{hs}^{m} - \sigma_{hs}^{b} = 0.0 - 583.29 = -583.29 \text{ MPa} \tag{6.8}$$

Analogous stresses obtained by the linearization of the fine mesh FE stress data are:

$$\text{at } x = 0 \qquad \sigma_{hs}^{s1} = \sigma_{hs}^{m} + \sigma_{hs}^{b} = 0 + 584.86 = 584.86 \text{ MPa}$$

$$\text{at } x = 4 \qquad \sigma_{hs}^{s2} = \sigma_{hs}^{m} - \sigma_{hs}^{b} = 0 - 584.86 = -584.86 \text{ MPa} \tag{6.9}$$

A comparison of linearized stress distributions plotted in Figure 6-5 shows that the difference between the stress distribution obtained using the nodal un-averaged stress data from 3D coarse mesh FE model and 3D fine mesh FE model is smaller (less than 1%) compared to the difference between the stress distribution obtained using the nodal averaged stress data from 3D coarse mesh FE model (GR3 method) and 3D fine mesh FE model (around 12%).

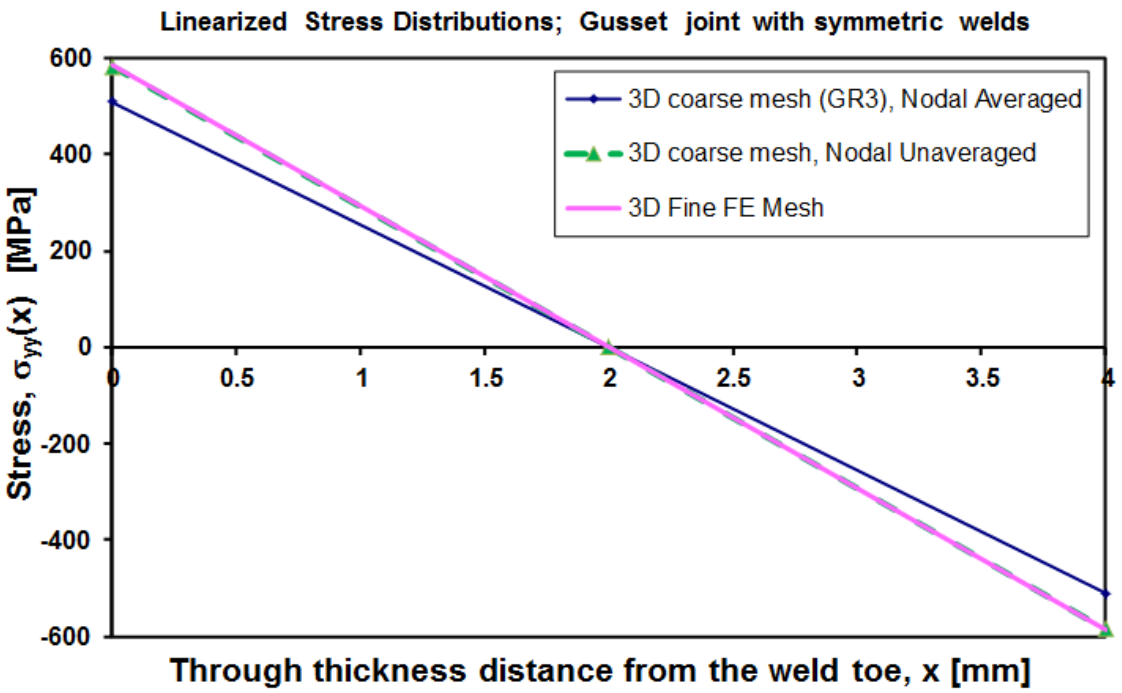

Figure 6-5: Linearized through thickness stress distributions in gusset edge weld joint

This indicates that the coarse FE mesh procedure using nodal un-averaged stress data could also provide reliable stress information for determination of the hot spot membrane and bending stress. More detailed investigation of this approach is recommended by analyzing various joint types under different loading conditions. One of the challenges with this method is that extra efforts are required to post-process the nodal-unaveraged FE stress data, while the nodal averaged FE stress data can be directly extracted in most of the FE packages.

6.4 Further investigations of the Total Fatigue Life concept

The Total Fatigue Life concept demonstrated in section 5.7 has been validated only for the cruciform joint; however more detailed investigation is recommended by analyzing various joint types, materials and loading configurations in order to better understand the robustness of this concept.

Chapter 7 Summary and Conclusions

During this work, the stress analysis and fatigue life estimation method applicable to welded structures has been developed. The method is based on a 3D coarse FE mesh model making it possible to analyze entire full scale welded structures without the necessity of modeling small geometrical features such as the weld toe radii, angle and other small geometrical discontinuities. The purpose of the method is to avoid very time and labor intensive accurate modeling of global and local geometrical features of welded structures but still provide sufficient stress information necessary for fatigue analyses. The modeling technique captures both the magnitude and the gradient of the hot spot stress near the weld toe which are necessary for calculating the stress concentration and the peak stress at critical cross-sections, e.g. at the weld toe. A procedure for the determination of the magnitude of the peak stress at the weld toe using the classical stress concentration factors (one for axial load and one for bending) has been proposed. The approach is based on the decomposition of the hot spot stress into the membrane and bending contribution. The method can be successfully applied to any combination of loading and weldment geometry. The stress concentration factors are used together with the hot spot membrane σ_{hs}^{m} and hot spot bending stress σ_{hs}^{b} at the location of interest in order to determine the peak stress at the weld toe and the through-thickness non-linear stress distribution. The knowledge of the peak stress at the weld toe enables application of the strain-life methodology for the assessment of the fatigue crack initiation life. The through-thickness stress distribution is the base for calculating stress intensity factors with the help of appropriate weight functions. Therefore the through-thickness stress distribution and the weight function method can be used for simulating the growth of fatigue cracks. The method is based on the observation that certain through thickness stress field properties are mesh independent and therefore they can be determined using relatively simple and coarse FE mesh models. The missing information concerning the actual stress concentration and non-linear through thickness distribution is added through appropriate post-processing of the coarse FE mesh data. It has been found from the validation studies that the difference between peak stresses obtained from the proposed

GR3 method and those determined using accurate and very fine FE mesh models did not exceed 10% and it is always conservative.

Further, welding process simulation model has been utilized to obtain information about the residual stress value at hot spot along with through thickness residual stress distribution at critical section. It has been shown that, fatigue crack initiation and propagation life predictions can then be made based on the combined effect of structural stress results obtained using the proposed methodology from 3D coarse mesh FE analysis and residual stresses obtained from the welding process simulation. The importance of including residual stresses during fatigue life estimation has been demonstrated as well.

The predicted total fatigue life has been compared with the experimental fatigue test data in order to further validate the accuracy of the proposed method and to demonstrate the overall process of fatigue life estimation utilizing structural stress results from the proposed methodology along with welding process simulation results. The experimental validation of the fatigue life calculated from the stress output data obtained using proposed methodology confirms good accuracy of the method.

A forward looking concept of estimating the total fatigue life by using the fracture mechanics method only has been demonstrated by using cruciform weld joint having incomplete penetration and misalignment. It has been shown that the stress data obtained using the proposed methodology can be used for the total fatigue life concept.

The proposed methodology provides a method to estimate the unique reference stress quantities which can be combined with geometry unique stress conc. factors to arrive at the required stress-strain information as needed for fatigue life analysis. The methodology accounts for local as well as global weldment geometry and allows the use of efficient 3D coarse mesh FE models to determine unique reference stress quantities. The methodology allows accounting for the manufacturing process effects (residual stress and its distribution, welding defects such as incomplete penetration). In conclusion, computationally effective methodology has been developed for reliable estimation of the fatigue life of large size welded structures under multiple modes of loading.

Finally, few recommendations have been made for the future work with the potential to further enhance the proposed methodology.

Bibliography

[1] Glinka G, "Fatigue & Fracture Mechanics - Analysis & Design," University of Waterloo, Lecture Notes 2011.

[2] Wolfgang Fricke, "Fatigue analysis of welded joints: state of development," *Marine Structures*, vol. 16, pp. 185-200, 2003.

[3] Niemi E, "Recommendations concerning stress determination for fatigue analysis of welded components," *IIW document Abington Publishers, Cambridge, UK*, pp. 1221-93, 1995.

[4] Fricke W, "Recommended hot-spot analysis procedure for structural details of ships and FPSOs based on round-robin FE analysis," *Int J Offshore & Polar Engg*, vol. 12, no. 1, pp. 40-8, 2002.

[5] Hobbacher A.F., "The new IIW recommendations for fatigue assessment of welded joints and components - A comprehensive code recently updated," *International Jornal of Fatigue*, no. 31, pp. 50-58, 2009.

[6] D. Radaj, C.M. Sonsino, and W. Fricke, "Recent developments in local concepts of fatigue assessment of welded joints," *International Journal of Fatigue*, no. 31, pp. 2-11, 2009.

[7] Wohler A, "Versuche Uber die festigkeit der Eisenbahnwagenachsen.," in *Zeitschrift fur Bauwesen 10; English summary. Engineering 4*, 1867, pp. 160-1.

[8] Goodman J., *Mechanics Applied to Engineering*, 8th ed. London: Longmans Green, 1914.

[9] Basquin O.H., "The Experimental Law of Endurance Tests," *Proc. ASTM*, vol. 10, no. 11, pp. 265-269, 1910.

[10] Palmgren A., "Die Lebensdauer von Kugellagern," *Zeitschrift des Vereins Deutscher Ingenieure*, vol. 68, no. 14, pp. 339-41, 1924.

[11] Miner M.A, "Cumulative Damage in Fatigue," *Trans. ASME, J. Appl. Mech*, vol. 67, pp. A159-64, 1945.

[12] Hobbacher A, *Recommendations for fatigue strength of welded components*.

Cambridge: Abington Publishers, 1996.

[13] "Structural Welding Code, Steel," AWS, ANSI/AWS D1.1-90, 1990.

[14] Niemi, W. Fricke, and S.J. Maddox, *Fatigue analysis of welded components, Designer's guide to the structural hot-spot stress approach*. Cambridge, England: Woodhead publishing limited, Sep 27, 2006.

[15] Hobbacher A, "Recommendations for fatigue design of welded joints and components," in *IIW XIII-2151r4-07/XV-1254r4-07 International Institute of Welding*, Dec 2008.

[16] Huther I., Gorski S., Lieurade H.P., Laborde, S., and Recho N., "Longitudinal non loaded welded joints geometrical stress approach," *Welding in the World*, vol. 43, no. 3, pp. 20–6, 1999.

[17] Niemi E and Tanskanen P, "Hot spot stress determination for welded edge gussets," *Welding in the World*, vol. 5, no. 44, pp. 31-7, 2000.

[18] Fricke W. and Bogdan R., "Determination of hot spot stress in structural members with in-plane notches using a coarse element mesh," in *nternational Institute of Welding. IIW-Doc. XIII-1870-01*, 2001.

[19] Radaj D and Sonsino CM, *Fatigue assessment of welded joints by local approaches*. Cambridge: Abington Publishers, 1998.

[20] Maddox S., "Recommended design S–N curves for fatigue assessment of FPSO," in *Proceedings of the ISOPE*, Stavanger, 2001.

[21] Maddox SJ., "Hot-spot stress design curves for fatigue assessment of welded structures," *Int J Offshore Polar Eng*, no. 12, pp. 134–41, 2002.

[22] Niemi E., "Structural stress approach to fatigue analysis of welded components—designer's guide.," in *IIW-Doc. XIII-1819-00/XV-1090-01, International Institute of Welding*, Paris, 2001.

[23] Dong P, Hong JK, and Cao Z., "Structural stress based master S–N curve for welded joints," in *IIW Doc XIII-1930-02/XV-1119-02. Int Inst Welding*, 2002.

[24] Dong P., "A structural stress definition and numerical implementation for fatigue analyses," *Intentaional Journal of Fatigue*, vol. 10, no. 23, pp. 865-76, 2001.

[25] Radaj D., *Design and analysis of fatigue-resistant welded structures*. Cambridge: Abington Publishers, 1990.

[26] Doerk O, Fricke W, and Weißenborn C., "Comparison of different calculation methods for structural stresses at welded joints," *Int Journal of Fatigue*, no. 25, pp. 359–69, 2003.

[27] Xiao ZG and Yamada K., "A method of determining geometric stress for fatigue strength evaluation of steel welded joints," *Int J Fatigue*, no. 26, pp. 1277–93, 2004.

[28] Noh B, Song J, and Bae S., "Fatigue strength evaluation of the load-carrying cruciform fillet-welded joints using hot spot stress," *Key Eng Mater*, pp. 324-325, 2006.

[29] Ilkka Poutiainen and Gary Marquis, "A fatigue assessment method based on weld stress," *International Journal of Fatigue*, no. 28, pp. 1037–1046, 2006.

[30] Wolfgang Fricke and Adrian Kahl, "Comparison of different structural stress approaches for fatigue assessment of welded ship structures," *Marine Structures*, no. 18, pp. 473-488, 2005.

[31] Radaj D, Sonsino CM, and Fricke W., *Fatigue assessment of welded joints by local approaches*, 2nd ed. Cambridge: Woodhead Publishing and Boca Raton CRC Press, 2006.

[32] Radaj D., "Review of fatigue strength assessment of nonwelded and welded structures based on local parameters," *Int J Fatigue*, no. 18, pp. 153–70, 1996.

[33] Radaj D, Lehrke HP, and Greuling S., "Theoretical fatigue-effective notch stresses at spot welds," *Fatigue Fract Eng Mater Struct* , no. 24, pp. 293–308, 2001.

[34] Langer B.F., "Fatigue failure from Stress Cycles of Varying Amplitude," *Journal of Applied Mechanics 59*, pp. 160-2, 1937.

[35] Neuber H., "Kerbspannungslehre," in *Springer-Verlag*, Berlin, 1937.

[36] Tavernelli J.F. and Coffin L.F., "Experimental support for generalized equation predicting low cycle fatigue," *Trans. ASME, J. Basic Eng.*, vol. 84, no. 4, pp. 533-38, 1962.

[37] Manson S.S. and Hirschberg M.H., "Fatigue behavior in strain cycling in low- and

intermediate cycle range," in *Sagamore Army Matls Research Conference*, 1963, pp. 133-178.

[38] Smith KN, Watson P, and Topper TH., "A stress–strain function for the fatigue of metals," *Journal of Materials*, vol. 5, no. 4, pp. 767–78, 1970.

[39] Topper T. H., Sandor B. I., and Morrow J., "Cumulative Fatigue Damage Under Cyclic Strain Control," *J. Materials*, vol. 4, no. 1, pp. 189-9, 1969.

[40] Neuber H., "Theory of Stress Concentration for Shear-strained Prismatic Bodies with Arbitrary Nonlinear Stress-strain Law," *ASME Journal of Applied Mechanics, ASME*, vol. 28, pp. 544-551, 1961.

[41] Matsuishi M. and Endo T., "Fatigue of Metals Subjected to Varying Stress," in *Japan Society of Mechanical Engineers*, Fukuoka, Japan, March 1968.

[42] Glinka G., "Energy density approach to calculation of inelastic strain–stress near notches and cracks," *Eng Fract Mech*, vol. 22, no. 3, pp. 485–508, 1985.

[43] Molski K. and Glinka G., "A method of elastic-plastic stress and strain calculation at a notch root," *Materials Science and Engineering*, vol. 50, no. 1, pp. 93-100, 1981.

[44] Manson S. S.(1953) and L. F. Coffin, "Behaviour of materials under conditions of thermal stress," in *NACA TN-2933 Trans. ASME*, 1954.

[45] Rakesh Goyal, Satyam Sahay, Eric Johnson, and Mohamad El-Zein, "Simulation and optimization of large welded structures," in *64th international conference on global trends in joining, cutting and surfacing technology by international institute of welding*, Chennai, July 2011.

[46] Irwin G.R., "Analysis of Stresses and Strains Near the End of a Crack Traversing a Plate," *Journal of Applied Mechanics*, vol. 24, pp. 361-4, 1957.

[47] Paris P.C., "The Growth of crack Due to Variations in Loads," Lehigh University, Bethlehem, Ph.D. Thesis 1960.

[48] Paris P.C., "Testing for Very Slow Growth of Fatigue Cracks," *Closed Loop*, vol. 2, no. 5, 1970.

[49] Schmidt R.A. and Paris P.C., "Threshold for Fatigue Crack Propagation and the Effects of Load Ratio and Frequency," in *ASTM STP 536, ASTM*, 1973, pp. 79-83.

[50] Elber W., "Fatigue Crack Closure under Cyclic Tension," *Eng. Fracture Mech.*, vol. 2, pp. 37-40, 1970.

[51] Paris PC., "Fracture mechanics and fatigue: a historical perspective," *Fatigue Fract Eng Mater Struct*, vol. 21, no. 5, pp. 535–40, 1998.

[52] Lie ST and Lan S., "A boundary element analysis of misaligned load-carrying cruciform welded joints," *Int J Fatigue*, vol. 20, no. 6, pp. 433–9, 1998.

[53] Nguyen NT and Wahab MA., "The effect of undercut and residual stresses on fatigue behaviour of misaligned butt joints," *Eng Fract Mech*, vol. 55, no. 3, pp. 453–69, 1996.

[54] Paris, P.C. and Erdogan F., "A critical analysis of crack propagation laws," *Journal of Basic Engineering*, no. D85, pp. 528-534, 1963.

[55] Walker EK, "The effect of stress ratio during crack propagation and fatigue for 2024-T3 and 7076-T6," *ASTM STP*, vol. 462, pp. 1–14, 1970.

[56] Forman R.G., Keamey V.E., and Engle R.M., "Numerical analysis of crack propagation in cyclic-loaded structures," *Journal of Basic Engineering, Trans. ASME 89, 459464.*, 1967.

[57] Dinda S and Kujawski D., "Correlation and prediction of fatigue crack growth for different R-ratios using Kmax and DK parameters," *Eng Fract Mech*, vol. 71, pp. 1779–90, 2004.

[58] Noroozi AH, Glinka G, and Lambert S, "A two-parameter driving force for fatigue crack growth analysis," *Int J Fatigue*, no. 27, pp. 1277-96, 2005.

[59] Noroozi AH, Glinka G, and Lambert S, "A study of the stress ratio effects on fatigue crack growth using the unified two-parameters fatigue crack growth driving force," *Int J Fatigue*, no. 29, pp. 1616–34, 2007.

[60] Glinka, G., Shen, G., "Universal Features of Weight Functions for Cracks in Mode I," *Engineering Fracture Mechanics*, vol. 40, no. 6, pp. 1135-1146, 1991.

[61] Kurihara M., Katoh A., and Kwaahara M., "Analysis on Fatigue Crack Growth Rates Under a Wide Range of Stress Ratio," *Journal of Pressure Vessel Technology, Transactions of the ASME*, vol. 108, no. 2, pp. 209-213, May 1986.

[62] Erkki Niemi, "Stress determination for fatigue analysis of welded components," in *IIS/IIW -1221-93 (ex doc XIII-1458-92,XV-797-92)* , 1993.

[63] Mattos R.J. and Lawrence F.V., "Estimation of the fatigue crack initiation life in welds using low cycle fatigue concepts," in *SAE SP- 424. Society of Automative Engineering*, Warrendale, PA, 1977.

[64] Hiroko Kyuba and Pingsha Dong, "Equilibrium-equivalent structural stress approach to fatigue analysis of a rectangular hollow section joint," *International Journal of Fatigue*, no. 27, pp. 85-94, 2005.

[65] Rakesh Kumar et al., "A Model Equation for the convection coefficient for thermal analysis of welding structures," in *8th International conference on Trends in Welding Research*, Pine Mountain, Georgia, USA , June 2008.

[66] Johnson Eric, "Progress toward a model based approach to the robust design of welded structures," Iowa State University, Graduate Theses and Dissertations Paper 13119, 2013.

[67] Monahan C. C., "Early fatigue cracks growth at welds," in *Computational Mechanics Publications*, Southampton UK, 1995.

[68] Chattopadhyay A, Glinka G, El-Zein M, Qian J, and Formas R., "Stress analysis and fatigue of welded structures," *Welding in the world*, vol. 55, no. 7, pp. 2–21, 2011.

[69] K. Iida and T. Uemura, "Stress Concentration Factor Formulas Widely Used in Japan," *Fatigue Fract. Engng Mater Struct* , vol. 19, no. 6, pp. 779-786, 1996.

[70] Mikheevskiy, G.,Glinka S., "Elastic–plastic fatigue crack growth analysis under variable amplitude loading spectra," *International Journal of Fatigue*, no. 31, pp. 1828–1836 , 2009.

Appendix A: Weight Function Parameters

Parameters of the weight function for a semielliptical crack in a finite thickness plate (Figure 2-8)

- **For the deepest point A**

$$\boldsymbol{m_A(x,a) = \frac{2F}{\sqrt{2\pi(a-x)}}\left\{1 + M_{1A}\left(1-\frac{x}{a}\right)^{\frac{1}{2}} + M_{2A}\left(1-\frac{x}{a}\right) + M_{3A}\left(1-\frac{x}{a}\right)^{\frac{3}{2}}\right\}}$$

$$M_{1A} = \frac{\pi}{\sqrt{2Q}}(4Y_0 - 6Y_1) - \frac{24}{5}$$

$$M_{2A} = 3$$

$$M_{3A} = 2\left(\frac{\pi}{\sqrt{2Q}}Y_0 - M_{1A} - 4\right)$$

where for $0 < a/c < 1$:

$$Q = 1.0 + 1.464\left(\frac{a}{c}\right)^{1.65}$$

$$Y_0 = B_0 + B_1\left(\frac{a}{t}\right)^2 + B_2\left(\frac{a}{t}\right)^4 + B_3\left(\frac{a}{t}\right)^6$$

$$B_0 = 1.0929 + 0.2581\left(\frac{a}{c}\right) - 0.7703\left(\frac{a}{c}\right)^2 + 0.4394\left(\frac{a}{c}\right)^3$$

$$B_1 = 0.456 - 3.045\left(\frac{a}{c}\right) + 2.007\left(\frac{a}{c}\right)^2 + \frac{1.0}{0.147 + \left(\frac{a}{c}\right)^{0.688}}$$

$$B_2 = 0.995 - \frac{1.0}{0.027 + \frac{a}{c}} + 22.0\left(1-\frac{a}{c}\right)^{9.953}$$

$$B_3 = -1.459 + \frac{1.0}{0.014 + \frac{a}{c}} - 24.211\left(1-\frac{a}{c}\right)^{8.071}$$

and

$$Y_1 = A_0 + A_1\left(\frac{a}{t}\right)^2 + A_2\left(\frac{a}{t}\right)^4 + A_3\left(\frac{a}{t}\right)^6$$

$$A_0 = 0.4537 + 0.1231\left(\frac{a}{c}\right) - 0.7412\left(\frac{a}{c}\right)^2 + 0.4600\left(\frac{a}{c}\right)^3$$

$$A_1 = -1.652 + 1.665\left(\frac{a}{c}\right) - 0.534\left(\frac{a}{c}\right)^2 + \frac{1.0}{0.198 + \left(\frac{a}{c}\right)^{0.846}}$$

$$A_2 = 3.418 - 3.126\left(\frac{a}{c}\right) - \frac{1.0}{0.041 + \left(\frac{a}{c}\right)} + 17.259\left(1 - \frac{a}{c}\right)^{9.286}$$

$$A_3 = -4.228 + 3.643\left(\frac{a}{c}\right) + \frac{1.0}{0.020 + \frac{a}{c}} - 21.924\left(1 - \frac{a}{c}\right)^{9.203}$$

and for 1 < *a/c* < 2

$$Q = 1.0 + 1.464\left(\frac{c}{a}\right)^{1.65}\left(\frac{a}{c}\right)^2$$

$$Y_0 = B_0 + B_1\left(\frac{a}{t}\right)^2 + B_2\left(\frac{a}{t}\right)^4$$

$$B_0 = 1.12 - 0.09923\left(\frac{a}{c}\right) + 0.02954\left(\frac{a}{c}\right)^2$$

$$B_1 = 1.138 - 1.134\left(\frac{a}{c}\right) + 0.3073\left(\frac{a}{c}\right)^2$$

$$B_2 = -0.9502 + 0.8832\left(\frac{a}{c}\right) - 0.2259\left(\frac{a}{c}\right)^2$$

$$Y_1 = A_0 + A_1\left(\frac{a}{t}\right)^2 + A_2\left(\frac{a}{t}\right)^4$$

$$A_0 = 0.4735 - 0.2053\left(\frac{a}{c}\right) + 0.03662\left(\frac{a}{c}\right)^2$$

$$A_1 = 0.7723 - 0.7265\left(\frac{a}{c}\right) + 0.1837\left(\frac{a}{c}\right)^2$$

$$A_2 = -0.2006 - 0.9829\left(\frac{a}{c}\right) + 1.237\left(\frac{a}{c}\right)^2 - 0.3554\left(\frac{a}{c}\right)^3$$

- **For the surface point B**

$$\boldsymbol{m_B(x,a) = \frac{2F}{\sqrt{\pi x}}\left\{1 + M_{1B}\left(\frac{x}{a}\right)^{\frac{1}{2}} + M_{2B}\left(\frac{x}{a}\right)^{1} + M_{3B}\left(\frac{x}{a}\right)^{\frac{3}{2}}\right\}}$$

$$M_{1B} = \frac{\pi}{\sqrt{4Q}}(30F_1 - 18F_0) - 8$$

$$M_{2B} = \frac{\pi}{\sqrt{4Q}}(60F_0 - 90F_1) + 15$$

$$M_{3B} = -(1 + M_{1B} + M_{1B})$$

where for $0 < a/c < 1$:

$$F_0 = \left[C_0 + C_1\left(\frac{a}{t}\right)^2 + C_2\left(\frac{a}{t}\right)^4\right]\sqrt{\frac{a}{c}}$$

$$C_0 = 1.2972 - 0.1548\left(\frac{a}{c}\right) - 0.0185\left(\frac{a}{c}\right)^2$$

$$C_1 = 1.5083 - 1.3219\left(\frac{a}{c}\right) + 0.5128\left(\frac{a}{c}\right)^2$$

$$C_2 = -1.101 + \frac{0.879}{0.157 + \frac{a}{c}}$$

and

$$F_1 = \left[D_0 + D_1\left(\frac{a}{t}\right)^2 + D_2\left(\frac{a}{t}\right)^4\right]\sqrt{\frac{a}{c}}$$

$$D_0 = 1.2687 - 1.0642\left(\frac{a}{c}\right) + 1.4646\left(\frac{a}{c}\right)^2 - 0.7250\left(\frac{a}{c}\right)^3$$

$$D_1 = 1.1207 - 1.2289\left(\frac{a}{c}\right) + 0.5876\left(\frac{a}{c}\right)^2$$

$$D_2 = 0.190 - 0.608\left(\frac{a}{c}\right) + \frac{0.199}{0.035 + \frac{a}{c}}$$

and for 1 < *a/c* < 2

$$F_0 = \left[C_0 + C_1\left(\frac{a}{t}\right)^2 + C_2\left(\frac{a}{t}\right)^4\right]\sqrt{\frac{a}{c}}$$

$$C_0 = 1.34 - 0.2872\left(\frac{a}{c}\right) + 0.0661\left(\frac{a}{c}\right)^2$$

$$C_1 = 1.882 - 1.7569\left(\frac{a}{c}\right) + 0.4423\left(\frac{a}{c}\right)^2$$

$$C_2 = -0.1493 + 0.01208\left(\frac{a}{c}\right) + 0.02215\left(\frac{a}{c}\right)^2$$

and

$$F_1 = \left[D_0 + D_1\left(\frac{a}{t}\right)^2 + D_2\left(\frac{a}{t}\right)^4\right]\sqrt{\frac{a}{c}}$$

$$D_0 = 1.12 - 0.2442\left(\frac{a}{c}\right) + 0.06708\left(\frac{a}{c}\right)^2$$

$$D_1 = 1.251 - 1.173\left(\frac{a}{c}\right) + 0.2973\left(\frac{a}{c}\right)^2$$

$$D_2 = 0.04706 - 0.1214\left(\frac{a}{c}\right) + 0.04406\left(\frac{a}{c}\right)^2$$

Appendix B: Welding Simulation Flow Chart